Fall 2012

# Characterization of expanded polystyrene (EPS) and cohesive soil mixtures

Nicholas Thomas Rocco

CHARACTERIZATION OF EXPANDED POLYSTYRENE (EPS)

AND COHESIVE SOIL MIXTURES

by

NICHOLAS THOMAS ROCCO

A DISSERTATION

Presented to the Faculty of the Graduate School of the

MISSOURI UNIVERSITY OF SCIENCE AND TECHNOLOGY

In Partial Fulfillment of the Requirements for the Degree

DOCTOR OF PHILOSOPHY

in

CIVIL ENGINEERING

2012

Approved by:

Ronaldo Luna, Advisor

Richard Stephenson

J. David Rogers

Neil Anderson

Louis Yu-Ning Ge

**ABSTRACT**

Soils modified with expanded polystyrene (EPS) particulates could be used as lightweight fill in a variety of installations including slopes for improved stability, embankments over compressible soils, and to reduce earth pressures next to structures.  The addition of low density EPS particulates into soil has a large effect on the mass and volumetric characteristics of these mixtures and their influence on mechanical properties is scarce in the literature.  A laboratory characterization program using clay mixed with EPS particulates was conducted for different dosages of EPS.  Soils were modified with up to 1.5% EPS by mass, which corresponds to approximately 45% EPS by volume.  This research focused on the laboratory evaluation of the individual constituents followed by the engineering characterization of composite mixtures at increasing percentages of EPS.  The preparation of unit element specimens for the mixtures were developed using slurry consolidation and mechanical compaction.  For each half percent increase in EPS content there was a reduction of 8% to 12% in dry unit weight and an increase in equivalent void ratio of 15 to 22%.  Therefore, the reduction in dry unit weight is significant for use as soil fill.  The evaluation of the mechanical properties of the soil/EPS mixtures included: swell, compression, and shear strength.  The low strain dynamic properties (shear modulus and damping) were examined using the following devices: resonant column apparatus, bender elements, and ultrasonic pulse velocity transducers.  Results indicate that the strength of the modified soils was not compromised with the addition of up to 1% EPS by mass.  The percent free swell and swell pressure reduce with increasing EPS content, but the compressional strain prior to inundation increases with increasing EPS content.  The dynamic properties indicate decreased shear stiffness with increasing EPS content, but the material damping is relatively unaffected by the EPS content.  Even though the shear modulus decreased in magnitude, the specimens exhibit elastic behavior for a wider range of strain.  Overall, the laboratory evaluation of these soil/EPS mixtures resulted in properties that are within the range of engineering use and could be considered as alternative construction materials in civil engineering applications.

# ACKNOWLEDGMENTS

**TABLE OF CONTENTS**

# LIST OF ILLUSTRATIONS

# LIST OF TABLES

# 1.    INTRODUCTION

The modification of soils to improve engineering performance is an established practice in geotechnical engineering. Mixing of soils with cement, or other pozzolanic materials such as fly ash or lime, for shallow fill or deep in-situ placements are common methods to improve performance of soil. A modified soil's reduced compressibility can also improve seismic performance of granular fills by reducing the liquefaction potential of a deposit. Researchers have utilized materials such as shredded tires (e.g. Bernal et al. 1996; Humphrey & Tweedie 2002; Grubb et al. 2007a), crushed glass (e.g. Wartmann et al. 2004; Grubb et al. 2006, 2007b), and geosynthetic products such as geofibers (e.g. Gregory 1996; Santoni et al. 2001) to modify soil behavior.

Closed-cell expanded polystyrene (EPS) geofoam has been utilized in geotechnical applications for the past three decades for a variety of uses including lightweight fill, thermal insulation, and compressible inclusions. There are situations where the installation of large geofoam pieces in the subsurface is not ideal and where mixing EPS particulates with soils could prove to be a viable alternative. Modified soils composed of typical fill material and EPS particulates could exhibit advantageous physical, mechanical, and dynamic properties. This research presents a detailed investigation of the laboratory characterization of a cohesive soil modified with EPS particulates. Strength, compressibility, and low strain dynamic properties were studied.

What initiated as an investigation into the ability to modify existing soils with EPS particulates to improve dynamic properties, eventually evolved into an overall investigation of the engineering properties of these modified soils as there was limited published research on the subject. Prior to understanding how these modified soils behaved with respect to dynamic energy, it seemed more prudent to characterize the particulate additive and more typical geotechnical properties such as compressibility and strength. Typical geotechnical properties such as compressibility and strength were evaluated for the modified soils as well as the material characterization of individual EPS particulates. Strength data was determined by performing unconsolidated undrained and consolidated undrained triaxial compression tests.

## 1.1.  OBJECTIVES OF INVESTIGATION

The primary objectives of this study were to report the engineering characteristics and behavior of a soil modified with EPS particulates through a rigorous, in-depth laboratory

investigation. Material characterization of the EPS particulates was accomplished using microscopy, scanning electron microscopy, and detailed mass and dimensional measurements. Engineering characterization of static properties for the modified soils were quantified by performing compaction, compression, swell, and triaxial strength tests. The reference soil used in the laboratory investigation was a commercially available, processed kaolin clay with consistent material properties so that the influence of different ratios of EPS particulates could be adequately evaluated from the test data. Testing was performed on both slurry consolidated and compacted specimens.

A secondary objective of the research was to assess if the low strain dynamic properties of a compacted soil were improved through the addition of EPS particulates. The role of laboratory testing for dynamic loads is to assess the stress-strain characteristics and material damping of the soil using metrics such as the Young's modulus (E), shear modulus (G), Poisson's ratio ($\nu$), and material damping (D). Low strain dynamic properties of the modified soils were quantified using the resonant column apparatus and ultrasonic and bender element pulse velocity measurements.

Low strain dynamic properties are important parameters in many geotechnical designs involving dynamic loads and vibrations as well as static structures that are designed to be far from failure. Small vibrations can prove to be disruptive to some sensitive equipment and must be considered for certain design scenarios such as medical facilities. Vibrations that are of concern to the geotechnical engineering practice can originate from a variety of sources, as shown in Figure 1.1. Dynamic loads can be introduced above the ground surface and transmit through a structure and into the ground surface thereby potentially affecting the foundation response. Traffic loadings on a roadway and industrial machine vibrations are examples of these types of loads. Conversely, dynamic loads can initiate at some distance from a structure and transmit through the soil prior to influencing a structure such as seismic events, mine blasting operations, and detonation of military munitions. The vibrations from these types of events are usually short-lived but can produce some of the most destructive motions. If a soil modified with EPS particulates exhibits an improvement in dynamic properties without a significant loss in strength, then they might provide a feasible additive in certain design scenarios.
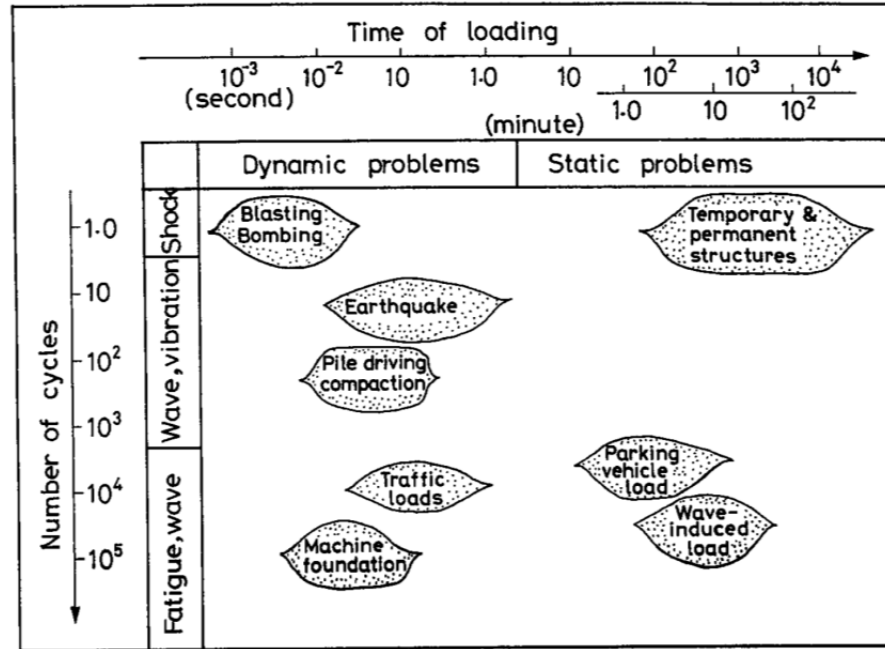
**Figure 1.1. Dynamic Problems in Geotechnical Engineering (Ishihara 1996)**

The primary questions that were answered with this research were:

- How does the addition of EPS particulates affect the strength of the soils?
- Did EPS modified soils exhibit changes in dynamic soil properties that would be advantageous in certain design scenarios?
- Based on the findings of the research program, what are the optimum mixing ratios for these soils and are these mixing ratios different for the modification of different engineering properties?

The idea of utilizing EPS particulates to modify soils developed from the desire to design a soil that provides improved dynamic performance. Improved dynamic performance is defined in this research as exhibiting increased damping of dynamic energy without a significant loss of material stiffness and strength. It is postulated that the EPS particulates will introduce "air pockets" within the modified soil, and thus provide increased damping by dispersion of transmitting energy waves. However it is unknown if the EPS particulates will saturate after a

specific pressure threshold or collapsed under certain confinements. Two working hypotheses that were considered throughout the research program are:

- The EPS particulate additives would not saturate under pressures and time periods of typical of geotechnical applications; and
- The EPS particulate additives would not significantly degrade the soil stiffness and strength as they constitute such a small percentage of the overall soil mass.

## 1.2. SCOPE OF LABORATORY INVESTIGATION

The scope of this study investigated how soils modified with EPS particulates changed the soil's engineering properties based on the results of a thorough laboratory testing investigation. Typical geotechnical characterization of static and dynamic soils properties were investigated using the following tests:

i. Compaction characteristics – Standard Proctor compaction tests (ASTM D698) were performed on pure clay and the EPS modified clay specimens to determine the influence of EPS particulates on the optimum moisture content and density of the specimens.

ii. Compression and swell characteristics – One dimensional compression and swell of compacted specimens were investigated on pure clay and EPS modified clay specimens according to ASTM D4546. Variations in specimen compression under different surcharge loads were investigated prior to inundation of the specimens and documentation of progressive swell or collapse with time. The influence of the EPS additives on the percent free swell and swell pressure was investigated and discussed.

iii. Strength characteristics – Strength and moduli for pure clay and EPS modified speciemsn were determined utilizing triaxial unconsolidated-undrained and triaxial consolidated-undrained compression tests. Testing was performed on both slurry and compacted specimens. Total and effective strength parameters were determined and discussed.

iv. Resonant column apparatus – Low to moderate strain shear moduli and material damping of test specimens were determined for cyclic torsional loads using the resonant column apparatus. The primary effect of EPS content was investigated as well as the secondary effects of confining pressure, void ratio, percent compaction, and saturation.

v.    Ultrasonic pulse velocity – Low strain moduli were determined for specimens utilizing ultrasonic pulse velocity transducers. The primary effect of EPS content was investigated.

vi.    Bender element pulse velocity – Low strain shear moduli of the specimens were determined with pulse velocity tests that utilized bender element transducers. The primary effect of EPS content was investigated as well as the secondary effects of confining pressure, void ratio, percent compaction, and saturation.

## 1.3. POTENTIAL IMPACTS OF RESEARCH

The addition of very low density EPS particulates into soil has a large effect on the mass and volumetric properties of the resulting modified soil mixtures and their influence on mechanical properties is scarce in the literature. The addition of EPS particulates has the potential to produce a modified soil with improved performance and a wide range of practical applications. EPS modified soils could be used as lightweight fill in slopes or embankments if they are shown not to have a significant reduction in strength. They could also be used to reduce earth pressures against structures if the EPS particulates function as compressible inclusions within the soil matrix. In addition the results of this research program could have implications in the vibrational isolation of structures and foundations if the modified soils maintain stiffness while improving energy damping.

A modified soil with reduced unit weight and significant void space could produce a composite material with many beneficial applications. With that in mind, the presented research investigated how the static and dynamic properties of a typical fill soil were improved by the addition of a closed-cell polystyrene particulate. Multiple mixing ratios and their effect on the static and dynamic behavior of the modified soils were investigated.

## 1.4. ORGANIZATION OF DISSERTATION

This thesis consists of eight chapters and associated appendices. Chapter 1 provides an overview of the research, the objectives and working hypotheses, and the scope of the research. Chapter 2 discusses the literature review that was performed in regards to modified soils, EPS materials, the determination and use of dynamic soil properties, and the piezoelectric phenomena that was utilized in the assessment of dynamic soil properties. Chapter 3 identifies the materials that were utilized in the laboratory investigation. Chapter 4 provides a review of the laboratory testing program and techniques used. Chapter 5 and Chapter 6 discuss the results and

interpretation of the static and dynamic properties of the modified soil specimens. Chapter 7 is a discussion of the results. Chapter 8 offers a summary, conclusion, and recommendations for future work.

## 2.   LITERATURE REVIEW

The first section of the literature review discusses how difficult soils have been modified in the past with other geomaterials to improve certain performance aspects.  As there are many different techniques and applications under the broad term "soil modification", this section is limited to soils modified with other particulate materials, thus topics such as soil grouting or dynamic compaction have been omitted.  The second section of the literature review discusses the production, manufacturing, specification, and typical properties of expanded polystyrene (EPS) geofoam products and their traditional uses in geotechnical engineering.

The final three sections of the literature review discuss the theory, experimental equipment, and empirical models used to determine the dynamic soil properties of soils. Although the experimental program realized for this research included significantly more testing than just measurement of low-strain dynamic soil properties, these procedures and techniques are well established in the industry and in our laboratory here at Missouri S&T.  Conversely, the measurement of low-strain dynamic soil properties is a relatively new development at Missouri S&T and new experimental equipment was developed to augment the equipment currently available at the university.

The third section of the literature review discusses dynamic soil properties and their use in geotechnical design.  Previous research is discussed and empirical models developed to estimate these properties are presented.  The fourth section discusses the development of laboratory techniques to measure the low strain dynamic properties of unit element soil specimens.  The final section of the literature review discusses piezoelectric phenomena and materials, and how these materials have been utilized in geotechnical engineering.

By no means is each topic covered exhaustively, but each provides the background to understand and appreciate the historical development and progress of each topic in the geotechnical engineering field of application and research.

### 2.1.  MODIFIED SOILS

**2.1.1.  Typical Soil Additives.**  Historically soils have been modified with a variety of particulate materials to alter behavior.  The modification of soils with rubber particles derived from discarded vehicular tires has been investigated.   Tire derived aggregate (TDA) has been utilized in geotechnical application for approximately two decades for a variety of applications. ASTM D6270 has been developed to help guide practitioners in the uses of TDA in the

subsurface and applicable laboratory testing to access engineering properties. Humphrey and Sandford (1993) performed a detailed laboratory investigation to determine the engineering properties of TDA. The authors advocated their use as lightweight fill for transportation applications over compressible subgrades. Bernal et al. (1996) discuss the use of TDA in the backfill for reinforced earth walls. Feng and Sutter (2000) performed resonant column testing to determine the dynamic properties of TDA mixed with sand. Nirmalan (2006) used a 70:30 soil to tire shred mixing ratio and performed undrained cyclic triaxial tests. Kim and Santamarina (2008) performed pulse velocity testing using bender element transducers to measure the shear wave velocity of TDA and sand mixtures. Kim and Kang (2011) created a flowable fill using a mixture of dredged soils, TDA, and ash. Results indicated that increasing rubber content decreased the strength but provided a more ductile, lightweight material. Senetakis et al. (2012) investigated the impact on laboratory measured dynamic soil properties of sandy soils modified with TDA. An empirical hyperbolic model was developed based on the test results. The authors conclude that increasing rubber content reduced the pore water pressure buildup at a given strain level.

Wartmann et al. (2004a,b) and Grubb et al. (2006) conducted laboratory investigations to evaluate the feasibility of utilizing crushed-glass to improve the engineering characteristics of highly compressible soils such as marine and river sediments and quarry fines. Crushing and utilizing glass from municipal curbside recycling programs presented an innovative use of a traditional waste stream. The authors found that the frictional strength of the fine-grained soil was considerably increased by the addition of crushed-glass while maintaining low hydraulic conductivity. Ultimately the authors believed this type of modified soil presented a viable option for a low-permeability fill material.

Natural and synthetic fibers have been mixed with soils to improve engineering properties. These soils are often referred to as fiber reinforced soils (FRS). Gregory (1996, 1997) used polypropylene fibers to modify soils for improved shear strength. Gregory (1999) presented an empirical relationship to estimate the increase in shear strength for FRS. Loehr et al. (2000) investigated the swell potential of FRS in the laboratory and results indicated improvements in swell potential were proportional the percentage of fibers introduced. Kumar and Tabor (2003) and Santoni et al. (2001) performed unconfined compression tests in the laboratory with sand – fiber mixtures and showed a significant improvement peak and residual strength with the addition of the fibers. The authors also defined an optimum mixing ratio and fiber length based on the results of the testing program. Ozkul and Baykal (2006, 2007) performed strength testing on soils modified with rubber fibers that were a waste product from re-

treading tires. Results indicated increased undrained and drained strength for the modified soils as compared to non-modified soils. Gregory (2011) discussed the successful repair of a highway embankment utilizing fiber-reinforced soils.

      **2.1.2.   Soils Modified with EPS Particulates.**   To date there is little published information and data for soils modified with EPS particulates. All available data was published within the last ten years for a few different engineered designs and research investigations, and the majority of the research has been within Asia. All previous studies have analyzed static loading conditions, but the impact of EPS particulates on the soil's dynamic properties has yet to be investigated. Table 2.1 below lists the published data available for soils modified with EPS particulates and the percent EPS utilized in those projects.

**Table 2.1. EPS Particulate Mixing Ratios**

| *Reference* | *Reported EPS Additive* |
|---|---|
| Tsuchida et al. (2001) | Not specified |
| Satoh et al. (2001) | Not specified |
| Yoon et al. (2004) | 1, 2, and 3% by mass |
| Liu et al. (2006) | 2, 3, 4, 5, and 6% by mass |
| Deng and Xiao (2008; 2010) | 0, 0.5, 1.5, and 2.5% by mass |
| Wei et al. (2008) | 0, 1.2, 2.3, 3.5, 4.6, and 100% by mass |
| Nataatmadja and Illuri (2009) | 0.3, 0.6, and 0.9% by mass |

      Satoh et al. (2001) and Tsuchida et al. (2001) discussed innovative field projects that utilized dredged soils mixed with EPS particulates and cement in land reclamation projects in Japan and South Korea, respectively. The mixing processes were performed in small batch plants to create a fluidized, modified soil that could be pumped into place. The low unit weight of EPS particulates yielded a light-weight material, and as is typical of cement treated soils, the final strengths were realized with time. The field component of the study demonstrated a successful pilot-scale application of this material, though the researchers noted that its application and durability under a wide range of field conditions warranted further investigation. The authors generally concluded that this type of flowable fill presents a viable alternative for projects with difficult access or irregular shapes where typical geofoam blocks are cumbersome. Satoh et al.

(2001) used CPT soundings to investigate the in-place properties of the installed EPS modified soil.

Yoonz et al. (2004) and Liu et al. (2006) performed unconfined compression tests on unit element soil specimens modified with EPS particulates and cement. Empirical relationships between the unconfined compressive strength, unit weight, cement ratio, EPS particulate percentage, and moisture content were developed. Evaluation of the engineering properties for these modified soil were based solely on the decrease in density and 7-day and 28-day compressive strength. Liu et al. (2006) noted that the addition of 2 – 6% EPS particulates by mass resulted in an approximate 190 – 570% increase by volume; a significant increase in void space! Data also indicated that increases in EPS ratios led to a decrease in unit weight and a decrease in strength. Interestingly the authors noted that the tangent modulus from the stress-strain data was not influenced by the EPS content.

Deng and Xiao (2008, 2010) mixed EPS particulates with sand to create a lightweight, non-structural fill and measured the stress-strain characteristics of these modified soils in the laboratory using triaxial testing techniques. Specimens with 0.5 – 2.5% EPS particulates by mass were prepared using vibration and moist tamping techniques. Direct shear test results indicated a decreasing friction angle with increasing EPS content. Consolidated-drained triaxial test results indicted decreasing strength with increasing EPS content and no peak strength was obtained in any specimen up to 15% axial strain. Volumetric behavior was completely contractive. Interestingly, the higher EPS content soils exhibited some apparent cohesion and a bi-linear failure envelope. Wei et al. (2008) mixed EPS particulates with sand and tested the dry mixtures in the direct shear apparatus. Results indicated that apparent cohesion increases and the internal friction angle decreases with increasing EPS content. Calculated shear strengths showed generally increasing shear strength for EPS / sand mixtures with increasing EPS contents, after which the shear strength decreased slightly when EPS contents exceeded 50%, by volume.

Nataatmadja and Illuri (2009) mixed EPS particulates into swelling soils to act as compressible inclusions. The EPS materials used in this research were produced by blending recycled materials from the packing industry and a 0.9% by mass mixing ratio was considered. Moisture density relationships, shrink-swell behavior, and hydraulic conductivity were discussed. Results indicated that the swell pressure was decreased by half and volumetric shrinkage upon desiccation was reduced by approximately 50%. The authors also reported that the hydraulic conductivity increased with increasing EPS content.

Arellano et al. (2009) discuss an innovative use of recycled polystyrene for drainage systems. The research used polystyrene packaging material that was melted and re-expanded to

an approximately 25mm cubic shape. The particulate material was encapsulated in a geotextile and drainage volumes were determined for different vertical loads.

## 2.2. GEOFOAM

**2.2.1. General.** Cellular plastic foam, or cellular geosynthetics, are manufactured products with an internal polymeric cell structure and are typically divided between two parent products: geocomb and geofoam. Geocomb is an open-cell material with a honeycomb cross-section that is manufactured in an extrusion process. They are a proprietary product and as of 2001 they were not available in the USA (Horvath 2001). Geofoam is a closed-cell material made from a variety of materials in one of two different manufacturing processes. Parent materials of geofoam can be divided into two different categories: inorganic and polymeric. Inorganic materials include cellular glass and foamed Portland cement concrete. Polymeric materials include polystyrene (PS), polyethylene (PE), and polyurethane (PUR) of which PS is the most common. Today, the term geofoam is more or less synonymous with PS geofoam, and for the remainder of this document will continue with this designation. PS geofoam is manufactured in either an extrusion or expansion process, and commonly referred to as XPS or EPS, respectively.

The engineering properties of PS particulates or regrind are not readily available in published literature, as the majority of published work has been on testing of the final, block-formed geofoam products (e.g. Horvath 1993; Negussey 2007; Osso and Romo 2011). Geosynthetic suppliers tend to reference geofoam density (ASTM D1622) and perform quality control testing to determine compressive strength (ASTM D1621), flexural strength (ASTM C203), and tensile strength (ASTM D1623) as needed. The density of geofoam is typically 20 kg/m$^3$ due to the large amount of void space. For comparison, this is approximately 1% of typical soil density.

**2.2.2. Manufacturing Process.** The most common cellular geosynthetics are closed-cell expanded polystyrene (EPS) geofoam. The primary component of polystyrene is styrene, which is formed from ethylene and benzene. Polystyrene is produced from styrene through a suspension polymerization process in a water solution (Figure 2.1). A specialty manufacturer of geofoam typically purchases polystyrene resin beads from a petroleum or chemical manufacturer, averaging 0.2 – 3mm in diameter, and containing a pentane or butane blowing agent inside.

EPS geofoam has a two-stage manufacturing process. During pre-expansion the resin beads are exposed to steam at a temperature of 100 - 110ºC under controlled pressure that softens the cell walls and expands the blowing agent to create a cellular structure within the particle, as

shown in Figure 2.1. An agitation paddle is used during pre-expansion to keep the beads from fusing together. As the beads are expanded, the density decreases and the lighter particles are forced to the top of the hopper and discharged. The final product, often called polystyrene pre-puff (PSPP) beads, are expanded up to 40 times the original resin bead size after the pre-expansion process (Liu et al. 2006). The bulk density after pre-expansion determines the density of the final geofoam product. After pre-expansion, the PSPP are transferred to storage hoppers where the cell walls cool and harden, and any remaining blowing agents diffuse through the cell walls and are replaced by ambient air. The molding stage involves heating the PSPP beads in steel molds where individual PSPP continue expansion and fuse together to form a specific geometry (Athanasopoulos et al. 1999), as shown in Figure 2.1. Typical densities of the final PS geofoam blocks is between 10 and 50 $kg/m^3$; with 20$kg/m^3$ being the most common (Negussey 2007). Scraps from trimming and cutting blocks are commonly ground down and recycled back with the PSPP prior to final molding. This material, called "regrind", can be 10 – 15% of the final product.
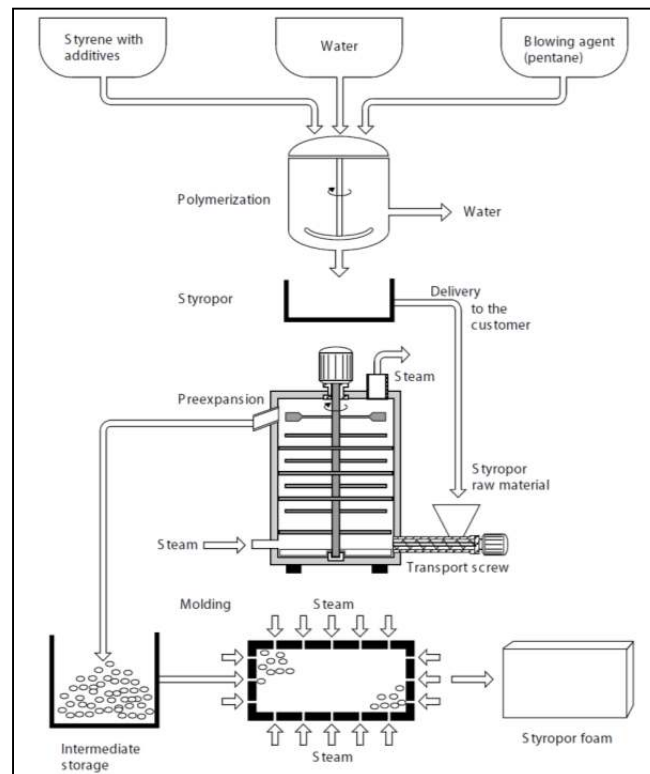


**Figure 2.1. Geofoam Manufacturing Process (BASF 2006)**

**2.2.3. Material Specifications.** ASTM Technical Committee D35 on geosynthetics has led the development of standards for the use of geofoam for civil engineering applications in the USA. A list of existing standards for EPS geofoam that are applicable to civil engineering applications that was adapted from Negussey (1997) and shown in Table 2.2.

**Table 2.2. Existing Standards for EPS Geofoam**

| Property | Standard | Title |
|---|---|---|
| Density | C-303 | Standard Test Method for Dimension and Density of Preformed Block and Board-Type Insulation |
| | D-1622 | Standard Test Method for Apparent Density of Rigid Cellular Plastics |
| Compressibility | D-1621 | Standard Test Method for Compressive Properties of Rigid Cellular Plastics |
| Tensile/Adhesion Properties | D-1623 | Standard Test Method for Tensile and Tensile Adhesion Properties of Rigid Cellular Plastics |
| Min. Construction Specifications | D-6817 | Standard Specification for Rigid Cellular Polystyrene Geofoam |
| Flexural Strength | C-203 | Standard Test Methods for Breaking Load and Flexural Properties of Block-Type Thermal Insulation |
| Water Absorption | C-272 | Standard Test Method for Water Absorption of Core Materials for Structural Sandwich Constructions |
| Shear Properties | C-273 | Standard Test Method for Shear Properties of Sandwich Core Materials |
| Insulation Specifications | C-578 | Standard Specification for Rigid, Cellular Polystyrene Insulation |
| Thermal Expansion | D-696 | Standard test method for coefficient of linear thermal expansion of plastics between -30°C and 30°C with a vitreous silica dilatometer |
| Combustion; Oxygen Index | D-2863 | Standard test method for measuring the minimum oxygen concentration to support candle-like combustion of plastics (Oxygen Index) |
| ** | D-7180 | Standard Guide for the Use of EPS Geofoam in Geotechnical Projects |
| Conformance Sampling | D-7557 | Standard Practice for Sampling of EPS Geofoam Specimens |

ASTM D1621 and D1622 typically utilize a 2-inch cube specimen for testing, whereas D1623 utilizes a "dog-bone" shaped specimen for gripping with the testing apparatus. ASTM D6817 was introduced in 2007 and helped address the minimum engineering parameters required for geofoam blocks utilized in the construction industry. The specification identifies the

minimum density; minimum compressive resistance at 1%, 5%, and 10% strain; minimum flexural strength; and minimum oxygen index. The use of ASTM D6817 is important in that it specifies the minimum compressive resistance for different types of geofoam utilized in civil engineering applications as well as providing a means to incorporate quality assurance (QA) inspections during construction.

EPS geofoam is manufactured to specified densities as shown in Table 2.3. The density of EPS materials are controlled during the manufacturing process by adjusting the amount of expansion of the resin beads during pre-expansion. These EPS density types are not always exactly followed during the manufacturing of geofoam materials for the geotechnical industry; for example the material used for this research program was approximately 32 kg/m$^3$ (2.0 lb/ft$^3$), and thus would be classified somewhere between a Type IX and Type XIV EPS material.

**Table 2.3. EPS Geofoam Types and Corresponding Densities**

| ASTM C578 Type | Density (kg/m$^3$) | Unit Weight (lb/ft$^3$) |
|---|---|---|
| XI | 12 | 0.70 |
| I | 15 | 0.90 |
| VIII | 18 | 1.15 |
| II | 22 | 1.35 |
| IX | 29 | 1.80 |
| XIV | 38 | 2.40 |
| XV | 46 | 2.82 |

**2.2.4. Usages and Previous Research Activities.** Geofoam has been used in the geotechnical industry for a few decades. The majority of existing research involves laboratory and field testing of EPS geofoam blocks. The first reported use of geofoam for lightweight fill in the USA was for a bridge approach in Michigan constructed over soft, lacustrine clay (Coleman 1974). Initially a conventional structural fill was installed for the approach, but prior to completion of the fill excessive lateral movement was noticed. The structural fill was removed and replaced with a lightweight fill comprised of approximately 1000m$^3$ of XPS plank bundles, that was reported to be performing as designed in 1997 (Negussey 1997). More recently, geofoam has been utilized in a wider variety of geotechnical applications. The most common application continues to be for lightweight fill applications in areas that are prone to excessive settlement, but other applications including the use of geofoam as a thermal insulator around

structures, as a compressible inclusion separating structures from swelling soils, or as an energy dissipater have been reported.

**2.2.4.1. Thermal properties.**   As a thermal insulator, geofoam has been underneath engineered pavements to minimize the depth of frost penetration and impede the negative effects of frost heave (Upright 1989) as well as to minimize the transmission of heat from structures to the subsurface in permafrost areas.  Horvath (1993) also discusses the potential energy saving by insulation of structures, pipes, and tunnels with EPS geofoam.

**2.2.4.2. Moisture absorption.**   According to BASF (2006), the cell walls of Styropor resin beads are impermeable and the only entry for water into EPS foam products is through small cracks and gaps between fused PS beads.  Thus, PSPP beads should be waterproof unless the cell walls have ruptured during the pre-expansion process.  BASF performed water absorption tests according to DIN 53434 standards and 28-day absorption was approximately 3% of the original volume.

Esch (1994) documented the exhumation of EPS products in permafrost areas underlying pavement in Alaska and reported moisture absorption tests performed on specimens.  Specimens had been buried for up to 20 years.  EPS geofoam exhibited from 1% - 6% absorption during that time, and XPS products exhibited negligible to approximately 3% absorption by mass.  Duskov (1997) measured water absorption in the laboratory and showed that the majority of absorption was in the first month of submersion and after one year the rate of absorption was negligible.  The average percent absorption by mass was 1.5% and the author believed the diffusion through cell walls was the primary transport mechanism.  The EPS Molders Association (2008) exhumed EPS type I paneling from approximately 2 meters below grade after 15-years of continuous installation and reported 4.8% moisture absorption.  Aabøe and Frydenlund (2011) reported on exhumed samples of EPS blocks that were 20 – 30 years old and showed that water absorption was around 1% by volume for sample above the groundwater table, around 4% for samples that were periodically submerged, and approximately 10% for completely submerged blocks.

**2.2.4.3. Compression behavior.**   As a compressible inclusion, geofoam has been installed adjacent to basement walls, abutments, and retaining walls to reduce lateral pressures against the structure.  Horvath (1997) discussed how EPS geofoam was used underneath slab-on-grade foundations over swelling soils instead of traditional elevated structural flooring. Applications that used geofoam over underground pipes and between earth retention structures and the soil were also discussed.  Athanasopoulos & Xenaki (2011) showed that the compressive strength of geofoam was a function of the density of the material and the confining stress.

**2.2.4.4. Stress – strain behavior.** Ossa & Romo (2009) discussed the three-stage stress -strain behavior exhibited by geofoam blocks tested in unconfined compression. The first stage was linear-elastic behavior that ends as the yield stress is reached. At stresses greater than the yield stress, the closed-form cells were ruptured and cell walls buckled with individual particulates within the geofoam matrix. This stage exhibited almost perfectly plastic behavior. The third stage was a strain hardening stage that occurred at strains greater than 60% and essentially was the frictional resistance between layers of stacked membranes within the specimen. Athanasopoulos & Xenaki (2011) believed that geofoam exhibits linear behavior at strains less than $10^{-2}$%, non-linear behavior at strain levels greater than $10^{-1}$%, and between these two thresholds the material exhibited "approximately linear" behavior.

**2.2.4.5. Dynamic properties.** Duskov (1997) performed ultrasonic pulse velocity tests on 20 kg/m$^3$ specimens and estimated a dynamic modulus of 10 - 15 MPa. The author also performed cyclic uniaxial tests to simulate traffic loadings and estimated a dynamic modulus of 6.1 – 8.3 MPa at stress conditions typical of road subbase material. Athanasopoulos et al. (1999) performed resonant column and cyclic uniaxial tests on unconfined specimens. Results indicated that stiffness increased with EPS material density but material damping was not affected. The authors noted the effects of loading frequency in the damping data. Modulus reduction curves were developed based on the measured data. Sivathayalan et al. (2001) used bender elements to measure the compressional wave velocity of 20 kg/m$^3$ EPS specimens. Results were used to estimate Young's modulus to be 14 – 22 MPa. Zarnani & Bathurst (2008) presented physical modeling of a rigid retaining wall backed with EPS geofoam cyclically loaded on a shaking table. Results from the tests were used to calibrate numerical models that are functions of EPS density, wall height, soil properties, and seismic loading. Murillo et al. (2009) performed centrifuge modeling of EPS isolation barriers to determine the influence of trench geometry and distance for dynamic source. Athanasopoulos & Xenaki (2011) showed that the small shear strain stiffness, $G_{max}$, of geofoam blocks increase with increasing material density and decreased with increasing confinement. Results also indicated a small strain damping ratio of 1.7%. Ossa & Romo (2011) performed resonant column and cyclic triaxial tests on specimens with three different densities; 24, 30, and 32 kg/m$^3$, respectively. Modulus reduction curves for different specimen densities and confining stresses were developed based on test measurements.

## 2.3.   DYNAMIC SOIL PROPERTIES

**2.3.1.   Introduction.**   The importance of understanding the relationship between dynamic soil properties and strain levels is vital for geotechnical engineers dealing with dynamic design scenarios.  For this document the term dynamic soil properties will refer to the shear modulus, G, and material damping as defined by the damping ratio, D.  This data is utilized in constitutive models, numerical simulations such as finite element and finite difference analyses that attempt to discretize the soil into unit elements each with specific material properties, vibration analyses, and ground response analyses.  Numerical analyses often require designation of the dynamic soil properties of each soil layer (i.e. transversely isotropic materials) to model soil response and soil-structure response in dynamic conditions.  Ground response analyses are used to determine how local site conditions will affect propagating waves.  In design applications, 1-D ground response analyses are commonly performed modeling the subsurface regime as a continuous layered system with each soil layer having specific dynamic properties.  Programs such as SHAKE model the soil in this manner.  Accurate modeling of site conditions in these analyses is dependent on the use of representative dynamic soil properties for the soils therein.

**2.3.2.   Shear Modulus.**   Dynamic stiffness is a measure of the resistance to cyclic shearing forces.  From a macroscopic viewpoint the stiffness of a particulate material is a function of: (1) the shape of the material; (2) the boundary conditions at the perimeter of the material; and (3) the stiffness of the constituent particles.  The shear modulus relates shear stresses to shear strains, as seen in Figure 2.2. The stiffness is at a maximum at zero strain and progressively decreases with increasing shear strain.  The maximum shear modulus, also called the low-strain shear modulus, is linear in nature, thus it represents a recoverable, elastic strain level.  It is commonly written as $G_{max}$ in the Americas and $G_0$ in Europe and Asia.  The low strain shear modulus is an important parameter for cyclic loadings that do not exceed a soil's elastic limit.  Analyses for dynamic loadings usually require $G_{max}$, as well as structures designed to remain far from failure.  At larger strains, the curve becomes non-linear, thus representing a transition to plastic, non-recoverable deformations.  The shear modulus at larger strains is represented by the secant shear modulus, $G_{sec}$, and is relevant only for the referenced strain level.

Soils are non-linear materials.  The shear modulus of a soil varies with strain levels, and many of the dynamic loadings relevant in geotechnical designs subject the soil to large oscillations in strain.  At low strains, the shear modulus is at a maximum, and modulus degradation occurs after surpassing some small-strain threshold.  Figure 2.3 is an example of a typical modulus reduction curve for soils and also identifies expected strains for typical geotechnical designs.
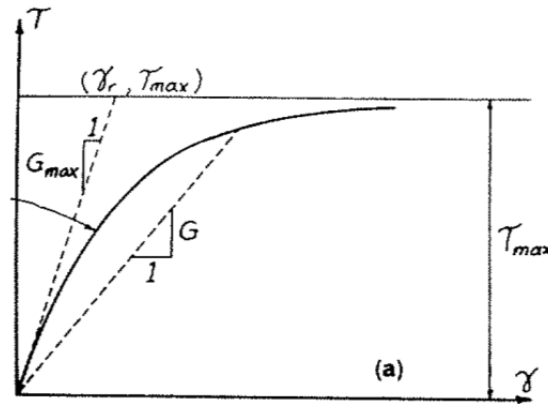
**Figure 2.2. Shear Modulus (Hardin & Drnevich 1972a)**
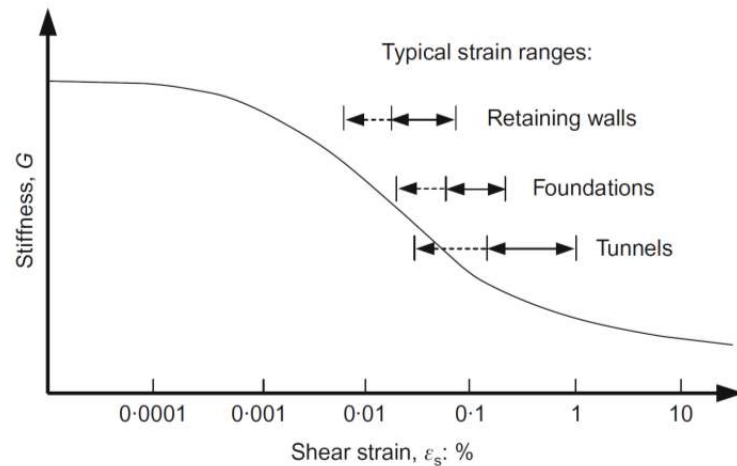


**Figure 2.3. Typical Shear Modulus Degradation of Soils (Atkinson & Sallfors 1991)**

In terms of a strain threshold, the maximum shear modulus is often simplified as the modulus at strains less than $10^{-3}\%$ shear strain. Vucetic and Dobry (1991) and Ishihara (1996) called this the "nonlinearity threshold"; defined as $\gamma_{tl}$ in Figure 2.4. Vucetic (1994) proposed to use the strain ratio corresponding to $G/G_{max} = 0.99$ as the nonlinearity threshold. At strains less than the nonlinearity threshold, the stress-strain behavior is linear elastic and thus shear strains are recoverable. At strains larger than the nonlinearity threshold, soil behavior transitions to nonlinear-elastic behavior but the strains are still recoverable. Dynamic loadings in this strain region demonstrate a hysteresis between the load and unload cycles, and the energy dissipated in the stress-strain loop are a function of local yielding and wear at particle contacts (Jardine 1992).

Soil behavior transitions to nonlinear-nonelastic above another strain threshold called the "volumetric strain threshold", shown as $\gamma_{tv}$ in Figure 2.4. Above the volumetric strain threshold, strains become irrecoverable.
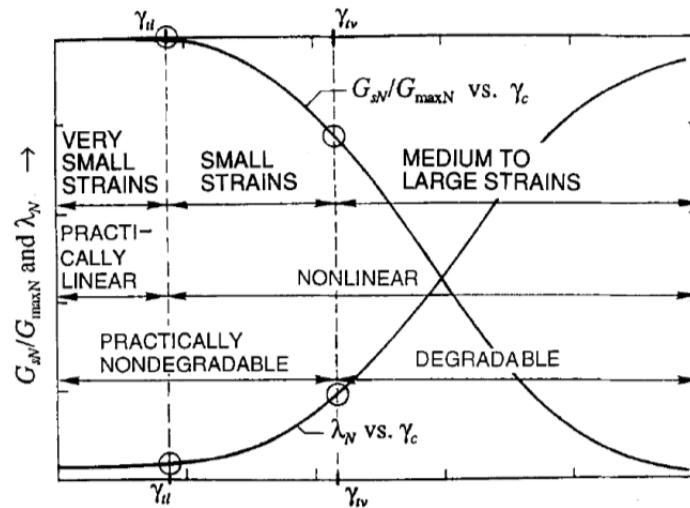


**Figure 2.4. Strain Thresholds for Dynamic Soil Properties (Vucetic 1994)**

Elastic stiffness is related to wave velocities. If it is determined that a soil will remain within a limited range of strains upon which elastic behavior controls material response, then the constrained modulus (M) and shear modulus (G) can be determined from measurements of the propagation velocity of compressional and shear waves in an infinite elastic medium as,

$$M = \rho * V_p^{\,2} \tag{2.1}$$

$$G = \rho * V_s^{\,2} \tag{2.2}$$

Where, $\rho$ is the mass density, $V_p$ is the compressional wave velocity, and $V_s$ is the shear wave velocity. Poisson's ratio ($v$) can also be determined from measurements of the P-wave and S-wave velocities as,

$$V_p = V_s * \sqrt{\frac{(1-\upsilon)}{(0.5-\upsilon)}} \tag{2. 3}$$

Young's modulus (E) and the bulk modulus (K) are additional relationships that correlate the strength of soil and deformation. The bulk modulus and Young's modulus are related to compressional wave velocity and the shear stiffness as,

$$V_p = \sqrt{\frac{\left(K + \frac{4}{3}G\right)}{\rho}} = \sqrt{\frac{E}{\rho} * \frac{(1-\upsilon)}{(1+\upsilon)(1-2\upsilon)}} \tag{2. 4}$$

If the wave equation is solved for wave velocities in an elastic rod; a typical geometry utilized in unit element specimens, the propagation velocity of P-waves is different than that shown in Equation 2.1. The P-wave velocity in an elastic rod is related to Young's modulus as,

$$E = \rho * V_p^{\,2} \tag{2. 5}$$

Compressional waves travel faster in an infinite, elastic medium compared to an elastic rod. The difference in velocities is related to the potential for lateral strains in an elastic rod affecting the overall volumetric strains, whereas in an infinite medium no lateral strains occur. The shear wave velocity is the same for infinite elastic mediums and elastic rods.

**2.3.3. Damping.** Damping is present in soils for all vibrations. The primary effect of damping is to transfer energy from the dynamic disturbance into the soil mass. In geotechnical engineering we are most concerned with damping in regards to soil-structure response.

Material damping in soils is primarily a function of two specific processes: (1) the frictional damping between soil particles often called internal damping; and (2) the viscous fluid-particle interaction and movement of pore fluid. Another less important influence is thermal damping. The individual mechanisms of material damping in soils cannot be exactly modeled as they are not completely understood, thus they are usually grouped together and represented by a more easily implemented material damping model.

Internal damping in a particulate material such as soils is a function of the interaction between adjacent particles. Frictional losses require strains to exceed the atomic size (approximately $10^{-7}$ mm) so that bonds are broken between particles and slippage takes place

(Santamarina 2001). At the low strain level common in elastic wave propagation, this type of damping is not expected.

Internal damping is usually modeled as hysteretic or visco-elastic damping. In a stress-strain curve a hysteretic loop is defined because the strain lags behind the stress during cyclic loading. The area inside the loop represents the energy dissipated by the soil in one cycle of loading; called the damping capacity ($\Delta W$). The specific damping capacity ($\Psi$) is a ratio of $\Delta W$ to the potential (stored) energy at maximum displacement, W (Richart et al. 1970). Using the stress-strain curve obtained from cyclic tests, $\Psi$ is the ratio of the area enclosed by the hysteresis loop to the total area under the hysteresis loop (Figure 2.5) as,

$$\Psi = \frac{\Delta W}{W} \tag{2.6}$$

Where, $\Psi$ is the specific damping capacity, $\Delta W$ is the area of the hysteresis loop, and W is the area underneath the triangle comprising the origin, secant shear modulus, and strain level.

The damping ratio (D) is commonly used in geotechnical engineering and represents the energy dissipated per radian of motion (Santamarina 2001). It is often represented as the ratio between system damping and critical damping in a SDOF system as,

$$D = \frac{c}{c_c} = \frac{c}{2\sqrt{km}} \tag{2.7}$$

Where, $c_c$ is the critical damping coefficient, c is the damping coefficient of the system, k is the stiffness and m is the mass. Critical damping represents the threshold between oscillatory motion and non-oscillatory motion. A system is over-damped if D >1 and under-damped if D < 1. In terms of the hysteretic damping, the damping ratio represents the ratio of energy lost per cycle to energy stored per cycle, as

$$D = \frac{\Delta W}{4\pi W} = \frac{1}{2\pi} \frac{A_{loop}}{G_{sec}\gamma_c^2} \tag{2.8}$$

Fluid damping is related to the flow mechanisms generated by the viscous movement of pore fluid between particles; one of the dominant mechanisms of damping in partially saturated

soils. During cyclic loadings, certain areas in the subsurface are in compression while adjacent areas are in tensions. This leads to "squirting" of pore fluid from one zone to another. Fluid losses in soils are frequency dependent; when free water is present in the pore spaces of saturated and partially saturated soils the dominant loss mechanisms are related to fluid flow (Santamarina 2001). Flow mechanisms have been modeled using Biot's theory (1956) which relates fluid movement and viscous damping to the application of external stresses.
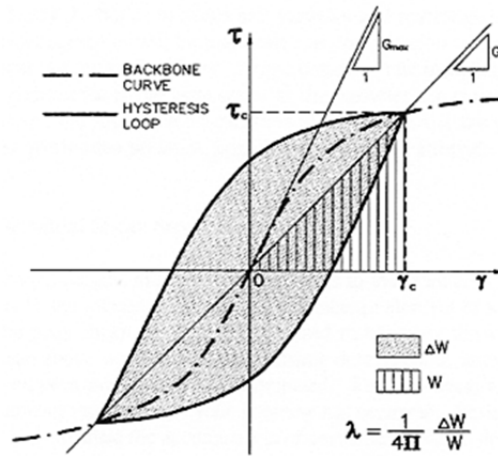


**Figure 2.5. Hysteresis Loop from Cyclic Test (Ishihara 1996)**

Material damping is not always represented by the lag of strain behind stress in cyclic tests, and other damping metrics are sometimes used in geotechnical engineering and more often used by the geological and structural engineering communities. The logarithmic decrement, $\delta$, is related to the decay of free-vibration in a SDOF system with viscous damping and essentially represents the loss of energy per cycle of motion. The measurement of this parameter is discussed in more detail in Section 2.4.1.5.

The coefficient of attenuation ($\alpha$) is the decrease in vibration amplitude with distance from a source as shown in Figure 2.6; thus it represents the loss of energy as a function of distance. The units of $\alpha$ are 1/distance. The coefficient of attenuation is related to the logarithmic decrement as,

$$\delta = \frac{2\pi v \alpha}{\omega} = \lambda \alpha \qquad\qquad (2.\ 9)$$

Where, v is the velocity, $\omega$ is the circular frequency, and $\lambda$ is the wavelength of the propagating wave.  The coefficient of attenuation is related to the damping ratio as,

$$\alpha = \frac{2\pi D}{\lambda} \qquad\qquad (2.\ 10)$$

Seismologists and geophysicists often work with the quality factor (Q) that is based on the frequency response of a damped spring-mass system under harmonic loadings (Graesser and Wong 1992).  It is related to the damping ratio as,

$$Q^{-1} = 2D \qquad\qquad (2.\ 11)$$

The loss factor is often used in vibration analyses.  The loss factor ($\eta$) represents a relationship between energy lost per radian of circular motion to the maximum potential energy during sinusoidal loadings, as

$$\eta = \frac{\Psi}{2\pi} = \frac{1}{2\pi} \frac{\Delta W}{W} \qquad\qquad (2.\ 12)$$

Overall there are several metrics to measure and describe damping in soils.  As it has been shown that damping of soils increases with strain levels, it is often convenient to use different metrics for different ranges of amplitude (Richart et al. 1970).
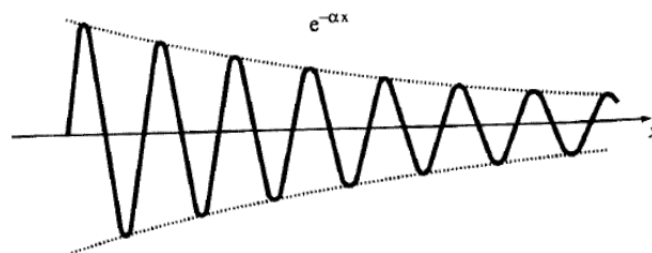


**Figure 2.6. Coefficient of Attenuation (Santamarina 2000)**

**2.3.4.    Previous Research into Dynamic Soil Properties for Cohesive Soils.**  A number of researchers have studied the relationship between dynamic soil properties and strain levels.  Shibuya et al. (2005) wrote:  "The use of proper soil stiffness considering its strain level dependency and stress state dependency in the deformation analysis is vitally important.  If the strain level can be predicted in advance, a linear-elastic analysis using a well-chosen stiffness would be of practical value.  If not, however, non-linear elastic or elasto-plastic approaches considering these factors would be more appropriate."

Hardin and Drnevich (1972b) summarized the main soil parameters affecting dynamic soil properties.  The primary factors included strain amplitude, effective stress, void ratio, number of cycles of loading, and degree of saturation for cohesive soils.  Dobry and Vucetic (1987) documented that dynamic soil properties are a function of void ratio, confining pressure, cementation, geologic age, overconsolidation ratio, plasticity index, degree of saturation and number of cycles of loadings, and influencing factors are listed Table 2.4.

**Table 2.4. Influence of Parameters on Dynamic Soil Properties of Cohesive Soils**
**(Dobry and Vucetic 1987)**

| Increasing Factor | $G_{max}$ | $G/G_{max}$ | Damping |
|---|---|---|---|
| Confining pressure, $\sigma_0'$ | Increase with $\sigma_0'$ | Stays constant or increases with $\sigma_0'$ | Stays constant or decreases with $\sigma_0'$ |
| Void Ratio, e | Decreases with e | Increases with e | Decreases with e |
| Geologic Age, $t_g$ | Increases with $t_g$ | May increase with $t_g$ | Decreases with $t_g$ |
| Cementation, c | Increases with c | May increase with c | May increase with c |
| Overconsolidation, OCR | Increases with OCR | Not affected | Not affected |
| Plasticity Index, PI | Increases with PI if OCR > 1; Stays approx. constant if OCR = 1 | Increases with PI | Decreases with PI |
| Cyclic Strain, $\gamma_c$ | ** | Decreases with $\gamma_c$ | Increases with $\gamma_c$ |
| Strain Rate, $\dot{\gamma}$ | Increases with $\dot{\gamma}$ | G increases with $\dot{\gamma}$; $G/G_{max}$ probably not affected if G and $G_{max}$ are measured at same $\dot{\gamma}$ | Stays constant or may increase with $\dot{\gamma}$ |
| Number of Loading Cycles, N | Decreases after N cycles of large $\gamma_c$ but recovers with time | Decreases after N cycles of large $\gamma_c$ ($G_{max}$ measured before N cycles) | Not significant for moderate $\gamma_c$ and N |

Hardin and Richart (1963) initially developed a relationship that related shear wave velocity to void ratio and confining stress.  Based on experimental measurements the authors noted that: (1) the shear wave velocity varies linearly with void ratio; and (2) the shear wave

velocity varies with the mean effective stress with a power of n/2. This relationship can be written as,

$$v_s = A(B-e)\sigma'^{n/2} \tag{2.13}$$

Where, A, B, and n are constants for different soil types. The relationship between density and void ratio is,

$$\frac{\rho}{\rho_s} = \frac{1}{1+e} \tag{2.14}$$

Where, $\rho$ and $\rho_s$ are the bulk and soil particle density, respectively, and e is the void ratio. If Equation 2.13 and Equation 2.14 are substituted into the equation relating shear wave velocity and the shear modulus (Equation 2.2) the following generic equation is developed,

$$G_{max} = \rho_s \frac{1}{1+e} A^2 (B-e)^2 \sigma'^n = A \frac{(B-e)^2}{1+e}\sigma'^n = A F(e)\sigma'^n \tag{2.15}$$

The relationship above has been modified by many different authors since its first introduction considering additional empirical data. Hardin and Black (1968; 1969) developed a classic simplified relationship to estimate $G_{max}$ of cohesive soils as,

$$G_{max} = 1230 * \frac{(2.973-e)^2}{1+e} * OCR^a * \sqrt{\sigma_m'} \tag{2.16}$$

Where, $G_{max}$ is defined in lb/in$^2$, e is the void ratio, OCR is the overconsolidation ratio, 'a' is a parameter dependent on soil plasticity and shown in Table 2.5, and $\sigma_m'$ is the mean effective stress in lb/in$^2$. The 'A" coefficient at the front of Equation 2.15 was an average, empirical value that fit the measured data and the void ratio expression was based on data from saturated kaolin specimens tested with a resonant column apparatus.

**Table 2.5. 'a' Parameter**

| PI | 'a' |
|------|------|
| 0 | 0 |
| 20 | 0.18 |
| 40 | 0.30 |
| 60 | 0.41 |
| 80 | 0.48 |
| >100 | 0.50 |

Commonly this relationship is used for clay soils with low plasticity. Its use for other soil types can be a stretch and thus it has been modified to fit measured data. Hardin (1978) modified the generic equation by replacing the original influence of void ratio by $F(e) = 1 / (0.3 + 0.7e^2)$ and Jamiolkowski et al. (1991) modified $F(e) = 1/e^{1.3}$ based on the Hertzian contact theory for spheres.

Hardin and Drnevich (1972b) used a hyperbolic relationship to correlate shear stress and shear strain during dynamic loadings. The basis of the model is shown in Figure 2.7 and it can be expresses as,

$$\tau = \frac{\gamma}{\dfrac{1}{G_{max}} + \dfrac{\gamma}{\tau_{max}}}$$
(2. 17)

Where, $\tau$ is the shear stress, $\gamma$ is the shear strain, $G_{max}$ is the maximum shear modulus and $\tau_{max}$ is the shear strength of the soil. The authors defined the reference strain ($\gamma_r$) shown in Figure 2.7 and defined as,

$$\gamma_r = \frac{\tau_{max}}{G_{max}}$$
(2. 18)

Harden and Drnevich (1972b) used a reference strain 0.1% for most "practical problems"; and Darendeli (2001) used a range from 0.01% – 0.1%. The equation for the normalized shear modulus is determined by dividing Equation 2.17 by the shear strain and rearranging terms as,

$$\frac{G}{G_{max}} = \left(1 + \frac{\gamma}{\gamma_r}\right)^{-1}$$ (2. 19)

Hardin and Drnevich (1972b) noted that the soil type had an influence on the stress-strain relationship as the hyperbolic model either slightly overestimated or underestimated measured stress-strain data, as shown in Figure 2.7. To account for these variations, the authors "distorted" the strain scale to improve the correlation between the model and recorded soil behavior. The hyperbolic strain, $\gamma_H$, replaced $\gamma/\gamma_r$ in Equation 2.19 and is defined as,

$$\gamma_H = \frac{\gamma}{\gamma_r}\left[1 + a \cdot e^{-b\frac{\gamma}{\gamma_r}}\right]$$ (2.20)

Where, 'a' and 'b' are coefficients that are used to adjust the normalized modulus reduction curve based on soil type and other secondary parameters. The hyperbolic relationship proposed by Hardin and Drnevich was the basis of many future empirical relationships.
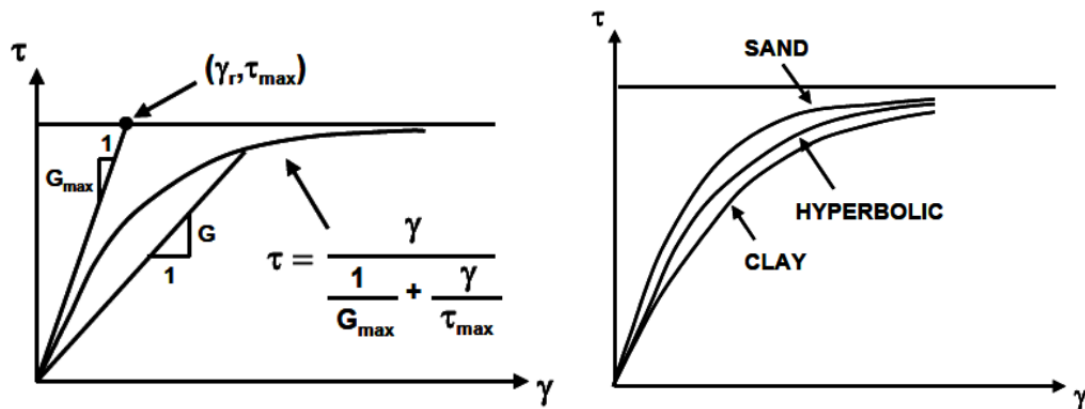


**Figure 2.7. Hyperbolic Soil Model (Hardin & Drnevich 1972b)**

Zen et al. (1978) documented the influence of PI in the modulus reduction curves for cohesive soils. Soils with higher plasticity tended to shift the curve to the right and showed a reduced rate of modulus reduction. Schneider et al. (1999) also showed increasing stiffness with increasing plasticity for residual soils.

Sun et al. (1988) and Vucetic and Dobry (1991) presented design graphs for the normalized modulus reduction curves for cohesive soil types that are commonly used in the industry.  The graphs of Sun et al. (1988) and Vucetic and Dobry (1991) were further separated into distinct curves that accounted for variations in plasticity.  The authors believed that PI was the most important influencing factor for cohesive soil and the void ratio was the second most important factor.  Sun et al. (1988) showed that the modulus reduction curves for cohesive soils were much more variable than those for cohesionless soils and recommended site-specific testing when dealing with cohesive soils.  As an example the relationship of Sun et al. (1988) is shown in Figure 2.8.

The generalized curves of the previous authors were all based on experimental data at atmospheric pressure, and thus they do not address the influence of confining pressure on the modulus reduction curve.  Sun et al. (1988) believed that the influence of confining stress for highly plastic clays was minimal.  Borden et al. (1996) showed that an increase in confining pressure from 25 to 100 kPa lead to a 2.5 times increase in the strain threshold of the modulus reduction curve.  Schneider et al. (1999) measured a 10 times increase in the strain threshold with changes in confining stress.
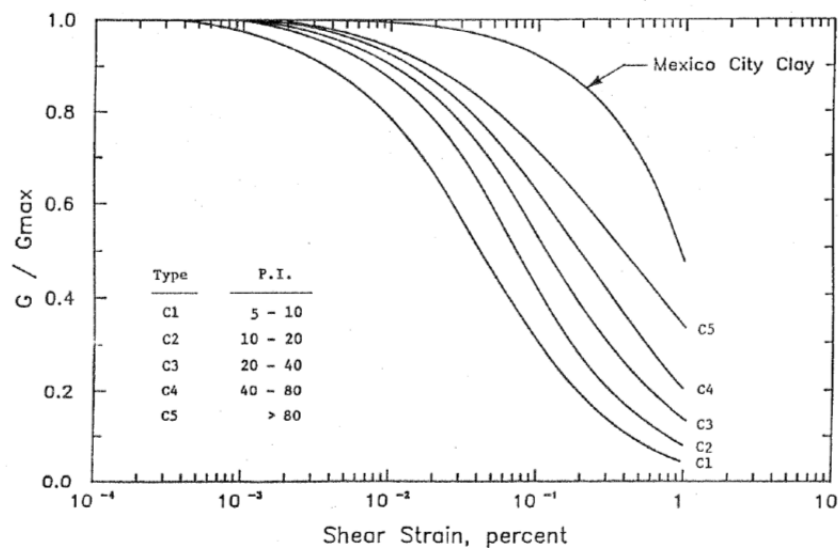


**Figure 2.8. Modulus Reduction Curves for Cohesive Soils (Sun et al. 1988)**

Ishibashi and Zhang (1993) developed empirical relationships that related the normalized modulus reduction curve to both soil plasticity and confining pressure as,

$$\frac{G}{G_{max}} = K(\gamma, PI)\sigma_0^{\,m(\gamma, PI)}$$

(2.21)

Where,

$$m(\gamma, PI) = 0.272 \left[ 1 - \tanh\left( \ln\left( \frac{0.000556}{\gamma} \right)^{0.4} \right) \right] e^{-0.0145 PI^{1.3}}$$

(2.22)

$$K(\gamma, PI) = 0.5 \left[ 1 + \tanh\left( \ln\left( \frac{0.000102 + n(PI)}{\gamma} \right)^{0.492} \right) \right]$$

(2.23)

$$n(PI) = \begin{pmatrix} 0.0 & for\ PI = 0 \\ 3.37x10^{-6}\ PI^{1.404} & for\ 0 < PI \le 15 \\ 7.0x10^{-7}\ PI^{1.976} & for\ 15 < PI \le 70 \\ 2.7x10^{-5}\ PI^{1.115} & for\ PI > 70 \end{pmatrix}$$

(2.24)

Where, PI is the plasticity index, $\gamma$ is the shear strain (not as a percentage), and $\sigma_0$ is expressed in kPa. The relationship is limited to confining pressures less than 1 MPa.

Additional research regarding the shear modulus of cohesive soils has been accumulated in the past forty years. Seed and Idriss (1970) recommended normalizing the shear modulus by the undrained shear strength for cohesive soils to account for a large variability between in-situ data and laboratory data that was attributed mainly to disturbance. Anderson and Stokoe (1978) discussed the duration of confining stresses acting upon soil influenced the shear modulus for soils. In general, there was an increase in the shear modulus with increasing time of confinement. The authors discussed the importance of this phenomenon when considering in-situ soils with design data derived from laboratory testing. The laboratory data represented a lower-limit of the available moduli of the soil in question. Another observation of Anderson and Stokoe (1978) was that small changes in effective confining pressures in situ, which could be expected from groundwater fluctuations or construction activities, can reduce the time derived increases in moduli. Conversely, Zen et al. (1986) did not find time rate effects for soils with plasticity indexes between 40 and 90.

Material damping has also been extensively studied in the past 40 years. Hardin and Drnevich (1972b) applied the hyperbolic model to measurements of material damping and proposed the following model to relate damping ratio to increasing strain levels,

$$\frac{D}{D_{max}} = \frac{\gamma_H}{1 + \gamma_H}$$

(2. 25)

Where, $D_{max}$ is the maximum damping ratio and $\gamma_H$ is the hyperbolic strain defined previously. Material damping is a function of soil type, confining pressure, number of loading cycles and frequency, and the constant 'a' and 'b' in the definition of hyperbolic strain (Equation 2.22) are used to adjust for these influences. Hardin and Drnevich (1972b) showed that material damping reaches an asymptotic value, $D_{max}$, at large strains.

Vucetic and Dobry (1991) presented design graphs for the damping ratio versus cyclic strain for cohesive soil types. Sun et al. (1988) stated that the design charts of Seed and Idriss (1970) had not changed and recommended their use. The relationship of Seed and Idriss (1970) predicted the mean relationship bounded by a broad range of potential values. The low-strain minimum damping ratio, $D_{min}$, is undefined in the design charts due to lack of data.

Ishibashi and Zhang (1993) developed a relationship that related the increase in damping ratio with increasing shear strain to the normalized modulus reduction curve; thus it is indirectly related to both soil plasticity and confining pressure, as

$$D = 0.333 \frac{1 + \exp\left(-0.0125 PI^{1.3}\right)}{2}\left[0.586\left(\frac{G}{G_{max}}\right)^2 - 1.547\left(\frac{G}{G_{max}}\right) + 1\right]$$

(2. 26)

The relationship is limited to confining pressures less than 1 MPa since it gives unreasonable estimates of damping at high confining pressures (Darendeli 2001). Santamarina (2001) provided a general guideline for low strain material damping of soils; approximately 1% to 5% for all soil types.

## 2.4.    LABORATORY MEASUREMENT OF LOW STRAIN DYNAMIC PROPERTIES

Both laboratory and field techniques have been developed to measure dynamic soil properties. These methods were discussed by Seed and Idriss (1970) and include: (1) measurement of stress-strain relationships in unit element specimens under cyclic loading

conditions; (2) forced vibration tests in unit element specimens and the field in an effort to determine the resonant frequency of the soil; (3) free vibration tests where the decay of motion is recorded; (4) measurement of wave velocities in the laboratory and field; and (5) measurement of ground response during seismic events. These different methods induce variable strains in the soil being tested, and thus not all are applicable in the "low strain range".

Typically there are two primary ways to measure the low-strain ($<10^{-3}$%) dynamic properties of soils in the laboratory: 1) resonant column testing methods; or (2) pulse velocity methods utilizing either ultrasonic transducers or bender element transducers. In theory elastic strains could be identified in other unit element tests by applying very small cyclic loadings, but problems are usually realized in attempting to accurately measure the strains induced. Dynamic properties at larger strain levels than $10^{-1}$% are most typically tested using the cyclic triaxial apparatus, but cyclic simple shear and cyclic torsional shear are also sometimes used. Resonant column, ultrasonic pulse velocity, and bender element pulse velocity testing were all completed as part of this research program.

The low-strain methods can be considered nondestructive, in that they do not significantly alter the sample during testing. The advantage of non-destructive testing (NDT) is that a single specimen can be used for a battery of tests, removing the potential for specimen variation to affect the measured results. Dynamic strains are very small during testing, approximately less than $10^{-3}$%, thus it is acceptable to assume that the geomaterial remains within the elastic range and conforms to elastic theory.

**2.4.1. Resonant Column Testing.** Resonant column (RC) tests are used to generate resonance in a test specimen through the application of torsional, and sometimes longitudinal or flexural (e.g. GDS resonant column system) wave motions. The resonant column test apparatus was initially developed to study the dynamic properties of rock. Through the contributions of Hardin and Richart (1963), Hardin and Music (1965), and Drenevich et al. (1978), among others the equipment and theory was modified to accommodate soil specimens. The objective of the test is to vibrate a soil specimen at the first-mode of resonance. First-mode resonance is defined as the frequency in which the maximum shear strain is realized in a specimen during a sweep of frequencies. In the first mode of resonance, all material within the specimen is vibrating in phase with the drive system. The methodology has been standardized as ASTM D4015 and is considered one of the most reliable methods to determine the low strain shear stiffness and material damping of soils. One of the main advantages of the test is the reliability and repeatability of the test results, but the primary disadvantage is that RC tests require specialized equipment.

**2.4.1.1. Equipment.** Traditional RC systems for soil testing were developed by Richart, Hall, Hardin, Drnevich, and Stokoe and continue to be used today (Woods 1994). Each apparatus includes a coil-magnet torsional force system, an accelerometer or velocity transducer to measure the motion, a displacement transducer to measure height changes in the specimen, and a confining chamber to apply pressure to a test specimen. There are multiple ways to apply a torsional load to specimen, but commonly the load is applied to the top of a specimen that is fixated at the base. More modern systems have replaced the coil-magnet drive system with an electrical motor.

Loads are typically applied with a "floating" motor that automatically adjusts as vertical strains occur and also allows for the application of anisotropic loads. The motor rests upon a cylindrical soil specimen. The motor can be hung from the top plate of the compression chamber to reduce the influence of its load on the specimen; if required. The base platen is connected to the drainage lines; and filter paper strips are often used to increase consolidation time. Good contact between the motor end platen and the specimen is important during testing, but usually the use of porous stones fastened to the end platens or textured end platens provide sufficient roughness (Drnevich 1985).

**2.4.1.2. Theory.** The determination of dynamic soil properties from the resonant column apparatus is based on linear-elastic vibrational theory as discussed by Hardin (1965). The analytical solution assumes a Kelvin-Voigt soil model with constant shear modulus (G) and viscous damping (c), as well as constant strains throughout the length of the specimen. The equation of motion for a rod undergoing torsional vibration is given by Hardin (1965) as,

$$\frac{\partial^2 \theta}{\partial t^2} = \frac{G}{\rho}\left(\frac{\partial^2 \theta}{\partial x^2}\right) + \frac{c}{\rho}\left(\frac{\partial^3 \theta}{\partial x^2 \partial t}\right) \tag{2.27}$$

Where, $\theta$ is the angle of rotation, $\rho$ is the mass density of the specimen, and x and t are derivatives with respect to distance and time, respectively. The solution to Equation 2.27 is determined by applying the appropriate boundary conditions: (1) no rotation of the specimen at the base and (2) the torque at the top of the specimen must be equal to the applied torsional vibration (Khan et al. 2008). The frequency equation of motion for the fixed-free resonant column results as,

$$\frac{I_{Soil}}{I_{System}} = \left(\frac{\omega H}{V_s}\right)\tan\left(\frac{\omega H}{V_s}\right) \tag{2. 28}$$

Where, $I_{soil}$ is the mass moment of inertia of the soil specimen; $I_{system}$ is the mass moment of inertia of the drive system and end platens; $\omega$ is the angular frequency of the first torsional vibration mode; H is the height of the soil specimen; and $V_s$ is the shear wave velocity. The frequency equation (Equation 2.28) can be used to calculate the velocity of an elastic, homogeneous soil specimen. The case applies both to the case of steady-state vibration and free-vibrational decay. The mass moment of inertia for the drive-system is determined through a calibration process utilizing a metallic specimen of known dimensions and properties prior to testing soils.

During the frequency sweep test the maximum rotational response as recorded by the accelerometer defines the resonant frequency. The angular frequency can be computed from the measured resonant frequency as,

$$\omega = 2\pi f_{res} \tag{2. 29}$$

**2.4.1.3. Measurement of shear strain.** The maximum shear strain in the soil specimen during torsional testing varies from a maximum at the specimen surface to zero at the central axis, as shown in Figure 2.9. There is also a variation in shear strain from the fixed base of the specimen to the free end; this condition is considered during the derivation of the frequency equation. Shear strain at any point along the cross-sectional area can be calculated as,

$$\gamma(R) = \frac{R * \theta_{max}}{H} \tag{2. 30}$$

Where, $\theta_{max}$ is the maximum angle of rotation, and R is a specific distance in question from the central axis of the specimen. Since the shear strain is not constant throughout the specimen, and equivalent shear strain factor is commonly used to represent the overall average strain. Drnevich (1985) recommended two-thirds the radius and Chen and Stokoe (1979) recommended a value of 0.82 of the radius. ASTM D4015 specifies 0.8 of the radius. For the tests performed as part of this research an equivalent strain factor of 0.707 was used and Equation 2.30 was adjusted as,

$$\gamma_{Avg} = 0.707 * (\frac{R * \theta_{max}}{H})$$

(2. 31)

During testing the recorded acceleration must be integrated with respect to time to determine the angular displacement, as

$$u = -\frac{\ddot{u}}{\omega^2} = -\frac{\ddot{u}}{4\pi^2 f_{res}^{\,2}}$$

(2. 32)

Where, u is the rotational displacement, ü is the recorded acceleration, $f_{res}$ is the resonant frequency, and $\omega$ is the resonant angular frequency. Finally the maximum angle of rotation, $\theta_{max}$, is determined as,

$$\theta_{max} = \frac{u}{R_{sensor}}$$

(2. 33)

Where, $R_{sensor}$ is the radius to the center of the attached accelerometer.
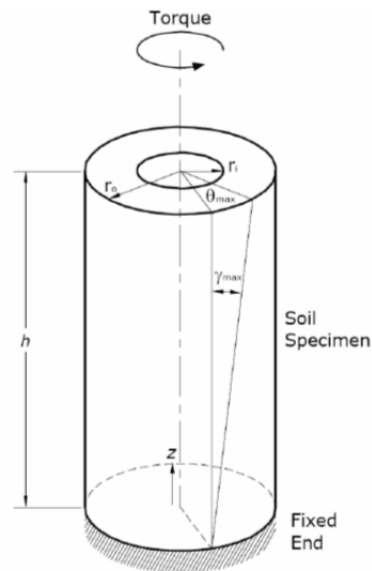


**Figure 2.9. Variation in shear strain in resonant column specimen (Padilla 2004)**

**2.4.1.4. Measurement of shear modulus.** Using the measured resonant frequency of a specimen, the specimen length, and the moment of inertia of the specimen the shear wave velocity can be calculated from the frequency equation of motion (Equation 2.28). Assuming the soil specimen is responding elastically during resonant column testing, the shear modulus is determined from Equation 2.2. The shear modulus is the same for drained or undrained conditions since the shearing motion results in essentially no volume changes within the specimen. In addition the influence of pore water pressure is negligible as water has no shear stiffness.

**2.4.1.5. Measurement of damping.** Traditionally, material damping was computed by monitoring the current sent to the drive system and the resulting acceleration of the specimen. Recently more automated testing systems (e.g. GCTS RC device used at Missouri S&T) do not monitor the current sent to the drive system, and thus material damping is determined from the logarithmic decrement of a free-vibration test or from measuring the width of the frequency response curve near resonance; often termed the half-power bandwidth method. Measurements of material damping can be influenced by the RC apparatus. System damping can also result from poor coupling of the torsional motor and the specimen.

If a specimen is set into free vibration, the amplitude of the vibrations will decrease and eventually completely attenuate. The reduction in the amplitude of the vibrations is a function of the internal, material damping of the specimen and the decay is similar to that of a viscously damped system (Richart et al. 1970). The response of a single degree of freedom soil specimen in free vibrational decay can be described by the solution of,

$$\theta(x,t) = Ce^{-D\omega_n t} \sin(\omega_d t + \phi) \sin\left(\frac{\omega_n L}{V_s}\right) \tag{2. 34}$$

Where, $\theta$ is the angle of rotation, C is a constant, D is the damping ratio, $\phi$ is the phase angle, $\omega_n$ is the natural frequency and $\omega_d$ is the damped frequency. A typical free vibrational response recorded in the laboratory is shown in Figure 2.10. The ratio between any two successive positive or negative peaks in Figure 2.10 is,

$$\frac{z_n}{z_{n+1}} = e^{-\omega_n D(t_n - t_{n+1})} = e^{\frac{2\pi D}{\sqrt{1-D^2}}} \tag{2. 35}$$

Where, $t_{n+1} = (t_n + 2\pi) / \omega_d$. The logarithmic decrement ($\delta$) is found by taking the natural logarithm of Equation 2.35 as,

$$\delta = \ln(\frac{z_i}{z_{i+1}}) = \frac{2\pi D}{\sqrt{1-D^2}}$$

(2. 36)

The logarithmic decrement can also be determined for non-successive positive or negative peaks as,

$$\delta = \frac{1}{n}\ln(\frac{z_i}{z_{i+n}}) = \frac{2\pi D}{\sqrt{1-D^2}}$$

(2. 37)

Where, $\delta$ is the logarithmic decrement, z is the maximum amplitude of an initial cycle, and n represent the number of peaks separating the segment in question.
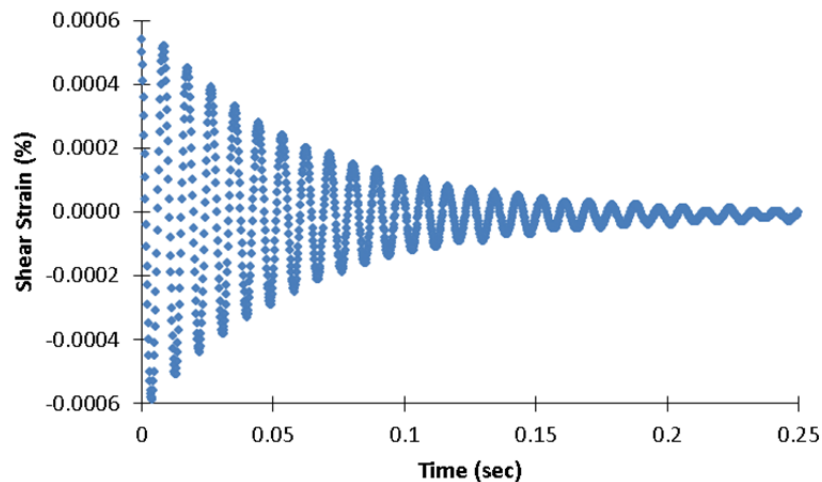


**Figure 2.10. Typical Free-Vibration Response in Soils**

The half-power bandwidth method of assessing material damping involves measuring the width of the frequency response curve near resonance (Richart et al. 1970) as shown in Figure 2.11. The frequency response curve characterizes a single-degree-of-freedom system to a constant force excitation at variable frequencies. The resonant frequency is defined as the

frequency upon which the maximum response is observed in the specimen. Frequencies above and below the resonant frequency corresponding to 0.707 of the maximum response are utilized to calculate the logarithmic decrement as,

$$\delta = \frac{\pi}{2} \frac{f_2^2 - f_1^2}{f_{res}^2} \sqrt{\frac{A^2}{A_{max}^2 - A^2}} \frac{\sqrt{1 - 2D^2}}{1 - D^2}$$  (2. 38)

When the damping ratio (D) is small, and A is set to equal 0.707A$_{max}$, Equation 2.38 becomes,

$$\delta = \pi \frac{f_2 - f_1}{f_{res}}$$  (2. 39)

And the damping ratio (D) is,

$$D = \frac{1}{2} \frac{f_2 - f_1}{f_{res}}$$  (2. 40)

Where, $f_1$ and $f_2$ correspond to the frequency at $\pm 0.707$Amax of a frequency response curve. The quality factor, Q, has also been related to the width of a frequency response curve as,

$$Q = \frac{f_{res}}{f_2 - f}$$  (2. 41)
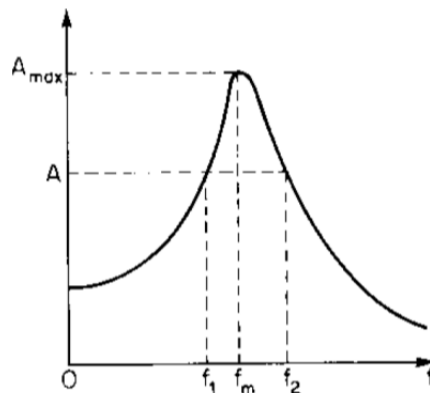


**Figure 2.11. Typical Frequency Response Curve (Richart et al. 1970)**

**2.4.2.   Pulse Velocity Testing.**  Two different pulse tests are available to measure the propagation of waves in geomaterials: (1) ultrasonic pulse test and (2) bender element test.  Pulse transmission methods allow the direct measurement of wave velocity which is different than resonant column methods.  Pulse tests can be arranged to produce either compressional, P-waves or shear, S-waves (Figure 2.12).  P-waves produce volumetric strains and thus travel at a speed that is a function of the undrained volumetric stiffness of the soil.  Shear waves produce shear strains without changes in unit volume.

Wave velocity can be defined as the velocity at which a disturbance propagates in a material, and it is a function of the material, material structure, and type of excitation.  Wave velocity calculations are calculated from the measured travel time (t) between a transmitting transducer and a receiving transducer and the specimen length (L) between the two transducers as,

$$V = \frac{L}{t} \tag{2. 42}$$

Precise time measurements are realized with electronic equipment.  Another parameter of wave transmission is the particle velocity.  For compressional waves, particle velocity is parallel to the wave propagation direction (Figure 2.12a), whereas for shear waves particle velocity is perpendicular to the wave direction (Figure 2.12b & Figure 2.12c).  Thus shear wave velocity and subsequently the shear modulus are dependent on the direction of propagation and the direction of particle velocity.  For anisotropic soils the maximum shear moduli are commonly defined as,

$$G_h = \rho * V_{s,h}^2 \tag{2. 43}$$

$$G_v = \rho * V_{s,v}^2 \tag{2. 44}$$

Where, $G_v$ is the shear stiffness for shear waves with particle motion in the vertical plane and $G_h$ is the shear stiffness for shear waves with particle motion in the horizontal plane.  For homogeneous specimens tested in the laboratory, $G_v = G_h$ as the soil structure is essentially the same in all directions. Measurements of shear wave velocity in-situ using geophysical techniques are commonly different for different particle velocity directions and this is attributed to natural variations in soil structure (Atkinson 2000).

Compressional waves introduced in the laboratory are often referred to as longitudinal waves. Longitudinal waves are simply compressional waves that for all intents and purposes are one-dimensional; essentially the transmission distances are so short that spherical expansion of the wave does not influence the wave characteristics. Compressional wave velocity is commonly used in partially saturated tests, as an indication of the degree of saturation as the wave propagation through a specimen is a function of the pore fluid. The shear wave velocity is not affected by the degree of saturation.
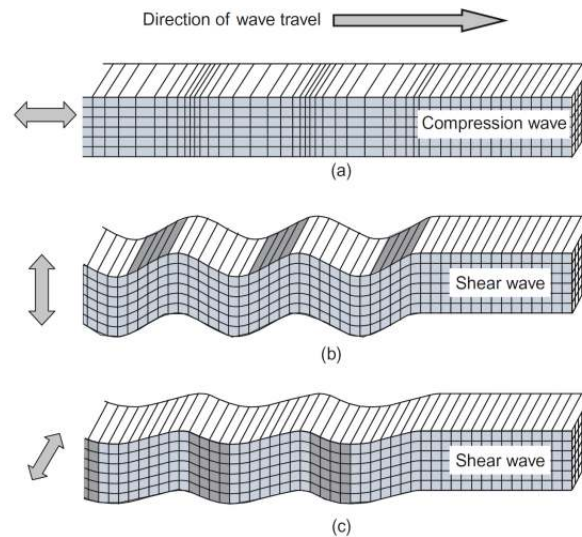


**Figure 2.12. Compressional and Shear Wave Travel (Clayton 2011)**

**2.4.2.1. Bender element testing.** Bender elements are utilized in geotechnical testing to generate waves within soils. The bender element test utilizes two piezoelectric ceramics with a metallic electrode sandwiched between them, and they are often referred to as a piezoelectric biomorph. Bender elements are partially fixated into end platens and the exposed cantilever portion is embedded into the specimen. Traditionally, bender elements have been used to induce and receive waves in laboratory specimens at low strain levels, and they can be installed to produce either P-waves or S-waves. Bender elements are used in combination with a power source, function generator and signal receiver to measure the wave velocity and estimate the soil moduli at low strain levels.

Given the amount of research using bender elements in the past few decades there has been a large variety of equipment, signal, and signal analyses techniques documented and discussed. Recently, Yamashita et al. (2009) published the results of an international parallel

bender element tests that included 23 different researchers from 4 continents. Based on their finding, they proposed the following bender element recommendations:

i. There is no optimum bender element size or embedment length;

ii. Time delay of the test system and direction of the initial motion should be measured by directly contacting the bending actuator and bending receiver;

iii. Frequency of the transmitted wave should be adjusted so that it equals the dominant frequency of the received signal;

iv. Sampling interval should be smaller than 1/100th of the expected arrival time;

v. Voltage resolution should be more than 1/100th of the largest amplitude of the received signal; and

vi. No specific travel time determination methodology is recommended, but matching of the transmitted and received signal frequencies is vital in peak-to-peak direct time measurements and cross-correlation measurements.

These recommendations were used to guide the development of bender elements and testing of modified soil specimens for this research program.

2.4.2.1.1. **Bender element transducers.** Bender element transducers are comprised of two or more layers of piezoelectric ceramics sandwiched together with a metallic center electrode separating the piezoelectric pieces. There are two types of bender element polarization schemes: parallel polarized (Y-poled) and cross-polarized (X-poled) bender elements. The polarization of the piezoelectric materials on each half of the biomorph are shown in Figure 2.13. With the appropriate electrical connects and upon application of a voltage, one half of the biomorph extends and the opposite half contracts due to the opposing polarity on each side of the bender element. When the electrical signal reverses, as is the case of a sine wave, the opposite motion occurs. The entire bender element vibrates under application of a continuous alternating current. Bender elements also operate in reverse, such that when they are strained they produce a voltage that can be monitored and related back to the actual deformation. Thus the bender element is a transducer that converts electrical energy to mechanical energy and a sensor that converts mechanical energy to an electrical signal.
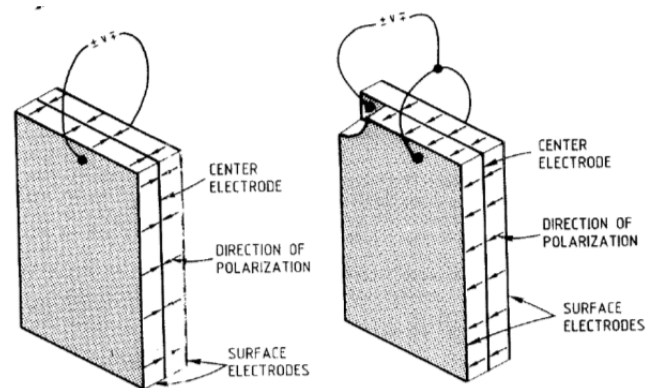
**Figure 2.13. Polarization of Bender Elements (Dyvik and Madshus 1985)**

There are two distinct wiring schemes for bender elements; elements wired in series (Figure 2.14a) and elements wired in parallel (Figure 2.14b).
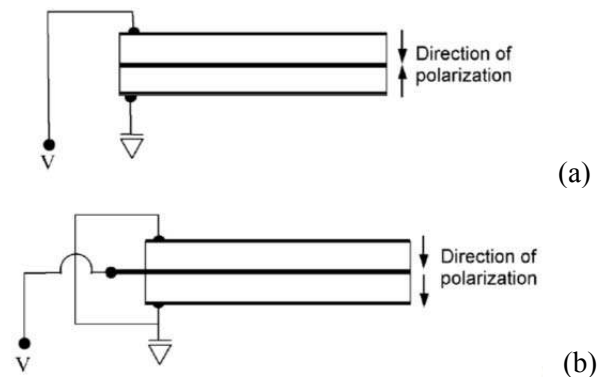


**Figure 2.14. Bender Element Wiring Schemes for S-wave transducers**

**(Lee and Santamarina 2005)**

It is commonly referenced in the literature that X-poled bender elements wired in series are more efficient sensors and Y-poled bender elements wired in parallel are more efficient transducers of S-waves (e.g. Leong et al. 2005). As these transducers are typically operated at less than their resonant frequencies, they are essentially operating as capacitors. A quick investigation into the governing equations and constants allows us to understand why this is commonly assumed. Capacitance (C) is related to electrical charge (Q) and voltage (V) as,

$$C = \frac{Q}{V} \qquad \qquad \textbf{(2. 45)}$$

And very generally the capacitance of a bender element can be determined from its physical and electrical properties as,

$$C = \frac{\varepsilon_0 Ak}{t} \qquad \qquad \textbf{(2. 46)}$$

Where, $\varepsilon_0$ is the permittivity of free space, k is the dielectric constant, A is the surface area and t is the thickness of the bender element.  Assuming Q, $\varepsilon_0$, A, and k are constant for a given test then the voltage produce is influence by only the thickness of the piezoelectric material.  As seen in Figure 2.14, the thickness separating the positive and negative leads of the X-poled bender element wired in series is twice the thickness of the Y-poled element wired in parallel.  Inspection of Equation 2.45 and Equation 2.46 show that the capacitance is decreased for the X-poled bender element wired in series and subsequently the voltage is increased as compared to a Y-poled bender element wired in parallel.  To summarize, the X-poled element wired in series generates a larger voltage for a given deflection, and is thus better suited as a receiving sensor for S-wave pulse tests.  The Y-poled element requires less voltage for a given deflection and is thus a better actuator for S-wave pulse tests.

Lings and Greening (2001) introduced an innovative, alternate wiring scheme for bender elements that allowed them to function as both bending and extending actuators; thus they could produce either P- or S-waves given a specific input signal.  Essentially they showed that X-poled bender element wired in parallel and Y-poled bender element wired in series produce P-waves. The relevant bender element polarities and wiring schemes are listed in Table 2.6.

**Table 2.6. Bender Element Transducer Characteristics**

| Element Polarity | Wiring Scheme | Wave Type | Transducer Type |
|---|---|---|---|
| Parallel | Parallel | S-wave | Transmitter |
| Cross | Series | S-wave | Receiver |
| Parallel | Series | P-wave | Receiver |
| Cross | Parallel | P-wave | Transmitter |

Stain levels near the transmitting transducer can be greater than $10^{-3}\%$, but due to attenuation of the signal the average strain levels in specimens are much lower (Nakagawa et al. 1996). Thus, bender element testing is considered a NDT technique. The resonant frequency of bender elements in air is a function of the transducer size, piezoelectric elastic constants, and mass density (Lee and Santamarina 2005), and in general the resonant frequency of bender elements when embedded in soil specimens is larger than that of bender elements in air.

**2.4.2.1.2.** **Bender element embedment length.** Proper selection of the embedment length of bender elements into soil specimens has been discussed in the literature. Increased embedment results in greater coupling between the elements and the specimen and a cleaner shear wave (Gohl and Finn 1991). Disadvantages include: (1) there is increased sample disturbance with increased embedment length; and (2) additional compressional wave energy is generated during S-wave testing thus complicating the interpretation of the received waveform. Between one-third to one-half of the bender element length is typically embedded into the soil specimen but there is considerable variability between researchers. Recently Yamashita et al. (2009) summarized that there is no optimum embedment length.

**2.4.2.1.3.** **Test specimen size.** The influence of specimen size on bender element tests has been investigated. The ASTM standard for ultrasonic pulse testing (ASTM D2845) has been used to confine acceptable specimen sizes for bender element testing; the standard recommends a length-to-diameter ratio (L/d) of less than 5 for testing. Leong et al. (2005) believed that most laboratories used a length to diameter ratio (L/d) of 0.3 to 2.5. Arroyo et al. (2006) performed numerical modeling simulations of bender element test for various specimen geometries and concluded that measurements of specimen stiffness were influenced by geometry. Slender geometries had the largest influence on measurements. Ultimately the authors recommended that all published data of wave velocities and stiffness need to be documented with the test specimen size.

Bender element research has been more focused on confining the wavelength ratio, which is defined as the ratio of the distance between the two bender elements to the input signal wavelength ($L/\lambda$). The proper selection of the wavelength ratio is important to separate higher velocity near field effects from lower velocity pure shear waves. The actuation of bender elements results in a portion of the energy being transmitted as a transient P-wave, which has a larger velocity than the shear wave. This transient phenomenon was recognized in geophysical field testing by Sanchez-Salinero et al. (1986) and was called the near-field effect (NFE). The NFE results from a portion of the shear wave energy traveling at the speed of a compression wave. The effect is transient, but in small laboratory specimens it can affect results. The authors

performed a geophysical wave analysis in the field and showed that for minimal separation between the signal source and receiver two separate wave arrivals could be distinguished. For shear wave transmissions the first arrival was a low amplitude wave traveling with the speed of a compressional wave, but it was determined to be a function of the shearing motion in the soil. The larger second wave arrival traveled at the speed of a shear wave and represented the shearing motion in the soil skeleton. The NFE is also present in compression wave transmissions, but the near field component propagates at the speed of a shear wave and therefore it does not influence the arrival of the primary compressional wave due to its slower speed and high rate of attenuation. The two primary ways to reduce the NFE are either to increase the separation distance between the signal source and receiver or to increase the frequency of the transmitted signal. An alternative to qualitatively assessing the arrival of the near-field component is to perform simultaneous P- and S-wave tests. This methodology enables the direct determination of the P-wave velocity that then can be used to interpret the received signal during the S-wave test. Sanchez-Salerino et al. (1986) recommended a wavelength ratio greater than 2. Jovicic et al. (1996) showed that no NFE was present for a wavelength ratio of 8. Pennington et al. (2001) recommended a ratio between 2 and 10. Leong et al. (2005) recommended a wavelength ratio of at least 3.33 based on experimental results. Pulse velocity standard (ASTM D2845) recommends a wavelength ratio greater than 10.

       **2.4.2.1.4.** **Input signal.** Typically a single square (e.g. Dyvik & Madshus 1985; Viggiani and Atkinson 1995) or sinusoidal pulse (e.g. Arulnathan et al. 1998; Pennington et al., 2001) is used to actuate the bender element transmitter. Sine waves are composed almost entirely of one specific frequency, whereas square waveforms are composed of a variety of frequencies. Leong et al. (2005) determined that a sine wave allows easier determination of the wave arrival, and recommended it use over square waves. As frequency analysis techniques have become more popular to determine travel times, the use of sine waveforms has increased. It is generally acknowledged that the mechanical movement of the bending transmitter is different than the input waveform. Lings and Greening (2001) and Rio (2006) attributed this to inertial effects. Rio (2006) used a laser velocimeter to measure bending transmitter in a free-space at multiple frequencies. Greening and Nash (2004) mounted a strain gauge on a bending transmitter, but acknowledged that the installation altered the mechanical behavior of the element. Pallara et al. (2008) measured bender actuator deformations in the air with laser techniques and showed that deformations were different than input waveforms. Results also indicated that at frequencies greater than the first mode resonant frequency the deformation of the bending actuator becomes

increasingly complex, thus the authors recommended operating bender actuators only at frequencies less than the first mode resonant frequency.

Both pulse and continuous signals have been used. Pulse signals generate only a transient response in the specimen, whereas continuous signals generate both transient and steady-state responses. The voltage sent to the bending element transmitter is different in the literature. The most typical voltage is ±10 V, but some researchers amplify the transmitting signal (e.g. Leong et al. 2009). Piezoelectric bender element manufacturers commonly rate the elements for a specific maximum voltage, after which de-lamination of the piezoceramics from the metallic center electrode can occur if exceeded.

A range of input frequencies have been used; from 5 Hz (Dyvik & Madhaus 1985) to 20 MHz (Lee et al. 2007). Soil generally acts as low-pass filters and thus higher frequency noise is attenuated preferentially. Variations in frequency affect dispersion of the transmitted wave and subsequent attenuation of wave energy. Dispersion occurs when wave energy impacts the specimen boundary or small irregularities in the specimen and it can also lead to wave conversion from shear to compressional. Variations in the wavelength ratio can also affect the attenuation the transmitted signal and complicate estimates of damping. Nonetheless, the primary control on input frequency is in relation to the wavelength ratio as discussed previously.

**2.4.2.1.5.** **Travel time determinations.** Wave velocities are determined from specimen geometries and measurement of the induced wave travel time between transducers using Equation 2.35. Travel time determinations are either from direct time measurements (e.g. Clayton et al. 2004; Leong et al. 2005) or indirect time measurements (e.g. Brocanelli and Rinaldi 1998; Lee and Santamarina, 2005). Direct travel time methods are advantageous in the fact that they are easily and efficiently implemented in a test program, whereas indirect travel time methods are advantageous in the fact that they can reduce some of the variability associated with direct travel time measurements. Direct time measurements are highly dependent on the quality of the measured signals, and thus on the quality of the bender element manufacturing, wiring, and peripheral electronics. Arroyo et al. (2003) discussed how different definitions of travel time can lead to differences of up to 50% of the average value; which subsequently affects the estimated modulus by the square of the estimated wave velocity.

The first task when evaluating a recorded waveform from bender elements is to analyze the signal to noise ratio (SNR). The SNR is defined as the ratio of signal amplitude to noise amplitude for a recorded signal. Leong et al. (2005) recommended a SNR of at least 4 dB, which corresponds to a unit less SNR of approximately 2.5. Clayton (2011) stated that signal to noise ratios less than 10 are unacceptable. Once it is determined that a sufficiently clean waveform has

been recorded the recorded wave signature can be used to evaluate travel times between the two bender element transducers.

        **2.4.2.1.6.**   <u>**Direct travel time determinations.**</u>    Direct time measurements are based on plots of transmitted and received voltages versus time. The analysis attempts to match portions of a transmitted signal with the received signal; for example the first peak or the first deflection. Direct time measurements often use stacking of repeated signals in an effort to emphasize the received signal, reduce background noise, and ultimately increase the SNR.

        The point of arrival of a wave can be determined as one of four specific points on the recorded wave signature: (A) point of first deflection; (B) point of first signal reversal after the first deflection; (C) the point where signal crosses the relative horizontal axis; (D) point of the first major peak, as shown on a generalize waveform in Figure 2.15. The ASTM D2845 standard for ultrasonic pulse testing bases travel time on the point of first deflection, Point A, but this location in the recorded wavelet is often influenced by near-field effect.
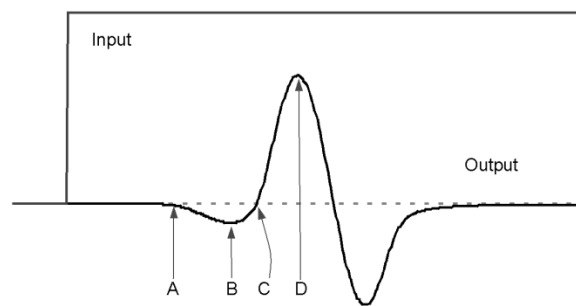


**Figure 2.15. Interpretation of Wave Arrival (Lee and Santamarina 2005)**

        The use of characteristic points was introduced by Viggiani and Atkinson (1995) and uses engineering judgment to match portions of the transmitted and received waveforms, and thus it is commonly variable for different interpretations. A final direct travel time analysis technique called the peak-to-peak method uses the time difference between the first peak of the transmitted signal and the first major peak of the received signal. To utilize this methodology it is important to use an input sinusoidal waveform and confirm that the received wavelet is of a similar frequency as the transmitted wave. If the frequencies are grossly different between the two signals and measured travel time will be influenced by the frequency mismatch.

**2.4.2.1.7.** **Indirect travel time determinations.** Indirect time measurements analyze attributes of the transmitted and received waveforms in an effort to determine travel time between the two transducers. The coherence between the two signals is determined using the cross-correlation function, and thus this method is commonly called the cross-correlation method. The method was first developed by Mancuso et al. (1989) for use in geophysical cross-hole tests. The cross-correlation function is a function of the degree of correlation between two signals versus the time delay between the signals. It can be written analytically as,

$$CC_{TR}(t) = \lim_{T_r \to \infty} \frac{1}{T_r} \int_{T_r} R(T) T(t+\tau) dT \qquad (2.47)$$

Where, T(t) is the transmitted signal, R(t) is the received signal, $T_r$ is the length of the time record and $\tau$ is the time delay between signals. Coherence is plotted against travel time and the travel time is determined as the time difference to the maximum cross-correlation value (Viggiani and Atkinson 1995).

An alternate procedure uses the cross-power spectrum (Viggiani and Atkinson 1995; Greening and Nash 2004; Ferreira et al. 2006) which is essentially a Fourier transformation of the cross-correlation function between the transmitted and received signals. Time domain measurements are often converted to the frequency domain to identify the frequency components of the signals. Ultimately plots of the absolute value of phase angle against frequency are determined by performing a frequency sweep, and the travel time between bender elements is determined from the linear portion of the curve, such that

$$t = \frac{\Phi_{angle}}{2\pi f} \qquad (2.48)$$

Alignment of the bender elements is critical when using the cross-correlation methods (Leong, personal communication). Yamashita et al. (2009) discussed that sometimes a second peak in the cross-correlation method is larger than the first peak due to dispersion or reflections.

**2.4.2.1.8.** **Comparison of travel time determinations.** There has been criticism of both direct and indirect time measurements. Some believe direct time measurements are too subjective and advocate the use of indirect measurements, but as stated before, a general consensus on data interpretation has not been achieved.

Arulnathan et al. (1998) believed that both direct time measurements using characteristic peaks and indirect time measurements using cross-correlation methods were not ideal due to specimen boundary effects, near-field effects, and signal distortion. Arroyo (2001) used statistical analysis to compare different travel time methodologies, and he found that no methodology was distinctly better than the others. Greening et al. (2003) showed that direct time measurements usually estimate shear wave velocities in excess of the estimates from indirect techniques. Greening and Nash (2004) believed that indirect time measurements that deconvolute a signal into the frequency domain provide more information about the relationship between the transmitted and received signal and allow for more robust engineering judgment during determination of travel time. Chan (2012) compared different methodologies and showed that first deflection, peak-to-peak direct time measurements, and cross-correlation methods appeared to converge at frequencies between 10 and 20 kHz, but cross-power spectrum methods predicted significantly lower wave velocities. The author agreed that indirect methods do offer more insight into relationship between the signals, but the estimated wave velocities have not been proven to be better and the rigors of these methods negate one of the primary advantages of bender element testing; it's simplicity.

Multiple researchers have discussed the need for the transmitted and received signals to be of similar frequency components for the cross-correlation and cross-power spectrum methods to be used, but this can be difficult to determine based on the attenuation and dispersion that occurs from generation of a signal, transmission through a specimen, and reception on the opposing specimen end. Yamashita et al. (2009) stated that adjusting the input frequency sent to the bender element transmitter does not significantly affect the frequency components of the received signal. The authors stated that increased frequency difference between the signals would indicate a lower confidence in a direct travel time measurement. Ultimately they did not recommend a specific methodology but stated that peak-to-peak measurements and cross-correlation measurements must contain similar frequencies between the transmitted and received signals.

**2.4.2.2. Ultrasonic pulse velocity testing.** The ultrasonic pulse test utilizes piezo-electric crystals to convert electrical signals to mechanical waves. The term "ultrasonic" is reserved for wave transmissions that are above the upper limit of the audible sound frequency; approximately 20 kHz. There are two typical test modes in ultrasonic testing: pulse-echo and through transmission. The pulse-echo utilizes one transducer to generate a short pulse of ultrasonic waves that propagate into the material in question, as shown in Figure 2.16. Reflections of the wave occur at boundaries separating materials of differing densities, voids, or

anomalies and the reflected waves travel back to the original transducer that also acts as a receiver. If the transmitting and receiving transducers are separate, this is sometimes called the pitch-catch mode as shown in Figure 2.17. The measured quantities are the amplitude of the reflected wave, or echo, and the transit time from transmitter to receiving transducer (Krautkramer and Krautkramer 1990). The through transmission method utilizes two transducers oriented on opposite sides of a material; one for transmission and one for receiving. Only transit time of the propagating wave is measured. The ultrasonic equipment utilized in this research is based on the through transmission mode of ultrasonic testing and relies on specialty end platens fitted with piezoelectric crystals.
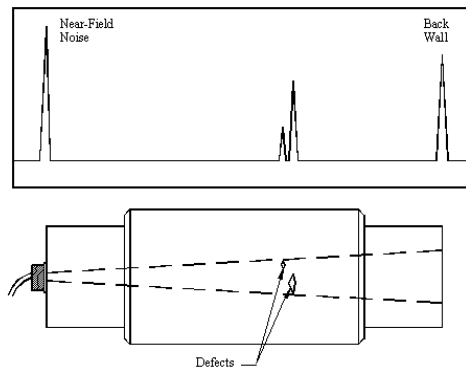


**Figure 2.16 Pulse-Echo Ultrasonic Transmissions**
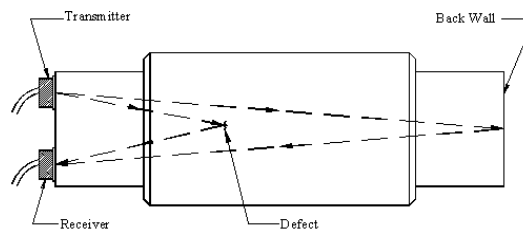


**Figure 2.17. Pitch-Catch Ultrasonic Transmissions**

According to Nakagawa et al. (1996) an ultrasonic wave transmission can produce both a fast P-wave and a slow P-wave propagating through a soil specimen. The fast P-wave has both a high and low frequency component, and is independent of backpressure for testing of saturated

specimens. Conversely, the slow P-wave shows a distinct correlation with backpressure; velocity decreases as pressure decreases. The slow P-wave travels through the specimen by viscous hydrodynamic movements. The velocity of the slow P-wave depends on the compressibility of the soil skeleton.

The choice of specimen geometry and input signals to excite the transmitting ultrasonic crystal are similar to that used in bender element testing as discussed in preceding sections.

**2.4.2.2.1.    Interpretation of ultrasonic pulse velocity data.**  In general the interpretation of ultrasonic pulse velocity measurements is identical to that used for bender elements. Both direct and indirect travel time determinations can be used.  de Alba and Baldwin (1991) applied both digital filters and signal stacking to improve the recorded signal.  A bandpass filter was applied to the signal filtering out all frequencies except a 2.5 – 4.0 kHz bandwidth around the dominant frequency of the transducers.  Stacking of repeated signals was also performed; the authors recommended between 35 and 100 stacked signals to remove background noise. Determination of damping ratios from the waveform of ultrasonic wave transmissions is difficult given wave reflects and refractions that absorb transmitted energy and Stephenson (1978) concluded that this could not be accurately done.

**2.4.2.3. Comparison of resonant column and pulse velocity tests.**  Both resonant column and ultrasonic pulse velocity test methods have developed sufficiently to obtain widespread acceptance of test methodologies and interpretation, and thus both methods have been standardized by ASTM as D4015 and D2845, respectively.  Bender element testing methods and interpretation are still the subject of much debate, and thus the development of standardized test procedures is still in development by ASTM (ASTM WK-23118).  The variations in equipment, methods and data interpretations remain significant obstacles to the acceptance of bender elements providing a robust estimate of shear modulus and potentially material damping.

Resonant column methods have the advantage of being able to apply various levels of strain to a specimen from low-strain to moderate strain levels.  Moderate strain levels are defined at $10^{-1}$ to $10^{-3}$ %.  Pulse velocity tests only apply small strains, and the strain levels are difficult to measure during testing.  Both methods are deficient in the sense that the strain levels during testing are variable throughout the test specimen.

During pulse velocity testing, the density of a specimen and the wave velocity are determined by direct measurement, whereas in resonant column testing wave velocities are a function of specimen resonance.  Dyvik & Madshus (1985) were the first researchers to install bender elements into a resonant column apparatus and good agreement was obtained for shear wave velocity measurements for cohesive soil specimens.  Thomann and Hryciw (1990) obtained

good agreement between bender element pulse tests and resonant column tests on undrained cohesionless specimens at various confining pressures and attributed the small differences in measurements to the differences in strain levels between the two testing methods. Nakagawa et al. (1996) performed comparative testing between the two methodologies and determined that shear wave velocities from resonant column tests were less than velocities determined from pulse testing. Differences were approximately 30% for overconsolidated clays and 7% for sands. The authors believed the difference in measurements were influenced by the volume of the specimen affected by the testing procedure. Pulse testing measures a specimen's response to elastic energy along a direct wave path, whereas the resonant column method uses measurements of specimen stiffness from the entire specimen. As laboratory specimens are typically more disturbed along their perimeter, resonant column measurements are commonly less than pulse measurements (Nakagawa et al. 1996). Ferreira et al. (2006) also performed simultaneous resonant column and bender element testing in a modified resonant column apparatus. Travel time determination for the bender element tests were performed using both direct-time and indirect-time methods based on the frequency content of the recorded wave signature. Results indicated that both direct and indirect-time measurements produced results that were similar to the resonant column results, but the authors noted that the methodologies cannot be fully automated and require variable degrees of engineering judgment.

One large disadvantage of pulse velocity methods as compared to resonant column tests is that the measurement of material damping is often difficult to realize. Damping estimates from pulse velocity tests have been performed but are often influenced by wave reflections and refractions at boundary surfaces and from inherent radiation damping that is a function of spherical spreading of the transmitted wave. Johnson (1981) discussed that material damping measurements from ultrasonic methods are greater than those from resonance methods due to the difference in frequency between the two methodologies. Measured damping decreased with increasing confining pressure and for soils and was a function of effective stress.

One of the largest advantages of pulse transmission tests over resonant column tests is that they are easily modified to work in other geotechnical equipment; such as the triaxial cell, consolidometer, centrifuges, and even resonant column equipment. Multiple pulse tests can be performed on a test specimen, and variations in soil moduli and damping can be determined as consolidation progresses or at different levels of pore water pressure generation in a triaxial test.

## 2.5. PIEZOELECTRICITY IN GEOTECHNICAL ENGINEERING

**2.5.1. Introduction.** Piezoelectricity is a phenomena in which certain materials deform when subjected to an electric field. It was discovered in 1880 by Jacques and Pierre Curie for some crystalline minerals such as quartz (Moulson and Herbert 1990), and it was later determined that metal oxide-based ceramics also exhibit this behavior. Essentially there are two types of piezoelectrics: (1) crystalline materials having natural piezoelectricity such as quartz; and (2) ceramics that get their piezoelectricity by being polarized in an electric field at elevated temperatures (Krautkramer and Krautkramer 1990). Ceramics manufactured from lead zirconate titinate (PZT) and lead titanate (PT) have high sensitivity to applied voltages and are the most commonly used piezoelectric transducers.

Piezoelectric materials develop an electrical charge on their surface when a mechanical stress is applied. A reversal of the direction of the applied stress leads to a reversal of the polarity of the charge generated. This is termed the direct piezoelectric effect, as shown in Figure 2.18. This property allows piezoelectrics to be used in devices used to detect strain, movement, force, pressure or vibrations; commonly found in force, acoustic and ultrasonic sensors.
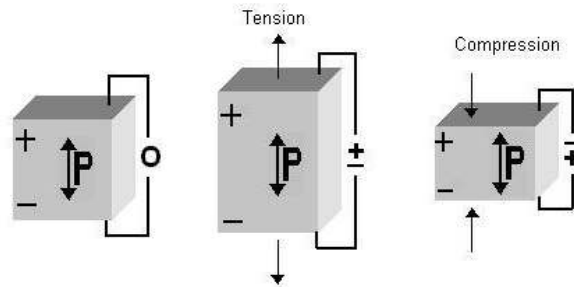


**Figure 2.18. Direct Piezoelectric Effect (from Boston Piezo-Optics, Inc.)**

It was later discovered that these piezoelectric materials behaved in a similar manner when subjected to an electrical field. Piezoelectric materials strain when placed in an electrical field. This phenomenon is termed the inverse piezoelectric effect. When the direction of the electrical field is reversed, the direction of deformation is also reversed. The inverse piezoelectric effect forms the basis of the design of transducers used to generate strain, movement, force, pressure or vibrations (Krautkramer and Krautkramer 1990).

The direction in which tension or compression induces strain in a piezoelectric material causes an electrical polarization to develop parallel to the direction of the applied strain. This direction is termed the piezoelectric axis. It is possible to generate various strain directions in a piezoelectric material through different combinations of material orientation and the applied electrical field (Krautkramer and Krautkramer 1990). To generate elongation of a material a voltage is applied parallel to the piezoelectric axis, as shown in Figure 2.19. Conversely, a voltage applied perpendicular to the piezoelectric axis will generate a shearing motion.
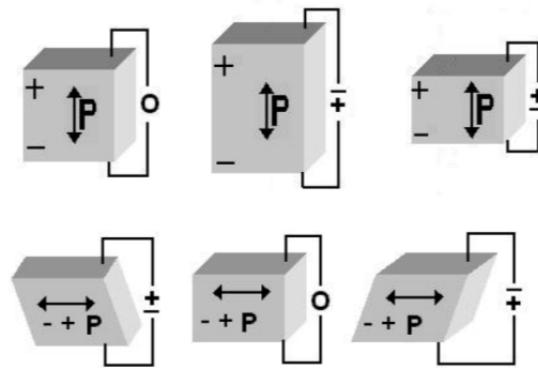


**Figure 2.19. Application of Voltages and Subsequent Strain in Piezoelectrics (from Boston Piezo-Optics, Inc.)**

The stresses and strains developed by the piezoelectric effect are related to electrical parameters through the piezoelectric constants; $d_{ij}$, $g_{ij}$, and $k_{ij}$. These constants have different values for different directions and different materials.

The constant $d_{ij}$ is defined as the piezoelectric strain constant which relates the mechanical strain experienced by a piezoelectric material to the applied electrical field. This parameter is also referred to as the charge constant. The subscripts define the direction of the electrical field and the direction of strain, respectively. The strain constant also represents the amount of charge developed relative to the stress applied along a specific axis. The strain constant is an important indicator of a material's ability to act as a suitable actuator or transmitter.

The constant $g_{ij}$ is defined as the piezoelectric voltage constant which relates the electrical field generated by a piezoelectric material for a given material strain. The subscripts define the direction of the electrical field and the direction of applied stress or strain in the

material; respectively. The voltage constant is an important indicator of a material's ability to act as a sensor or receiver.

The electromagnetic coupling factor, $k_{ij}$ defines the efficiency that a piezoelectric material converts electrical energy to mechanical energy or vice versa. The subscripts define the direction in which the electrical field is applied and the direction of the mechanical energy is applied, respectively. Coupling factors are typically quoted by piezoelectric suppliers. Typical piezoelectric ceramics can convert 30 – 75% of the energy delivered to the material in on form to the other form (APC International 2002). A high coupling factor is desirable for efficient energy conversion. Quartz on the other hand has a coupling factor of 0.1, thus it is seldom used in material testing.

A piezoelectric material actuated with an alternating current changes dimensions cyclically at the frequency of the applied electrical field. The frequency at which the element vibrates most readily in response to the applied electrical field, and thus most efficiently converts electrical energy to mechanical energy, is termed the resonant frequency. The resonant frequency is a function of piezoelectric material, shape and volume. At frequencies less than the resonant frequency, piezoelectrics are essentially capacitors (Huebner 2011).

**2.5.2.   Development of Piezoelectric Transducers in Geotechnical Engineering.**
Piezoelectric elements of various materials, shapes, and operational frequencies are utilized in geotechnical laboratory and field testing. The development of these materials for geotechnical testing has been evolving for over four decades.

Initially piezoelectric crystals were developed to generate waves in rock specimens, but when utilized in soils differences in the stiffness of the crystals and soil led to large impedance contrasts. It is important to closely match the impedance of the transducers and tested material to optimize the transmission of waves. Lawrence (1963) is reported as the first to use piezoelectric crystals in the geotechnical field; using piezoelectric crystals pressed against both ends of a Shelby tube sample to measure compressional wave velocity. Lawrence (1965) modified laboratory end platens with twelve ceramic piezoelectric elements orientated around the circumference of each platen. The piezoelectrics were wired in parallel, so they generated a torsional load on an attached specimen when a voltage as applied. The piezoelectrics utilized were not very sensitive and thus there was difficulty in detecting the initial arrival of waves. Gregory and Podio (1970) developed a piezoelectric device for measuring both P-wave and S-wave in rock materials; it functioned as a pitch-echo transducer/receiver. Shirley and Anderson (1975) used piezoelectric ceramic disks mounted in deep ocean sediment corers to obtain P-wave velocities. Stephenson (1978) used piezoelectric crystals bonded to unit element specimen end

platens to measure both P-wave and S-wave velocity in a specimen; the equipment was mounted into a uniaxial compression device to ensure consistent coupling of the end platens and the specimen.

Piezoelectric transducers were eventually developed that more closely matched the impedance characteristics of soils. Shirley and Hampton (1978) and Shirley (1978) discuss the development of the first bending piezoelectric transducer used to generate S-waves in the marine sediments, and they introduced the term "bender element" to the industry. The transducers were composed of two piezoelectric ceramics of opposing polarity glued together; typically called piezoelectric bender elements. Schultheiss (1981) was the first to introduce bender elements into the end platens of a triaxial cell to measure S-wave velocity. De Alba et al. (1984) used piezoelectric crystals and biomorph transducers both fixated into an end platen to measure elastic soil properties and relate them to the liquefaction potential of sands. The authors believed encapsulating the bender elements in the end platens prevented potential damage of the transducers during insertion into soil specimens. They determined that the shear wave velocities were slightly higher than those predicted by the Hardin and Richart equation (Hardin and Richart 1963). Dyvik and Madhaus (1985) confirmed the accuracy of bender element measurement of S-wave velocities by mounting the equipment into a Hardin-type resonant column device and comparing the $G_{max}$ estimated with each test. Thomann and Hryciw (1990) obtained good agreement between bender element pulse tests and resonant column tests on undrained cohesionless specimens at various confining pressures and attributed the small differences in measurements to the differences in strain levels between the two testing methods. Lings and Greening (2001) introduced an innovative, alternate wiring scheme for bender elements that allowed them to function as both bending and extending actuators; thus they could produce either P- or S-waves given a specific input signal.

**2.5.3. Advantages and Disadvantages.** The advantages of pulse velocity testing using either ultrasonic pulse velocity crystals or bender elements to measure wave velocities in soil specimens is the simplicity in their implementation in a geotechnical laboratory, the flexibility in their installation with different equipment and test procedures, the low cost of the transducers, and the ability to measure wave velocities in two directions in an effort to model anisotropic soils.

Piezoelectric materials have been quite useful in a range of geotechnical applications, but pulse velocity testing has several disadvantages that affect their use in soils. Weak transmitted signals, poor coupling between transducers and the soil, near field effects, and high operating frequencies all tend to weaken and distort the recorded signals. Piezoelectric crystals have proven to be effective at generating P-waves in soils, but their ability to generate S-waves is

suspect given the minimal contact between the element and the soil and the impedance contrasts. Velocity measurements in dry materials are difficult because of significant attenuation of the signal in particulate material (de Alba et al. 1984). Bender elements offer an improved method for measuring S-wave velocities since the transducers typically produce a stronger signal because the impedance match between the transducers and the soil specimen is improved as compared to ultrasonic platens. As the bender elements are intimately coupled to the soil, as compared to ultrasonic piezoelectric crystals housed within end platens, they overcome some of the problems of poor coupling and subsequent weak signals.

One operational advantage of ultrasonic tests over bender element tests is that the transducers are less prone to electrical failure from moisture migration in the specimen and cell fluid. Ultrasonic transducers are sealed within a specimen end platen and thus are separated from moisture. Problems with bender elements often arise during the insertion of the transducers into the specimen which can damage the waterproofing around the piezoelectric. Once a bender element is damaged electronically the equipment must be dismounted and changed; a tedious and time-consuming process.

# 3. MATERIALS

The following discussion of research materials considers only the discrete constituents utilized in this research. Discussion of specimen preparation techniques is included in Chapter 4 and specific specimen properties are noted during discussion of the experimental tests results; Chapters 5 and 6.

## 3.1. EPS PARTICULATES

**3.1.1. Source of Material.** Bulk samples of PS resin beads, EPS particulates, and EPS re-grind material were obtained from VersaTech Inc., a regional supplier of EPS materials for the engineering, manufacturing, and packaging industries. A site visit to the production facility located in Fredericktown, MO was made on February 25, 2011 to inspect the source material and fabrication process for EPS products utilized in engineering applications. PS resin beads utilized at the VersaTech facility were obtained from BASF Chemical Company under the tradename Styropor®. Bulk samples of various EPS particulates, virgin PS resin beads, and recycled EPS re-grind material were delivered to Missouri S&T on May 13, 2011 from VersaTech personnel. EPS particulate densities of 10, 16, 24, and 32 $kg/m^3$ were received, identified, and stored for future use.

**3.1.2. Stereoscopy.** Initially EPS particulates were visually inspected using a Fisher Scientific trinocular stereoscope (Model No. 12-562-5) with a primary magnification of 0.7x – 4.5x and an enhanced magnification from 7x – 45x utilizing magnification eyepieces. The central port of the trinocular was fitted with a C-mount adapter to directly attach a DSLR camera. Images from 15x – 45x magnification were obtained with a Panasonic Lumix G2 camera attached directly to the C-mount adapter; without the use of a traditional camera lens. Illumination for the images was provided by a Fisher Scientific fiber optic light source (Model No. 12-562-36), but both a haloing effect and high reflectivity of the surface rendered the images somewhat difficult to assess. In general, the surfaces of the EPS particulates appear to be a continuous, textured and dimpled membrane without any noticeable cracks or large voids. The shape is spheroidal but not perfectly spherical. All stereoscopy images are located in the Appendix.

**3.1.3. Scanning Electron Microscopy.** EPS particulates were also investigated using a Hitachi S4700 field emission scanning electron microscope (SEM), which under optimal conditions can magnify images upwards of 500,000x and resolve features as small as two nanometers. The SEM utilized proprietary Windows-based software provided by Hitachi to

control the SEM and capture the images in a *.tiff format. Specimens must be electrically conductive at the surface for imaging and grounded to prevent the accumulation of electrostatic charge, thus the EPS particulates were prepared with water-based carbon paint to adhere them to an aluminum stub and coated with 60/40 gold palladium, as shown in Figure 3.1. Seven different EPS particulate specimens were prepared for image capture with the SEM as shown in Table 3.1.
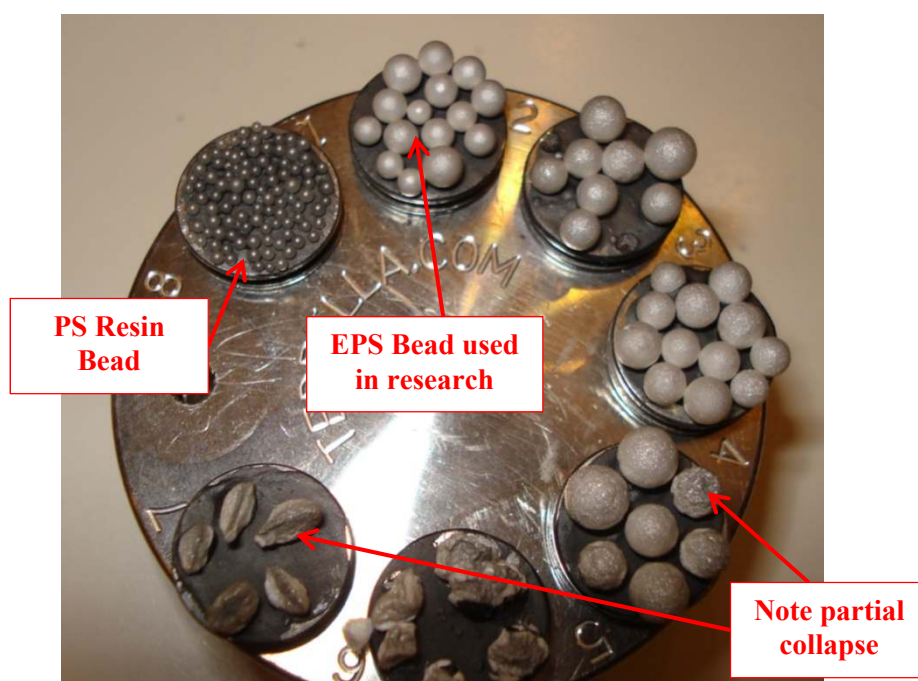


**Figure 3.1. Particulates after SEM**

**Table 3.1. SEM Imaging of EPS Particulates**

| No. | Identification | SEM Magnification Range |
|---|---|---|
| 1 | Polystyrene (PS) Resin Bead | 30x, 250x ,1000x, 5000x, 10000x, 20000x |
| 2 | EPS Particulate (~32 kg/m$^3$) | 30x, 250x ,1000x, 5000x, 10000x, 20000x |
| 3 | EPS Particulate (~24 kg/m$^3$) | 30x, 250x ,1000x, 5000x, 10000x, 20000x |
| 4 | EPS Particulate (~16 kg/m$^3$) | 30x, 250x ,1000x, 5000x, 10000x, 20000x |
| 5 | EPS Particulate (~10 kg/m$^3$) | 30x, 250x ,1000x, 5000x, 10000x, 20000x |
| 6 | EPS Re-grind | 30x, 250x ,1000x, 5000x, 10000x |
| 7 | EPS Particulate half-sphere | 30x, 250x ,1000x, 5000x, 10000x |

The "half-sphere", No. 7 on Figure 3.1, was a very low density EPS particulate (~10 kg/m$^3$) that was mechanically cut in half with a knife to view the internal structure of the particulate. During imaging, the specimens were contained within a vacuum of approximately 10$^{-6}$ Pascals and the electron beam was operated using a 5 kV charge. Upon removal of the specimens from the vacuum the half-spheres, re-grind material, and some of the lowest density particulates collapsed; as shown in Figure 3.1. All SEM images can be found in the Appendix.

SEM images were analyzed to estimate the diameter of PS and EPS particulates. A public domain image processing program called ImageJ imported the SEM files and was able to perform digital length measurements. The SEM files have a scale bar printed directly on the images that is manually calibrated with ImageJ to set the spatial distance to pixels ratio. Once this ratio was set, multiple diameter measurements were made for each PS and EPS particulate and recorded. All linear measurements made from the SEM images are recognized to be in error given the three-dimensional nature of the particulates, and actual diameter lengths are probably slightly longer than those measured. The combined use of stereoscopy and SEM at various levels of magnification provided a comprehensive assessment of the surface texture of the PS resin beads and EPS particulates as shown in Figure 3.2 and Figure 3.3



a)  30x Magnification                    b)  250x Magnification
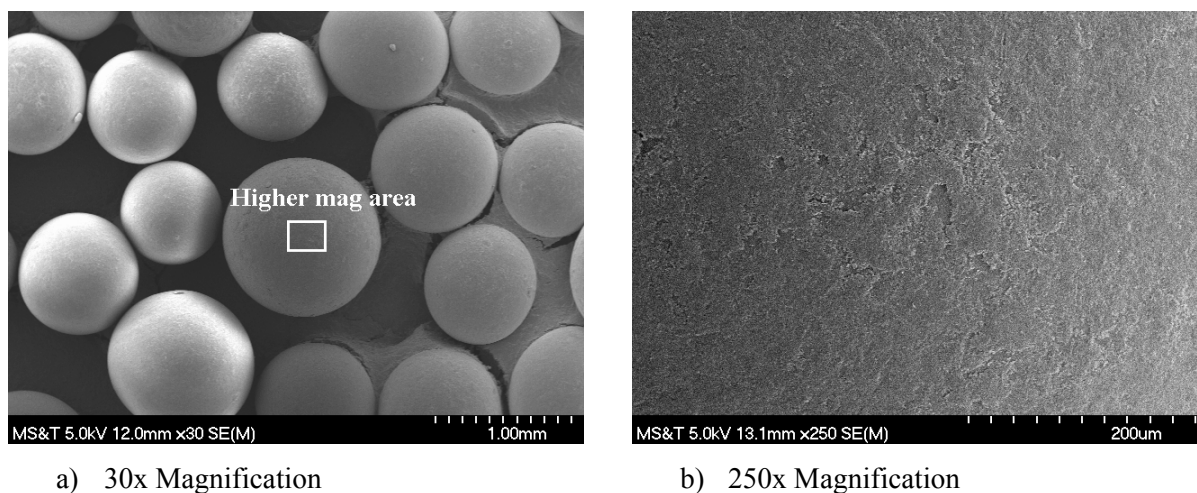
**Figure 3.2.  SEM Images for PS Resin Bead**

The PS resin bead surface is a continuous, textured membrane with a fused flakey structure. The surface texture is rough, but higher magnification images gave no indication of conduits or voids into the internal spaces. In general the surface texture of the EPS particulates is

similar to description based on the stereoscopy images. Comparison of the different density EPS particulates showed an increase in the amount of voids in the textured surface membrane of the particles as the density decreases, or more simply, as the amount of expansion increased. It is unclear how far these surface voids penetrate into the internal structure of the particulates, but higher magnification images indicated the voids close off very near the surface of the particle. Both the EPS regrind material and the half-sphere offer a detailed view of the internal honeycomb structure of the EPS particulates. The internal structure is composed of fused foam cells with thin, translucent cell walls. Intermittent, larger internal voids are also present.



a) 30x Magnification      b) 250x Magnification
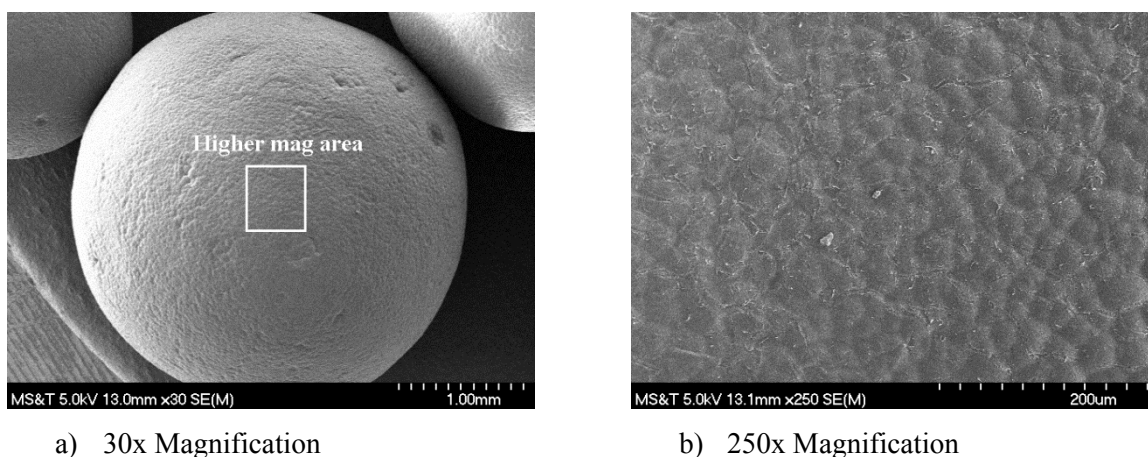
**Figure 3.3. SEM Images for EPS Particulate (~32 kg/m$^3$)**

**3.1.4. Particle Mass.** Mass measurements were obtained using a Mettler Toledo XS205 digital scale with precision to $10^{-4}$ grams. Particles of EPS and PS resin beads were measured cumulatively in sets of 50 particles. Three sets of measurements were obtained for the PS resin beads and EPS particulates, thus 150 individual measurements of individual particle mass were obtained. In addition, 50 mass measurements were obtained of a lower density EPS particulate. A summary of all mass measurements are shown in Table 3.2.

**Table 3.2.  Measured Mass of Particulates (grams)**

| Material Type | Avg. | Min. | Max. | Standard Dev. |
|---|---|---|---|---|
| PS Resin Bead | 0.00036 | 0.00012 | 0.00097 | 0.00013 |
| EPS Particulate (~32 kg/m3) | 0.00065 | 0.00011 | 0.00150 | 0.00031 |
| EPS Particulate (~16 kg/m3) | 0.00040 | 0.00017 | 0.00060 | 0.00009 |

**3.1.5.  Particle Density.**  Estimates of particle density were obtained by combining the mass measurements with the measurements of diameter obtained from the SEM images.  All results are shown in Table 3.3.  The measured density of EPS particulates agrees well with data reported in published literature.  Deng and Xiao (2010) authors reported an average density of 0.03 $g/cm^3$ for EPS particles with diameters between 2 – 4 mm, and Wei et al. (2008) reported an average density of 0.0368 $g/cm^3$ for EPS particles with diameters between 2 – 3 mm.

**Table 3.3.  Measured Density and Unit Weight of Particulates**

| Material Type | $g/cm^3$ | $kg/m^3$ | $lb/ft^3$ |
|---|---|---|---|
| PS Resin Bead | 0.942 | 942.0 | 58.8 |
| EPS Particulate (~32 $kg/m^3$) | 0.051 | 51.0 | 3.18 |
| EPS Particulate (~16 $kg/m^3$) | 0.033 | 33.1 | 2.06 |

**3.1.6.  Water Absorption.**   An attempt was made to measure the water absorption properties of EPS particulates using a procedure modified from ASTM C272.  Absorption can be defined as the increase in mass of a particle due to water penetrating into the pores, during a specific period of time, but not including water adhering to the outside surface of the particles. Initially 50 grams of EPS particulates were placed into a fine mesh soil sieve and submerged for 24 hours.  Upon removal from the water bath, there was significant difficulty in removing the particulates from the mesh sieve, and once completely removed the particulates took over 4 hours to surface air dry via constant agitation and a heated fan.  An alternate procedure was attempted in which a large culinary "tea-ball" was used to contain the EPS particulates during submersion. The tea-ball had to be suitably ballasted to the base of the submersion tank in order not to float. Upon removal from the water bath, the entire tea-ball was dipped in alcohol in an effort to displace surface moisture, similar to the procedure outlined in ASTM C272, and removed.  The tea-ball was manually shaken to remove moisture and mass readings were obtained each minute

until no appreciable changes were noted. Three separate experiments were performed in this manner, but all tests took over 45 minutes until mass readings converged to a consistent value. Nonetheless, the mass change of the EPS particulates was so small that the accuracy of the digital scale significantly affected the measured moisture change. Given the difficulties in surface drying of the particles and the large mass mismatch between the particles themselves and the apparatus used to contain them gave the impression that the measurements were not very accurate. Comparison of the measurements with published data for geofoam (Esch 1994; Duskov 1997; Aabøe and Frydenlund 2011) confirmed that the measurements were not very accurate.

## 3.2. KAOLIN

Due to heterogeneities and difficulties in sampling in-situ soils it is common to use manually prepared homogeneous soil specimens. Many researchers have used specimens prepared from kaolin for a variety of reasons. The advantages of kaolin were summarized by Rossato et al. (1992) as: (1) commercial availability; (2) relatively high permeability; (3) relatively large particle size which helped with optical studies; and (4) a large existing database of test data. Imerys (Kentucky-Tennessee Clay Co.) #6 Tile kaolin was used in this research as the parent soil type for the modified soil specimens since it is a well-documented material for geotechnical research, had high plasticity, and tended to exhibit well-defined dynamic properties at low strain levels.

### 3.2.1. Mineralogy.
Clay minerals are formed through a prolonged process from a variety of parent materials, including feldspars, micas, and limestone. The weathering process includes disintegration, oxidation, hydration, and leaching. Prolonged weathering at high temperatures, often in tropical conditions, with ferric iron parent rocks promotes the formation of minerals of the kaolinite group (Chen 1988). Kaolinite minerals tend to be much less expansive than other clay minerals such as illite or montmorillonite.

One of the most important properties of fine-grained soils is the mineralogical composition (Chen 1988). Silica sheets and alumina sheets combine to form the basic structural units of clay particles. Kaolinite is a two layer material having a single silica tetrahedral sheet joined by a single alumina octahedral sheet to form a "2-to-1" lattice structure.

In a clay-water-air system, the water within the clay is called adsorbed water; the water and ions within the clay lattice constitute the diffuse double layer. Both attractive and repulsive forces surround clay particles. The attractive forces promote the attraction of dipolar water molecules and include: a) electrostatic forces; and b) Van der Waal forces. Electrostatic forces result from the interaction between positively charged clay edges and negatively charged clay

surfaces. Van der Waal forces result from the mutual influence of electronic motion between atoms, and are the most important of the attractive forces (Seed et al. 1960). As more water molecules are attracted to a clay particle, a net repulsive force develops between the diffuse double layers of adjacent particles due to the dipolar nature of the water molecule (Mitchell 1993).

   **3.2.2. Classification.** Commercially available powdered kaolinite (#6 Tile) was purchased from L&R Specialties Inc., located in Nixa, Missouri. Four individual hydrometer tests (ASTM D422) were performed on samples of the kaolinite and results are shown in Figure 3.4. Results indicate that approximately 85% of the soil is clay-sized particles (defined as less than 2 μm) and the remaining material is silt-sized particles. All tested soils passed the #200 sieve. Two different tests were performed to measure the Atterberg Limits (ASTM D4318). The average liquid limit was approximately 56% and the average plastic limit was 27%, resulting in a plasticity index (PI) of 29. The kaolinite is considered non-active; as the activity approximately equaled 0.33; and had a specific gravity of 2.64. The measured activity agreed well with published data (Holtz and Kovacs 1981; Nelson and Miller 1992). The soil plotted slightly above the A-line on the plasticity chart (Figure 3.5) and is best classified as a CH/MH according to Unified Soil Classification System (USCS) and an A-7-6 soil according to the American Association of State Highway and Transportation Officials (AASHTO) classification system.
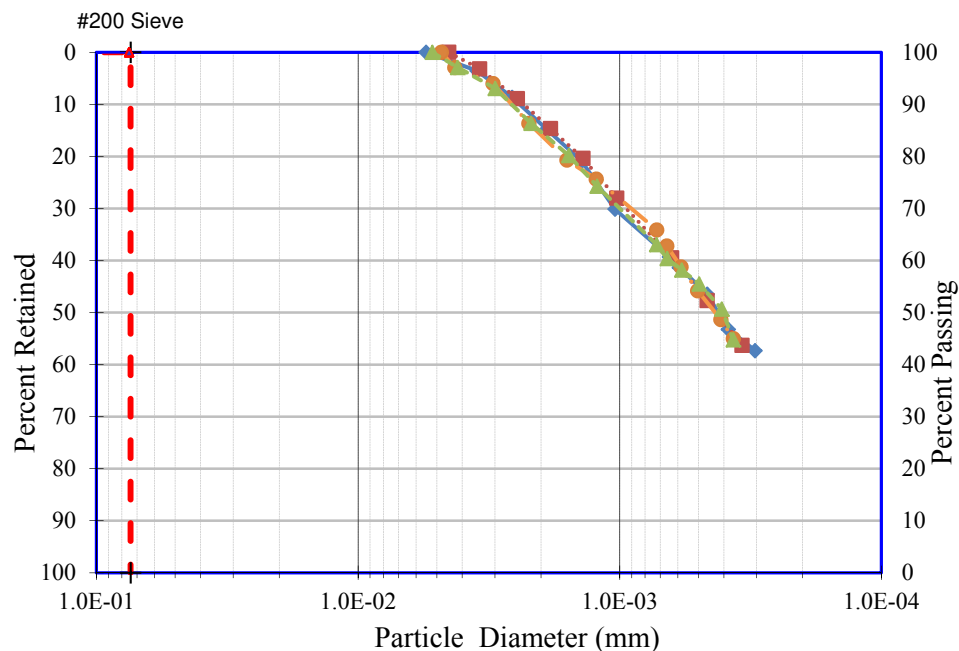


**Figure 3.4. Results of Hydrometer Analyses**
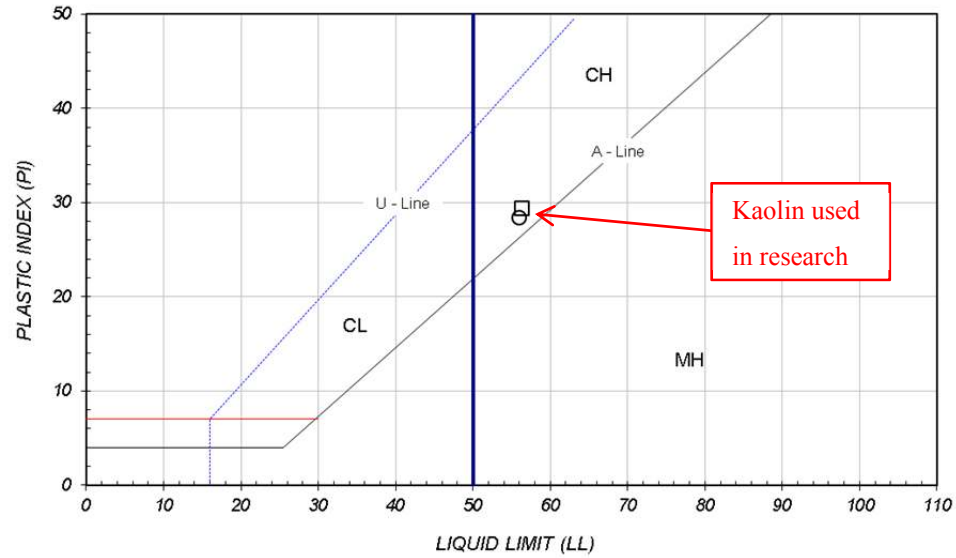
**Figure 3.5.  Kaolin plotted on Plasticity Chart**

### 3.3.    WATER

Distilled water was used throughout the experimental program.  The water originated from the universities' coal-fired power plant and was piped to the laboratory; a distance of approximately 0.5 km.

## 4. LABORATORY TEST PROGRAM

The following chapter discusses the laboratory equipment and techniques utilized throughout the testing program. Much of the underlying theory in regards to low-strain dynamic tests was introduced previously in Chapter 2.

### 4.1. SPECIMEN PREPARATION

Three different modified soil specimens were prepared in addition to a pure kaolin specimen that served as a baseline in which to analyze data trends. During the specimen preparation process, the kaolin and EPS particulates were mixed according to specific mass ratios. Table 4.1 lists the specimens prepared as part of this research program; mix ratios by volume are based on an EPS particulate mass density previously referenced in Table 3.3 of this report.

Table 4.1. Research Test Specimens

| Specimen ID | Measured Mix Ratio by Mass, % (Kaolin : EPS) | Calculated Mix Ratio by Volume, % (Kaolin : EPS) |
|---|---|---|
| Kaolin | n/a | n/a |
| Modified A | 99.5 : 0.5 | 79.4 : 20.6 |
| Modified B | 99.0 : 1.0 | 65.7 : 34.3 |
| Modified C | 98.5 : 1.5 | 55.9 : 44.1 |

Two different specimen preparation techniques were utilized during this research program: slurry consolidation and static undercompaction. The primary reason slurry consolidation techniques were used was to produce specimens without interlift density variations and an approximate 100% degree of saturation. Moist preparation techniques such as the static undercompaction methodology used in this research commonly develop density variations between lifts that can affect energy transmissions during pulse velocity testing and render it difficult to estimate material damping losses.

**4.1.1. Slurry Consolidated Specimens.** Approximately 300 mm diameter (11-¾ inch) large diameter specimens were prepared with kaolin and various amounts of EPS additives. The kaolin was moisture conditioned at approximately 150% of the measured liquid limit using distilled water and allowed to hydrate at least 24 hours prior to use. The appropriate water-to-

solids ratio was determined through a trial and error process; and the utilized ratio was deemed to provide a thick enough slurry to avoid floating the EPS particles to the surface during mechanical mixing but thin enough to be poured into the large diameter consolidometer.  Prior to pressing the slurry, the kaolin was mixed for approximately 10 minutes with a Hobart A-200 20-quart mixer on the low setting and pre-determined mass of EPS particulates were introduced into the mixture. The slurry was transferred to the large consolidometer and consolidated under one-dimensional conditions, as shown in Figure 4.1.  Vertical loads were initially applied with dead weights and after approximately 3 days loadings were transferred to a GeoTest S5720 strain controlled load frame set at the lowest strain rate of approximately 0.0254 mm/min (0.001 in/min).  The large diameter specimen was consolidated in the load frame until a constant vertical stress of approximately 150 kPa was obtained.  Drainage was provided at both the top and bottom of the specimen using needlepunched, non-woven polypropylene geotextile married to a porous HDPE filter board.



**Figure 4.1. Slurry Consolidation (98.5% Kaolin : 1.5% EPS)**

After reaching the target vertical stress on the specimen, the specimen was extruded from the consolidometer (Figure 4.2), cut into coarse blocks, wrapped in plastic cling wrap, enclosed in zip-lock bags, and stored in a moisture-controlled room for future testing. Each extruded specimen was between 175 – 200 mm (7 – 8 inches) in height. The samples were normally-consolidated in the large-diameter apparatus, but were likely to have become overconsolidated upon removal due to swelling and some intake of free water. When needed for unit element testing, the specimens were trimmed from the coarse pieces and the ends were discarded. Slurry specimens were utilized for the following tests: triaxial strength tests; resonant column tests; and pulse velocity tests.
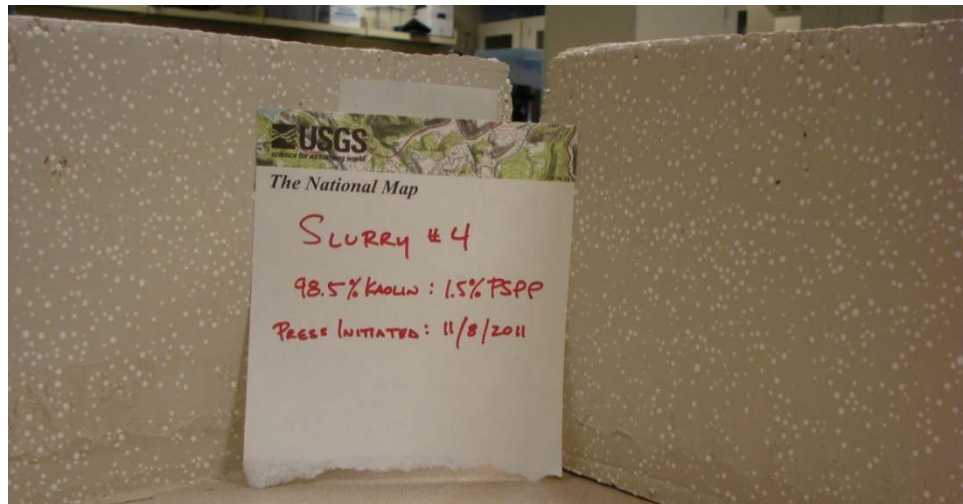


**Figure 4.2. Slurry Consolidated Specimen**

**4.1.2. Compacted Specimens.** Compacted specimens were prepared using a 71 mm diameter (2.8-inch) cylindrical, vertically split miter box mold modified with a top collar for additional height. Soil, EPS particulates, and water were mixed at the appropriate mass ratios and allowed to hydrate for at least 24 hours prior to pressing. Specimens were prepared in five lifts using the undercompaction method (Ladd 1978) and statically pressed in a triaxial load frame under a constant rate of strain of 5 mm/min (0.2 in/min) to the appropriate lift height, as shown in Figure 4.3.

Upon completion, the split mold was removed and the specimen was measured and weighed to determine the density. It was noted that during remolding some segregation of the

EPS particulates occurred while transferring the moist mixture to the mold using a funnel. The particles tended to move towards the top and sides of the placed lifts. Care was taken during preparation to thoroughly mix each lift after placing in the mold to reduce the segregation of soil and EPS.
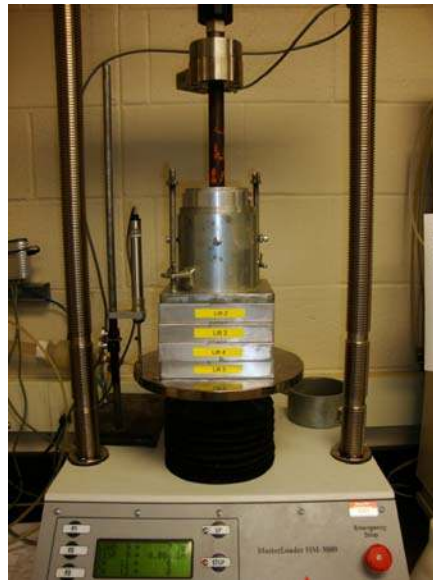


**Figure 4.3. Static Undercompaction of Specimens**

     **4.1.3. Specimen Uniformity.** To ensure that both slurry consolidated and compacted specimens were uniform some specimens were cut into sections, the mass and geometric dimensions were obtained, and each section was dried to determine the moisture content. Two different slurry consolidated specimens were fine-trimmed to dimensions similar to those tested in triaxial compression and further dissected to determine uniformity. Results of the measurements to ensure specimen uniformity are shown in Table 4.2.

     The measured water contents in the middle portions of the slurry consolidated specimens were greater than the top or bottom of the specimen which affected the measured dry unit weight. This phenomenon was expected given the large-diameter consolidometer in which the specimens were prepared provided drainage at the top and bottom of the specimens.

**Table 4.2. Measurements to Confirm Specimen Uniformity**

| Preparation Technique | Mix Ratio (by mass) | Section | Dia. (cm) | Length (cm) | Vol. (cm$^3$) | Mass (g) | $\omega$ (%) | $\gamma_d$ (kN/m$^3$) |
|---|---|---|---|---|---|---|---|---|
| Slurry Consolidation | 99.5 : 0.5 | Top | 4.84 | 3.41 | 62.88 | 99.87 | 0.396 | 11.2 |
| | | Middle | 4.91 | 3.60 | 68.26 | 105.21 | 0.412 | 10.7 |
| | | Bottom | 4.81 | 3.17 | 57.46 | 92.98 | 0.401 | 11.3 |
| | 99 : 1 | Top | 5.08 | 3.77 | 76.31 | 103.34 | 0.408 | 9.4 |
| | | Middle | 5.13 | 3.97 | 82.13 | 102.02 | 0.425 | 8.6 |
| | | Bottom | 5.11 | 3.11 | 63.65 | 91.25 | 0.413 | 10.0 |
| Compacted | 99.5 : 0.5 | Top | ** | ** | ** | ** | 0.270 | ** |
| | | Middle | ** | ** | ** | ** | 0.271 | ** |
| | | Bottom | ** | ** | ** | ** | 0.273 | ** |

One compacted specimen was tested for uniformity after undergoing pulse velocity testing, as the dynamic test did not significantly alter the moisture content or dimensions of the specimen. There were difficulties cutting the compacted specimens into smaller sections as the edges of each section tended to crumble during the cutting process. Meaningful geometric dimensions could not be measured on the cut sections, but material from each section was used to obtain moisture contents. Results indicated that the moisture content of the compacted specimen were much more uniform throughout the specimen than the slurry consolidated specimens which would be expected given the controlled manner in which these specimens were prepared. Given the difficulty in directly measuring the density of the compacted specimens, the majority of tests that utilized these specimens were performed in duplicate to critically assess specimen variation from subsequent test measurements.

## 4.2. COMPACTION TESTING

Compaction tests measure the relationship between specimen unit weight, or density, and moisture content. The results are used to identify the moisture content that generates the maximum dry density under a specific compacted effort, for a given soil, typically called the optimum moisture content. Laboratory moisture-density relationships were developed for pure kaolin and kaolin-EPS particulate mixtures using standard compactive effort (ASTM D698). A 101.5 mm (4-inch) diameter mold was utilized for all tests. Air-dry powdered kaolin and EPS particulates were manually mixed with distilled water, sealed in air-tight containers, and allowed to hydrate for at least 24 hours prior to compaction. An automatic compaction hammer

manufactured by Ploog Engineering Company was utilized for all tests. Final moisture content determinations used the entire compacted specimen.

## 4.3.    COMPRESSION – SWELL TESTING

Measurements of the stress-strain relationship in compressible soils often use the one-dimensional consolidometer. The compression curve realized for a soil specimen is a relationship between the applied vertical stress and the volume change in the specimen. Various test procedures have been developed and are in use to measure the compression curve for soils. The ASTM procedure (ASTM D4546) contains three separate methodologies; termed Method A, Method B, and Method C. In addition, another procedure was developed along the eastern slope of the Rocky Mountains to deal with regional overconsolidated claystone and shale and is called the Denver swell test. (Chao et al. 2011) All tests can be used to determine the swell pressure defined as the minimum stress required to prevent swelling upon inundation and the percent free swell defined as the percent swell upon inundation with no significant vertical pressure.

One-dimensional compression and swell tests for compacted specimens of pure kaolin and kaolin-EPS particulate mixtures were performed using the wetting-after-loading procedure (Method A) described in ASTM D4546. This particular methodology has also been called the "swell under load" procedure (Feng et al. 1998). The procedure attempts to mimic a typical stress scenario a soil could experience in the field; where after construction significant time could pass prior to exposure to water. The test was utilized for this research project to determine if the addition of EPS particulates significantly affected the measured compression and swell response of a compacted specimen as defined by the swell pressure and percent free swell.

The general purpose of Method A is to determine the magnitude of compression and swell of multiple soil specimens under different surcharge loadings. Surcharge loadings are typically termed the inundation pressure. Since Method A utilizes multiple specimens, it is a good choice for reconstituted specimens where specimen uniformity can be assured (Chao et al. 2011). According to ASTM D4546, the inundation pressure is applied to the specimen for a maximum of one hour. This amount of time was deemed sufficient for the specimens to reach equilibrium under the respective loads. After the initial dry compression, each sample is inundated and the deformation is monitored. Typical test results for multiple specimens tested according to Method A are shown in Figure 4.4.
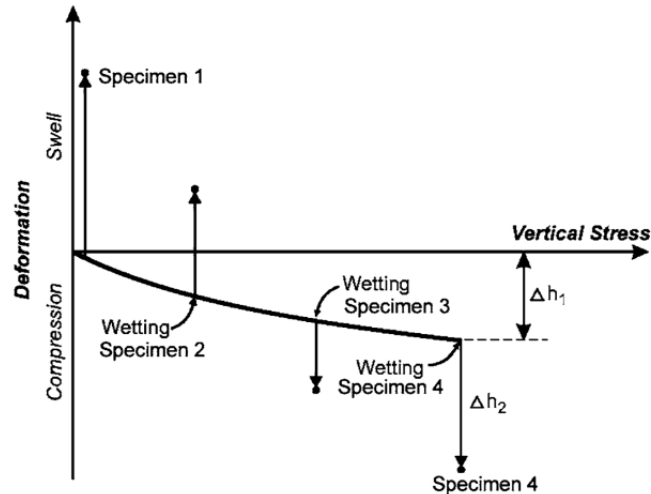
**Figure 4.4.  Compression Curve from Method A (ASTM D4546)**

Compacted specimens were utilized for compression/swell tests.  Soil mixtures were prepared at the optimum moisture content, determined according to the procedures discussed in Section 4.2, and allowed to hydrate at least 24 hours prior to compaction.  Prepared soils were compacted directly into 63.5 mm (2.5-inch) diameter consolidation rings, as shown in Figure 4.5. Test specimens were compacted to 90% maximum dry density in one lift using a rubber mallet to achieve the desired density.  Specimens were approximately 19.1 mm (0.75 inch) in height.  The finished surface was set below the ring perimeter to ensure only axial deformation within the laterally constrained ring occurred upon swelling.  The consolidation ring and specimens were set into a floating-ring consolidation chamber between porous stones without filter paper and a 1 kPa (20 lb/ft$^2$) seating load was applied prior to the application of the inundation pressure.

The specimens were statically loaded under a constant stress until stable vertical deformations were obtained, always less than 60 minutes, after which the specimen was inundated with distilled water.  Six different inundation pressures were used:  1 kPa (20 lb/ft$^2$), 23.9 kPa (0.25 tons/ft$^2$), 47.9 kPa (0.5 tons/ft$^2$), 95.8 kPa (1.25 tons/ft$^2$), 239.4 (2.5 tons/ft$^2$), and 478.8 (5.0 tons/ft$^2$) vertical stress.  The lowest inundation pressure represented free swell conditions.  Plastic wrap was placed over the specimen during testing to avoid moisture loss in the specimen.  Deformations were systematically tracked at time intervals typical of a consolidation test after inundation.  Upon completion of the test, final height measurements and the final moisture content were determined.  A lever-arm consolidometer was used to apply loadings and vertical deformations were automatically monitored with a digital LVDT and data

acquisition system. The compressibility of the loading apparatus was not determined for these tests as the data was utilized to determine general trends rather than actual design values.
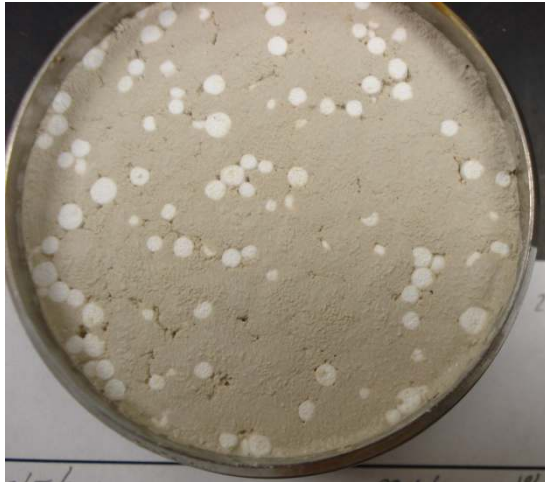


(a)  63.5 mm diam. consolidation ring          (b) Compaction mold placed over consol. ring

**Figure 4.5.  Prepared Specimen for Compression – Swell Testing (99% Kaolin : 1% EPS)**

## 4.4.     TRIAXIAL STRENGTH TESTING

Both unconsolidated-undrained (UU) and isotropically consolidated-undrained (CU) triaxial compression tests were performed during the testing program. The UU test attempts to model the response of a soil deposit to a very rapid loading and prior to the onset of subsequent consolidation and drainage. One problem with the UU test is that the effective stress of the soil remains unknown throughout the test. The CU test is used to determine the strength and stress-strain relationship of a soil sample that is initially saturated and consolidated, and where drainage is restricted during shearing. The test attempts to model the response of a soil deposit to a rapid loading and prior to the onset of subsequent consolidation and drainage. The procedures outlined in ASTM D2850 and ASTM D4767 were generally followed and deviations from the procedures are noted.

UU testing utilized both slurry consolidated and compacted specimens while CU testing utilized slurry specimens only. Compacted specimens targeted both 90% and 95% relative compaction, but given the friction along the sides of the mold realized densities were approximately 88% and 94% relative compaction. Slurry specimens were obtained from coarse sections cut from the large slurry consolidated specimen. Individual samples were trimmed into

to an approximate 50 mm (2.0-inch) diameter by 100 mm (4.0-inch) tall cylindrical sample. Specimens were trimmed with the vertical axis parallel to the consolidation direction in the consolidometer. The trimmings were used to determine the initial moisture content for each specimen. Diameter and height measurements were taken at three separate locations and the specimen mass was recorded. After trimming was completed the samples were assembled with the appropriate end caps, filter paper, porous stone, inserted into a latex membrane, and mounted into a compression chamber. Filter papers, porous stones, and the membrane were de-aired and saturated prior to use. Compacted specimens did not require further trimming after remolding and were assembled and mounted in the triaxial chamber in a similar manner as the slurry specimens.

Since drainage and consolidation are not allowed during the UU test, the drainage valves were closed and the chamber pressure was increased to the appropriate cell pressure. Slurry specimens were tested under a cell pressure of 172, 344, and 690 kPa (25, 50, and 100 psi) and compacted specimens were tested at a cell pressure of 69, 172, and 344 kPa (10, 25, and 50 psi).

A uniaxial mechanical compression load frame (Humbdoldt Master Loader HM-3000) was used to shear the specimens. Two different load frames were used throughout the testing program; local laboratory designations "Devices 1" and "Device 2", respectively. A 1000-lb Strainsert universal load cell (S/N 03319-1) was calibrated and mounted on Device 1 and a 2500-lb Strainsert universal load cell (S/N 05655-1) was calibrated and mounted on Device 2. The vertical compression was completed under a constant strain rate of 0.5% per minute, until approximately 15% vertical strain had been attained. Vertical deformations were monitored with an LVDT and vertical loads were monitored with a load cell mounted outside of the pressurized chamber. Recorded data was corrected for the influence of the confining pressure on the load cell, for membrane stiffness, and for the increase in sample area with increasing strain.

Specimens that were tested in CU conditions were backsaturated maintaining a stress difference of 34.5 kPa (5 psi) between the backpressure and the cell pressure. Specimens were assumed to be saturated once the pore pressure B-value exceeded 0.95. B-values were checked after each stage of backpressure saturation, and if the required B-value was not obtained, both the backpressure and cell pressure were increased by 69 kPa (10 psi). Once saturation had been achieved, the specimens were consolidated at effective stresses of 172, 344, and 690 kPa (25, 50, and 100 psi) and drainage from the specimen was monitored using a burrette. The consolidation process typically continued for approximately 1 day. Once primary consolidation was complete, the drainage lines were closed and the sample was sheared. Shearing rates were based on the recorded consolidation data, as defined in ASTM D4767. Shearing was completed at a slow rate

so that equalization of pore pressures occurred throughout the specimen during testing; as pore pressures were measured only at the base of the specimen.

## 4.5. RESONANT COLUMN TESTING

**4.5.1. General.** All RC tests performed for this research utilized a resonant column – torsional shear system manufactured by Geotechnical Consulting and Testing Systems (GCTS). This equipment utilizes an electric motor to apply a cyclic torsional load to a fixed-free specimen, as shown in Figure 4.6. The servo motor was manufactured by MCG (Model No. OB23002) and driven with a sinusoidal varying voltage. The advantage of using a sinusoidal voltage is that the signal produced has one dominant frequency. Testing initiated with a sweep of input frequencies at a constant excitation voltage. During the frequency sweep, the shear deformation imposed on the specimen was not constant for all frequencies. In general, most RC testing was performed at frequencies less than 200 Hz, which agreed well with the range of 20 to 260 Hz referenced by Hardin and Drnevich (1972a). During the frequency sweep tests the step between tested frequencies was 0.25 Hz, and each tested frequency experienced 20 cycles of torsional loading to condition and stimulate the specimen and an additional 5 cycles of motion in which movements were recorded by the data acquisition system prior to stepping to the next, higher frequency. After the frequency sweep was completed, the system returned to the resonant frequency, torsionally loaded the specimen for a few cycles of motion, and the power to the motor was removed. The free vibration decay of motion was subsequently recorded with the accelerometer. Rotational deformations were monitored during testing with an accelerometer attached near the excitation force and vertical deformations were monitored with a LVDT.
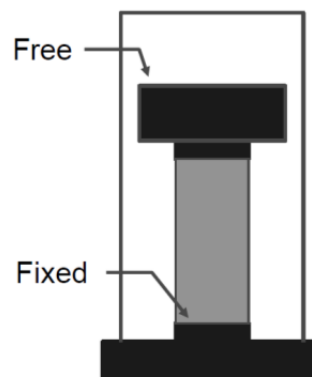


**Figure 4.6. Fixed – Free Resonant Column Apparatus (Drnevich, personal file)**

During testing, essentially only two quantities were monitored and measured: (1) the power sent to the drive system and (2) the output of the accelerometer. The power to the drive system was used to determine the torsional force applied to the specimen. The output from the accelerometer was double integrated to determine the induced deformation in the sample. The definition of resonance depends on apparatus and specimen characteristics. For the equipment utilized in this research, resonance was defined as the frequency which generated the maximum shear strain during a sweep of relevant frequencies, as shown in Figure 4.7.

Drnevich (1985) discussed using the maximum amplitude to define the resonant frequency and concluded that for systems with low damping and at low amplitude strains this procedure gives fairly accurate results, but errors increased at larger strains since the underlying equations are based on phase relationships between the applied torque and resulting motion in the specimen.

**4.5.2. Equipment Calibration.** A load calibration procedure was completed to determine the relationship between the power sent to the servo motor and the strains induced by the motor on the test specimen. The load calibration was performed by testing an aluminum calibration specimen in the RC apparatus and mounting a torque load cell to the electric motor drive shaft. A Tovey RT-25 torque load cell was used. The calibration procedure defined the torque output to a relative percent full scale (PFS) of the motor. A torque conversion factor of 0.0373 N-m / PFS (0.33 lb-in / PFS) was determined. After the load calibration process the torque load cell was removed for routine testing.
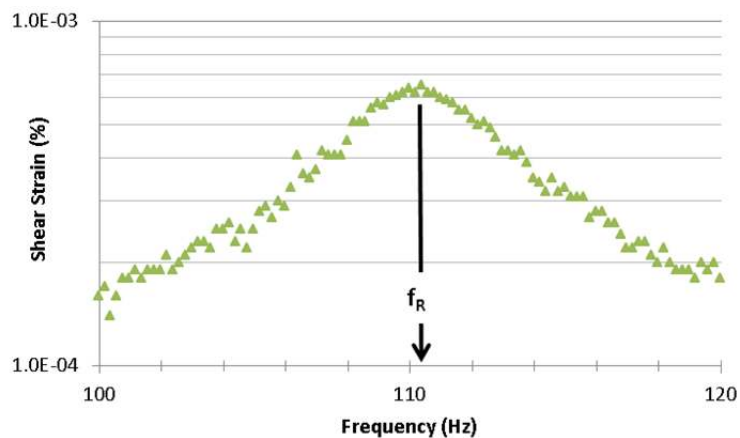


**Figure 4.7. Frequency Response of RC Test**
**(98.5% Kaolin : 1.5% EPS @ Torque = 0.0112 N-m)**

Additional calibration procedures were required to determine the stiffness and damping of the resonant column equipment and pressure chamber. The procedure utilized a calibration rod made from a 6061-T6 tempered aluminum alloy which was considered to have a constant torsional stiffness and negligible material damping. Simplifying the servo motor of the RC apparatus as a torsional pendulum under harmonic motion and the aluminum rod as a torsional spring, the resonant frequency of the first mode of vibration is,

$$\omega_1 = \sqrt{\frac{k}{I_{System} + I_{rod}}}$$

(4. 1)

Where, k is the torsional stiffness of the aluminum rod, $I_{System}$ is the mass moment of inertia of the drive system and chamber, and $I_{rod}$ is the moment of inertia of the aluminum rod. The resonant frequency of the aluminum rod can be adjusted by adding weights to the top of the aluminum rod yielding a modified equation as,

$$\omega_2 = \sqrt{\frac{k}{I_{System} + I_{rod} + I_{mass}}}$$

(4. 2)

Where, $I_{mass}$ is the moment of inertia of the added mass and is based on its geometry and mass. The calibration procedure was performed by applying a frequency sweep to the aluminum rod with and without the added mass. The applied force was determined through a trial and error process to produce a signal that did not saturate the attached accelerometer. The frequency sweeps define $\omega_1$ and $\omega_2$, and calibration tests measured resonant frequencies of 76.5 Hz and 62.0 Hz, respectively. $I_{System}$ was determined by solving equation 4.1 and equation 4.2 as,

$$I_{System} = \frac{\left(I_{rod} + I_{mass}\right)\omega_2^2 - I_{rod}\omega_1^2}{\omega_1^2 - \omega_2^2}$$

(4. 3)

The determined moment of inertia of the resonant column system was 822.4 kg – mm$^2$. Since the specimen top cap was not utilized in the calibration process, this needed to be added to the calculated moment of inertia, and the resulting final $I_{system}$ was 1036.4 kg – mm$^2$. Ultimately the determined value of $I_{system}$ was used in Equation 2.28 to determine the shear velocity in a test specimen.

The data from the calibration tests on the aluminum rod was also used to determine the inherent damping of the RC system. The measured damping determined from the free-vibrational decay data were 1.04% and 0.43% without and with the added mass, respectively. The measured damping determined using the half-power bandwidth method applied to the frequency sweep data were 3.68% and 2.41% without and with the added mass, respectively. Discussions with the GCTS technical support staff (Peter Goguen, GCTS personal communication) could not definitively identify if the measured value with the added mass or without should be used as the calibration value. As a result an average of the two values was used to reduce measured damping values from actual test specimens.

**4.5.3. Experimental Procedure.** Resonant column testing was performed on both slurry consolidated and compacted specimens. Specimen dimensions were approximately 71 mm diameter by 142 mm height. Compacted specimens were allowed to stabilize for approximately 24 hours after remolding prior to RC testing. Specimens were directly mounted on textured bottom and top platens and enclosed in a hydrated latex membrane to reduce moisture loss during testing. Changes in height of the specimen upon increases in chamber pressure were monitored with a LVDT.

The specimens and RC equipment were enclosed in a triaxial chamber and air pressure was used for specimen confinement. Initially the use of air pressure was thought to significantly affect the moisture content of specimens throughout the test program, and the chamber was partially filled with a fluid. Discussion with the manufacturer (Peter Goguen, GCTS personal communication) recommended against the use of water as a confining fluid as the humidity in the chamber could potentially damage the electric servo motor. Mineral oil was also tried but it was determined that latex membranes quickly deteriorate upon contact with this oil. Silicon oil was found to not react with the membranes, but ultimately the loss in moisture of tested specimens was not significant enough to necessitate the use of a confining liquid.

A multistage testing approach was used for all specimens tested in an effort to extract the behavior of the soils to increasing strain levels as well as increased confining pressures. To study the effect of confining pressure on the dynamic properties of the modified soils, the tests were conducted at confining pressure from 10 to 200 kPa (1.5 – 29 lb/in$^2$). Specimens were initially tested with only a small seating pressure of 10 kPa applied to the chamber to ensure good contact between the motor and specimen. Multiple measurements were obtained at each confining pressure as the voltage sent to the drive-motor was subsequently increased. Typically strains ranging from approximately $10^{-4}$ to $10^{-2}$ percent were realized for each specimen at each individual confining pressure. Drainage was not allowed during testing. After a round of testing

was completed, the chamber pressure was increased and the specimen was allowed to compress for at least 15 minutes prior to additional testing based on procedures used by Amini (1995). In general the entire multi-stage testing routine from mounting of the specimen to dismounting took approximately 3 hours. The final moisture content was determined for all tested specimens and results indicated that moisture loss during testing was less than 1%.

### 4.6.    PULSE VELOCITY TESTING

**4.6.1.    General.**   Two different pulse tests were used to measure the propagation of waves in test specimens: (1) bender element test and (2) ultrasonic pulse velocity test. Pulse velocity testing was primarily performed on compacted soil. Slurry specimens were not tested with pulse velocity techniques because of two main reasons: (1) the variability in specimen density/void ratio and dynamic soil properties from the resonant column tests indicated that the compacted specimens were better able to identify the influence of EPS content; and (2) the potential use of the EPS modified soils was more applicable to a placed fill and thus compacted specimens would provide a more realistic model of potential field installations. Attempts were made to measure the transmission of both P-waves and S-waves. Measurements of P-wave and S-wave velocity were used to determine soil moduli according to Equations 2.2 and Equation 2.5, respectively.

**4.6.2.    Bender Element Testing.**  Bender elements are utilized in geotechnical testing to generate waves within soils. Traditionally, bender elements have been used to induce and receive waves in laboratory specimens at low strain levels, and they can be installed to produce either P-waves or S-waves. Bender elements are piezoelectric wafers that are used in combination with a power source, function generator and signal receiver to measure the wave velocity and estimate the soil moduli at low strain levels.

**4.6.2.1. Transducer production.**  Large pieces of X-poled and Y-poled bender elements of dimensions 32 mm x 64 mm were machined down to sizes typically used in geotechnical applications using equipment from the Materials Science research group at Missouri S&T. The recommended size for laboratory testing is approximately 12mm x 8mm x 0.6mm; assuming that the average particle diameter is less than 1mm (Santamarina 2001). On average sixteen bender elements could be realized from a large sheet. The process of cutting the piezoelectric elements initially utilized a Chevalier FSG-618 grinder with an attached diamond cutting blade with a 1.3 mm (50 mil) thickness, but it was quickly determined that this cutting blade caused extensive cracking along the edges of the piezoelectric material. Final cutting was realized using an Aremco 5200 dicing saw with a 0.15 mm (6 mil) thick diamond cutting blade with a low

concentration, medium mesh grit obtained from UKAM Industrial Tools. The Aremco saw requires a 3" diameter cutting blade with a 5/8" arbor size. The thinner blade resulted in no cracking along the edges of the piezoelectric material. Grinding of the piezoelectric material to expose the metallic center electrode was realized with the Chavalier surface grinder with a 120-grit grinding wheel, but grinding was also performed manually with a precision file set. All machining processes used in this research are detailed in the Appendix.

After the bender elements were cut to the appropriate size and the center electrode was exposed, the elements were wired according to the recommendations of Lings and Greening (2001) to operate as bender-extenders. The signal wires used through all electrical connections were 3-conductor shielded cables to reduce electrical leaks and electromagnetic noise. The elements were waterproofed with at least five coats of polyurethane after wiring. The polyurethane also helped protect and reinforce the elements and solder locations.

Elements must be properly insulated to prevent electrical short circuits and cross-talk. Cross-talk is an electromagnetic phenomenon where the source and receiving transducers are coupled (Lee and Santamarina 2005). Cross-talk results in the receiver element recording the transmitted signal almost instantaneously after the application of a voltage, as show in Figure 4.8.
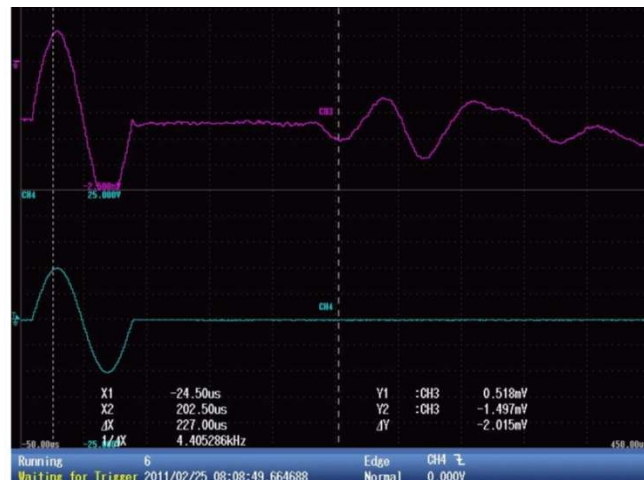


**Figure 4.8.  Cross-Talk Phenomena**

**(Cyan = Transmitted Signal ; Magenta = Received Signal)**

To prevent cross-talk between the transmitter and receiver the elements were wrapped in teflon tape, the shielding ground wire from the cables was inserted over the tape, and the entire

element was wrapped in aluminum tape.  The grounded aluminum tape essentially created a faraday cage around the element.  A final coat of polyurethane was applied over the aluminum tape.  The entire cross-sectional detail of a prepared bender element is shown in Figure 4.9.
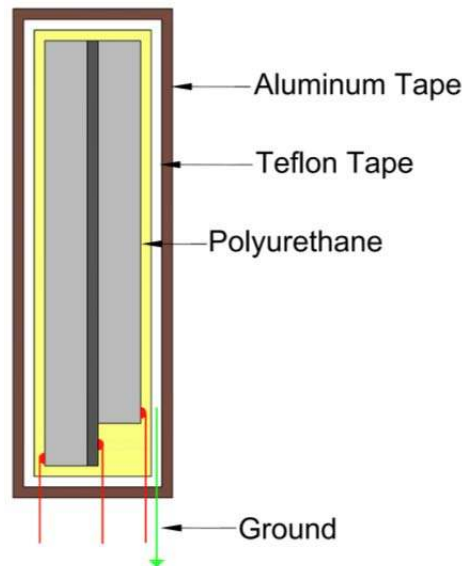


**Figure 4.9.  Bender Element Detail**

**4.6.2.2. Peripheral electronics.**   The various components of the bender element test system are summarized in Table 4.3 and shown in Figure 4.10.  In addition to the Yokogawa oscilloscope, two other oscilloscopes were evaluated to monitor and record the wave travel times. First an Agilent 54622A dual channel scope was utilized, but it was determined that the 8-bit A/D converter was not sufficient to accurately access the wave arrivals.   This concurs with observations of Leong et al. (2004) who ultimately recommended a 12-bit A/D converter at a minimum.  A Picoscope model #4227 PC-based oscilloscope was also utilized but the voltage sensitivity was not sufficient, especially for weak signals typical of P-wave transmission in bender element tests.  The Picoscope records were digitally amplified after acquisition but this process also amplified the background noise rendering the record difficult to interpret.   An additional disadvantage of the Picoscope equipment is that it did not have the capabilities to average repeated signals to improve the signal-to-noise ratio.

**Table 4.3.  Peripheral Electronics for Pulse Velocity Testing**

| Equipment | Manufacturer | Model |
|---|---|---|
| Bender Element Transducers | Piezo Systems, Inc. | T220-A4-503 (X and Y) |
| Ultrasonic Transducers | GCTS Testing Systems | ULT-100 |
| Signal Generator | Hewlett Packard / Agilent | 33120A |
| Amplifier | Piezo Systems, Inc. | EPA-104 |
| Oscilloscope | Yokogawa | DL850 + 701250 module |
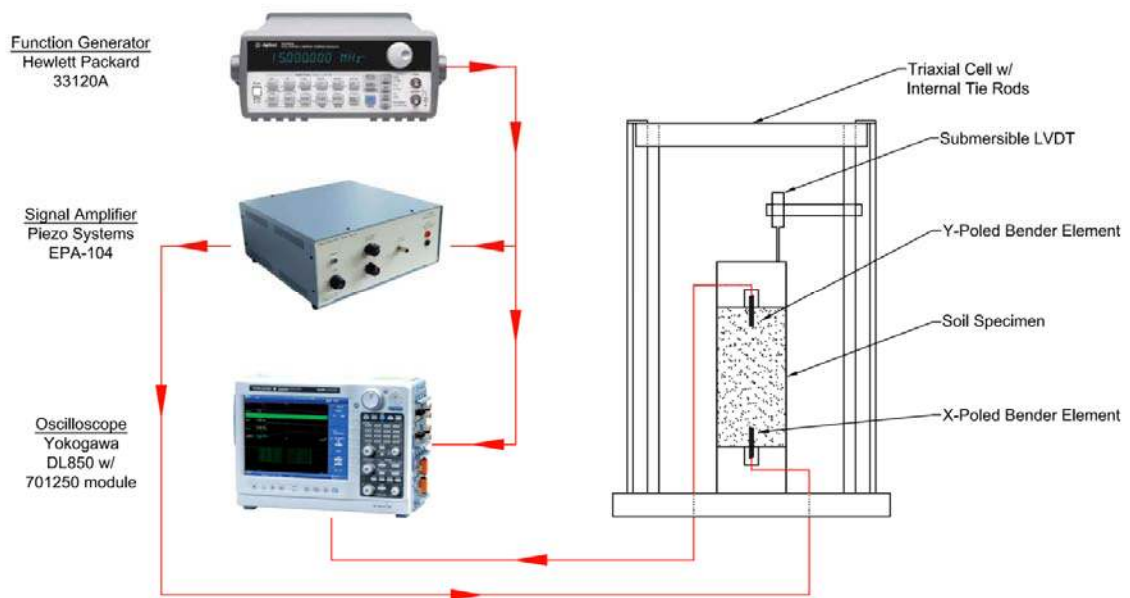


**Figure 4.10.  Bender Element Test System**

**4.6.2.3. Equipment calibration.**  The time delay of the electric signal from the source (signal generator) to the actuation of the bender element needed to be determined and subtracted from measured travel time of wave transmissions.  The calibration process involved manually holding the cantilevered bender elements together and recording the transmission of both P-waves and S-waves, as shown in Figure 4.11.  The time lag between the transmission of the signal and the reception of the signal was determined as 4.2 μsec and 3.8 μsec for P-waves and S-waves, respectively.  The time delay was removed from all subsequent travel time determinations.
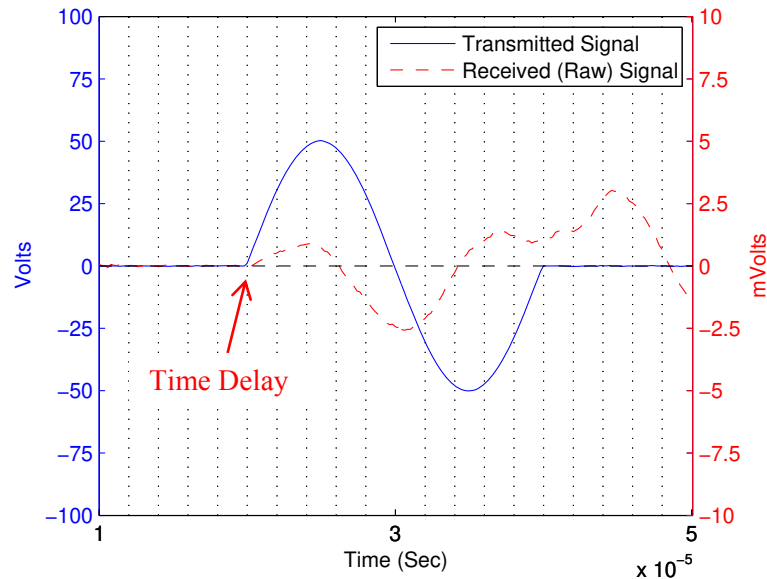
**Figure 4.11. Tip-to-Tip Calibration of P-wave Transmission**

It is commonly recommended that initially a broad frequency pulse (i.e. square waveform) be transmitted through each test specimen and the received signal power spectrum analyzed to determine the dominant frequency of the wave signature. The frequency of the transmitted wave is then adjusted to match the dominant frequency and a sine waveform is used (Yamashita et al. 2009). Alternately multiple wave transmission tests can be performed at a range of frequencies that bracket the dominant frequency. Calibration tests with pure kaolin specimens showed that the dominant frequency changed between specimens and thus was influenced by the installation of the transducers into the soil. The transducer's behavior is different when operating in a free space as compared to when they are partially retrained and coupled to a test specimen. It was also noted that the dominant frequency was a function of confining pressure and thus changed during different stages of the test program for each specimen. Based on these results it was best to perform multiple wave transmissions at a variety of frequencies and then determine the appropriate travel time of the wave pulse while considering measurements from all the recorded wave signatures.

    **4.6.2.4. Bender element testing program.** The bender element testing program utilized as part of this research project is summarized as follows:

    i.    A single, sinusoidal wave pulse was generated using the function generator. The sinusoidal pulse was transmitted at a range of frequencies. In general S-wave pulses were transmitted at frequencies of 5, 10, 20 and 40 kHz and P-wave pulses were

transmitted at frequencies of 5, 10, and 20 kHz. The pulse signal from the signal generator was directly connected to the digitizing oscilloscope through a coaxial BNC tee connection and used as a trigger for the data recorder.

ii. Maximum output of the function generator was limited to ±10 volts. The signal from the function generator was fed into a power amplifier which raised the voltage up to ±100 volts. Through a trial-and-error process, this voltage was deemed sufficient to drive the bender elements so that enough energy was imparted on the specimen.

iii. The amplified signal was fed to the bender element transmitter mounted in the specimen end platen.

iv. The bender element transmitter converted the electrical pulse into a small amplitude mechanical pulse based on its piezoelectric properties.

v. The bender element receiver converted the mechanical energy that propagated through the specimen into an electrical signal that was monitored with the oscilloscope. Received waves were recorded with an oscilloscope utilizing a 12-bit vertical resolution A/D convertor at a sampling rate of 1 MS/sec and recorded an approximate $1000 - 2000$ μsec record.

vi. The entire routine was repeated approximately 100 times, with a 1 second delay between triggered signals. The oscilloscope averaged all the recorded waveforms and generated one single "stacked" waveform for archiving and analysis.

Testing of a single bender element specimen required approximately two days for material preparation and specimen remolding and approximately 1 hour for each stage of pulse velocity testing. Typically five different stages of testing were completed for each specimen at increasing confining pressures, and thus all pulse transmissions were completed in approximately five hours for each specimen. Overall, approximately three days were required in total for each specimen.

**4.6.3. Ultrasonic Pulse Velocity Testing.** The ultrasonic pulse velocity tests utilize piezoelectric crystals to convert electrical signals to mechanical waves. The through transmission method of ultrasonic testing utilizes two transducers oriented on opposite sides of the test specimen; one for signal generation and one for signal reception. Only transit time of the propagating wave is measured. The ultrasonic equipment utilized in this research was based on the through transmission mode of ultrasonic testing and relied on specialty end platens fitted with piezoelectric crystals.

**4.6.3.1. Ultrasonic transducers.**    The ultrasonic crystals used in this research were housed within 70 mm diameter specimen end platens with a stiff diaphragm separating the crystal from the specimen, and they relied on transmission of waves through the platen face.  The platens contain one central crystal capable of generating compressional waves and six additional crystals orientated around the circumference of the platen capable of generating shear waves (Figure 4.12).   The piezoelectric crystals strain (vertically for P-wave transmissions and horizontally for S-wave transmissions) when a voltage pulse is applied and generate a voltage when they are mechanically strained; thus both platens can be utilized as a transmitter or receiver.   The transducers were constructed and sealed for installation in a saturated triaxial chamber. One reoccurring criticism of ultrasonic testing is that the piezoelectric crystals are not in direct contact with the soil specimen and thus weak signals are common.



**Figure 4.12.  Piezoelectric Crystals Mounted in Specimen End Platens**

**4.6.3.2. Peripheral electronics.**  The ultrasonic transducers utilized in this research were originally part of an overall test system that included a pulse generator and receiver as well as a data acquisition system.  The system was essentially a "black box" with user control over the type of wave generated and minimal control over the test data.  The system could be improved with additional control of the applied signal sent to the ultrasonic transducers and the data acquisition. A modified wire extension was produced so a generic signal generator could control the ultrasonic end platens, as shown in Figure 4.13.  The wire extension consisted of a female multi-pin connector (Hirose HRS HR10-7P-4S73) with an attached multi-wire shielded cable.  The red line was connected to the S-wave piezoelectric crystals, the black line was connected to the P-wave piezoelectric crystal, and the green and white wires were connected to the ground wire on

the ultrasonic platens. The other components of the modified ultrasonic test system are shown in Figure 4.14 and listed in Table 4.3.
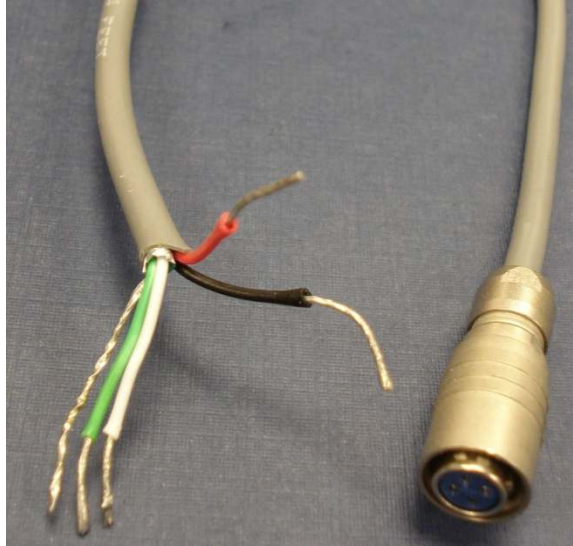


**Figure 4.13.  Modified Wire Extension for Ultrasonic Platens**

 

**4.6.3.3. Equipment calibration.** The manufacturing process of the piezoelectric crystals and the bonding to the platen define the dominant frequency.  The shear and compressional piezoelectric crystals have natural frequencies between 200 and 1000 kHz during isolated operation (Leong et al. 2004).  The materials used to cement the crystals to specimen end platens and attaching the transducers to a stiff diaphragm that separates them from the tested specimens alter the dominant frequency, and thus one could expect the dominant frequency to vary between different test systems.  As the manufacturer of the ultrasonic platens did not specify the dominant frequency of the end platens, this was determined with a calibration test.  The calibration process involved obtaining measurements with the two platens pressed against each other; a "face-to-face" test.  A ±50V low frequency square wave pulse signal was applied to the transmitting ultrasonic transducers and the received signal was recorded and analyzed.  A second test was performed by sending the pulse signal to the opposite transducer.  Square waves were utilized as they are broad spectrum signals and contain both low and high frequency content.
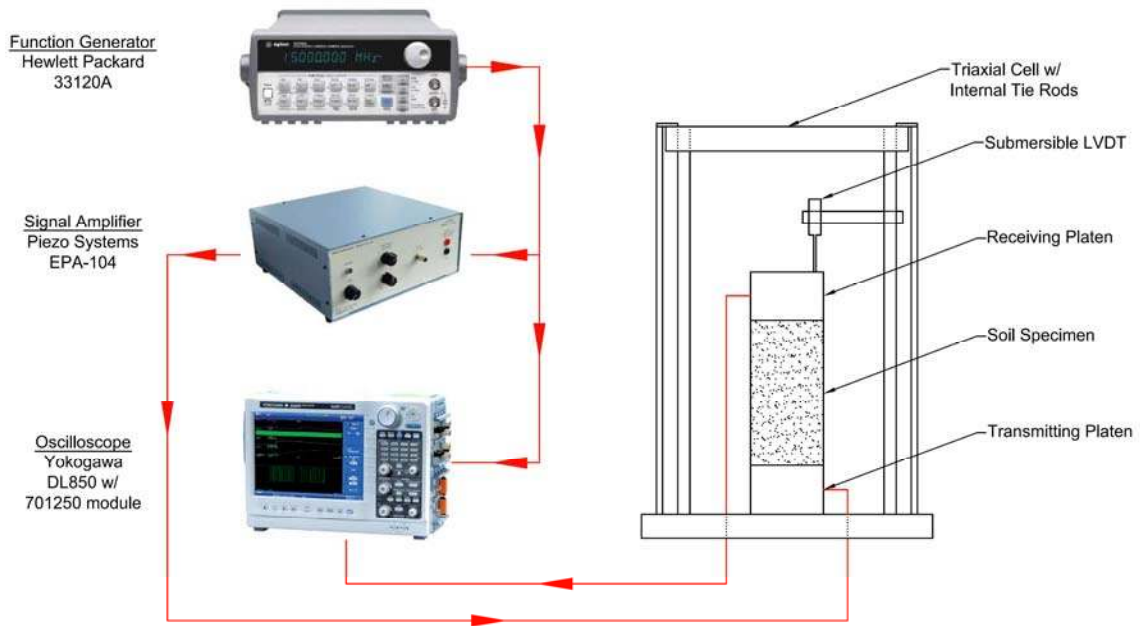
**Figure 4.14.  Ultrasonic Test System**

The frequency spectra of the compressional and shear wave signals from the face-to-face calibration tests are show in Figure 4.15 and Figure 4.16.  The frequency spectrum of the compressional wave calibration process shows a distinct peak around 95 kHz, and the frequency spectra of the shear wave shows a primary peak around 73.5 kHz.  Based on this calibration; all compressional wave tests were performed at a frequency of 95 kHz and all shear tests were performed at a frequency of 75 kHz.  This observation is different than that documented by Weidinger (2007) using the same ultrasonic equipment.  Weidinger (2007) reported a dominant frequency of 46 kHz and 39 kHz for the P-wave and S-wave transducers, respectively.  Interestingly, Weidinger's data indicates a secondary peak at approximately 95 kHz and 74 kHz, and the current calibration process indicates very minor secondary peaks that coincide with Weidinger's dominant frequencies.

Another observation from the face-to-face calibration tests was that the energy delivered by the transducers during a P-wave test is significantly greater than that delivered during S-wave tests.  This observation is partially affected by the coupling factor of the shear mode, $k_{31}$, is only half of the coupling factor of the compressional mode; $k_{33}$ (Shi 1998).  Other factors such as the attachment of the transducers to the end platen diaphragm can also affect the coupling and transmission of energy to the soil specimens.
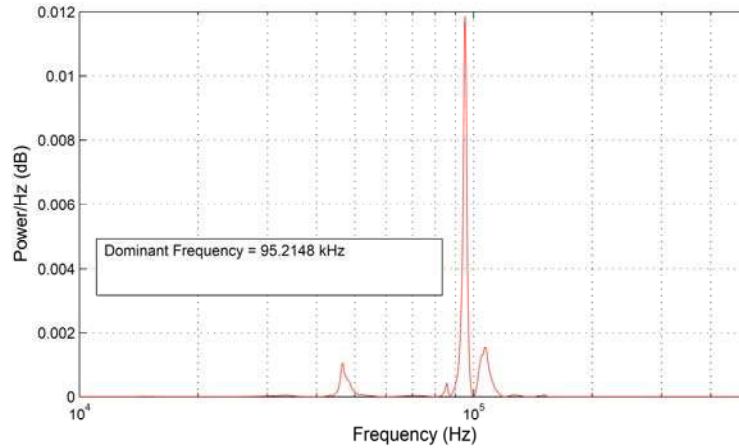
**Figure 4.15. Dominant Frequency of Ultrasonic P-wave Transducers**
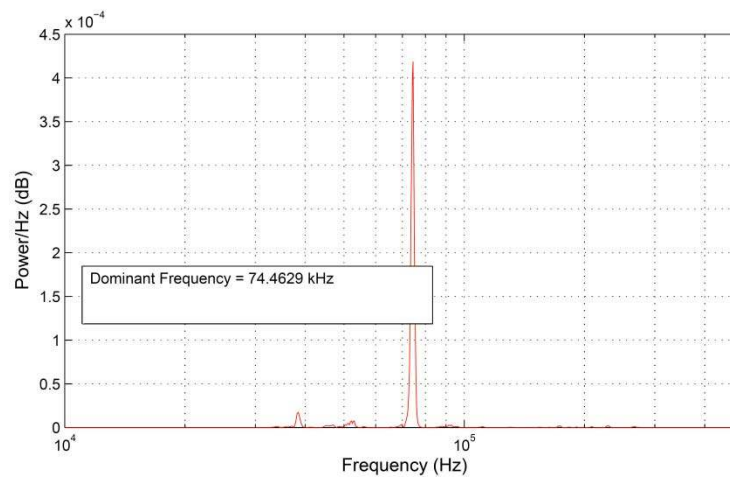


**Figure 4.16.  Dominant Frequency of Ultrasonic S-wave Transducers**

Due to the time delay from the response of the electronic equipment and the presence of a stiff diaphragm on the end platen faces between the piezoelectric crystals and the specimen, there will be a delay from the transmission of the pulse wave as it propagates through the diaphragm. A calibration procedure was performed to determine the face delay time so that it could be removed from the recorded travel time of the wave pulses.  A face-to-face calibration tests was performed.  If no delay is present, then the recorded signal from the receiving transducer would originate at 0 seconds.  The face delay for compression and shear wave signals was determined to

be 4.0 and 5.3 μsec, respectively.  Both compression and shear waves were propagated from the bottom platen to the top platen throughout the testing program.

      **4.6.3.4.**      **Ultrasonic pulse velocity testing program.**  The generalized testing program is summarized as follows:

i.      A single, sinusoidal wave pulse was generated using the function generation.  The frequency of the signal was either 95 or 75 kHz depending on whether P-waves or S-waves are induced in the specimen.  The pulse signal was directly connected to the digital oscilloscope through a coaxial BNC tee connection and used as a trigger for the data recorder.

ii.      Maximum output of the function generator was limited to ±10 volts.  The signal was fed into a power amplifier which raised the voltage up to ±50 volts.  This voltage was determined to be sufficient to drive the piezoelectric crystals so that enough stress energy was imparted on the specimen.

iii.      The transmitting signal was fed to the actuating ultrasonic transmitter mounted in the specimen end platen.

iv.      The ultrasonic transmitter converted the electrical pulse into a small amplitude mechanical pulse based on its piezoelectric properties.

v.      The ultrasonic receiver converted the mechanical energy that had propagated through the specimen into an electrical signal that was monitored with the oscilloscope.  The oscilloscope was automatically triggered by the initial transmitter pulse and recorded an approximate $1000 - 2000$ μsec record.

vi.      The entire routine was repeated approximately 100 times, with a 1 second delay between triggered signals.  The oscilloscope averaged all the recorded waveforms and generated one single "stacked" waveform for archiving and analysis.

The testing of a single ultrasonic pulse velocity specimen required approximately two days for material preparation and specimen remolding and approximately 1 hour for each stage of pulse velocity testing.  Typically five different stages of testing were completed for each specimen at increasing confining pressures, and thus all pulse tests were completed in approximately five hours for each specimen.  Overall, approximately three days were required in total for each specimen.

An acoustic couplant can be used to ensure uniform contact between the end platen transducers and the specimen.  Krautkramer and Krautkramer (1990) referenced water, glycerin,

petroleum jelly, grease, and oil as potential couplants. Leong et al. (2004) reported a significantly improved signal using a thin layer of fiberglass resin jelly. Weidinger (2007) investigated honey, fiberglass resin jelly, vacuum grease, petroleum jelly, ultrasound jelly, and no couplant. Plastic and latex membranes were utilized to separate the soil specimen and the couplant and avoid absorption. There are also concerns of couplant be absorbed into partially saturated specimens. Data from this research indicated that no couplant produced the strongest pulses and thus no couplant was used.

## 5.   RESULTS – STATIC PROPERTIES

The following chapter presents the results of experimental tests that were used to determine how static properties varied with EPS content.  The following geotechnical tests were performed:  compaction, one-dimensional compression – swell, unconsolidated-undrained triaxial compression, and consolidated-undrained triaxial compression tests.  Further discussion of the test results is presented in Chapter 7.

### 5.1.   INFLUENCE OF EPS CONENT ON UNIT WEIGHT AND VOID RATIO

The addition of very low density EPS particulates into soil had a large effect on the mass and volumetric properties of the resulting modified soil mixtures.  The effect of increasing EPS content on the dry unit weight of slurry consolidated and compacted unit element specimens is shown in Figure 5.1.  The reduction in dry density with each half percent increase (0.5%) in EPS content is between 8% and 12% on average.  A general rule of thumb would be to estimate a 10% reduction in dry unit weight for each half percent of EPS content.

The calculation of void ratio requires the determination of the voids within the soil. Voids are typically considered to include both air space and water space between soil particles. For the purposes of this discussion it is assumed that the closed-cell EPS particulates are completely impermeable, thus each particle is comprised of a solid membrane, a honeycombed internal structure, and internal air mass.   Considering the density measurements of EPS particulates (Table 3.3), it is seems reasonable to assume that the they are more similar to a unit volume of air ($\rho_{air} \approx 1.204$ kg/m$^3$ @ 20°C) rather than a unit volume of soil ($\rho_{soil} \approx 1400 - 2000$ kg/m$^3$).  For the remainder of this report an equivalent void ratio is used instead of the traditional void ratio used in geotechnical engineering.  The equivalent void ratio ($e_{eq}$) is defined as,

$$e_{eq} = \frac{V_{Voids} + V_{EPS}}{V_s} \tag{5.1}$$

Where $V_{voids}$ is the volume of the water and air, $V_s$ is the volume of the soil particles, and $V_{EPS}$ is the volume of the EPS particulates.  The effect of increasing EPS content on the equivalent void ratio of slurry consolidated and compacted specimens is shown in Figure 5.2.  The increase in equivalent void ratio with each half percent increase (0.5%) in EPS content is between 15% and 25% on average.
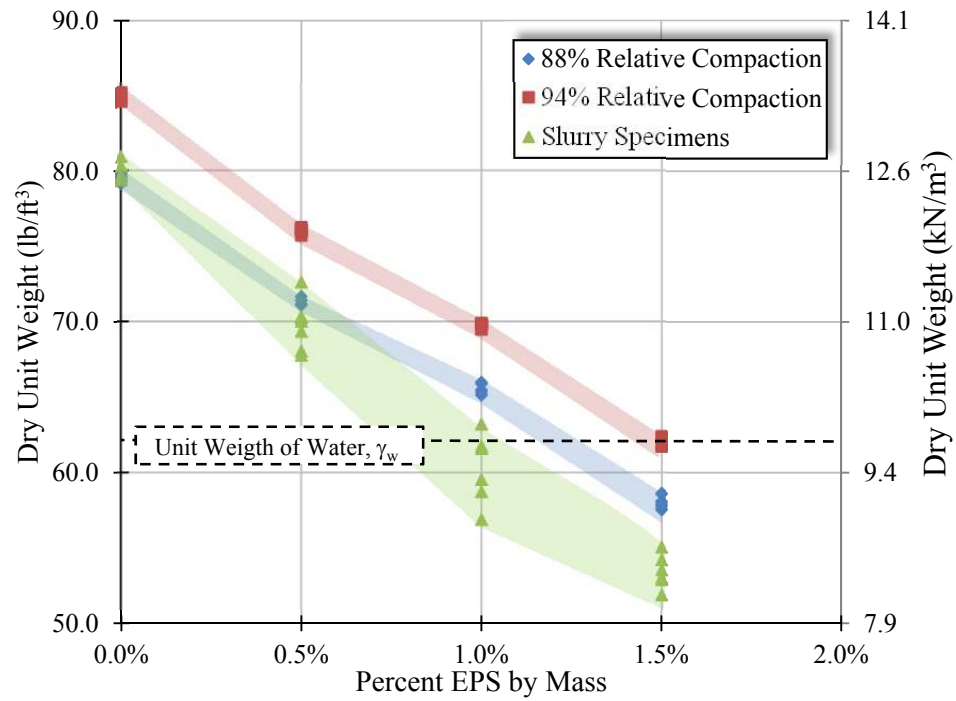
**Figure 5.1.  Effect of EPS Content on Dry Unit Weight**
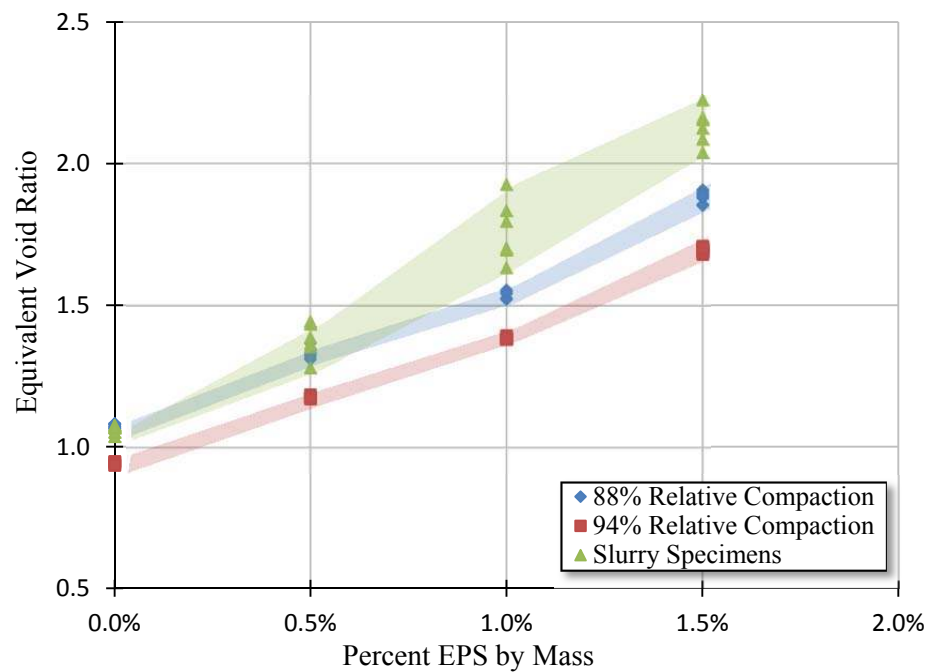


**Figure 5.2.  Effect of EPS Content on Equivalent Void Ratio**

**5.2.    MOISTURE – UNIT WEIGHT RELATIONSHIP**

Based on the data from the Standard Proctor tests, compaction curves were developed for a pure kaolin specimen and for the three different kaolin – EPS particulate mixtures investigated. Each different soil was tested with replicas to verify reproducibility in the results.  Figure 5.3 displays the compaction curves.  The zero air void (ZAV) curve for a 100% saturated specimen and curves for decreasing saturation levels using a specific gravity of 2.64 (kaolin).
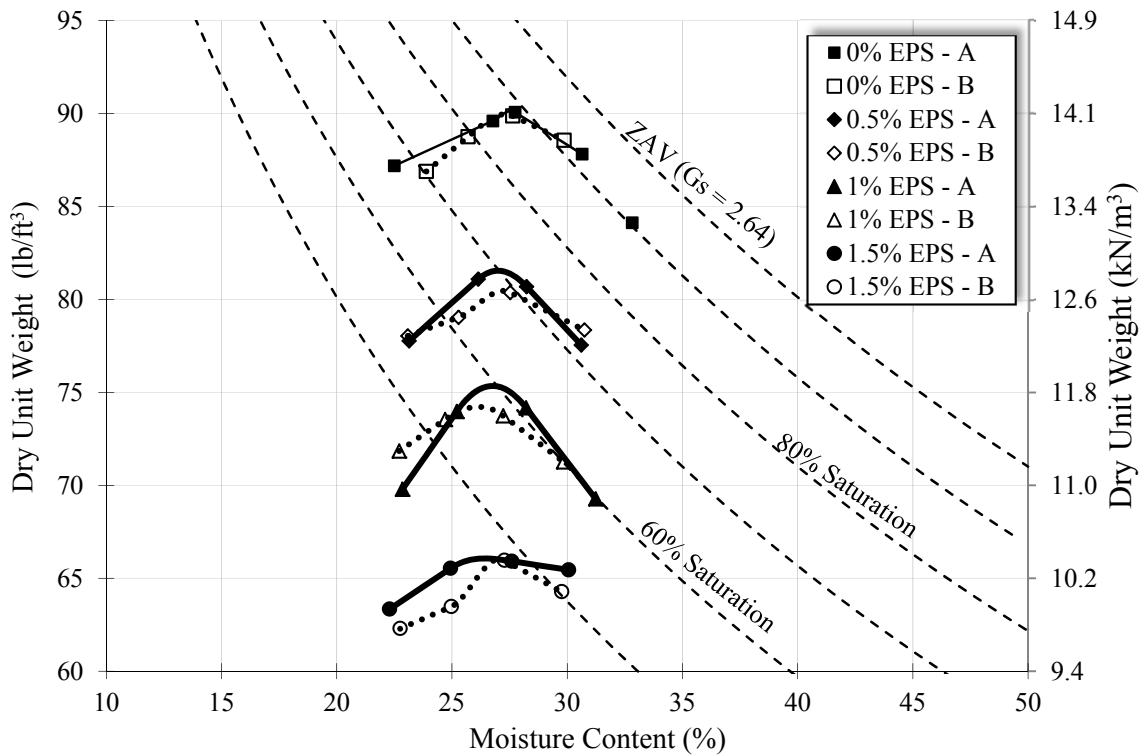


**Figure 5.3.  Moisture – Unit Weight Relationship**

The compaction curves were constructed by fitting a second-order polynomial to the data. Best engineering judgment was utilized in selection of the maximum dry unit weight ($\gamma_{d,max}$) and optimum moisture content ($\omega_{opt}$); as summarized in Table 5.1.

**Table 5.1.  Maximum Dry Unit Weight and Optimum Water Content**

| Mix Ratio (% Kaolin : % EPS, by mass) | I.D. | $\omega_{opt}$ (%) | $\gamma_{d,max}$ (lb/ft$^3$) | $\gamma_{d,max}$ (kN/m$^3$) |
|---|---|---|---|---|
| 100 : 0 | A | 27.6 | 90.2 | 14.2 |
|  | B | 27.3 | 90.0 | 14.1 |
|  | Avg. | 27.5 | 90.1 | 14.2 |
| 99.5 : 0.5 | A | 27.0 | 81.6 | 12.8 |
|  | B | 27.2 | 80.5 | 12.6 |
|  | Avg. | 27.1 | 81.1 | 12.7 |
| 99 : 1 | A | 26.8 | 75.4 | 11.9 |
|  | B | 26.2 | 74.2 | 11.7 |
|  | Avg. | 26.5 | 74.8 | 11.8 |
| 98.5 : 1.5 | A | 26.4 | 66.1 | 10.4 |
|  | B | 27.1 | 66.1 | 10.4 |
|  | Avg. | 26.8 | 66.1 | 10.4 |

## 5.3.     COMPRESSION – SWELL CHARACTERISITCS

The initial and final water content, initial dry unit weight, equivalent void ratio, and initial degree of saturation of the compacted specimens tested in one-dimensional compression – swell tests are noted in Table 5.2.  Six individual specimens were tested for the pure clay and each of the mix ratios specified in Table 4.1.  Each compacted specimen was initially loaded with a specific surcharge loading for a brief period and ultimate deformations were recorded.  The specimen was then inundated and the deformation with time was recorded.  Typical data recorded after inundation of the specimens is shown in Figure 5.4.  The presented data was adjusted to represent an initial height of 1.9.1 mm (0.75 inches) for all the specimens and surcharge loadings. The data was analyzed to determine the end of primary compression or swell, which was chosen as the intersection of two tangents to each curve.  This is identical to Casagrande's logarithm of time fitting method commonly used for consolidation tests.

The swell and collapse strains were determined from the deformation versus time data after inundation of the specimens.  The vertical strain is simply the ratio of the vertical deformation at the end of primary compression as determined from the data in Figure 5.4 and the original height of the specimen.  Data from the remainder of the tested specimens are shown in the Appendix.

**Table 5.2. Compression – Swell Test Specimen Properties**

| Mix Ratio (% Kaolin : % EPS, by mass) | Load | | $\omega_i$ (%) | $\gamma_{d,i}$ (kN/m$^3$) | $e_{eq}$ (**) | $S_i$ (%) | $\omega_f$ (%) |
|---|---|---|---|---|---|---|---|
| | (kPa) | (lb/ft$^2$) | | | | | |
| 100 : 0 | Free Swell | | 26.2 | 12.9 | 1.011 | 68.4 | 43.3 |
| | 23.9 | 500 | 27.5 | 12.8 | 1.031 | 70.4 | 40.5 |
| | 47.9 | 1000 | 27.6 | 12.7 | 1.035 | 70.4 | 37.8 |
| | 119.7 | 2500 | 27.5 | 12.8 | 1.029 | 70.6 | 36.0 |
| | 239.4 | 5000 | 27.0 | 12.8 | 1.023 | 69.7 | 33.0 |
| | 478.9 | 10000 | 27.6 | 12.7 | 1.034 | 70.5 | 31.3 |
| 99.5 : 0.5 | Free Swell | | 26.3 | 11.5 | 1.259 | 55.4 | 44.3 |
| | 23.9 | 500 | 26.0 | 11.6 | 1.251 | 55.1 | 39.0 |
| | 47.9 | 1000 | 26.0 | 11.6 | 1.251 | 55.2 | 38.8 |
| | 119.7 | 2500 | 26.0 | 11.6 | 1.251 | 55.1 | 36.1 |
| | 239.4 | 5000 | 25.9 | 11.6 | 1.249 | 55.0 | 33.7 |
| | 478.9 | 10000 | 25.9 | 11.6 | 1.249 | 55.0 | 31.5 |
| 99 : 1 | Free Swell | | 26.5 | 10.5 | 1.497 | 47.2 | 45.3 |
| | 23.9 | 500 | 26.7 | 10.6 | 1.477 | 48.2 | 39.9 |
| | 47.9 | 1000 | 26.7 | 10.6 | 1.479 | 48.1 | 38.5 |
| | 119.7 | 2500 | 26.0 | 10.6 | 1.463 | 47.4 | 36.5 |
| | 239.4 | 5000 | 26.0 | 10.6 | 1.462 | 47.4 | 33.6 |
| | 478.9 | 10000 | 26.4 | 10.6 | 1.467 | 48.0 | 30.9 |
| 98.5 : 1.5 | Free Swell | | 27.0 | 9.3 | 1.818 | 39.8 | 45.9 |
| | 23.9 | 500 | 27.0 | 9.3 | 1.821 | 39.7 | 41.6 |
| | 47.9 | 1000 | 27.0 | 9.3 | 1.820 | 39.8 | 37.8 |
| | 119.7 | 2500 | 27.0 | 9.3 | 1.818 | 39.8 | 35.5 |
| | 239.4 | 5000 | 27.0 | 9.3 | 1.817 | 39.8 | 32.5 |
| | 478.9 | 10000 | 27.0 | 0.95 | 1.821 | 39.7 | 30.1 |

An entire testing sequence for one specific modified soil type is shown in Figure 5.5. This data covers both the application of the surcharge loading and subsequent compression followed by inundation and swelling or collapse. The data for the remainder of the specimens tested is shown in the Appendix. Inundation test data is combined for different mix ratios and different surcharge loadings and shown in Figure 5.6. Typically data plots as a straight line on a semi-log scale, but for these tests a second order polynomial equation provided a better fit. The highest stress point for the pure kaolin specimen and the 1.5% EPS modified soil were omitted from the polynomial fit.

The swell pressure is determined from the fitted curve at zero vertical strain and the percent free swell was defined as the percent swell after inundation for the specimens with only small seating load applied. These data are listed in Table 5.3.
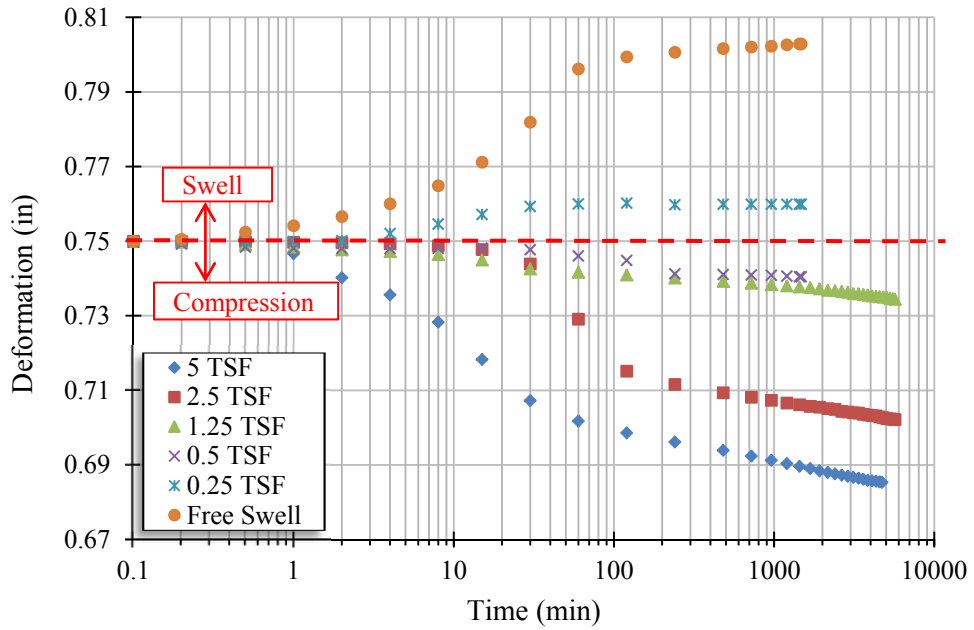
**Figure 5.4.  Deformation versus Time after Inundation (99% Kaolin : 1% EPS)**
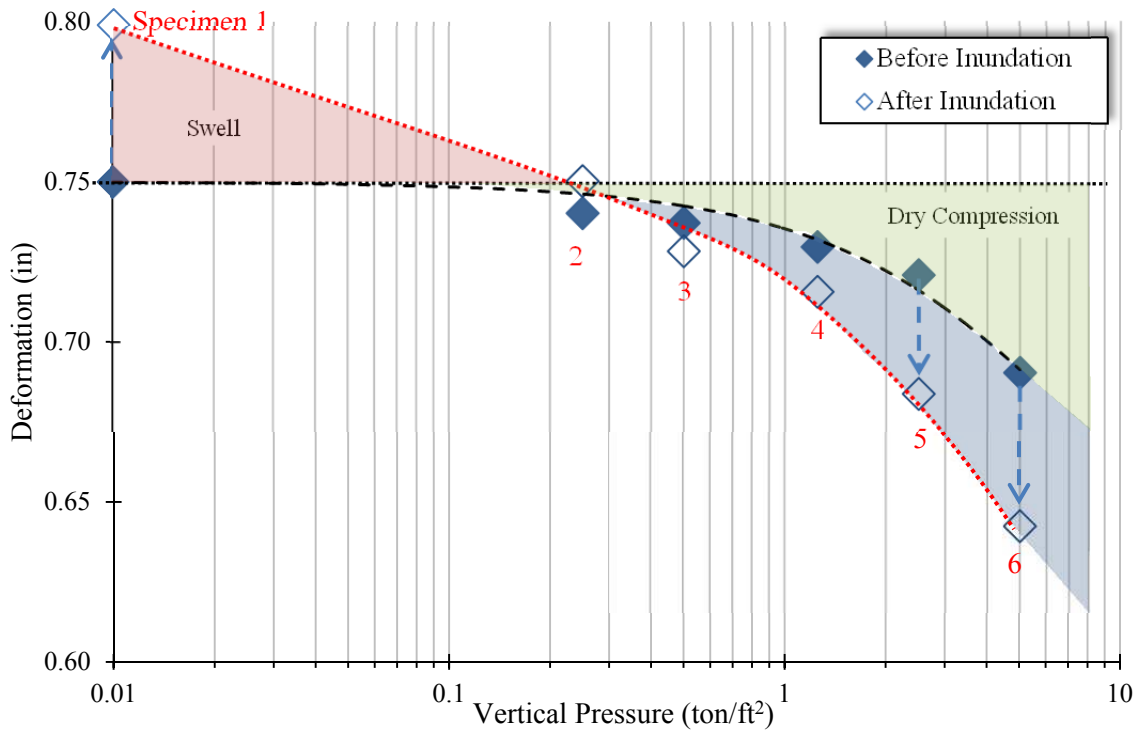


**Figure 5.5.  Deformation versus Applied Stress (99% Kaolin : 1% EPS)**
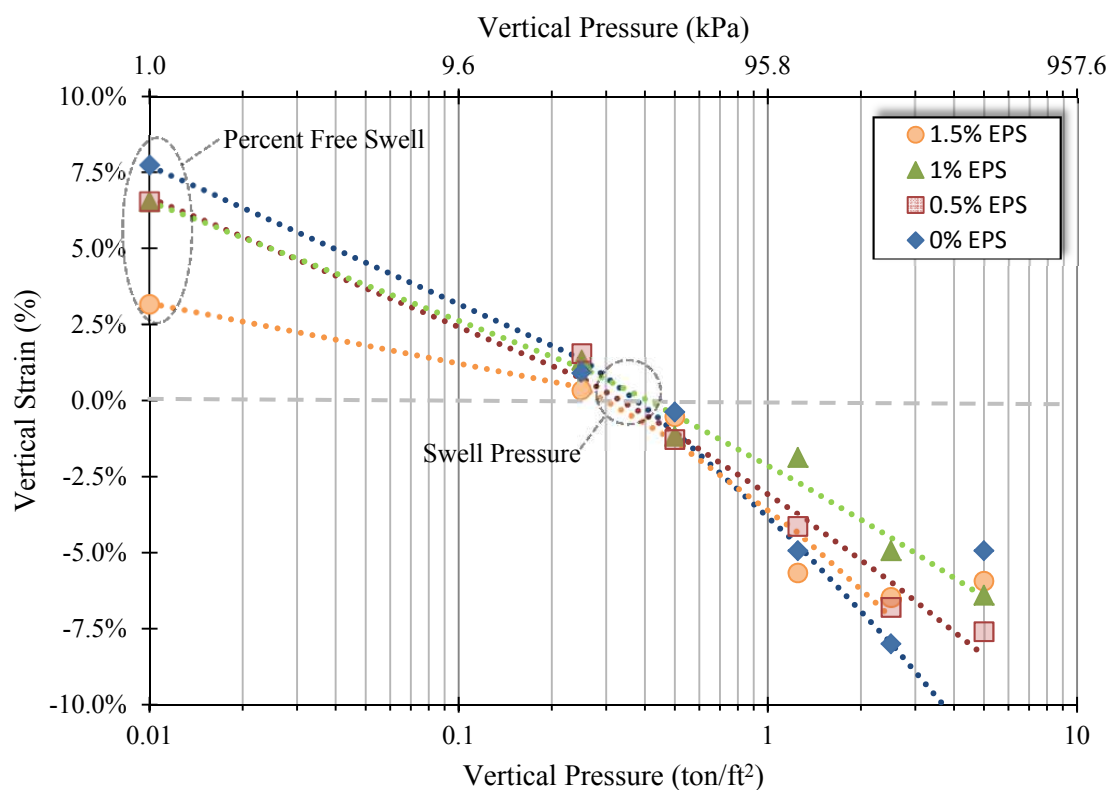
**Figure 5.6. Stress versus Wetting-Induced Swell – Collapse Strain**

**Table 5.3. Percent Free Swell & Swell Pressure**

| Mix Ratio (% Kaolin : % EPS, by mass) | Free Swell | Swell Pressure | |
|---|---|---|---|
| | (%) | (ton/ft$^2$) | (kPa) |
| 100 : 0 | 7.7 | 0.38 | 36.4 |
| 99.5 : 0.5 | 6.5 | 0.34 | 32.6 |
| 99 : 1 | 6.5 | 0.40 | 38.3 |
| 98.5 : 1.5 | 3.2 | 0.30 | 28.7 |

Results indicated that the introduction of less than 1% EPS content by mass does not significantly affect either the free swell potential or swell pressure of the cohesive soil specimens, but the influence of EPS content was noted for larger percentages of EPS particulates. Specimens with 1.5% EPS content exhibited a significant reduction in free swell potential and a measureable reduction in the swell pressure. Further discussion of the swell-compression results is located in Chapter 7.

## 5.4. STRENGTH

Slurry consolidated and statically undercompacted specimens were utilized for triaxial testing. Slurry specimens were utilized for isotropically consolidated undrained triaxial testing and unconsolidated undrained triaxial testing was completed on both slurry and compacted specimens.

**5.4.1. Unconsolidated Undrained Triaxial Tests.** Unconsolidated undrained (UU) triaxial compression tests do not allow for drainage during application of the confining pressure or during shearing. Pore water pressures are not measured, and thus the effective stress during testing is unknown. Results of UU tests are typically plotted on a Mohr diagram. The UU test is applicable for both saturated and partially saturated compacted soils with no drainage during the application of loading.

**5.4.1.1. UU triaxial test specimen properties.** Initial conditions of the slurry consolidated specimens are summarized in Table 5.4 and for compacted specimens are summarized in Table 5.5.

**Table 5.4. Properties of Slurry Consolidated UU Triaxial Test Specimens**

| Mix Ratio (% Kaolin : % EPS, by mass) | $\sigma_{cell}$ (kPa) | $\omega_i$ (%) | $\gamma_{d,i}$ (kN/m$^3$) | $\rho_{d,i}$ (g/cm$^3$) | $e_{eq}$ | S (%) |
|---|---|---|---|---|---|---|
| 100 : 0 | 172.4 | 40.0 | 12.7 | 1.30 | 1.036 | 100 |
| | 344.7 | 40.0 | 12.5 | 1.28 | 1.066 | 99.5 |
| | 689.5 | 39.6 | 12.6 | 1.29 | 1.051 | 99.5 |
| 99.5 : 0.5 | 172.4 | 39.9 | 11.0 | 1.12 | 1.365 | 77.5 |
| | 344.7 | 39.7 | 10.7 | 1.09 | 1.434 | 73.5 |
| | 689.5 | 40.0 | 11.4 | 1.16 | 1.281 | 82.9 |
| 99 : 1 | 172.4 | 40.4 | 9.4 | 0.95 | 1.795 | 60.0 |
| | 344.7 | 40.9 | 9.7 | 0.99 | 1.695 | 64.3 |
| | 620.5 | 41.0 | 9.2 | 0.94 | 1.834 | 59.6 |
| 98.5 : 1.5 | 172.4 | 40.4 | 8.3 | 0.85 | 2.161 | 50.1 |
| | 344.7 | 41.0 | 8.3 | 0.85 | 2.154 | 51.0 |
| | 689.5 | 41.1 | 8.5 | 0.87 | 2.085 | 52.8 |

**Table 5.5. Properties of Compacted UU Triaxial Test Specimens**

| Mix Ratio (% Kaolin : % EPS, by mass) | $\sigma_{cell}$ (kPa) | $\omega_i$ (%) | $\gamma_{d,i}$ (kN/m$^3$) | $\rho_{d,i}$ (g/cm$^3$) | $e_{eq}$ | S (%) | Relative Compaction (%) |
|---|---|---|---|---|---|---|---|
| 100 : 0 | 68.9 | 28.4 | 12.5 | 1.27 | 1.078 | 69.6 | 88.0 |
| | 172.4 | 28.3 | 12.4 | 1.27 | 1.082 | 69.0 | 87.8 |
| | 344.7 | 27.9 | 12.5 | 1.27 | 1.072 | 68.7 | 88.2 |
| | 68.9 | 28.2 | 13.3 | 1.36 | 0.943 | 79.0 | 94.1 |
| | 172.4 | 28.2 | 13.4 | 1.36 | 0.934 | 79.7 | 94.6 |
| | 344.7 | 28.3 | 13.4 | 1.36 | 0.936 | 79.8 | 94.5 |
| 99.5 : 0.5 | 68.9 | 27.2 | 11.2 | 1.14 | 1.319 | 54.7 | 88.0 |
| | 172.4 | 27.9 | 11.2 | 1.14 | 1.330 | 55.7 | 87.7 |
| | 344.7 | 28.0 | 11.2 | 1.14 | 1.327 | 56.0 | 87.7 |
| | 68.9 | 27.6 | 12.0 | 1.22 | 1.176 | 62.3 | 93.8 |
| | 172.4 | 27.9 | 12.0 | 1.22 | 1.179 | 62.8 | 93.7 |
| | 344.7 | 27.8 | 12.0 | 1.22 | 1.172 | 63.0 | 94.0 |
| 99 : 1 | 68.9 | 27.2 | 10.3 | 1.05 | 1.542 | 47.0 | 87.6 |
| | 172.4 | 27.2 | 10.2 | 1.04 | 1.555 | 46.6 | 87.0 |
| | 344.7 | 27.1 | 10.3 | 1.05 | 1.548 | 46.7 | 87.3 |
| | 68.9 | 27.1 | 11.0 | 1.12 | 1.384 | 52.2 | 93.3 |
| | 172.4 | 27.1 | 11.0 | 1.12 | 1.380 | 52.4 | 93.4 |
| | 344.7 | 27.1 | 11.0 | 1.12 | 1.386 | 52.1 | 93.2 |
| 98.5 : 1.5 | 68.9 | 27.6 | 9.1 | 0.93 | 1.891 | 39.1 | 87.6 |
| | 172.4 | 27.6 | 9.1 | 0.92 | 1.903 | 38.9 | 87.1 |
| | 344.7 | 27.5 | 9.0 | 0.92 | 1.907 | 38.6 | 87.0 |
| | 68.9 | 27.1 | 9.7 | 0.99 | 1.694 | 42.9 | 93.9 |
| | 172.4 | 27.3 | 9.7 | 0.99 | 1.700 | 43.0 | 93.6 |
| | 344.7 | 27.4 | 9.7 | 0.99 | 1.705 | 43.1 | 93.5 |

**5.4.1.2. UU triaxial test stress – strain data.** The stress – strain data for the triaxial UU tests are shown in Figure 5.7 through Figure 5.9. Failure conditions for each specimen are indicated in Table 5.6 through Table 5.8. For this research program failure was defined as the maximum deviator stress obtained prior to 15% axial strain. Raw data recorded during testing and recorded by the data acquisition system is included on the data CD in the Appendix.

**Figure 5.7. UU Triaxial Test Results for Slurry Consolidated Specimens (Deviator Stress vs. Axial Strain)**
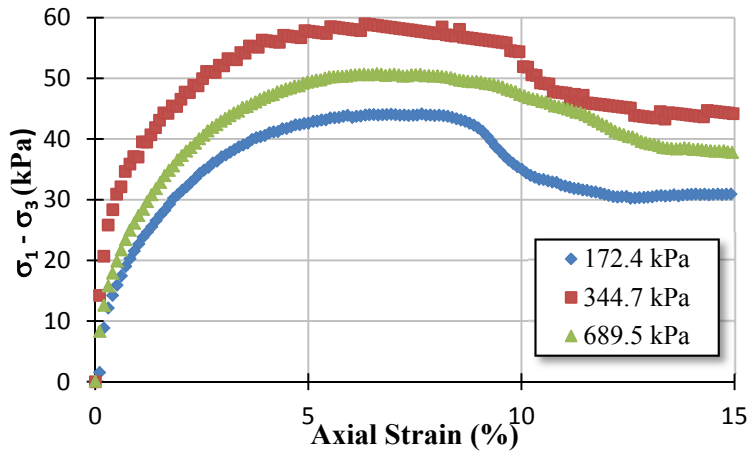
a)   100% Kaolin ($\gamma_d \approx 12.6$ kN/m$^3$)
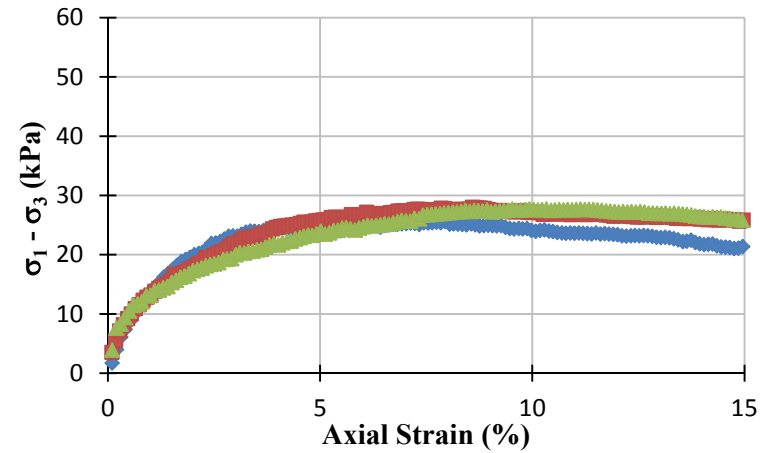
c)   99% Kaolin : 1% EPS ($\gamma_d \approx 9.5$ kN/m$^3$)
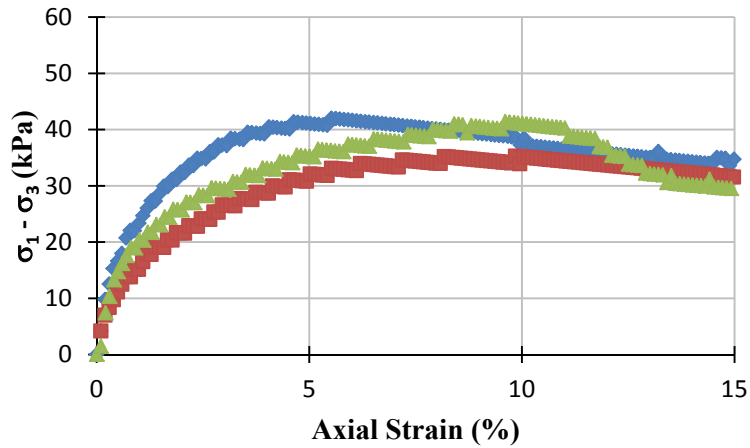
b)   99.5% Kaolin : 0.5% EPS ($\gamma_d \approx 11.0$ kN/m$^3$)
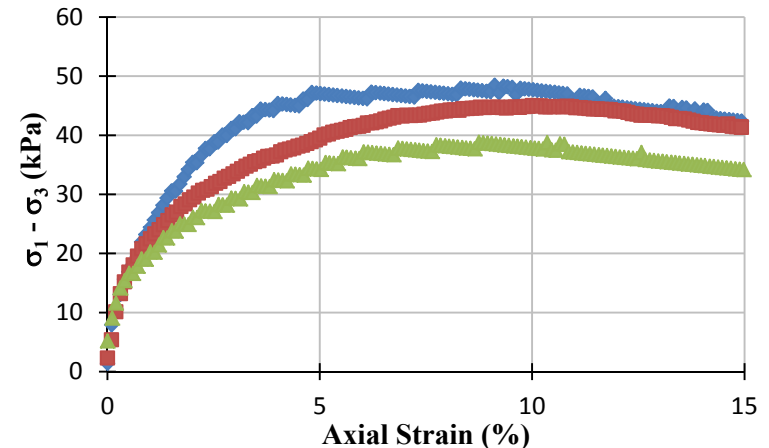
d)   98.5% Kaolin : 1.5% EPS ($\gamma_d \approx 8.4$ kN/m$^3$)
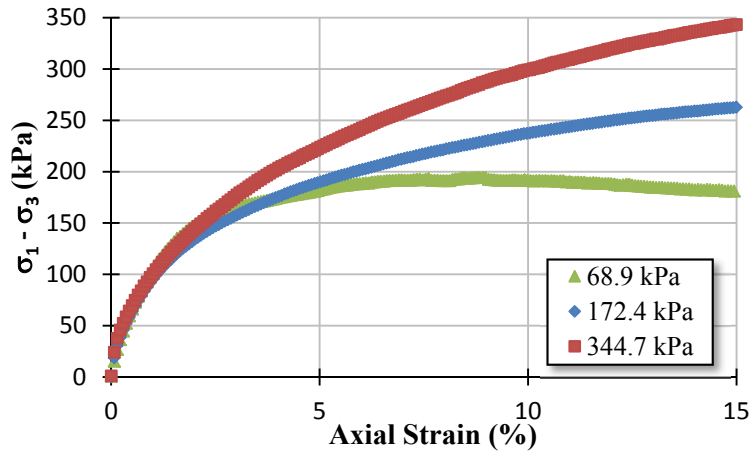
a)   100% Kaolin ($\gamma_d \approx 12.4$ kN/m$^3$)
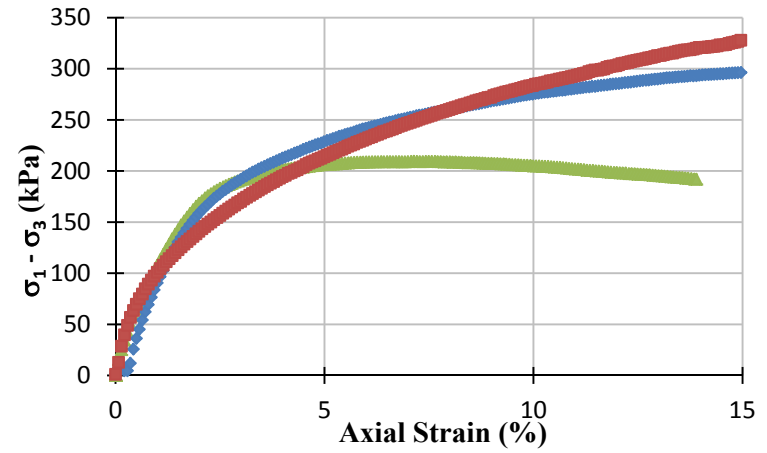
c)   99% Kaolin : 1% EPS ($\gamma_d \approx 10.3$ kN/m$^3$)
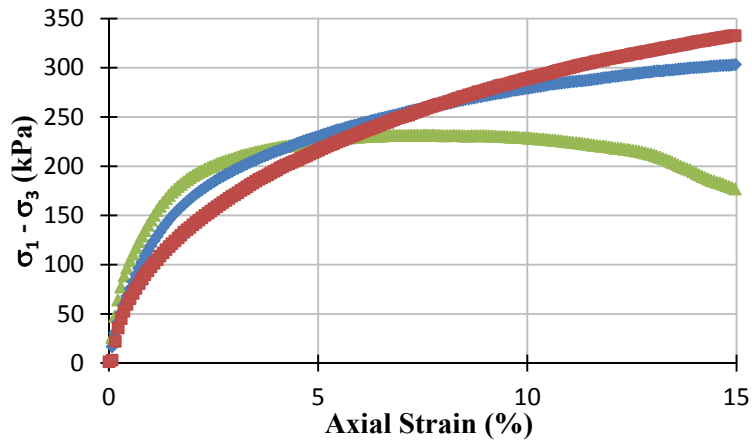
b)   99.5% Kaolin : 0.5% EPS ($\gamma_d \approx 11.2$ kN/m$^3$)
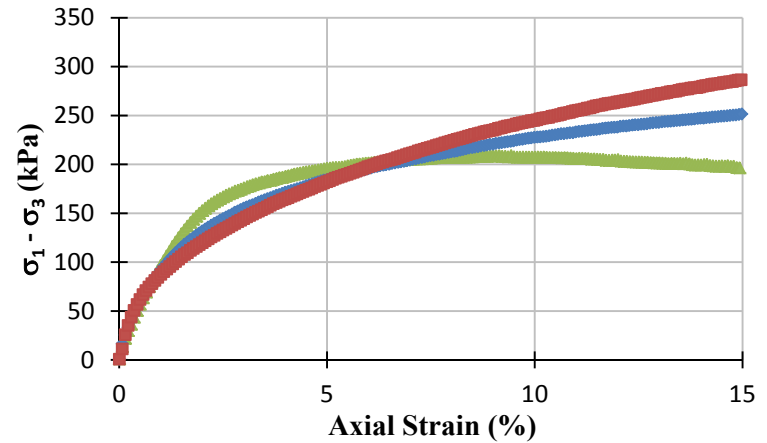
d)   98.5% Kaolin : 1.5% EPS ($\gamma_d \approx 9.1$ kN/m$^3$)

**Figure 5.8. UU Triaxial Test Results for Compacted Specimens (Relative Compaction ≈ 88%)**
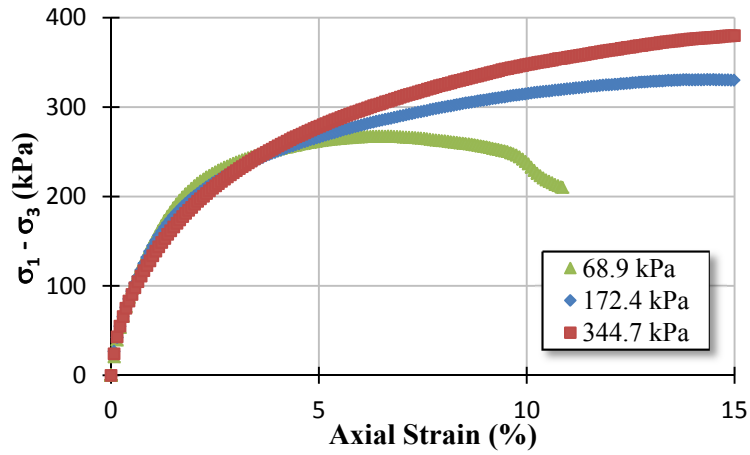
a)   100% Kaolin ($\gamma_d \approx$ 13.4 kN/m$^3$)
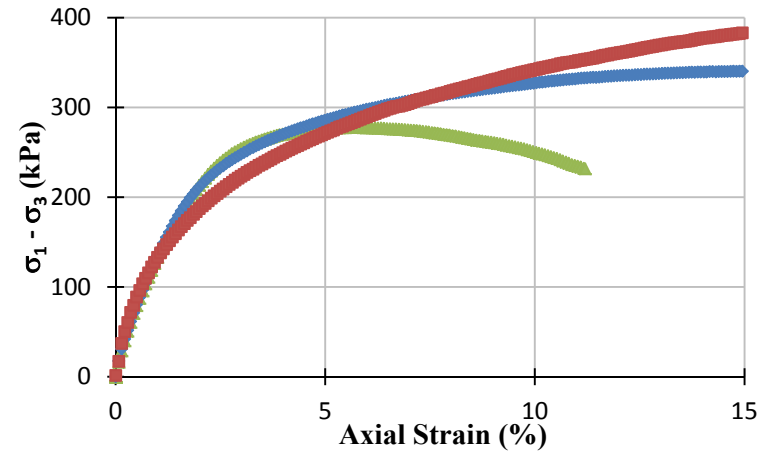
c)   99% Kaolin : 1% EPS ($\gamma_d \approx$ 11.0 kN/m$^3$)
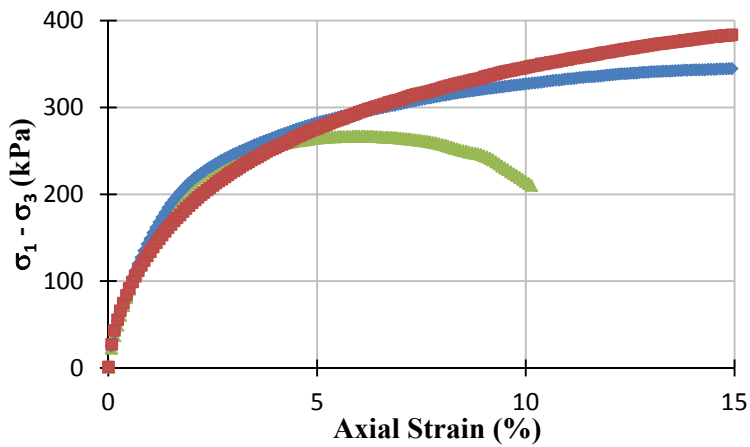
b)   99.5% Kaolin : 0.5% EPS ($\gamma_d \approx$ 12.0 kN/m$^3$)
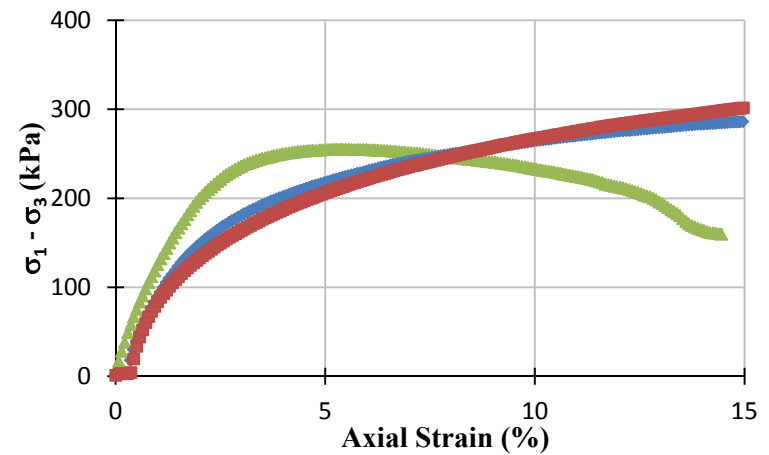
d)   98.5% Kaolin : 1.5% EPS ($\gamma_d \approx$ 9.7 kN/m$^3$)

**Figure 5.9. UU Triaxial Test Results for Compacted Specimens (Relative Compaction $\approx$ 94%)**

**Table 5.6. Failure Conditions for Slurry Consolidated UU Triaxial Test Specimens**

| Mix Ratio (% Kaolin:% EPS, by mass) | $\sigma_{cell}$ (kPa) | $\varepsilon_f$ (%) | $\sigma_{dev,f}$ (kPa) |
|---|---|---|---|
| 100 : 0 | 172.4 | 7.7 | 44.1 |
| | 344.7 | 6.3 | 59.0 |
| | 689.5 | 6.6 | 50.7 |
| 99.5 : 0.5 | 172.4 | 5.5 | 42.0 |
| | 344.7 | 9.9 | 35.2 |
| | 689.5 | 9.6 | 41.4 |
| 99 : 1 | 172.4 | 6.3 | 25.7 |
| | 344.7 | 8.6 | 28.0 |
| | 620.5 | 9.5 | 27.7 |
| 98.5 : 1.5 | 172.4 | 9.1 | 48.5 |
| | 344.7 | 10.0 | 45.0 |
| | 689.5 | 8.7 | 38.8 |

**Table 5.7. Failure Conditions for Compacted UU Triaxial Specimens**

**(Relative Compaction ≈ 88%)**

| Mix Ratio (% Kaolin:% EPS, by mass) | $\sigma_{cell}$ (kPa) | $\varepsilon_f$ (%) | $\sigma_{dev,f}$ (kPa) |
|---|---|---|---|
| 100 : 0 | 68.9 | 8.9 | 194.4 |
| | 172.4 | 15.0 | 263.4 |
| | 344.7 | 15.0 | 344.7 |
| 99.5 : 0.5 | 68.9 | 7.6 | 231.7 |
| | 172.4 | 15.0 | 304.1 |
| | 344.7 | 15.0 | 334.4 |
| 99 : 1 | 68.9 | 7.1 | 209.6 |
| | 172.4 | 15.0 | 297.2 |
| | 344.7 | 15.0 | 328.9 |
| 98.5 : 1.5 | 68.9 | 9.4 | 208.9 |
| | 172.4 | 15.0 | 252.3 |
| | 344.7 | 15.0 | 288.2 |

**Table 5.8.  Failure Conditions for Compacted UU Triaxial Specimens**

**(Relative Compaction ≈ 94%)**

| Mix Ratio (% Kaolin:% EPS, by mass) | $\sigma_{cell}$ (kPa) | $\varepsilon_f$ (%) | $\sigma_{dev,f}$ (kPa) |
|---|---|---|---|
| 100 : 0 | 68.9 | 6.7 | 267.5 |
|  | 172.4 | 14.3 | 330.9 |
|  | 344.7 | 15.0 | 381.3 |
| 99.5 : 0.5 | 68.9 | 6.1 | 266.8 |
|  | 172.4 | 15.0 | 344.7 |
|  | 344.7 | 15.0 | 384.7 |
| 99 : 1 | 68.9 | 5.5 | 277.9 |
|  | 172.4 | 14.7 | 340.6 |
|  | 344.7 | 15.0 | 384.0 |
| 98.5 : 1.5 | 68.9 | 5.3 | 255.1 |
|  | 172.4 | 15.0 | 286.8 |
|  | 344.7 | 15.0 | 302.7 |

**5.4.1.3. UU triaxial strength parameters and moduli.**    The stress-strain data from the triaxial UU tests was analyzed to determine strength parameters.  Saturated soils testing in UU triaxial compression tend to have nearly horizontal failure envelopes regardless of the confining pressures on the specimen as the pore water reacts against any increase in pressure.  Essentially there is no increase in effective stress without drainage and thus no increase in shear stress would be expected.  For saturated soils the undrained shear strength ($S_u$) is characterized by a cohesion intercept and no friction angle.

Since the slurry consolidated triaxial UU specimens were saturated, or for the modified soil specimens the soil matrix was saturated, the testing program exhibited a nearly linear failure envelope.  The reported undrained shear strength in Table 5.9 is an average of the recorded maximum shear strength from three confining pressures tested.  The tangent modulus for each specimen was determined from the strain-strain test data.  The initial tangent modulus was determined by fitting a hyperbolic relationship to the measured stress-strain data using the procedures described by Kondner (1963).  The secant modulus ($E_{50}$) was determined for the specimens at 50% of the deviator stress at failure.

**Table 5.9. Undrained Shear Strength & Moduli of Slurry Consolidated Specimens**

| Mix Ratio (% Kaolin:% EPS, by mass) | $\sigma_{cell}$ (kPa) | $E_{tangent,i}$ (MPa) | $E_{50}$ (MPa) | $S_u$ (kPa) |
|---|---|---|---|---|
| 100 : 0 | 172.4 | 4.2 | 2.3 | 25.5 |
| | 344.7 | 9.7 | 6.9 | |
| | 689.5 | 4.2 | 3.1 | |
| 99.5 : 0.5 | 172.4 | 4.9 | 3.0 | 20.0 |
| | 344.7 | 2.6 | 1.5 | |
| | 689.5 | 3.1 | 1.8 | |
| 99 : 1 | 172.4 | 2.7 | 1.4 | 13.8 |
| | 344.7 | 2.3 | 1.3 | |
| | 620.5 | 1.9 | 1.3 | |
| 98.5 : 1.5 | 172.4 | 5.8 | 2.3 | 22.1 |
| | 344.7 | 3.7 | 2.0 | |
| | 689.5 | 3.8 | 1.5 | |

Partially saturated soils will behave differently than saturated soils in UU tests. The pore air in partially saturated soils is readily compressible. Increases in confining pressure during a UU test lead to compression of air voids thus decreasing the specimen volume and subsequently increasing the specimen density. In addition, as the volume of air is decreased, the saturation level increases. Strength would be expected to increase in partially saturated specimens with increasing confining pressure. A suite of partially saturated soils tested at various confining pressures usually exhibit a curve failure envelop until a threshold confining pressure is reached. Above this threshold confining pressure all the air voids are compressed in the specimen, saturation reaches 100%, and a typical horizontal failure envelope for saturated specimens develops. For each specimen the undrained shear strength was evaluated at $\phi = 0$, and thus it is simply half of the recorded deviator stress.

The measured undrained shear strength of the UU triaxial compression tests for specimens compacted to 88% and 94% relative compaction are shown in Figure 5.10 and Figure 5.11, respectively. The data and calculated soil moduli are listed in Table 5.10 and Table 5.11for specimens compacted to 88% and 94% relative compaction, respectively.
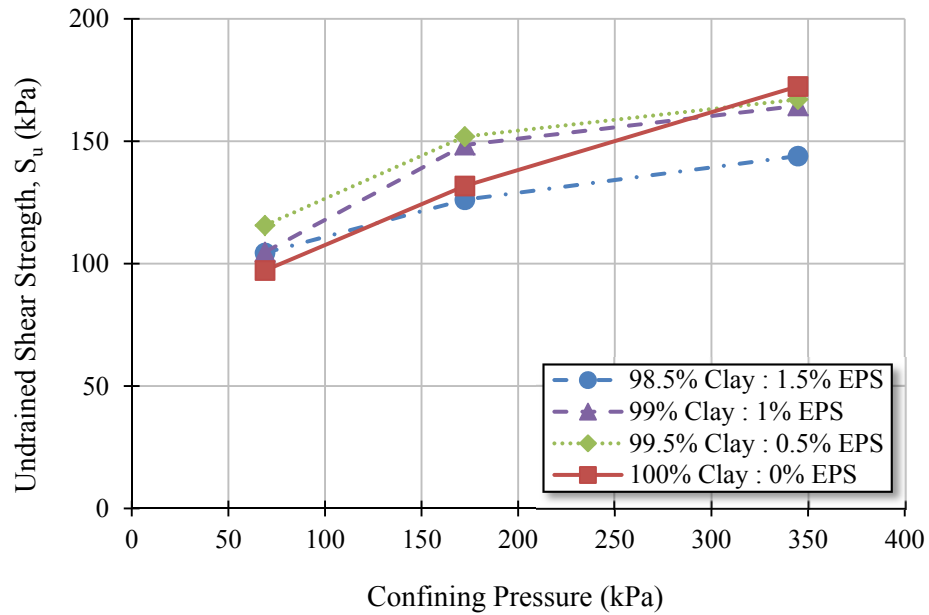
**Figure 5.10. Undrained Shear Strength for Compacted UU Triaxial Specimens**
**(Relative Compaction ≈ 88%)**
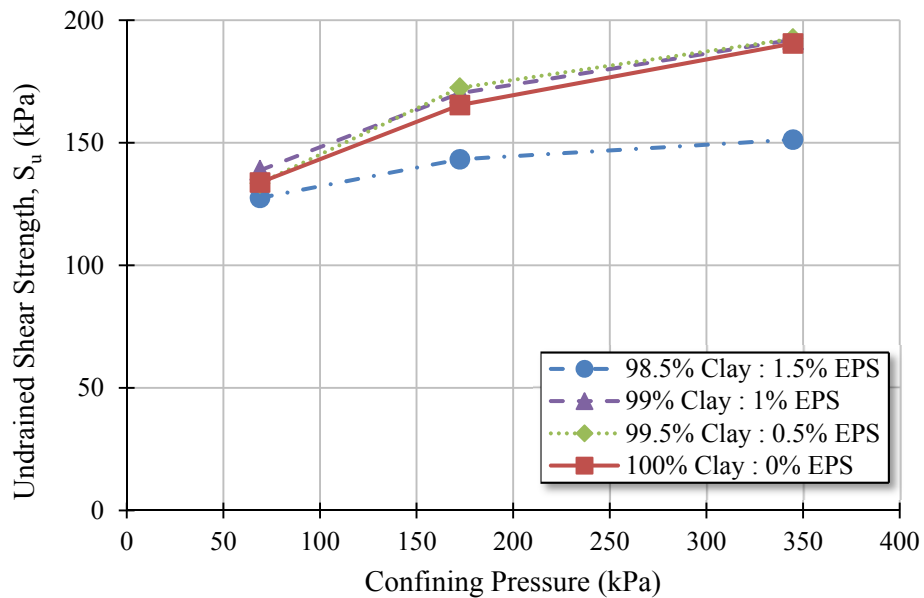


**Figure 5.11. Undrained Shear Strength for Compacted UU Triaxial Specimens**
**(Relative Compaction ≈ 94%)**

**Table 5.10.  Moduli for Compacted UU Triaxial Specimens (Relative Compaction ≈ 88%)**

| Mix Ratio (% Kaolin:% EPS, by mass) | $\sigma_{cell}$ (kPa) | $E_{tangent,i}$ (MPa) | $E_{50}$ (MPa) |
|---|---|---|---|
| 100 : 0 | 68.9 | 22.2 | 10.9 |
| | 172.4 | 10.7 | 6.8 |
| | 344.7 | 11.1 | 6.0 |
| 99.5 : 0.5 | 68.9 | 38.3 | 17.7 |
| | 172.4 | 15.7 | 9.6 |
| | 344.7 | 10.1 | 5.8 |
| 99 : 1 | 68.9 | 23.0 | 11.0 |
| | 172.4 | 13.3 | 8.2 |
| | 344.7 | 10.8 | 5.9 |
| 98.5 : 1.5 | 68.9 | 19.7 | 9.4 |
| | 172.4 | 11.7 | 7.0 |
| | 344.7 | 9.0 | 4.8 |

**Table 5.11.  Moduli for Compacted UU Triaxial Specimens (Relative Compaction ≈ 94%)**

| Mix Ratio (% Kaolin:% EPS, by mass) | $\sigma_{cell}$ (kPa) | $E_{tangent,i}$ (MPa) | $E_{50}$ (MPa) |
|---|---|---|---|
| 100 : 0 | 68.9 | 32.8 | 15.8 |
| | 172.4 | 20.3 | 12.9 |
| | 344.7 | 16.8 | 9.5 |
| 99.5 : 0.5 | 68.9 | 30.0 | 15.3 |
| | 172.4 | 23.8 | 13.4 |
| | 344.7 | 16.4 | 9.3 |
| 99 : 1 | 68.9 | 23.8 | 13.1 |
| | 172.4 | 23.0 | 12.4 |
| | 344.7 | 15.7 | 9.2 |
| 98.5 : 1.5 | 68.9 | 23.0 | 12.6 |
| | 172.4 | 12.5 | 7.6 |
| | 344.7 | 9.6 | 6.0 |

### 5.4.2.  Consolidated Undrained Triaxial Tests.

**5.4.2.1. CU triaxial test specimen properties.**  Consolidation pressures utilized during CU testing were greater than vertical pressures during the slurry consolidation process to ensure all specimens were normally consolidated upon loading.  Initial and final conditions of test specimens are summarized in Table 5.12 and Table 5.13.

**Table 5.12. Initial Properties CU Triaxial Test Specimens**

| Mix Ratio (% Kaolin : % EPS, by mass) | $\sigma_3'$ (kPa) | $\omega_i$ (%) | $\gamma_{d,i}$ (kN/m$^3$) | $\rho_{d,i}$ (g/cm$^3$) | $e_{eq,i}$ | S (%) |
|---|---|---|---|---|---|---|
| | | | *Initial Properties* | | | |
| 100 : 0 | 172.4 | 39.8 | 12.5 | 1.27 | 1.073 | 97.9 |
| | 344.7 | 40.5 | 12.5 | 1.27 | 1.076 | 99.4 |
| | 689.5 | 40.5 | 12.5 | 1.28 | 1.067 | 100.0 |
| 99.5 : 0.5 | 172.4 | 40.3 | 11.1 | 1.13 | 1.354 | 79.4 |
| | 344.7 | 40.8 | 10.9 | 1.11 | 1.388 | 78.3 |
| | 689.5 | 40.8 | 10.7 | 1.09 | 1.443 | 75.3 |
| 99 : 1 | 172.4 | 41.2 | 8.9 | 0.91 | 1.925 | 57.4 |
| | 344.7 | 40.8 | 9.7 | 0.99 | 1.702 | 64.3 |
| | 689.5 | 41.3 | 9.9 | 1.01 | 1.633 | 67.9 |
| 98.5 : 1.5 | 172.4 | 40.8 | 8.4 | 0.86 | 2.124 | 51.9 |
| | 344.7 | 41.1 | 8.7 | 0.88 | 2.038 | 54.5 |
| | 689.5 | 41.2 | 8.2 | 0.83 | 2.223 | 50.0 |

Saturation of the modified soil specimens was interesting considering the questionable impermeability of the EPS particulates as well as questions of their lack of rigidity and potential collapse during backpressure saturation and B-value checks. Results from the saturation process indicated that the EPS particulates were stiff enough to not collapse or change volume significantly during B-value checks that applied an approximate 68.9 kPa undrained load on the specimen. As shown in Table 5.13 all B-values of the specimens indicate that saturation was obtained or nearly obtained prior to undrained loadings.

**5.4.2.2. CU triaxial test stress – strain data and stress paths.** The stress-strain plots and stress paths for the CU triaxial tests are displayed in Figure 5.12 through Figure 5.15 below. The deviator stress versus vertical strain and excess pore water pressure versus vertical strain data confirm that all specimens were normally consolidated. Excess pore water pressures increased throughout the shearing process. Raw data recorded during testing and recorded by the data acquisition system is included in the data CD in the Appendix. Failure conditions for each specimen are indicated in Table 5.14. For this research program failure was defined as the maximum deviator stress obtained.

**Table 5.13.  Post-Consolidation Properties CU Triaxial Test Specimens**

| Mix Ratio (% Kaolin : % EPS, by mass) | $\sigma_3'$ (kPa) | Post-Consolidation Properties | | | | | | |
|---|---|---|---|---|---|---|---|---|
| | | $\gamma_{d,test}$ (kN/m³) | $\rho_{d,test}$ (g/cm³) | $e_{eq,test}$ | $S_{test}$ (%) | B-value | $t_{50}$ (min) | Shear Rate (mm/min) |
| 100 : 0 | 172.4 | 13.3 | 1.35 | 0.949 | 100.0 | 0.97 | 80 | 50.8e-4 |
| | 344.7 | 14.4 | 1.47 | 0.797 | 100.0 | 0.99 | 95 | 50.8e-4 |
| | 689.5 | 15.6 | 1.59 | 0.660 | 100.0 | 0.97 | 76 | 50.8e-4 |
| 99.5 : 0.5 | 172.4 | 12.2 | 1.24 | 1.141 | 82.1 | 0.98 | 75 | 63.5e-4 |
| | 344.7 | 12.7 | 1.29 | 1.052 | 82.7 | 0.96 | 65 | 63.5e-4 |
| | 689.5 | 13.2 | 1.34 | 0.980 | 80.4 | 0.96 | 58 | 71.1e-4 |
| 99 : 1[1] | 172.4 | 9.8 | 1.00 | 1.674 | 57.0 | 0.97 | ?? | 30.5e-2 |
| | 344.7 | 11.4 | 1.16 | 1.292 | 65.0 | 0.99 | 95? | 50.8e-4 |
| | 689.5 | 12.3 | 1.25 | 1.128 | 70.0 | 0.97 | 65 | 63.5e-4 |
| 98.5 : 1.5 | 172.4 | 9.2 | 0.94 | 1.863 | 50.9 | 0.96 | 70 | 58.4e-4 |
| | 344.7 | 10.0 | 1.02 | 1.627 | 53.2 | 0.99 | 70 | 58.4e-4 |
| | 689.5 | 10.1 | 1.03 | 1.600 | 46.9 | 0.99 | 56 | 73.7e-4 |

Note: [1]Air pressure used to maintain the backpressure and cell pressure of specimens was reduced overnight due to a leak in the pressure tank for two of the 99% Kaolin : 1% EPS specimens.  The pressure reduced to approximately 415 kPa overnight, and thus the backpressure was not affected but the cell pressure was reduced.  With the loss of pressure the specimens responded by swelling.   Once pressure was restored, consolidation was re-initiated.

**Table 5.14.  Failure Conditions for CU Triaxial Tests**

| Mix Ratio (% Kaolin:% EPS, by mass) | $\sigma_3'$ (kPa) | $\varepsilon_f$ (%) | $\sigma_{dev,f}$ (kPa) | $u_{excess,f}$ (kPa) | $\sigma_{1,f}$ (kPa) |
|---|---|---|---|---|---|
| 100 : 0 | 172.4 | 5.8 | 123.4 | 135.8 | 295.8 |
| | 344.7 | 9.3 | 182.0 | 212.4 | 526.8 |
| | 689.5 | 8.7 | 308.9 | 389.6 | 998.4 |
| 99.5 : 0.5 | 172.4 | 7.5 | 108.9 | 125.5 | 281.3 |
| | 344.7 | 7.3 | 168.9 | 195.1 | 513.7 |
| | 689.5 | 7.6 | 309.6 | 363.4 | 999.1 |
| 99 : 1 | 172.4 | 8.1 | 90.3 | 92.4 | 262.0 |
| | 344.7 | 10.8 | 163.4 | 194.4 | 513.7 |
| | 689.5 | 7.5 | 311.0 | 382.7 | 1000.4 |
| 98.5 : 1.5 | 172.4 | 12.5 | 104.8 | 104.8 | 277.2 |
| | 344.7 | 11.0 | 182.7 | 213.7 | 527.4 |
| | 689.5 | 9.5 | 314.4 | 356.5 | 1003.9 |
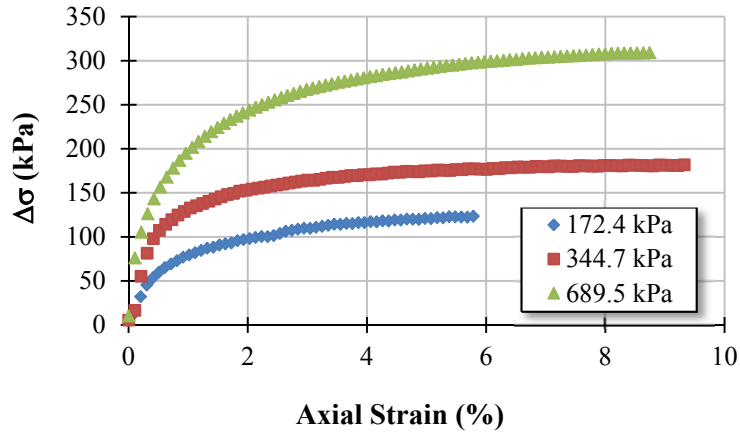
a)  Deviator Stress vs. Axial Strain
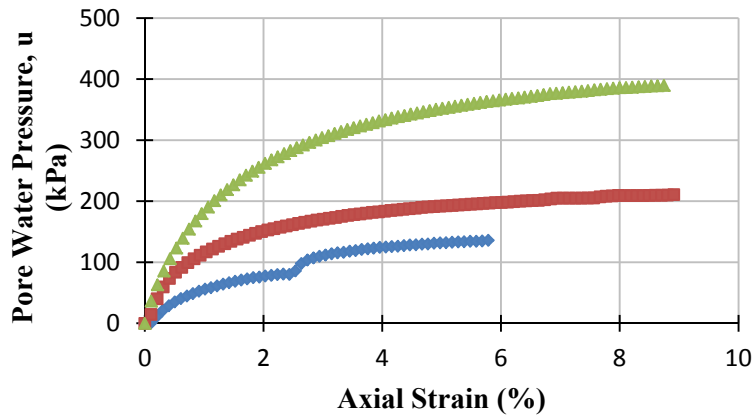
b)  Excess Pore Water Pressure vs. Axial Strain
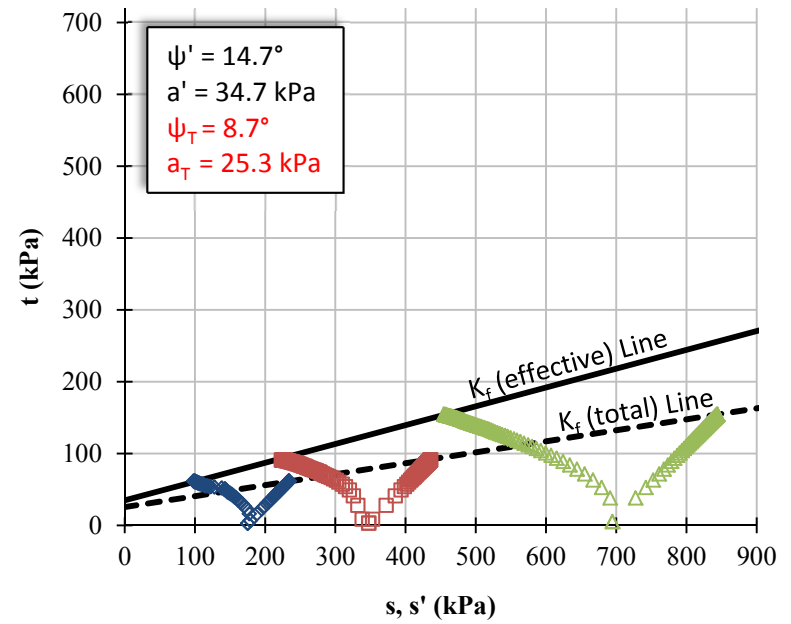
c)  Mean Stress vs. Deviator Stress (s – t)

**Figure 5.12. CU Triaxial Test Results for 100% Kaolin Specimen**
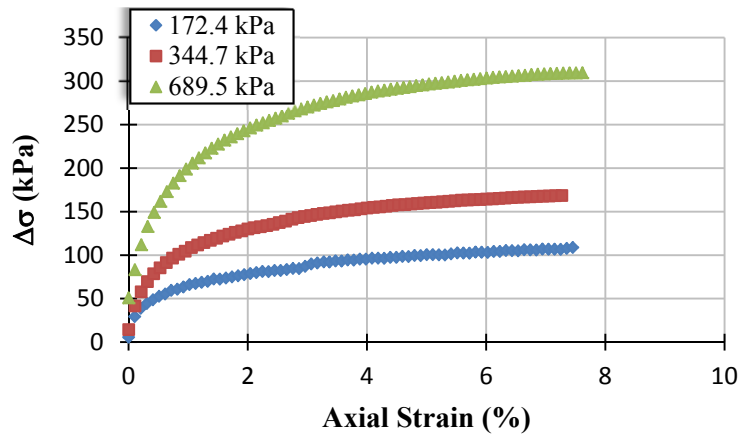
a)   Deviator Stress vs. Axial Strain
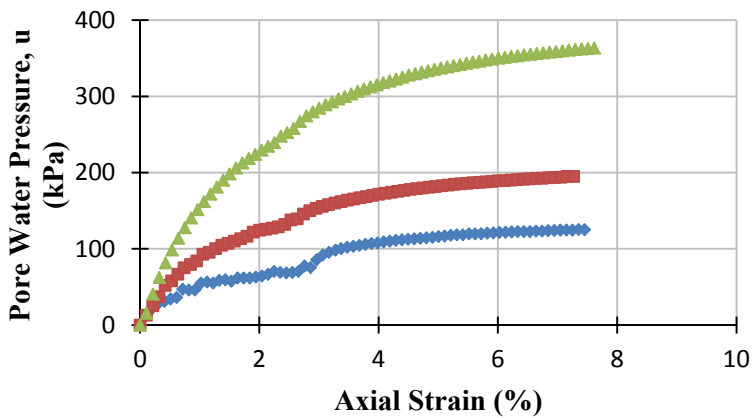


b)   Excess Pore Water Pressure vs. Axial Strain
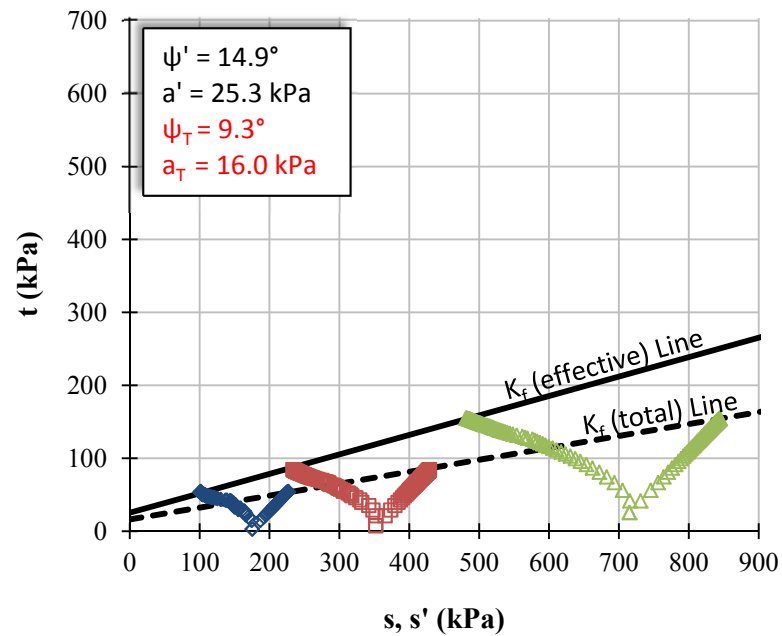


c)   Mean Stress vs. Deviator Stress (s – t)

**Figure 5.13.  CU Triaxial Test Results for 99.5% Kaolin : 0.5% EPS Particulate Specimen**
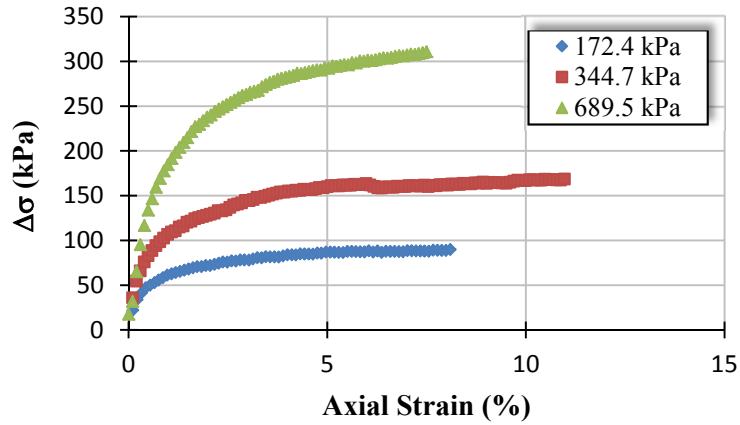
a)    Deviator Stress vs. Axial Strain
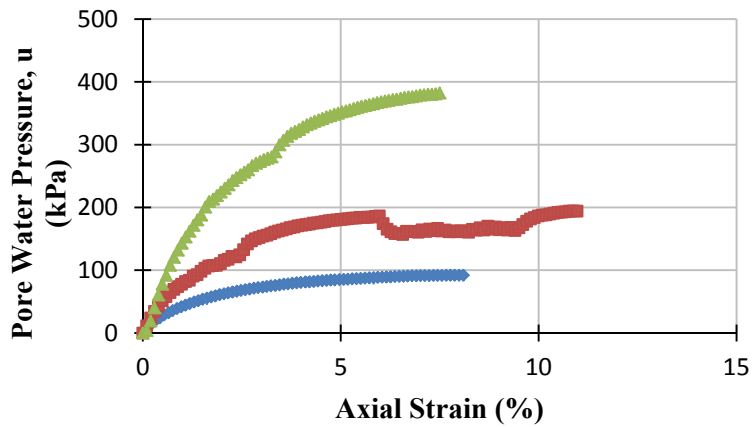


b)    Excess Pore Water Pressure vs. Axial Strain
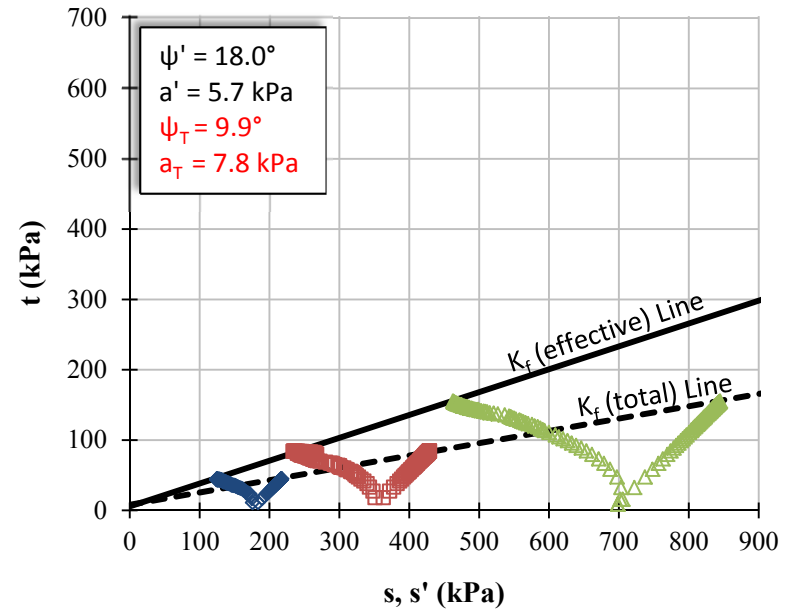


c)    Mean Stress vs. Deviator Stress (s – t)

**Figure 5.14.  CU Triaxial Test Results for 99% Kaolin : 1% EPS Particulate Specimen**
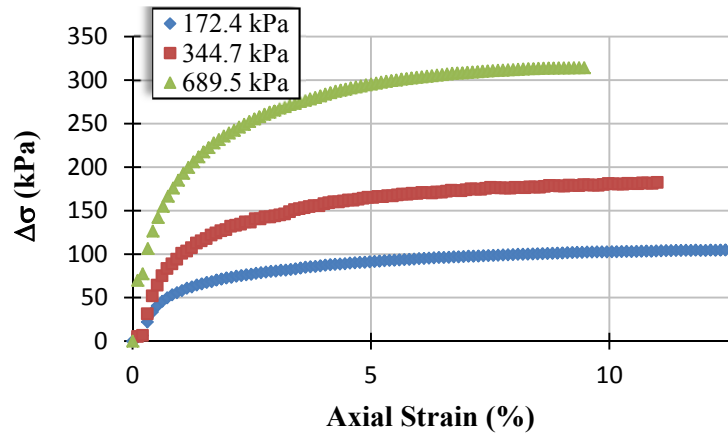
a)    Deviator Stress vs. Axial Strain
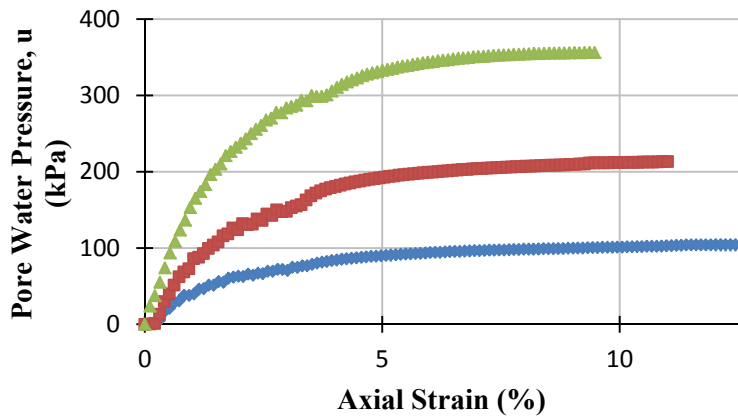


b)    Excess Pore Water Pressure vs. Axial Strain
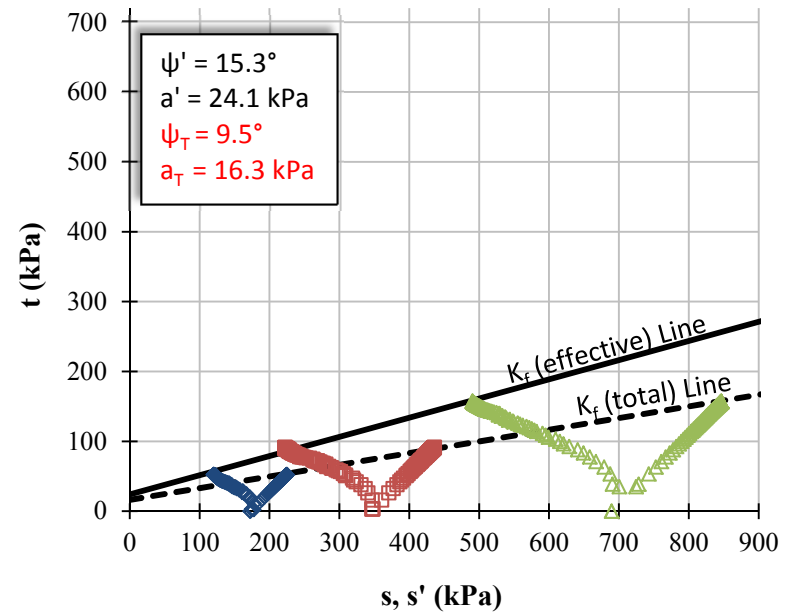


c)    Mean Stress vs. Deviator Stress (s – t)

**Figure 5.15.  CU Triaxial Test Results for 98.5% Kaolin : 1.5% EPS Particulate Specimen**

**5.4.2.3. CU triaxial strength parameters and moduli.**   The stress-strain data from the triaxial CU tests was analyzed to determine strength parameters.  The mean stress and deviator stress at failure were determined for all specimens and plotted.  The data was converted to polar coordinates and linearized following the procedures of Handy (1981) to correctly account for data variability.  The linear regression of the three points for each specimen defined the $K_f$ line, upon which the strength parameters (cohesion and friction angle) were determined from trigonometric conversions.

The tangent modulus for each specimen was determined from the strain-strain test data. The initial tangent modulus was determined by fitting a hyperbolic relationship to the measured stress-strain data using the procedures described by Kondner (1963).  The secant modulus ($E_{50}$) was determined for the specimens at 50% of the deviator stress at failure.

**Table 5.15.  CU Triaxial Strength Parameters & Moduli**

| Mix Ratio (% Kaolin:% EPS, by mass) | $\sigma_3{}'$ (PSI) | $\phi'$ (deg) | $c'$ (kPa) | $\phi_T$ (deg) | $c_T$ (kPa) | $E_{tangent,i}$ (MPa) | $E_{50}$ (MPa) |
|---|---|---|---|---|---|---|---|
| 100 : 0 | 25 | | | | | 17.7 | 10.8 |
| 100 : 0 | 50 | 15.2 | 35.9 | 8.8 | 25.5 | 37.7 | 22.3 |
| 100 : 0 | 100 | | | | | 48.6 | 27.4 |
| 99.5 : 0.5 | 25 | | | | | 13.6 | 9.2 |
| 99.5 : 0.5 | 50 | 15.5 | 26.2 | 9.4 | 16.5 | 25.1 | 13.5 |
| 99.5 : 0.5 | 100 | | | | | 64.4 | 22.9 |
| 99 : 1[1] | 25 | | | | | 17.1 | 10.9 |
| 99 : 1[1] | 50 | 19.0 | 6.2 | 10.1 | 8.3 | 29.1 | 17.0 |
| 99 : 1[1] | 100 | | | | | 39.6 | 20.5 |
| 98.5 : 1.5 | 25 | | | | | 10.3 | 6.4 |
| 98.5 : 1.5 | 50 | 15.9 | 24.8 | 9.6 | 16.5 | 18.6 | 10.8 |
| 98.5 : 1.5 | 100 | | | | | 41.0 | 24.3 |

Note:   [1]During consolidation a loss of panel pressure resulted in swelling of two of the specimens, and influenced shearing rates and subsequently specimen response.

# 6.    RESULTS – DYNAMIC PROPERTIES

The following chapter presents the results of experimental tests that were used to determine variations in dynamic soil properties with increasing EPS content. Low to intermediate torsional cyclic strains were applied to unit element specimens using the resonant column apparatus, and pulse velocity transmissions were performed using both bender element and ultrasonic pulse velocity transducers. Results from resonant column testing presented here are a summary. All results are presented in a tabulated form in the Appendix and raw data files recorded by the data acquisition system are also included in the Appendix. Measurements and post-processing of the data is presented herein and further discussion of the results is located in Chapter 7.

## 6.1.    RESONANT COLUMN

**6.1.1.    Specimen Properties.** Both slurry consolidated and compacted specimens were tested in the resonant column apparatus. In general, compacted specimens were prepared to 88% and 94% of the maximum dry density as defined in Section 5.2. All resonant column tests using compacted specimens were performed in duplicate for each specific soil to EPS particulate mix ratio and each relative compaction. Specimen characteristics for the compacted and slurry specimens are listed in Table 6.1 below. After testing of the specimens was completed, the samples were dismounted and dried to determine the final moisture content. On average, each specimen lost approximately 0.2% moisture (by mass) during the testing process, and thus air diffusion through the membrane was assumed to be negligible.

**6.1.2.    Results of Frequency Sweep.** As discussed in Section 4.5, the first portion of the resonant column test measured the specimen's response to a range of input frequencies at a constant torsional force. Figure 6.1 displays typical frequency response curves for a suite of measurements made at increasing torsional force on one specific specimen. The recorded shear strain levels, as defined by Equation 2.31, are plotted on a semi-log scale. The maximum recorded shear strain at each applied force defines the resonant frequency of the specimen. The shear strain is normalized by the maximum shear strain in Figure 6.2.

**Table 6.1.  Summary of Resonant Column Specimen Properties**

| Mix Ratio (% Kaolin:% EPS, by mass) | ID | $\omega_i$ (%) | $\gamma_{d,i}$ (kN/m³) | $\rho_{d,i}$ (g/cm³) | $e_{eq}$ | S (%) | Relative Compaction (%) |
|---|---|---|---|---|---|---|---|
| 100 : 0 | A | 27.7 | 12.6 | 1.28 | 1.063 | 68.8 | 88.6 |
| | D | 28.0 | 12.5 | 1.28 | 1.069 | 69.1 | 88.4 |
| | E | 28.5 | 13.3 | 1.36 | 0.947 | 79.4 | 93.9 |
| | F | 28.5 | 13.3 | 1.36 | 0.948 | 79.4 | 93.9 |
| | Slurry | 40.5 | 12.4 | 1.27 | 1.084 | 98.6 | n/a |
| 99.5 : 0.5 | A | 28.6 | 11.3 | 1.15 | 1.311 | 57.9 | 88.3 |
| | B | 27.1 | 11.0 | 1.12 | 1.369 | 52.5 | 86.2 |
| | C | 28.2 | 12.0 | 1.22 | 1.175 | 63.7 | 93.9 |
| | D | 28.1 | 11.9 | 1.21 | 1.187 | 62.8 | 93.3 |
| | Slurry | 40.6 | 11.0 | 1.12 | 1.368 | 78.8 | n/a |
| 99 : 1 | A | 27.3 | 10.4 | 1.06 | 1.522 | 47.8 | 88.2 |
| | B | 26.6 | 10.4 | 1.06 | 1.526 | 46.5 | 88.1 |
| | C | 28.2 | 10.9 | 1.11 | 1.395 | 53.9 | 92.9 |
| | D | 28.1 | 11.0 | 1.12 | 1.382 | 54.2 | 93.4 |
| | Slurry | 41.9 | 9.7 | 0.99 | 1.690 | 66.1 | n/a |
| 98.5 : 1.5 | A | 26.6 | 9.2 | 0.94 | 1.855 | 38.4 | 88.6 |
| | B | 26.6 | 9.2 | 0.94 | 1.852 | 38.5 | 88.7 |
| | E | 27.3 | 9.8 | 1.00 | 1.687 | 43.4 | 94.2 |
| | G | 27.3 | 9.8 | 1.00 | 1.686 | 43.4 | 94.2 |
| | Slurry | 41.2 | 9.0 | 0.92 | 1.915 | 57.7 | n/a |
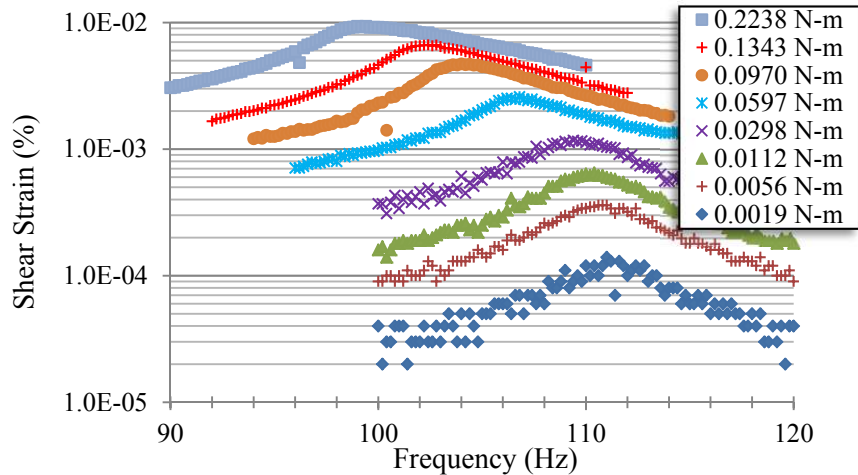


**Figure 6.1.  Frequency Response Curves**

**(98.5% Kaolin : 1.5% EPS Specimen G @ $\sigma_{cell}$ = 25kPa)**
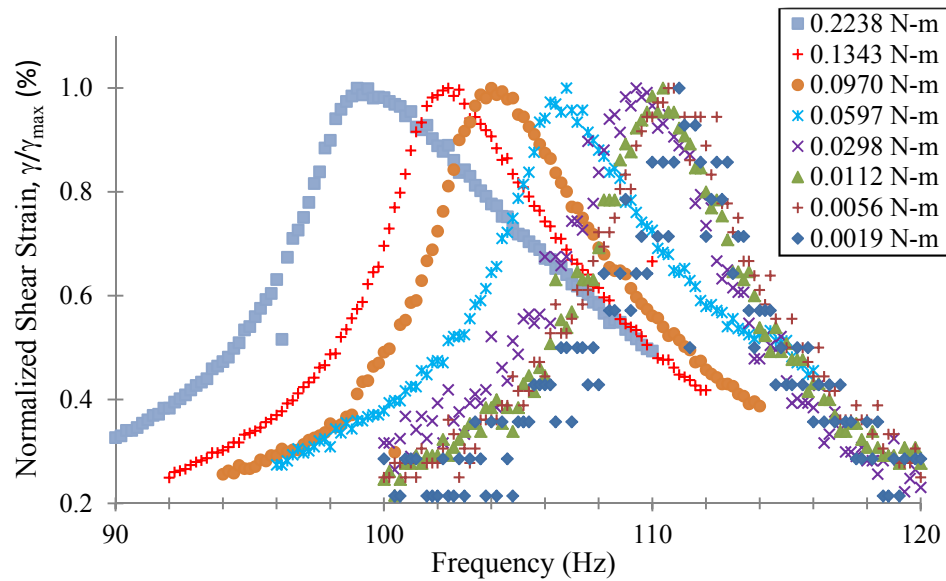
**Figure 6.2. Normalized Frequency Response Curve**
**(98.5% Kaolin : 1.5% EPS Specimen G @ $\sigma_{cell}$ = 25kPa)**

One result of increasingly larger torsional strains applied to the specimen is to decrease the resonant frequency; implying that the frequency response curve shifts to the left. At low strains the curves are symmetrical, which is indicative of linear-elastic soil behavior. With increasing strain level the frequency response curves shift to a lower resonant frequency and become more asymmetrical which indicates the initiation of non-linear behavior. The shear modulus is indirectly calculated from the resonant frequency (Section 2.4.1); thus the decrease in resonant frequency with increasing strain level coincides with the decrease in shear modulus. One final observation is the increased scatter at lower strain levels that systematically reduced at higher strains. The scatter is likely a function of the resolution of the accelerometer mounted on the resonant column apparatus.

Figure 6.3 displays discrete measurements from twenty cycles of forced vibration applied to the specimen at the resonant frequency. Data for increasing torsional force is displayed. The data shows that as the cyclic shear strain increased the area of the hysteresis loops subsequently increased which indicates increased damping according to Equation 2.6.
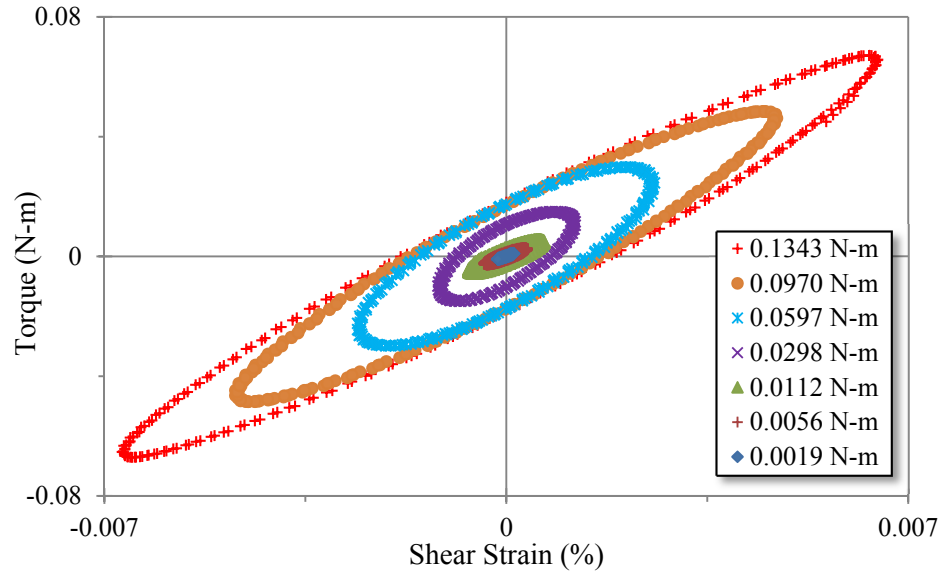
**Figure 6.3. Torque vs. Strain (98.5% Kaolin : 1.5% EPS Specimen G @ $\sigma_{cell}$ = 25kPa)**

**6.1.3.    Results of Free Vibration Decay.**  The final portion of the resonant column test involved measuring the free-vibration decay of motion in the specimen.    Figure 6.4 presents typical data from the free-vibration portion of the resonant column test.
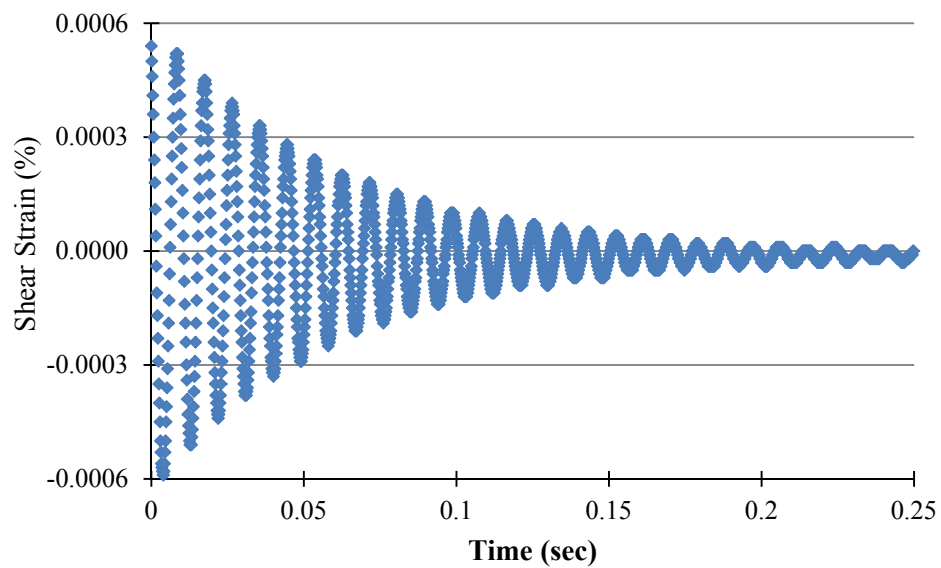


**Figure 6.4.  Free Vibrational Decay (98.5% Kaolin : 1.5% EPS Specimen G @ $\sigma_{cell}$ = 25kPa)**

The damping ratio, D, was used to quantify material damping and was calculated from the logarithmic decrement of free vibrations recorded after removal of torsional loading. The damping ratio was calculated from Equation 2.29 in which the logarithmic decrement was assumed to be constant for the initial cycles of motion. The data acquisition software used with the resonant column directly calculated the damping ratio from the free vibrational decay tests, but the raw data was analyzed independently to confirm the software's calculations. Figure 6.5 shows the independent determination of the logarithmic decrement for a 100% kaolin slurry consolidated specimen at a confining pressure of 25 kPa. Relative maxima and minima from the free vibration data were both used in the calculations. The logarithmic decrement becomes increasingly non-linear with increasing strain levels and number of cycles. Optimally, ten cycles of motion were used to estimate the logarithmic decrement. For example, the specimen at a cyclic shear strain of 0.025% in Figure 6.5 exhibited increasing non-linear behavior at cycles greater than six, and thus the damping ratio was calculated only for the minima and maxima for the first six cycles.

Table 6.2 shows the damping ratio as determined by the data acquisition system software versus the independent calculation of the damping ratio. Results indicated a good match in the damping ratio, and thus all data presented considers only the damping ratio as calculated by the data acquisition system software.
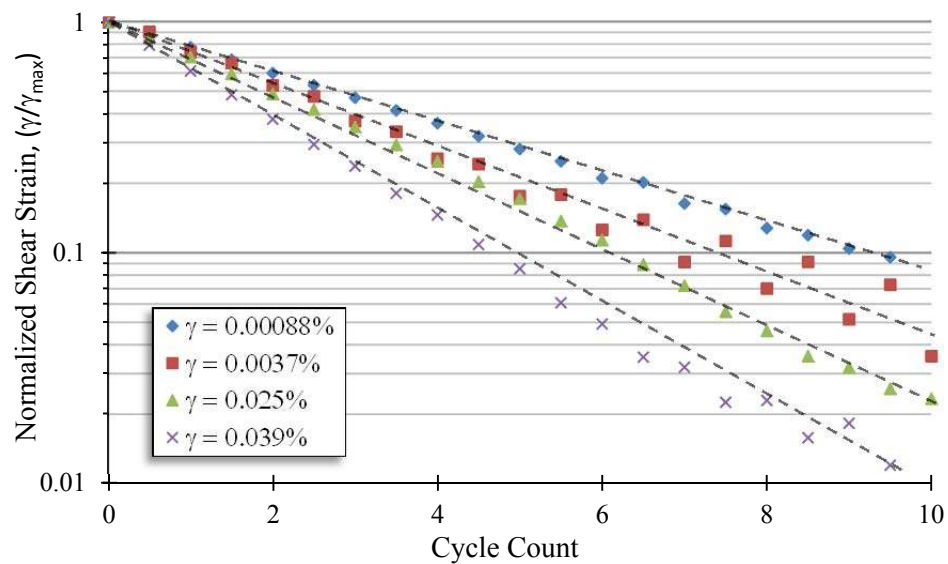


**Figure 6.5. Effect of Strain Level on Logarithmic Decrement**

**(100% Kaolin Slurry Specimen @ $\sigma_{cell}$ = 25kPa)**

**Table 6.2. Comparison of Damping Ratio (100% Kaolin Slurry Specimen @ $\sigma_{cell}$ = 25kPa)**

| I.D. | DAQ Damping Ratio (%) | Calculated Damping Ratio (%) |
|------|------------------------|-------------------------------|
| 010 | 3.49 | 3.53 |
| 011 | 3.73 | 3.70 |
| 012 | 3.95 | 3.98 |
| 013 | 4.01 | 4.07 |
| 014 | 4.92 | 4.97 |
| 015 | 5.71 | 5.94 |
| 017 | 6.18 | 6.17 |
| 018 | 7.51 | 7.41 |

**6.1.4. Shear Modulus Degradation Curves.** Figure 6.6 and Figure 6.7 display the shear modulus degradation curves for pure kaolin and modified soil specimens compacted to 88% and 94% relative compaction, respectively. Each specimen was tested at confining pressures of 10, 25, 50, 100, and 200 kPa. During testing, the shear modulus was first determined at the lowest possible strain level followed by progressively larger strain levels. Resonant column measurements made on the slurry consolidated specimens did not exhibit clear trends in terms of the shear stiffness magnitude, and it is believed that this is primarily due to the variations in the slurry consolidation process, density differences, and disturbance of the soft specimens during trimming and mounting in the resonant column apparatus. Tabulated data from the resonant column tests and the output files from the data acquisition program are presented for all specimens in the Appendix. Modulus reduction curves are often normalized by the maximum shear modulus. The normalization process easily allows identification of the percent reduction in the shear modulus for a given strain level. Figure 6.8 and Figure 6.9 display the shear modulus degradation curves normalized by the maximum shear modulus for specimens compacted to 88% and 94% relative compaction, respectively, and Figure 6.10 is the normalized modulus reduction curves for the slurry consolidated specimens.

**6.1.5. Variation of Damping Ratio with Cyclic Shear Strain.** Figure 6.11 and Figure Figure 6.12 display the variation in damping ratio with cyclic shear strain for pure kaolin and modified soil specimens compacted to 88% and 94% relative compaction, respectively, and Figure 6.13 is the data for the slurry consolidated specimens. Each specimen was tested at confining pressures of 10, 25, 50, 100, and 200 kPa. Only data from the free-vibrational decay portion of the resonant column test was used; damping measurements from the specimen frequency response or the hysteresis stress-strain loops were not conducted for this research. Measurements obtained are tabulated in the Appendix.
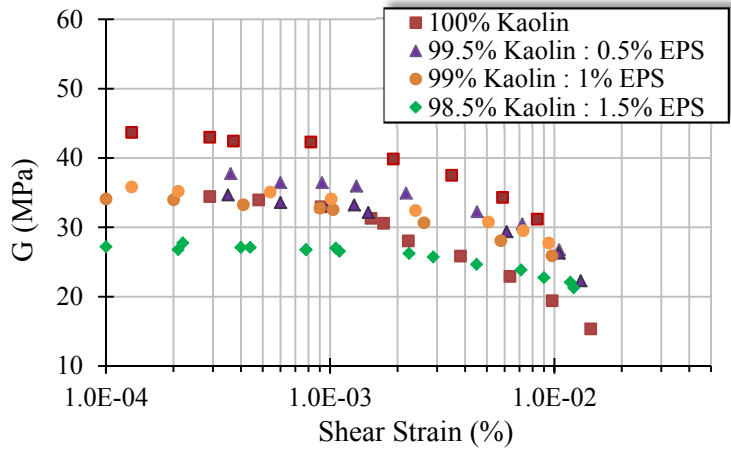
a)    25 kPa Confining Stress
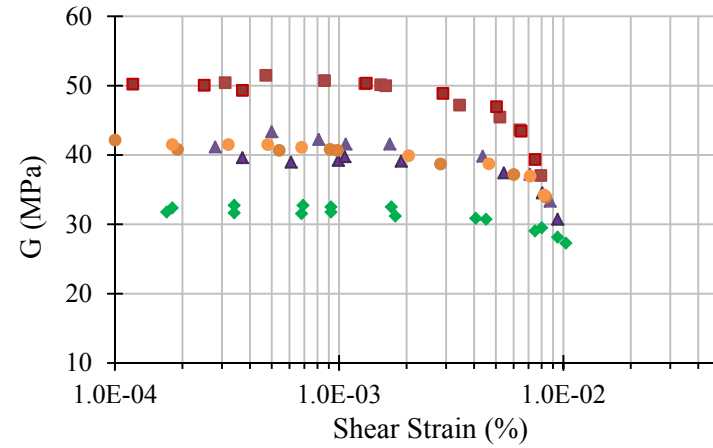
b)    50 kPa Confining Stress
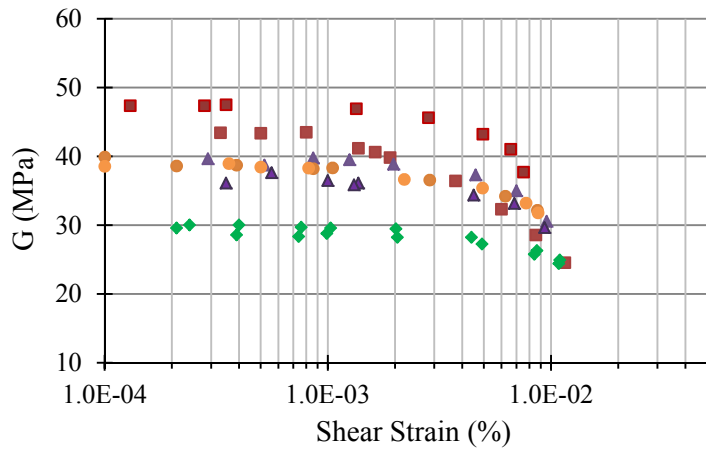
c)    100 kPa Confining Stress
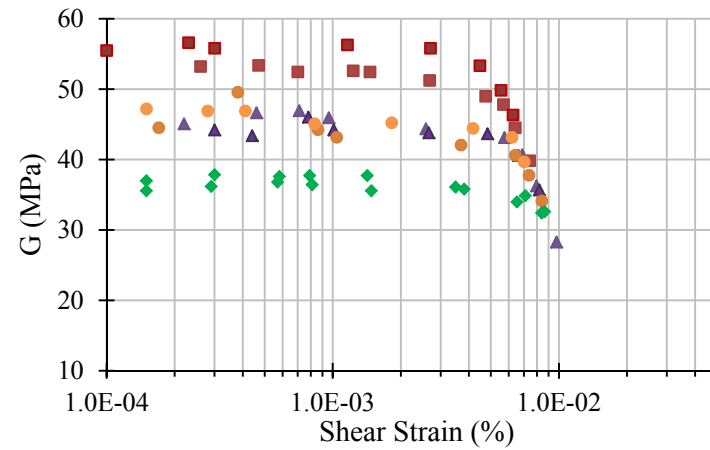
d)    200 kPa Confining Stress

**Figure 6.6. Modulus Degradation Curves (Compacted Specimens @ 88% Relative Compaction)**
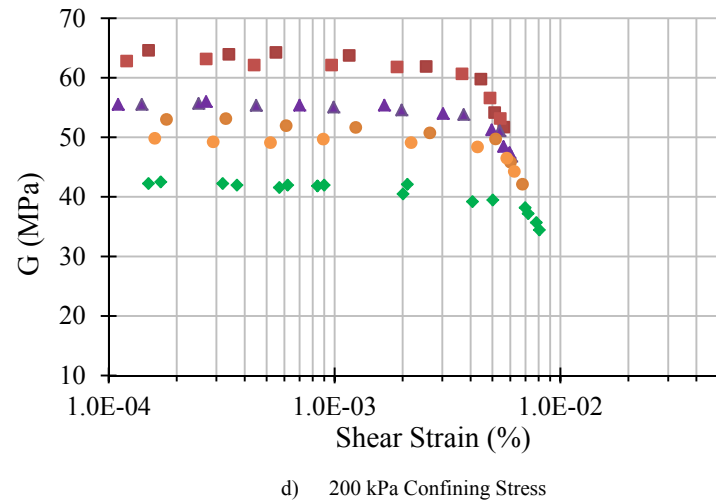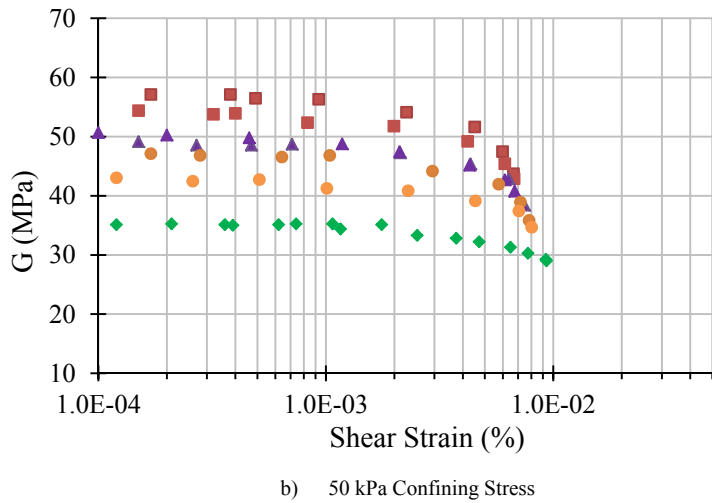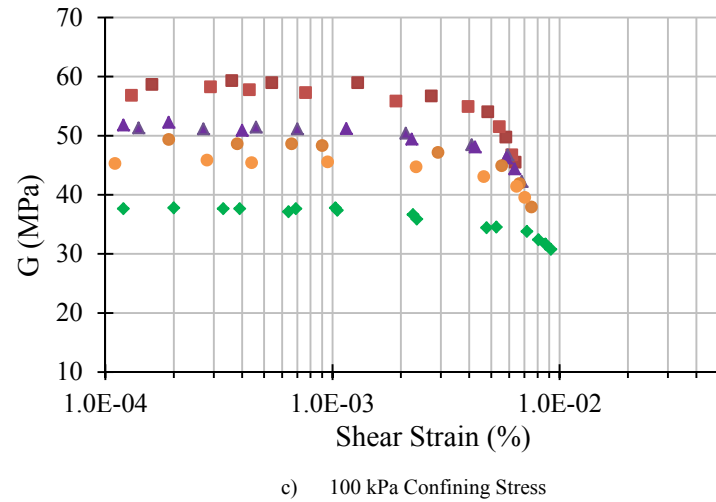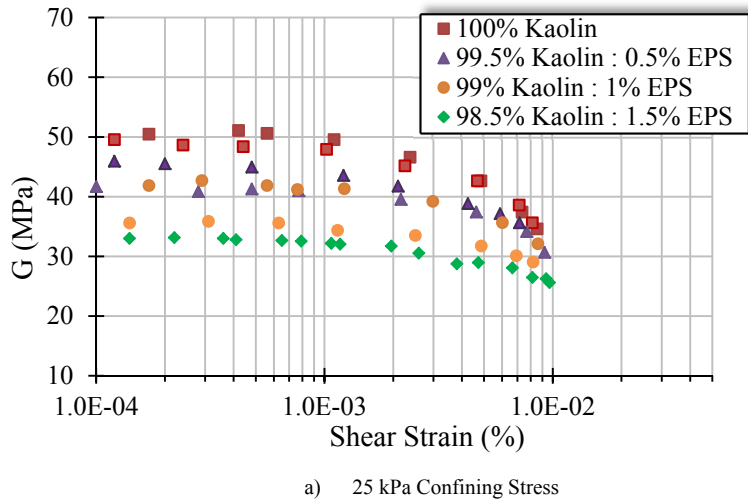
Figure 6.7. Modulus Degradation Curves (Compacted Specimens @ 94% Relative Compaction)
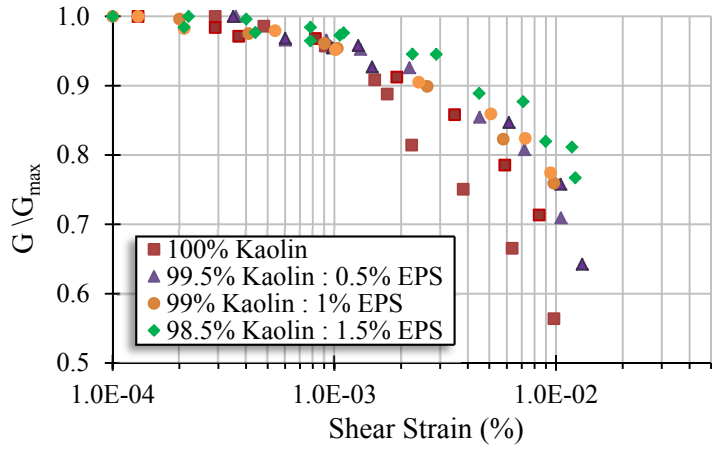
a)    25 kPa Confining Stress
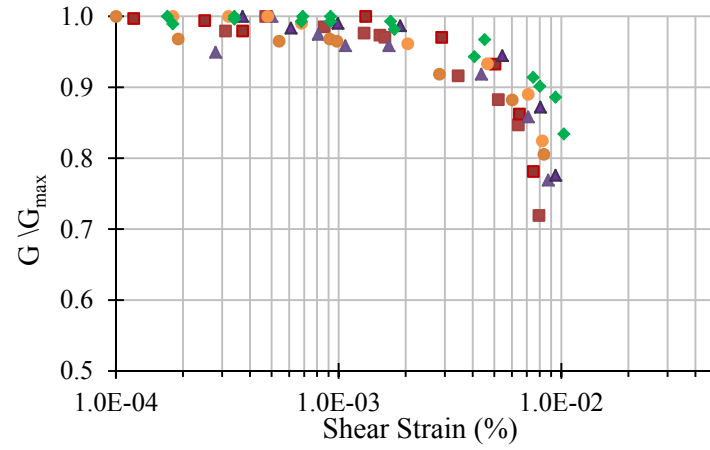
b)    50 kPa Confining Stress
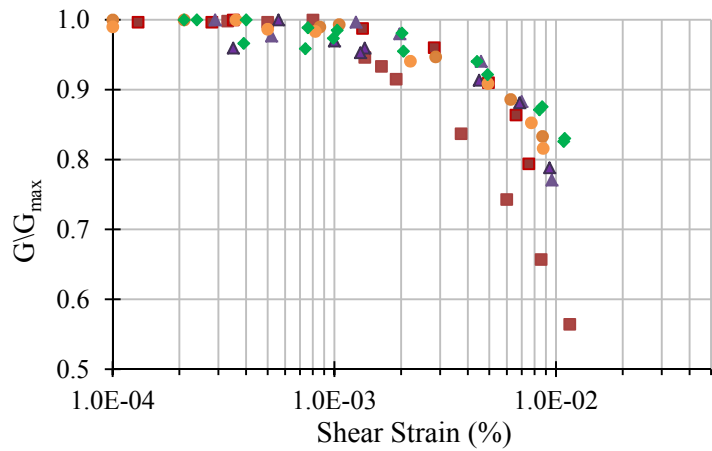
c)    100 kPa Confining Stress
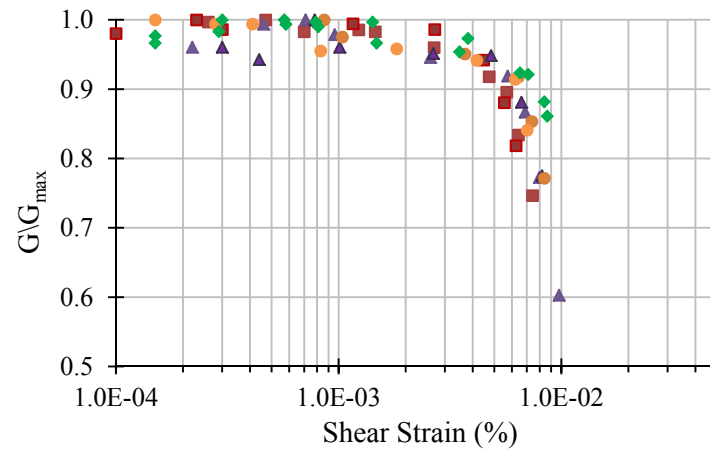
d)    200 kPa Confining Stress

**Figure 6.8. Normalized Modulus Degradation Curves (Compacted Specimens @ 88% Relative Compaction)**
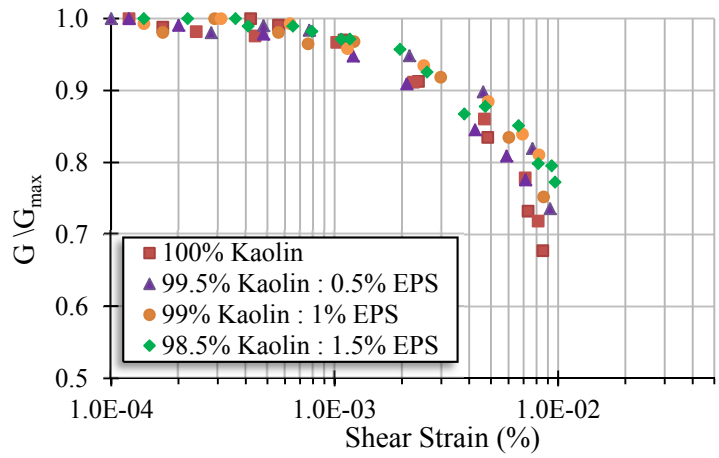
a)     25 kPa Confining Stress
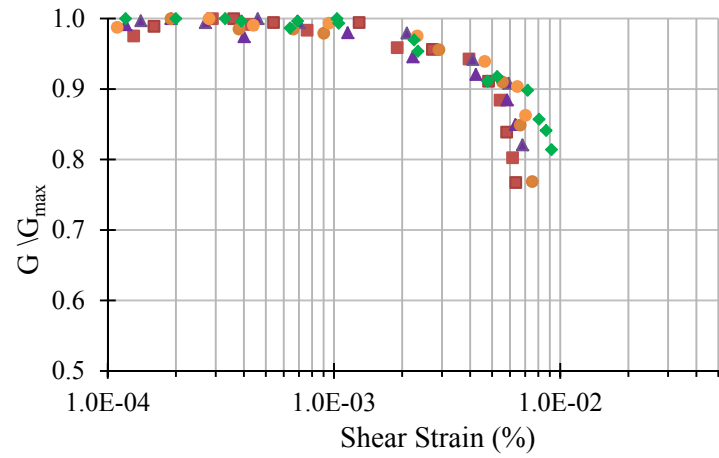
b)     50 kPa Confining Stress
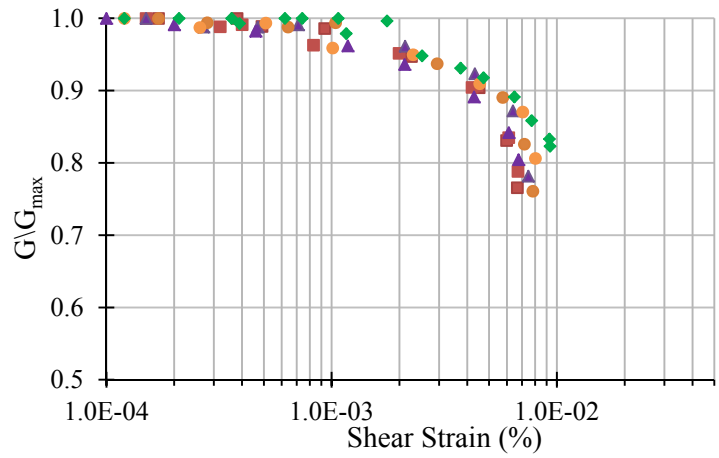
c)     100 kPa Confining Stress
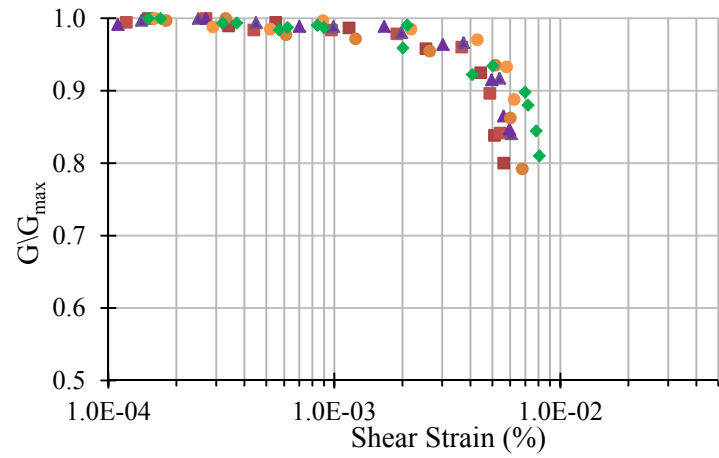
d)     200 kPa Confining Stress

**Figure 6.9. Normalized Modulus Degradation Curves (Compacted Specimens @ 94% Relative Compaction)**
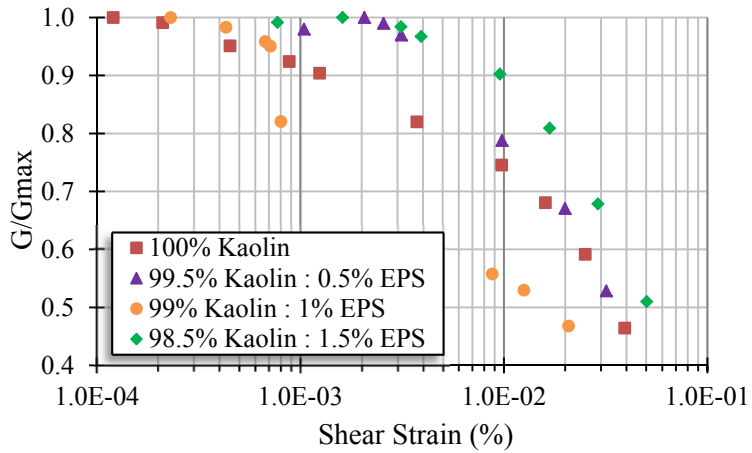
a)    25 kPa Confining Stress
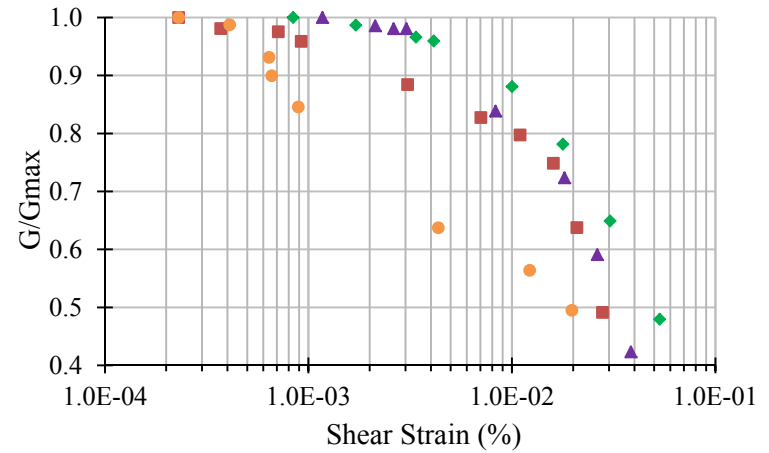
b)    50 kPa Confining Stress
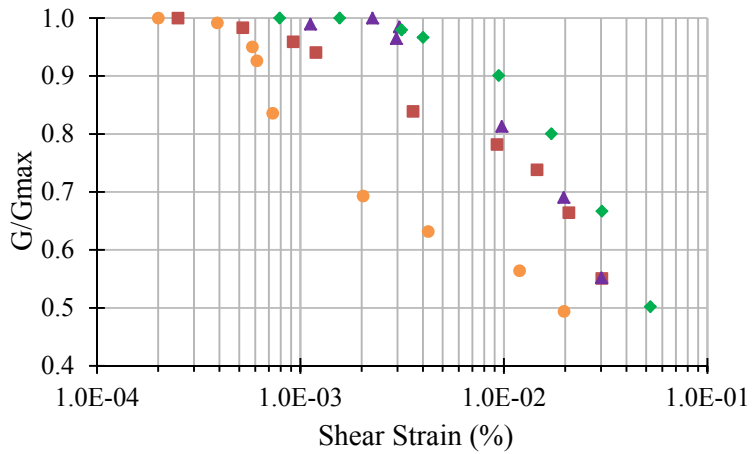
c)    100 kPa Confining Stress
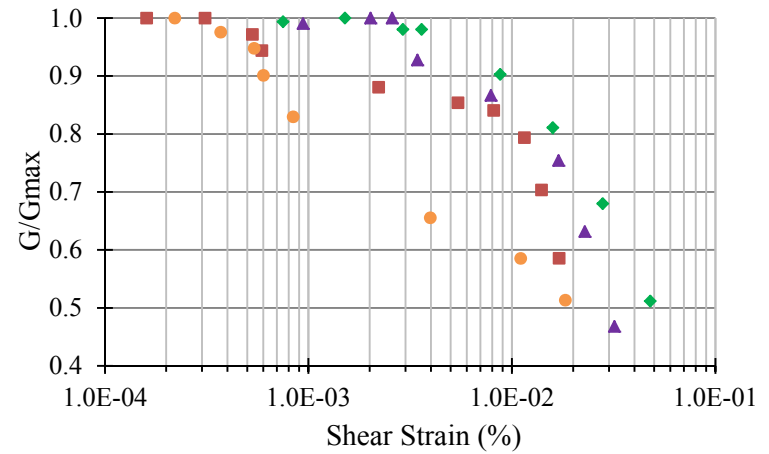
d)    200 kPa Confining Stress

**Figure 6.10. Normalized Modulus Degradation Curves (Slurry Consolidated Specimens)**
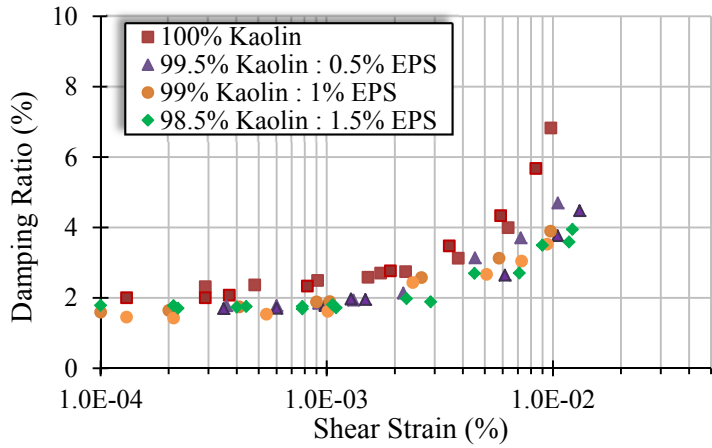
a)     25 kPa Confining Stress
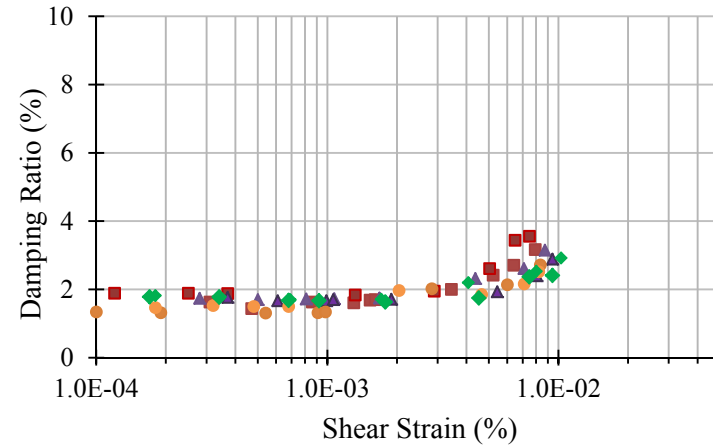
b)     50 kPa Confining Stress
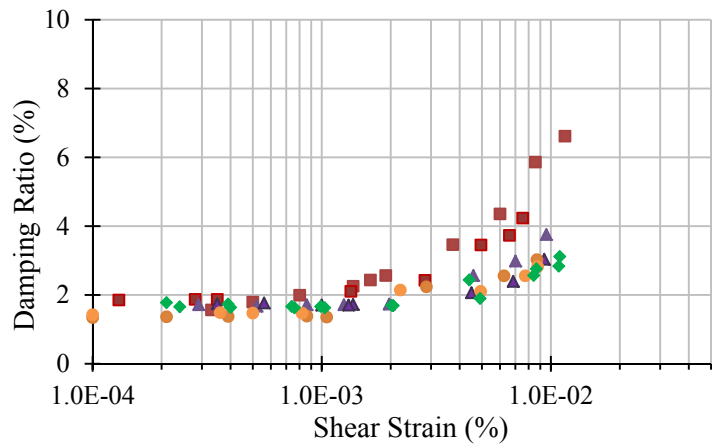
c)     100 kPa Confining Stress
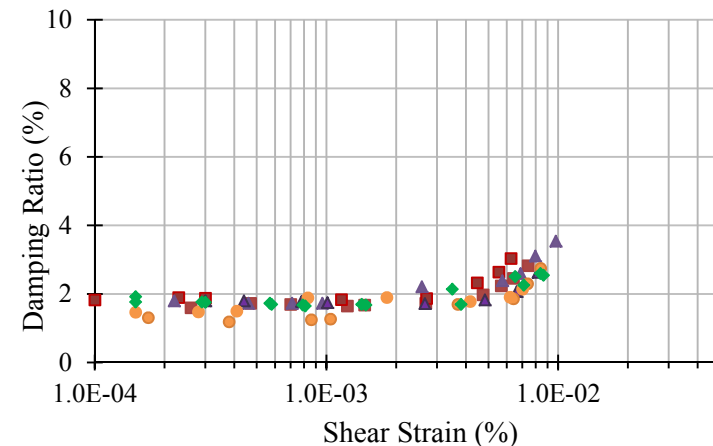
d)     200 kPa Confining Stress

**Figure 6.11. Damping Ratio versus Shear Strain (Compacted Specimens @ 88% Relative Compaction)**
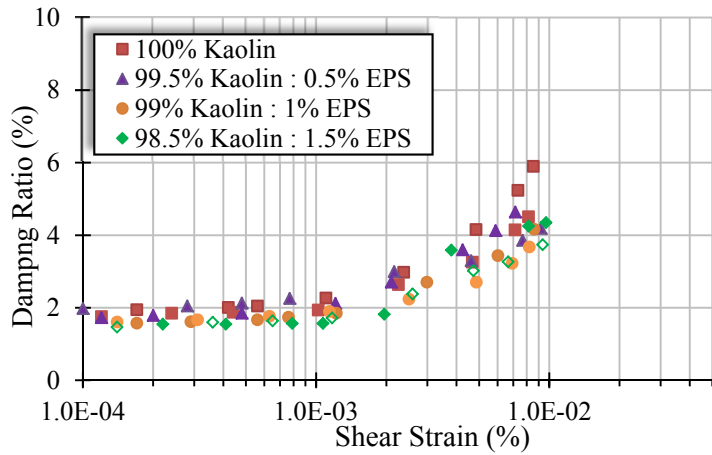
a)    25 kPa Confining Stress
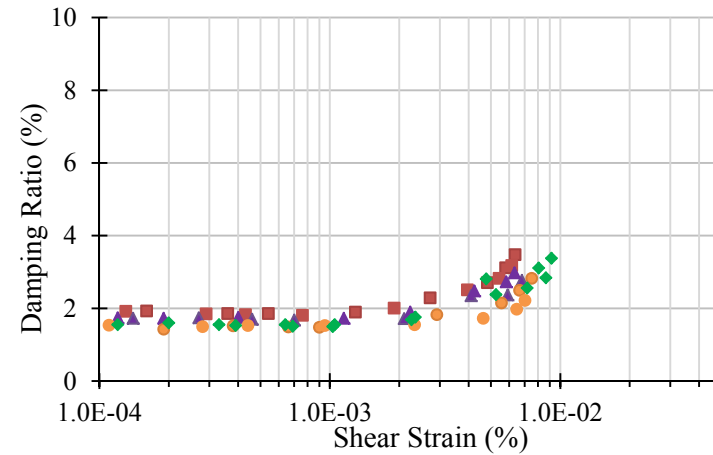
b)    50 kPa Confining Stress
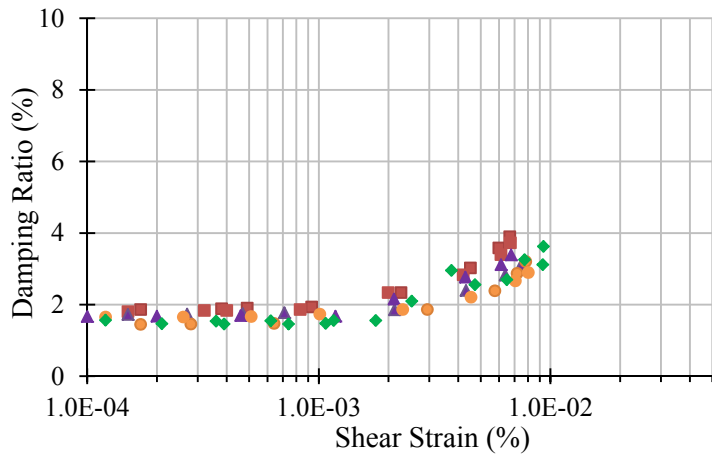
c)    100 kPa Confining Stress
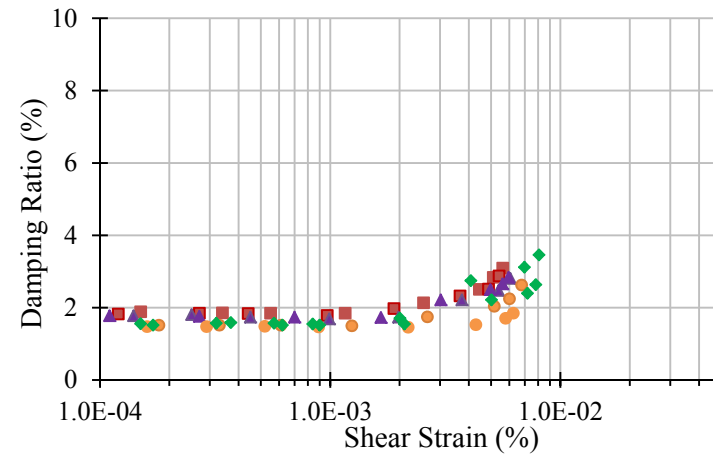
d)    200 kPa Confining Stress

**Figure 6.12. Damping Ratio versus Shear Strain (Compacted Specimens @ 94% Relative Compaction)**
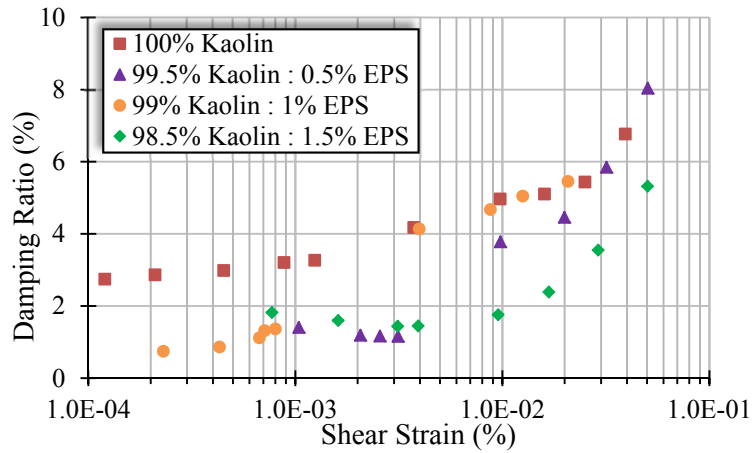
a.    25 kPa Confining Stress
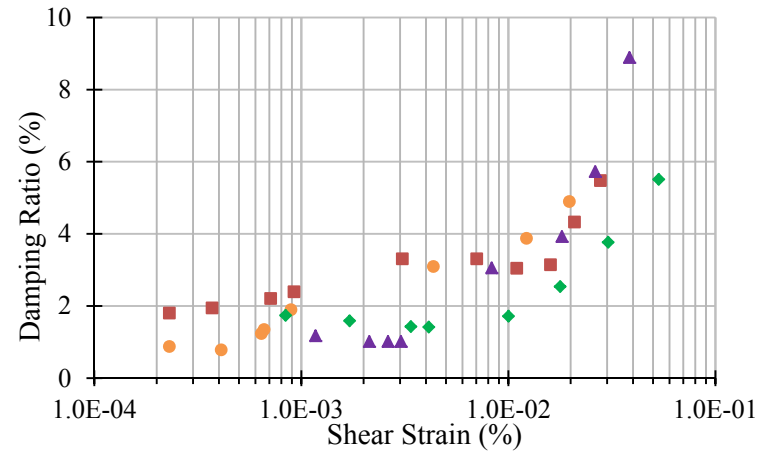
b.    50 kPa Confining Stress
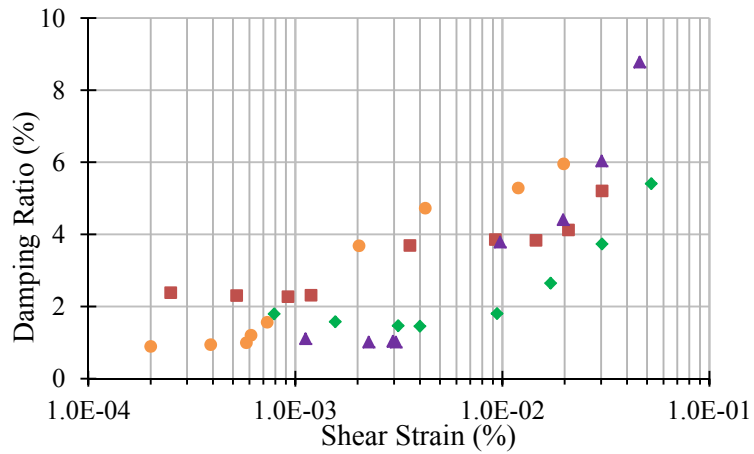
c.    100 kPa Confining Stress
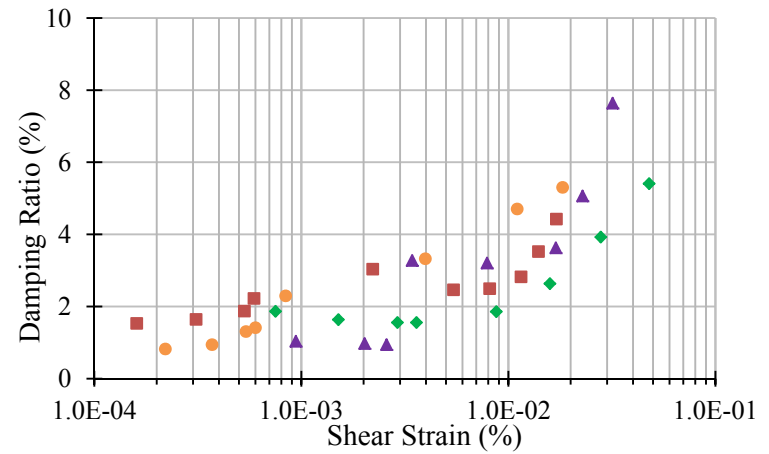
d.    200 kPa Confining Stress

**Figure 6.13. Damping Ratio versus Shear Strain (Slurry Consolidated Specimens)**

## 6.2. BENDER ELEMENT TESTS

**6.2.1. Specimen Properties.** Compacted specimens were tested in the resonant column apparatus. In general, specimens were compacted to 88% and 94% of the maximum dry density as defined in Section 5.2. All resonant column tests using compacted specimens were performed in duplicate for each specific soil to EPS particulate mix ratio and each relative compaction. Duplicate specimens were compacted at two different specimen lengths; approximately 78 mm and 145mm, respectively. Specimen lengths were arbitrarily selected to provide a more robust assessment of wave velocities when comparing duplicate specimens. Short specimens were compacted in the same mold as the longer specimens using three lifts of equal mass instead of five. Specimen characteristics for the bender element specimens are listed in Table 6.3 below.

**Table 6.3. Summary of Bender Element Specimen Properties**

| Mix Ratio (% Kaolin:% EPS, by mass) | ID | $\omega_i$ (%) | $\gamma_{d,i}$ (kN/m$^3$) | $\rho_{d,i}$ (g/cm$^3$) | $e_{eq}$ | S (%) | Relative Compaction (%) |
|---|---|---|---|---|---|---|---|
| 100 : 0 | 90S | 28.5 | 12.6 | 1.30 | 1.035 | 72.7 | 89.8 |
| | 90L | 28.2 | 12.7 | 1.29 | 1.052 | 70.8 | 89.1 |
| | 95S | 28.1 | 13.7 | 1.39 | 0.895 | 82.9 | 96.5 |
| | 95L | 28.2 | 13.5 | 1.38 | 0.916 | 81.2 | 95.4 |
| 99.5 : 0.5 | 90S | 27.6 | 11.1 | 1.13 | 1.338 | 54.7 | 87.3 |
| | 90L | 27.9 | 11.2 | 1.14 | 1.322 | 56.0 | 87.9 |
| | 95S | 27.4 | 12.0 | 1.22 | 1.171 | 62.1 | 94.0 |
| | 95L | 27.3 | 12.0 | 1.23 | 1.162 | 62.3 | 94.4 |
| 99 : 1 | 90S | 27.3 | 10.2 | 1.04 | 1.555 | 46.8 | 87.1 |
| | 90L | 26.8 | 10.5 | 1.07 | 1.500 | 47.7 | 89.0 |
| | 95S | 27.1 | 11.0 | 1.12 | 1.387 | 52.1 | 93.2 |
| | 95L | 26.8 | 11.2 | 1.13 | 1.358 | 52.6 | 94.4 |
| 98.5 : 1.5 | 90S | 27.7 | 9.1 | 0.92 | 1.899 | 39.1 | 87.3 |
| | 90L | 27.9 | 9.1 | 0.93 | 1.886 | 39.7 | 87.7 |
| | 95S | 27.4 | 9.7 | 0.99 | 1.704 | 43.1 | 93.6 |
| | 95L | 27.6 | 9.8 | 0.99 | 1.697 | 43.6 | 93.8 |

A multi-stage approach was used for bender element testing. Specimens were mounted in a triaxial chamber and initial pulse transmissions was recorded at atmospheric pressure. After testing was complete, the chamber pressure was increased and additional pulse transmissions were recorded. No drainage was allowed from the specimen during changes in cell pressure.

Pulse transmissions were performed at 0, 25, 50, 100, and 200 kPa in succession. After testing of the specimens was completed, the samples were dismounted and dried to determine the final moisture content. On average, each specimen lost approximately 0.2 – 0.4% moisture (by mass) during the testing process, and thus air diffusion through the membrane was assumed to be negligible.

      **6.2.2. Post-Processing of Wave Transmission Data.** Bender element pulse transmission tests were performed according to the procedures discussed in Section 4.6.2. Stacking of repeated signals was performed by the oscilloscope and discrete measurements of the wave pulse were post-processed using a routine in Matlab® (Mathworks 2011). Since the oscilloscope was directly attached to the signal generator and not the signal amplifier, the recorded signals needed to be multiplied by an amplification factor equal to the amplification setting. The Matlab routine allowed the option to simply plot the raw data or apply various processing techniques. Some signals contained low-frequency noise that was manifested as a linear ramping of the recorded signal in the time domain, as shown in Figure 6.14. This noise was removed by fitting a low frequency function to the original signal and subsequently subtracting the trend from the measured data (Santamarina and Fratta 2005). This filtering process is typically called signal detrending and is programmed in the Matlab routine in two parts. The first detrend process removes the linear ramping of the signal, and the second detrend process re-orientates the signal at the zero voltage axis.
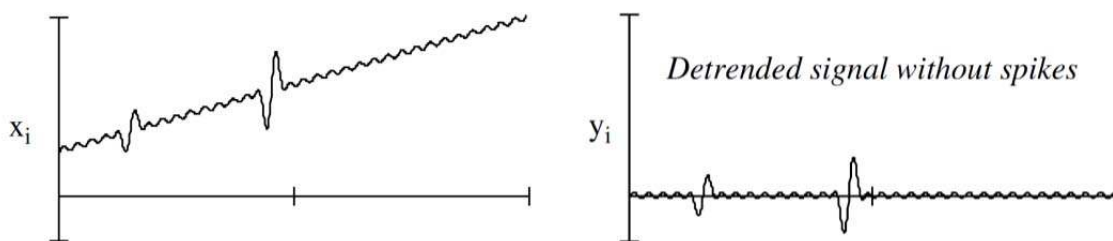


**Figure 6.14. Signal Detrending (from Santamarina & Fratta 2005)**

      The signal processing routine also allowed application of an $n^{th}$ order Butterworth band-pass filter by defining the low-pass cutoff frequency and high-pass cutoff frequency. An ideal band-pass filter allows a specific frequency band of the original signal to pass through the filter with distortion while suppressing frequencies greater than and less than the cutoff frequencies.

For all analyses the low-pass frequency was set at 1 – 2.5 kHz and the high-pass frequency was set at 25 - 50 kHz, but in general there was little improvement of the signal from the application of the band-pass filter.

   **6.2.3. Analysis of Pulse Transmissions.** After the recorded signals were processed using the procedures previously described, the data was plotted at a range of frequencies for each specimen at a specific cell pressure. Presentation of pulse transmission tests at a variety of frequencies can aid in the determination of the wave arrivals and also help to assess the influence of the near field effect, if any. In general S-wave pulses were transmitted at frequencies of 5, 10, 20 and 40 kHz and P-wave pulses were transmitted at frequencies of 5, 10, and 20 kHz. Typical results are shown in Figure 6.15 for S-wave pulse tests and Figure 6.16 for P-wave pulse tests. Relevant signal data is shown to the right of each plot. The P-wave transmissions at 5 kHz are quite poor as a portion of the wave energy arrives before the entire sinusoid has been transmitted.

   The frequency of the transmitting signal, $f_{in}$, is simply the frequency of the generated sinusoid pulse. The characteristic frequency of the received signal, $f_{out}$, was determined by frequency analysis of the recorded wavelet. The travel time of the signal from the tip of the transmitting bender element to the tip of the receiving bender element, $\Delta t$, will be discussed in more detail below. The specimen length to wavelength ratio, $L_{tt}/\lambda$, was determined for each specimen and frequency using the following relationship:

$$L_{tt} / \lambda = L_{tt}\left(\frac{f}{V}\right) = f\Delta t \qquad\qquad \textbf{(6. 1)}$$

   The ratio of transmission length to wavelength needed consideration for its influence on the near-field effect. Direct time measurements based on the first deflection of the received signal can be influenced by the near field effect, as discussed in Section 2.4.2. The measured wavelength ratios indicated that near-field effects would not need to be considered for pulse transmissions at frequencies of greater than 5 kHz, but the pulse transmissions using a 5 kHz signal were often influenced. Since the near field effect is not an issue for P-wave transmissions, the data in Figure 6.16 does not include the determination of $L/\lambda$ .
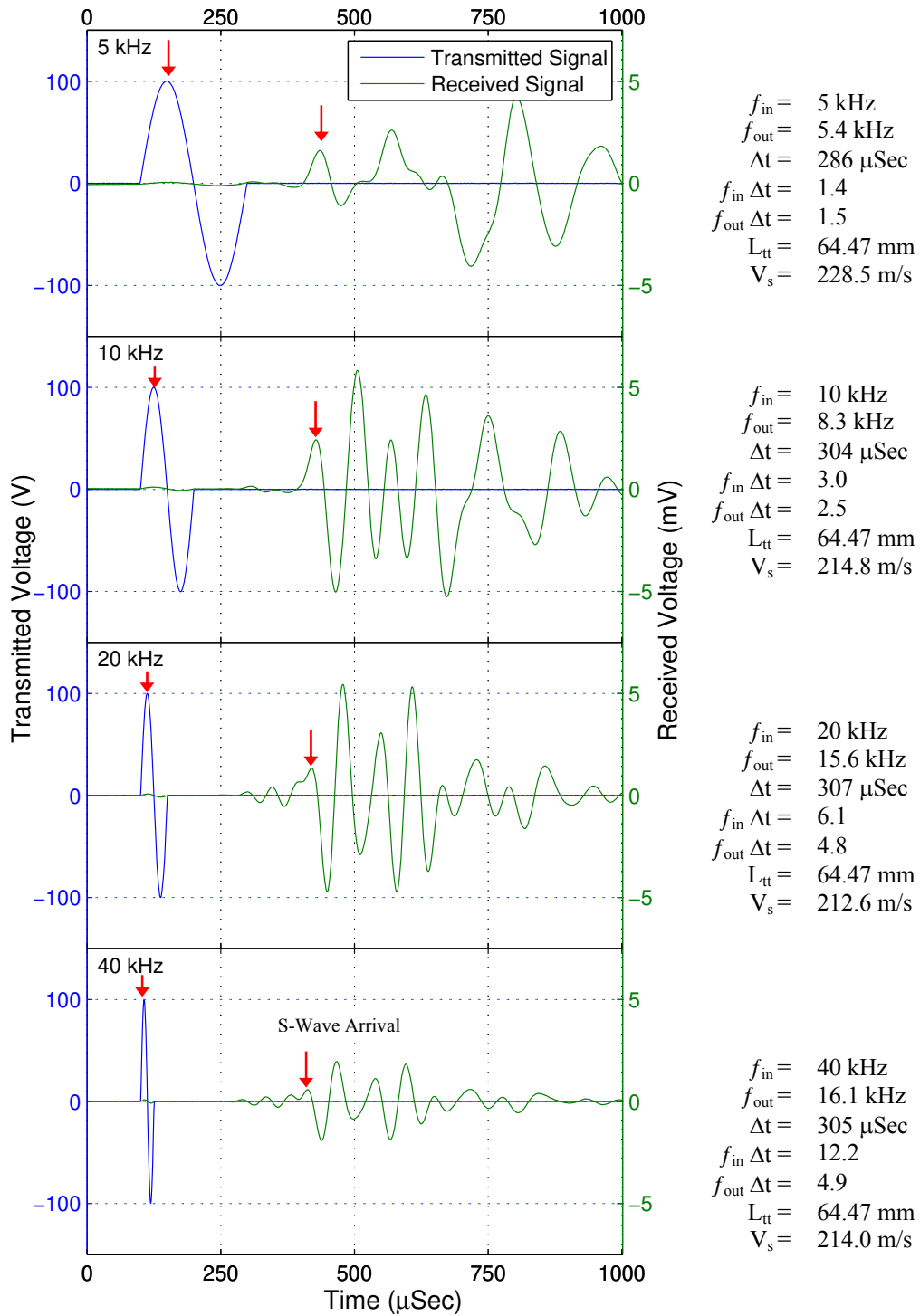
**Figure 6.15. Typical Bender Element S-wave Pulse Transmission (99.5% Kaolin : 0.5% EPS; 94% Relative Compaction; $\sigma_{cell}$ = vent)**
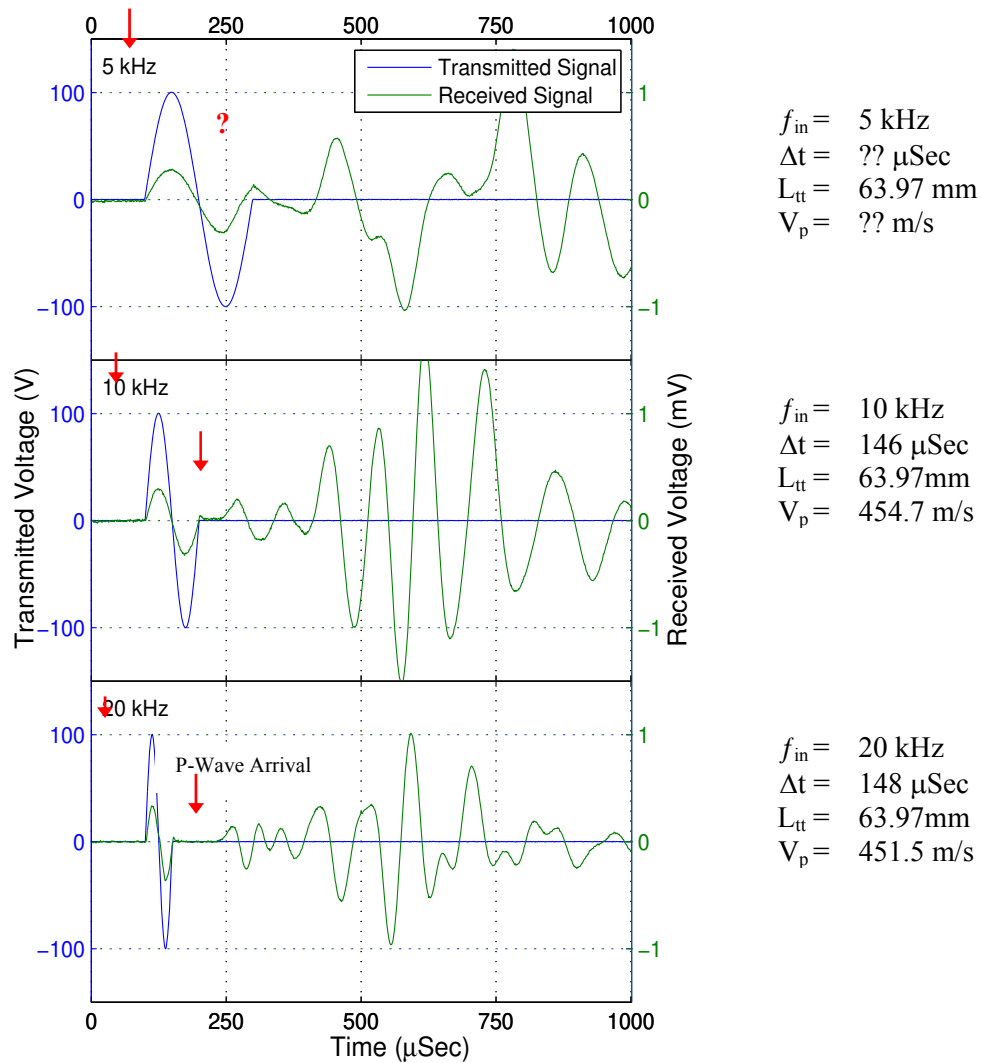
**Figure 6.16. Typical Extender Element P-wave Pulse Transmission**
**(99.5% Kaolin : 0.5% EPS; 94% Relative Compaction; $\sigma_{cell}$ = 50 kPa)**

The data in Figure 6.15 and Figure 6.16 indicate that both P-wave and S-wave pulse transmissions using bender-extender elements are influenced by both compressional and shear wave energy and thus measurement of both the velocities is important to assess each individual wave arrival. A simple cross-section of the bender elements embedded into a soil specimen also depicts how both compression and shear energy is generated during the transmission of S-wave pulses, as shown in Figure 6.17. This phenomenon, termed directivity by Santamarena (2001), is

in addition to any near field effects and increases the confusion in selecting the shear wave arrival. The generated compressional wave energy travels along the specimen boundaries and the initial arrival and reflection off the end platen can both influence the recorded wave signature.
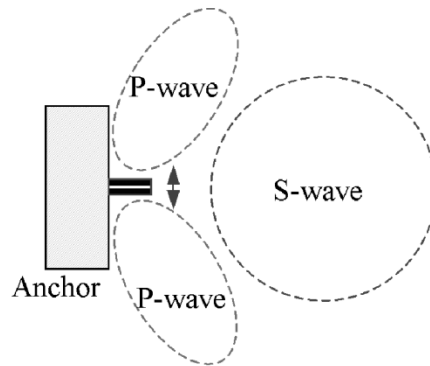


**Figure 6.17. Directivity of Bender Element S-wave Transmissions**
**(from Lee and Santamarina 2005)**

During P-wave pulse tests shear wave energy can also be generated if the bender elements are not perfectly aligned and vertical. Realistically the exact alignment and orientation of the bender elements is not possible, thus some shear energy is always present during P-wave testing. This occurrence is not much of a problem as the S-waves travel at a much slower speed than the P-waves and do not influence the determination of the P-wave arrival.

**6.2.4. Measured Wave Velocities.** All measurements of travel time for this research program utilized direct travel time measurements in the time domain. Various interpretation methodologies of direct travel time measurements were discussed in Section 2.4.2.1. Considering the factors that can affect the recorded wavelet, the determination of each wave arrival required careful consideration. P-wave velocities for 88% and 94% relative compaction specimens are shown in Figure 6.18 and Figure 6.19, respectively and the wave arrival was chosen as the point of first signal reversal, as previously identified in Figure 2.14. Wave arrivals were difficult to determine for the longest compacted specimens. Extender elements are relatively weak sources of dynamic excitation, and thus the small amount of energy imparted upon the specimens was attenuated during transmission.
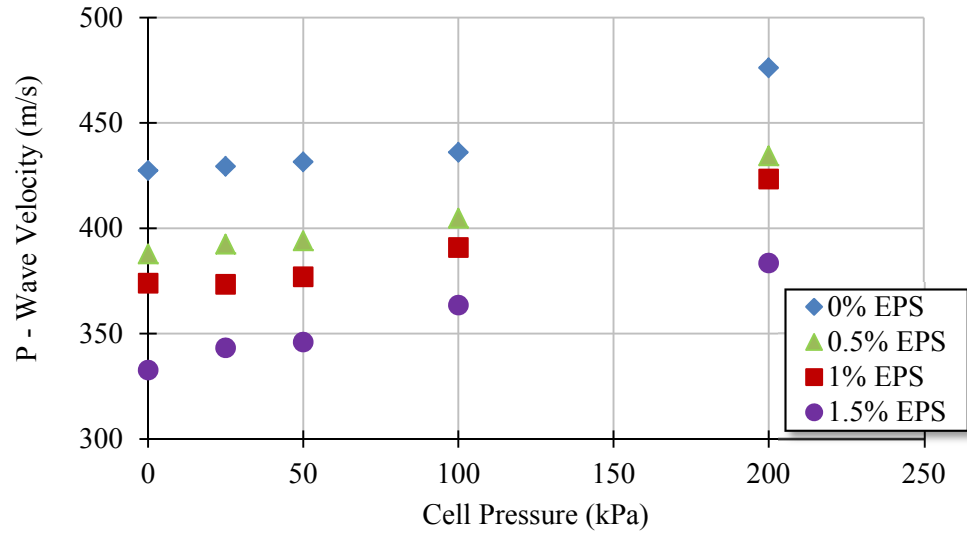
**Figure 6.18.  Measured P-wave (Compressional) Velocity (88% Relative Compaction)**
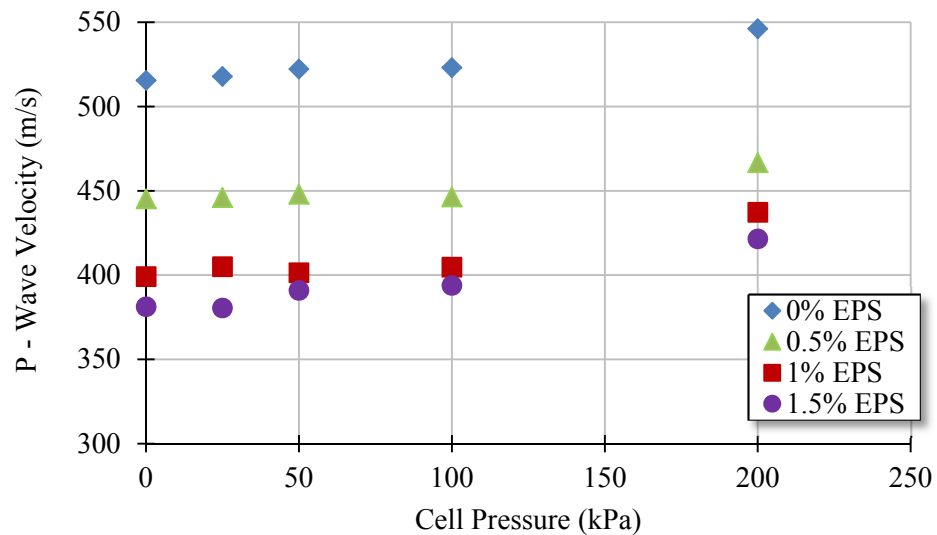


**Figure 6.19.  Measured P-wave (Compressional) Velocity (94% Relative Compaction)**

Measured S-wave velocities are shown in Figure 6.20 and Figure 6.21.  The data presented used the "peak – to – peak" methodology to determine the transmission time, which was previously described in Section 2.4.2.1.
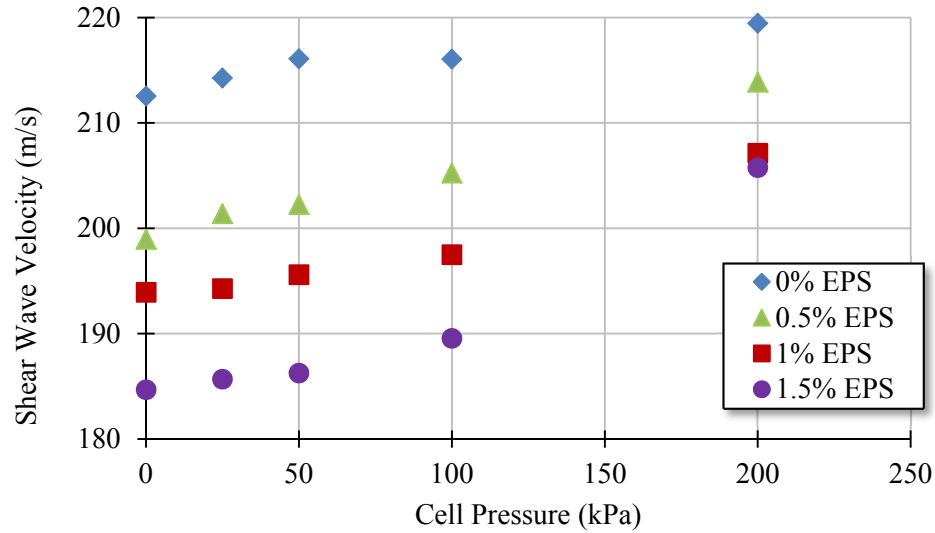
**Figure 6.20. Measured S-wave (Shear) Velocity (88% Relative Compaction)**
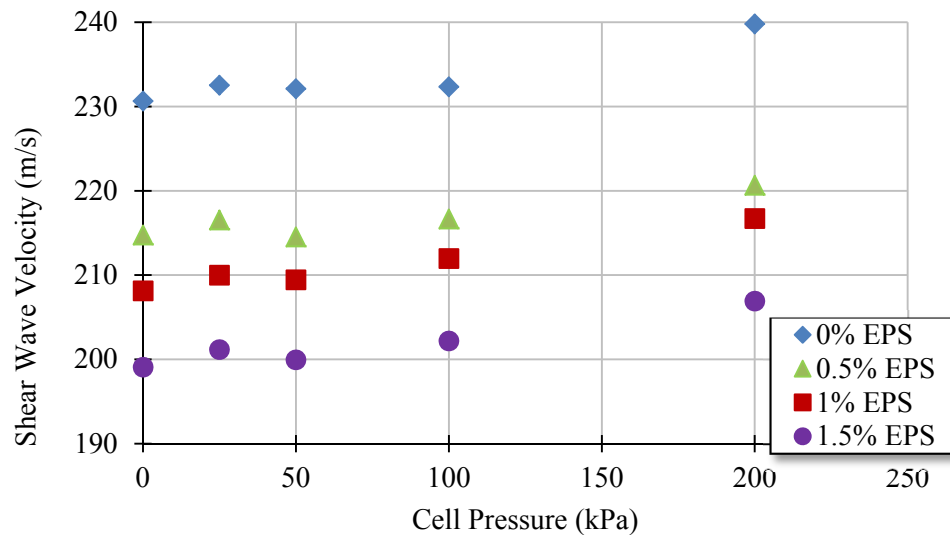


**Figure 6.21. Measured S-wave (Shear) Velocity (94% Relative Compaction)**

The measurements obtained with the duplicate short and long specimens were not overly precise, even though the general trend of decreasing shear wave velocity with increasing EPS content were the same for all specimen lengths. The differences are attributed to slight changes in specimen densities and the possibility that the transducers were influenced by direct contact

with EPS particulates during testing. For clarity only the data from the shorter specimens has been presented, and the remaining data is included in the Appendix.

**6.2.5. Dynamic Moduli.** The measurement of both compressional and shear wave velocities using the bender-extender transducers results in significantly more information regarding the material's dynamic soil properties. The shear modulus (G) and Young's modulus (E) were computed from the measured wave velocities using Equations 2.2 and 2.5, respectively.

Specimen density is required to determine dynamic moduli from wave velocities. For partially saturated specimens, volume change during increases in cell pressure cannot be reliably measured since compression of pore air constitutes a significant part of the overall volume change. In the testing reported within this report, compression of air voids constituted all the volume change as drainage was not allowed. Typically there are two primary ways to measure volume change in unsaturated specimens: (1) monitoring changes in the confining cell fluid; and (2) direct measurement of vertical and radial strain on the specimen. Since air was used as the confining cell fluid during bender element testing, specimen volume changes could not be reliably monitored by the changes in the cell fluid. Specimen changes were monitored by an attached vertical LVDT, but radial strain measurements were not realized during testing as the appropriate transducers were not available. Radial strains were estimated using the calculated Poisson's ratio ($\nu$) from the previous stress state that relied upon measurements of the P-wave and S-wave velocities. Poisson's ratio was calculated according to Equation 2.3. The following procedure was followed throughout bender element pulse testing to estimate changes in specimen density during increases in the confining pressure:

Stage 1: $\sigma_{cell}$ = Vent; $\rho$ based on specimen geometry, mass, and water content; measure $V_p$ and $V_s$ during pulse transmissions; calculate G, E, and $\nu$.

Stage 2: $\sigma_{cell}$ = 25 kPa; $\varepsilon_V$ determined from internal LVDT measurements; $\varepsilon_H$ calculated from $\varepsilon_V$ and $\nu$ (from previous Stage); $\rho$ based on changes in specimen length and radius as defined by $\varepsilon_H$ and $\varepsilon_V$; measure $V_p$ and $V_s$ during pulse transmissions; calculate G, E, and $\nu$ using updated $\rho$.

The shear moduli versus confining pressure are plotted in Figure 6.22 and Figure 6.23 for specimens compacted to 88% and 94% relative compaction, respectively. The figures include data synthesized from the duplicate, short and long specimens and results indicated that the duplicate specimens were uniform for each specific mix ratio.
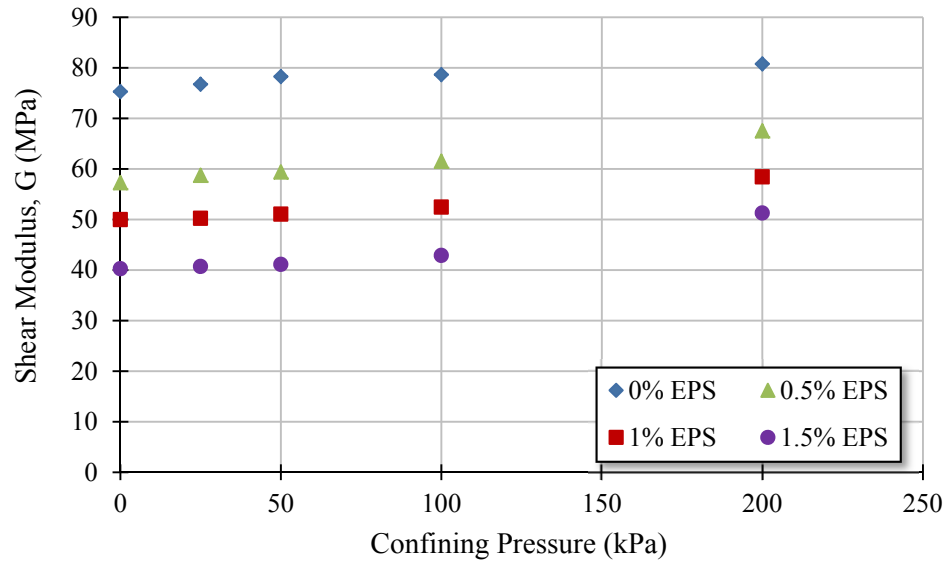
**Figure 6.22.  Shear Modulus vs. Confining Pressure (88% Relative Compaction)**
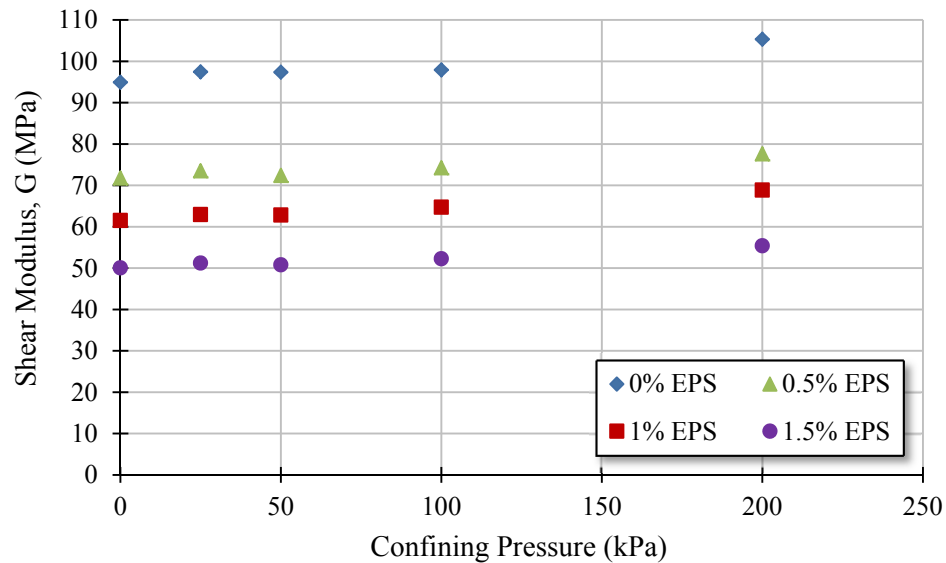


**Figure 6.23.  Shear Modulus vs. Confining Pressure (94% Relative Compaction)**

Similarly, Young's moduli versus confining pressures are plotted in Figure 6.24 and Figure 6.25 for specimens compacted to 88% and 94% relative compaction, respectively, and the data from the duplicate specimens also indicate the specimens were uniform for each specific mix ratio.
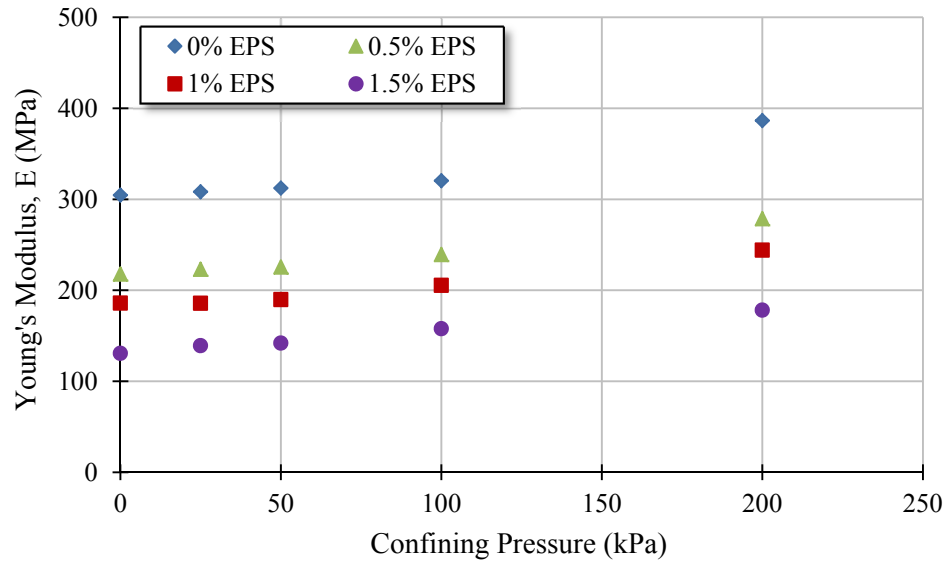
**Figure 6.24. Young's Modulus vs. Confining Pressure (88% Relative Compaction)**
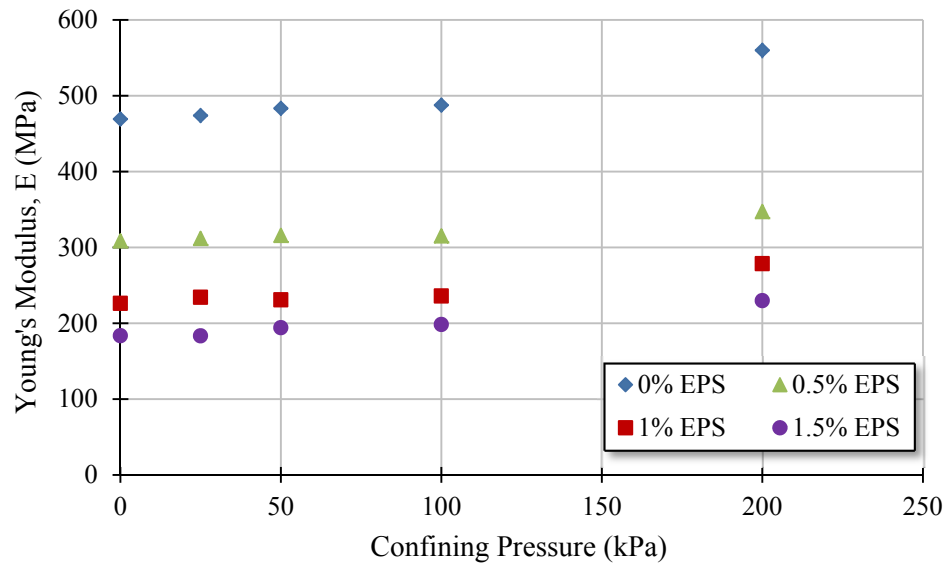


**Figure 6.25. Young's Modulus vs. Confining Pressure (94% Relative Compaction)**

The estimation of Poisson's ratio ($\nu$) required the determination of both compressional and shear wave velocities. Poisson's ratio was determined according to Equation 2.3 and the bulk modulus using Equation 2.4. Poisson's ratio versus confining pressures are plotted in Figure 6.26 and Figure 6.27 for specimens compacted to 88% and 94% relative compaction, respectively.
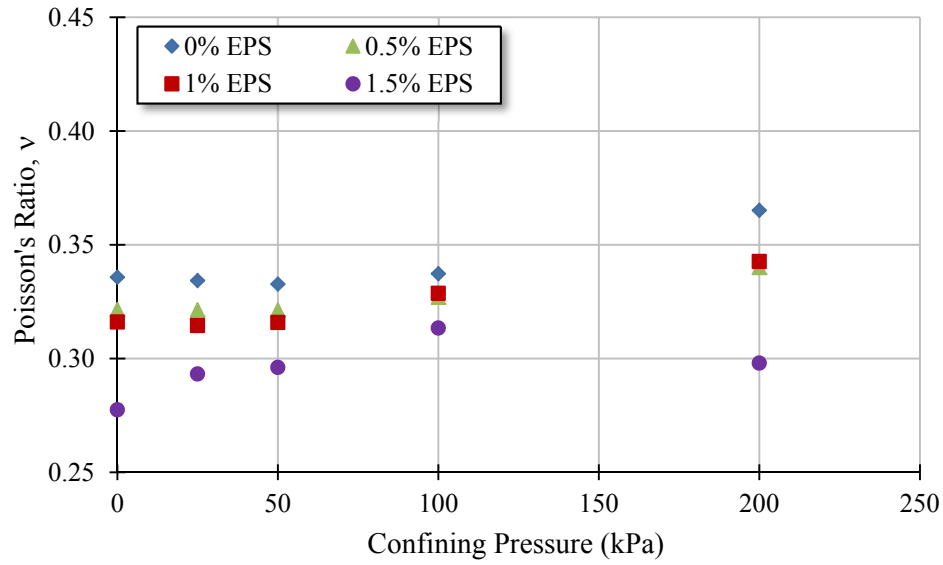
**Figure 6.26. Poisson's Ratio vs. Confining Pressure (88% Relative Compaction)**
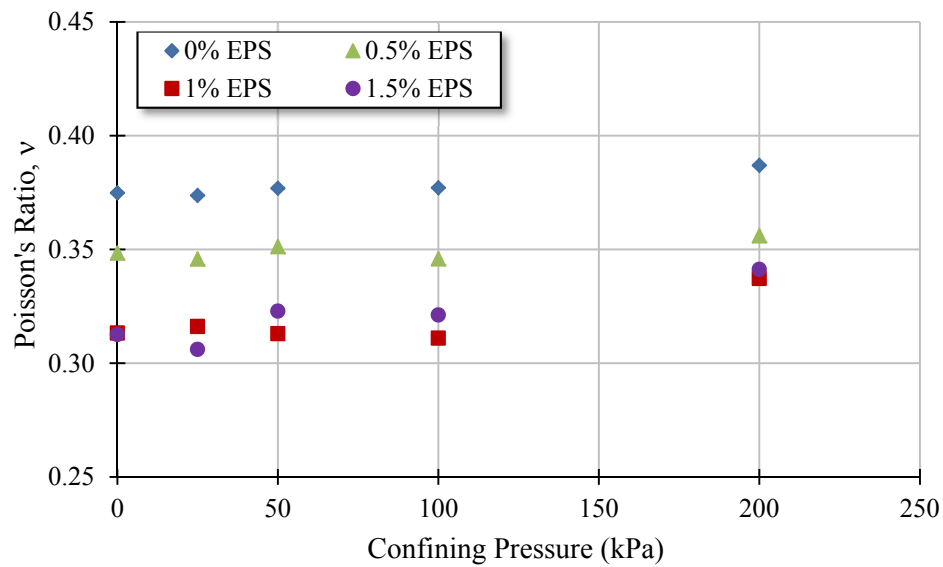


**Figure 6.27. Poisson's Ratio vs. Confining Pressure (94% Relative Compaction)**

## 6.3.    ULTRASONIC PULSE VELOCITY TESTS

**6.3.1.    Specimen Properties.**  Four different compacted specimens were tested using the ultrasonic pulse velocity equipment.  Both long and short specimens were remolded at densities of approximately 88% and 94% relative compaction.  In addition, three slurry consolidated specimens were tested.  Specimen properties are listed in Table 6.4.

Similar to the bender element tests, a multi-stage approach was used for ultrasonic pulse velocity testing.  Specimens were mounted in a triaxial chamber and initial pulse transmissions were recorded at 10 kPa cell pressure.  This small pressure was used to ensure good contact between the specimens and the end platen transducers.  After testing was complete, the chamber pressure was increased and additional pulse transmissions were recorded.  No drainage was allowed from the specimen during changes in cell pressure.  Pulse transmissions were performed at 10, 25, 50, 100, and 200 kPa in succession. After testing of the specimens was completed, the samples were dismounted and dried to determine the final moisture content.  On average, each specimen lost less than 0.5% moisture by mass during the entire multi-stage testing process, and thus air diffusion through the membrane was assumed to be negligible for these relatively short duration tests.

**Table 6.4.  Ultrasonic Pulse Velocity Specimen Properties**

| Mix Ratio (% Kaolin:% EPS, by mass) | Remold Type | ID | $\omega_i$ (%) | $\gamma_{d,i}$ (kN/m$^3$) | $\rho_{d,i}$ (g/cm$^3$) | $e_{eq}$ | S (%) | Relative Compaction (%) |
|---|---|---|---|---|---|---|---|---|
| 100 : 0 | Slurry | ** | 40.5 | 12.5 | 1.27 | 1.080 | 99.0 | n/a |
| 99.5 : 0.5 | Slurry | ** | 40.8 | 10.9 | 1.11 | 1.383 | 78.3 | n/a |
| 99 : 1 | Slurry | ** | 41.8 | 9.5 | 0.96 | 1.767 | 63.1 | n/a |
| 98.5 : 1.5 | Compacted | 1Long | 27.5 | 9.1 | 0.93 | 1.894 | 38.9 | 87.4 |
| | | 1Short | 27.1 | 9.1 | 0.93 | 1.884 | 38.6 | 87.7 |
| | | 3Long | 27.4 | 9.7 | 0.99 | 1.705 | 43.1 | 93.5 |
| | | 2Short | 27.1 | 9.7 | 0.99 | 1.705 | 42.6 | 93.5 |

**6.3.2.    Ultrasonic Pulse Velocity Transmissions.**  Ultrasonic pulse transmissions were performed according the procedures outlined in Section 4.6.3.  Stacking of repeated signals was performed by the oscilloscope and signal processing of the discrete signals were performed in a Matlab® using the techniques discussed previously in Section 6.2.2.

Initially an entire suite of ultrasonic pulse velocity transmissions tests were planned, similar to the bender element pulse transmission tests. Results from the first group of compacted specimens prepared (1.5% EPS by mass) indicated that attenuation of the ultrasonic pulse signals were too significant for both the longer, 145 mm, and shorter, 78 mm, specimen lengths. The S-wave arrival times were very difficult to determine given the signal to noise ratio and thus no clear initial deflection could be identified that conclusively indicated the wave arrival, as shown in Figure 6.28 and Figure 6.29 for long and short specimens, respectively. Likewise, the P-wave arrival times were also difficult to determine. The significant noise and ambiguity in selecting the appropriate wave arrival time resulted in modifying the testing program and reducing the number of ultrasonic tests performed.
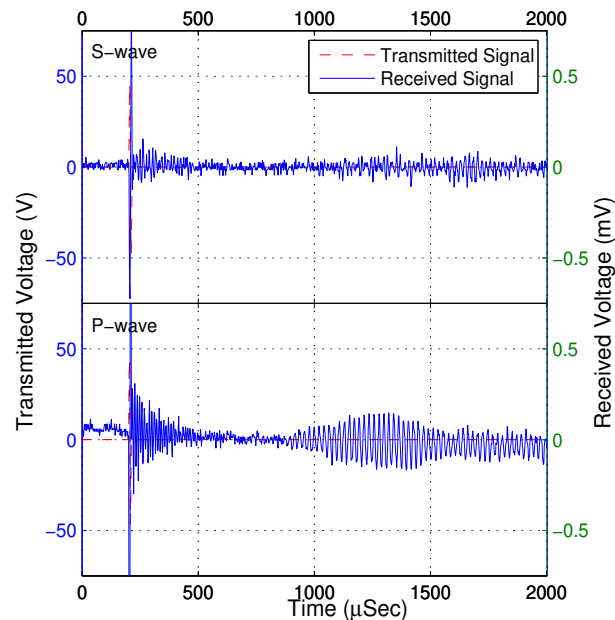


**Figure 6.28.  Ultrasonic Wave Signature**

**(98.5% Kaolin : 1.5% Kaolin Compacted Specimen 1Long @ $\sigma_{cell}$ = 50 kPa)**
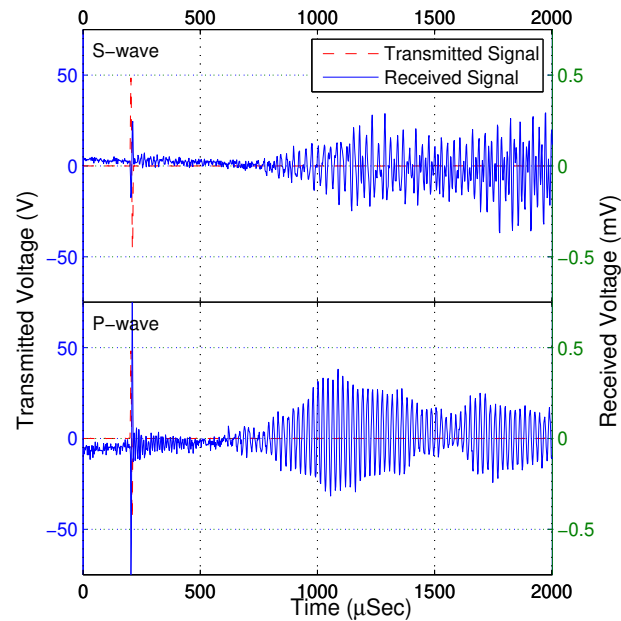
**Figure 6.29.  Ultrasonic Wave Signature**

**(98.5% Kaolin : 1.5% Kaolin Compacted Specimen 1Short @ $\sigma_{cell}$ = 50 kPa)**

Ultrasonic pulse transmissions for the slurry specimens were much stronger and thus arrival times were determined (note the difference in the received signal strength in Figure 6.29 and Figure 6.30).  In all cases the P-wave transmissions resulted in a stronger signal than the S-wave transmissions.  In addition, signals tended to decrease in strength with an increase in EPS content.  Wave arrivals were taken as the point of first deflection, as discussed in Section 2.4.2, for all signals, and the measured wave velocities for the slurry specimens are listed in Table 6.5. All raw data files of the transmitting and receiving transducers recorded by the oscilloscope during ultrasonic pulse velocity testing are included in the Appendix.

**Table 6.5.  Ultrasonic Pulse Velocities**

| Mix Ratio (% Kaolin:% EPS, by mass) | ID | $V_S$ (m/sec) | $V_P$ (m/sec) |
|---|---|---|---|
| 100 : 0 | Slurry | 590 – 650 | 1280 – 1570 |
| 99.5 : 0.5 | Slurry | 890 – 970 | 1080 – 1120 |
| 99 : 1 | Slurry | 950 – 970 | 1100 – 1130 |
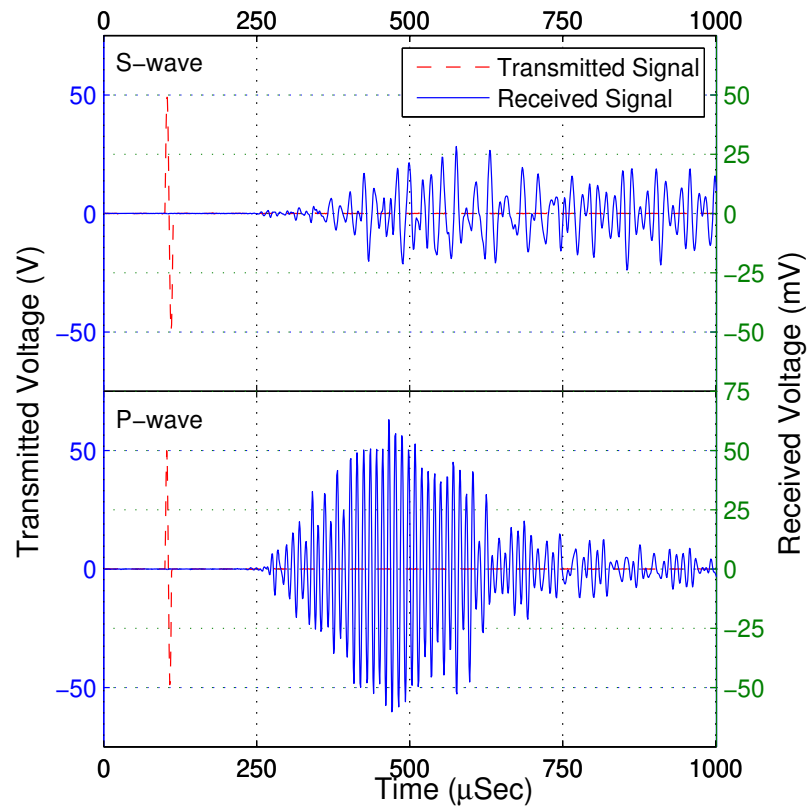
**Figure 6.30. Ultrasonic Wave Signature**

**(99% Kaolin : 1% EPS Slurry Specimen @ $\sigma_{cell}$ = 50 kPa)**

# 7.    DISCUSSION

The following chapter presents a detailed discussion of the static and dynamic properties of EPS modified soil specimens that were introduced in the preceding chapters.  The reader should note that references to results presented in Chapters 5 and 6 will be frequent throughout the following discussion.

## 7.1.    SWELL – COMPRESSION CHARACTERISTICS

The effect of increasing EPS content on the loads imposed on the soil skeleton can be shown by the data from the swell – compression tests performed, as shown in Figure 5.6. Compliance of the EPS particles reduced the swell potential of the soil mixtures at low pressures, thus the EPS particulates behaved as compressible inclusions within the soil matrix.  At higher pressures trends indicate that the increase in EPS content led to a decrease in the effective stress on the soil skeleton and thus a decrease in the overall vertical compression after inundation.  One could argue that the measurements were influenced by the replacement of a portion of the soil with EPS particulates, but it is believed that the EPS particulate operating as a compressible inclusion was the primary catalyst for the reduction in free swell.

Nattaatmadja & Illuri (2009) published laboratory test data from swell tests that showed the positive influence of EPS content on both the swell pressure and the percent free swell.  The EPS materials used in their research were produced by blending recycled materials from the packing industry and mixing with a sand / bentonite soil mixture.  Results indicated that the swell pressure was decreased by half or greater and the percent free swell was reduced by one-third to one-half for a 0.9% EPS content, by mass.  The reduction in the percent free swell reported in this research (Table 5.3) indicates an approximate 58% reduction in the free swell potential with the introduction of 1.5% EPS content.  The variation in swell pressure with increasing EPS content was generally inconclusive and but a slight decrease was noted.

Chen (1988) discussed the parameters that influenced the swell pressure and percent swell based on laboratory test results of remolded specimens and these are shown in Table 7.1. The influence of EPS content as determined by this research are also included in Table 7.1.

Table 7.1.  Factors Influencing Swell Characteristics (adapted from Chen 1988)

| Parameter (increasing) | Test Range | Swelling Pressure | Percent Swell |
|---|---|---|---|
| Initial Dry Density | 1.51 – 1.90 g/cm$^3$ | Increase | Increase |
| Initial Water Content | 5.8 – 19.4 % | Constant | Decrease |
| Initial Degree of Sat. | 61 – 93 % | Constant | Decrease |
| Specimen Thickness | 1.28 – 3.81 cm | Constant | Constant |
| Inundation Pressure | 48 – 335 kPa | Constant | Decrease |
| **EPS Content** | **0 – 1.5 % (by mass)** | **Slight Decrease** | **Decrease** |

## 7.2.   MOISTURE – UNIT WEIGHT RELATIONSHIP

Based on the moisture – unit weight data presented in Section 5.2, the increase in EPS content significantly affects the maximum dry unit weight of compacted soils but has little effect on the optimum water content.  The overall drop in dry unit weight was approximately 3.8 kN/m$^3$ (24 lb/ft$^3$) for specimens with 1.5% EPS content by mass.  Assuming a linear decrease in unit weight with increasing EPS particulates as shown in Figure 5.1, a general rule of thumb for cohesive soils would be a 1.25 kN/m$^3$ (8 lb/ft$^3$) decrease in dry density for each 0.5% EPS particulates by mass mixed into the soil.  Given the nearly parallel line of optimums, one could expect the soil matrix to dominate optimum moisture behavior for any percentage of EPS particulates; which could be useful data to guide field installation.  Nonetheless, it is expected that there is a threshold mixing ratio where the percentage of EPS particulates begins to more significantly affect the optimum moisture content, but based on this research program it exceeds 1.5% EPS content by mass.

## 7.3.   STATIC STRENGTH PROPERTIES

Initial studies of soils modified with EPS (Satoh et al. 2001; Tsuchida et al. 2001; Yoonz et al. 2004; Liu et al. 2006) relied upon the addition of cement to achieve acceptable strengths and the percentage EPS particulates were typically adjusted simply to reduce the unit weight.  More recent studies of cohesionless soils modified with EPS particulates present conflicting results, and until now the shear strength of soil mixtures consisting of EPS and cohesive soils has not been reported.

It is believed that the different techniques used to prepare the unit element specimens did not influence the comparison of data.  The differences in preparation methodologies for triaxial test specimens resulted in different internal structures of the kaolin soil skeleton.  The slurry consolidation process produced specimens with dispersed, parallel orientated clay particles.  Particle orientation was predominantly perpendicular to the direction of loading.  The static

compaction process that was performed for the clay soils prepared at the optimum water content produced specimens with more flocculated, randomly orientated clay particles. Classic documentation of strength tests on kaolin soils (Morgan 1967) reported similar strength parameters from slurry consolidated specimens and compacted specimens, and the author ultimately stated that "particle orientation had little effect on the strength behavior."

**7.3.1. UU Triaxial Results.** Failure of each specimen was defined as the maximum deviator stress obtained during shearing. For each specimen, the undrained shear strength was evaluated as half of the maximum deviator stress. Both the pure kaolin and EPS modified specimens exhibited nearly horizontal failure envelopes, and thus it was confirmed that the soil matrix was saturated. Saturation of the soil matrix in EPS modified soils cannot be determined by measurement of the percent saturation (Table 5.4), since the particulates will most likely always contain air space.

Surprisingly, the slurry consolidated specimens did not exhibit any distinct decrease in $S_u$ with increasing EPS content, as shown in Table 5.9. The 99% kaolin : 1% EPS particulate specimens exhibited much lower $S_u$ than the other mixtures, and this is attributed to the specimen preparation process. The variations in the measured $S_u$ are attributed to difficulties in controlling the effective stress imposed on bulk specimens during slurry consolidation.

A slight increase in the failure strain with increasing EPS content is noted in Table 5.6 and is an indication of increasing ductility and the influence of foam EPS particles. The initial tangent modulus and secant modulus (Table 5.9) generally indicate decreasing stiffness with increasing confining pressure but the influence of EPS content on the stiffness is unclear. Generally it was expected to see an increase in moduli with confining pressure and a decrease in moduli with increasing EPS content, but the measurements did not indicate any clear trends.

As expected, the compacted specimens exhibited a curved failure envelop, as shown in Figure 5.10 and Figure 5.11. The undrained shear strength increased with increasing confining pressure due to the compression of air voids. It is not believed that complete saturation of the soil matrix was obtained at the highest confining pressure (345 kPa), and thus undrained shear strengths would be expected to increase further at higher confining pressures. The undrained shear strength appeared to be influenced by EPS contents greater than 1% by mass. EPS contents below 1% did not exhibit any discernible reduction in undrained shear strength. Overall, the reduction in undrained shear strength for the EPS modified specimens appeared to increase with increasing confining pressure, and the initial tangent modulus and secant modulus (Table 5.10 and Table 5.11) decreased with both increasing EPS content and increasing confining pressure for all specimens. The weaker, less stiff behavior is attributed to the influence of increasing EPS

content as the porous nature of the foam material is not as stiff as the surrounding soil matrix. The reduction in stiffness with increasing confining pressure is poorly understood at this time.

Finally, the difference in the measured undrained shear strength of slurry consolidated and compacted specimens were primarily a function of the energy used to prepare the specimens, as the dry unit weight was very similar for the slurry and specimens compacted to 88% relative compaction.

### 7.3.2. CU Triaxial Results.

**7.3.2.1. Discussion of EPS content.** The saturation of specimens for CU triaxial testing presented some surprising data during the B-value checks. The pore pressure B parameter is used to ensure saturation of specimens, and considering that the EPS particulates were comprised primarily of air space it was initially assumed that acceptable B-values would not be obtained due to the assumed compliance and volume reduction of the EPS particles during undrained B-check loadings. Nonetheless, B-values greater than or equal to 0.96 (Table 5.13) were measured for all specimens with EPS inclusions. This indicated that the EPS particulates are sufficiently stiff not to compress or completely collapse under the applied backpressure or the 69 kPa (10 lb/ft$^2$) stress differential used during the B-value check. Maximum backpressures used during saturation were approximately 310 kPa (45 lb/ft$^2$). It should be noted that the typical definition of saturation is not applicable to determine the percent saturation for soils modified with EPS particulates given the assumed impermeability of the particles. The data in Table 5.12 shows that the calculated percent saturation decreases by approximately 15% for each 0.5% increase in EPS content (by mass). This decrease is primarily attributed to the air inside the EPS particulates that is believed to not be saturated under typical laboratory backpressures.

Consolidation data from the CU triaxial tests indicated that the inclusion of EPS particulates led to a small decrease in the time to 50% primary consolidation, $t_{50}$, as compared to the pure kaolin specimens. This is attributed to the volumetric replacement of a portion of the soil and water in a pure soil specimen by EPS particulates. Thus there was a reduced volume of water to remove from each specimen for a given effective stress.

The deviator stress versus axial strain data from the CU triaxial compression tests (Figures 5.12 – Figure 5.15) did not indicate any clear trends with increasing EPS content, except that the failure strain increased slightly. The slurry consolidated specimens were all considered normally consolidated since the lowest effective stress used during CU triaxial tests (172 kPa) exceeded the consolidation stress of approximately 150 kPa and unloading was never induced.

Pore pressure data indicated compressive behavior for all specimens; confirming the specimens were normally consolidated. An interesting phenomenon from the CU test data was

the momentary fluctuations in the pore water pressure for some of the specimens. One specimen containing 1% EPS particles, Figure 5.14, exhibited dilative behavior momentarily during shearing before resuming compressive behavior. These momentary fluctuations are believed to be a result of an experimental error with the pore pressure transducer, and likely not influenced by the EPS content. The pore pressure data did not indicate any distinct trends with increasing EPS content. It was initially believed that at high effective stresses some of the EPS particulates would collapse and thus there would be a rapid decrease in pore water pressure from the instantaneous increase in void space within the soil matrix, but this was not evident in the measured data. Excess pore water pressures at failure are similar for all specimens for a given effective stress.

Failure of each specimen was defined as the maximum deviator stress recorded during shearing. Strength parameters were defined in terms of Mohr – Coulomb failure criteria and summarized in Table 5.15. All specimens and EPS contents exhibited comparable strength parameters. The 99% kaolin : 1% EPS specimen series exhibited slightly stronger behavior than the other mix ratios, but this is primarily attributed to the fact that the specimen tested at 172 kPa (25 lb/ft$^2$) effective stress was sheared at an accelerated strain rate because the consolidation data was lost during a power outage. The increased strain rate led to an increase in the stress state at failure which subsequently affected the determination of the Mohr-Coulomb strength parameters. In addition, the 99% kaolin : 1% EPS specimen consolidated to 345 kPa swelled overnight during the same power outage prior to re-initiating consolidation, and this could have affected the measured data. The initial tangent modulus and secant modulus, $E_{50}$, increased with effective stress and decreased with EPS content. Both of these trends were expected since soils are typically stiffer at high effective stress states and EPS particulates are less stiff than the consolidated soil skeleton.

**7.3.2.2. Comparison of kaolin with published data.** The strength data determined for pure kaolin specimens was compared to published data in order to determine that reasonable data was realized during the experimental program, as shown in Table 7.2. Considering the differences in kaolin type and mineralogy, test procedures and equipment, and laboratory technicians the variations in strength parameters seem realistic. The data presented in this research seems to be approximately the median of the reported values in Table 7.2. This comparison provided confidence that CU triaxial measurements obtained for the EPS modified soils were representative of the influence of increasing EPS content.

**Table 7.2. Comparison of Mohr – Coulomb Strength Parameters for Kaolin Specimens**

| Citation | $\phi'$ (deg) | c' (kPa) | $\phi_T$ (deg) | $c_T$ (kPa) |
|---|---|---|---|---|
| This study | 15.2 | 35.9 | 8.8 | 25.5 |
| Oh et al. (2008) | 11.8 | 3.5 – 4.8 | 6.7 – 7.9 | 5.5 – 9.0 |
| Silvestri et al. (1988) | 19.0 | 34.5 | ** | ** |
| Allam & Sridharan (1979) | 24.5 | 4.1 | 19.9 | 14.5 |
| Parry & Nadarajah (1973) | 19.1 | 9.0 | ** | ** |

**7.3.2.3. Comparison of EPS modified soils with published data.** Deng and Xiao (2008, 2010) mixed EPS particulates with sand to create a lightweight, non-structural fill and measured that stress-strain characteristics of these modified soils in the laboratory using triaxial testing techniques. Specimens with 0.5 – 2.5% EPS particulates by mass were prepared using vibration and moist tamping. Consolidated-drained triaxial tests results indicted significant decrease in strength with increasing EPS content and no peak strength was obtained in any specimen up to 15% axial strain. Volumetric behavior was completely contractive. Interestingly, the higher EPS content soils exhibited some apparent cohesion and a bi-linear failure envelope. It is believed that the difference in strength parameters with increasing EPS content for Deng and Xiao's materials and the research presented herein are due to the difference in a sand soil skeleton and a clay soil skeleton. The inclusion of EPS particles within a drained sand skeleton replaces a certain percentage of the interlocking between individual sand grains with a more compliant, less stiff EPS material thus leading to a reduction in strength. Conversely the strength of moist clay soils are only partially influenced by particles interlocking but also influenced by interaction between the soil particles and pore water. The inclusion of EPS particulates into the matrix of a clay soil did not significantly influence the measured strength from triaxial CU tests.

## 7.4. MEASURED WAVE VELOCITY

The following section discusses the wave velocities directly measured using pulse velocity techniques, since these techniques required careful selection of the wave arrival times and thus were dependent on interpretation of laboratory measurements.

Analysis of variable frequency wave transmissions suggests that dispersion is occurring within the specimens, but for such short travel lengths this is unlikely. It is believed that the EPS particulates scattered the wave energy during transmission and thus slightly influenced travel times. This phenomenon is termed apparent attenuation and is most influential when the

wavelength approaches the average diameter of the heterogeneities. For this research, at a transmission frequency of 40 kHz and a velocity of approximately 200 m/sec the wavelength approaches the average size of the EPS particulates and thus this indicates why apparent attenuation is noted in the recorded data.

Shear wave splitting is another phenomenon that occurs in anisotropic materials in which a shear wave splits into horizontal and vertical components at the intersection of anomalies that subsequently propagate at different velocities. The time separation of the two split-waves is commonly used in the seismological studies to identify the location of anomalies. While shear wave splitting definitely occurred in the EPS modified specimens, the short specimen lengths did not allow a measureable difference in wave velocities, and the resulting conclusion is that shear wave splitting did not influence the measurement of wave velocities and is not relevant for laboratory studies.

**7.4.1.  Bender Element Wave Velocity.**  Bender element pulse transmission tests can indicate the influence of EPS content on the wave velocities. Measurements showed a decrease in wave velocities with increasing EPS content, and the specimens compacted to higher densities exhibited faster wave velocities (Figure 6.18 – Figure 6.21). These results are contradictory to observations of Schulteiss (1981) who performed similar tests on saturated clay specimens with methane gas bubbles. Measurements indicated shear wave velocity and shear modulus of the parent soil type and not that of a soil / gas composite, and the author believed that the high-frequency signals diverted around the gas voids and transmitted through the soil matrix. The influence of EPS content appeared to decrease with increasing cell pressure, and this could be a result of collapse of the EPS particulates at high pressures.

The compressional wave velocity to shear wave velocity ratio is typically between 1.5 and 2.0. Kramer (1996) referenced a value of 1.87 for typical geologic materials and Lee and Santamarina (2005) referenced a value of 1.5 for dry or unsaturated soils. Results from these tests indicate a wave velocity ratio between 1.7 and 2.4; which an average value of 2.0 and thus the measurements appear to be reasonable.

**7.4.2.  Ultrasonic Pulse Velocity Wave Velocity.** Measured P-wave velocities for the slurry consolidated specimens (Table 6.5) bracket the compression wave velocity of water, approximately 1470 m/sec, and agree with the theory introduced by Biot (1956). Biot's theory was based on analytical modeling of the individual and coupled behavior of a particulate medium and the pore fluid. Biot discussed the propagation of two types of compressional waves in a saturated porous medium; one that travels through an elastic porous soil skeleton, and one that travels through the pore fluid and is a function of hydrodynamic interactions. The measurements

made herein agree with Biot's theory, as the primary wave signature recorded during testing propagated through the pore water and measurements generally confirmed the velocity to be that of water. The portion of the energy that traveled through the soil skeleton was slower and thus arrived after the wave traveling with the velocity of water. The measurements also agree well with published data. Nakagawa et al. (1996) referenced velocities between 1513 – 1623 m/sec for slurry specimens of kaolin between 98 – 490 kPa effective stress and Leong et al. (2004) referenced velocities of 1405 and 1519 m/sec for 0 and 800 kPa effective stress states.

Measured S-wave velocities for the slurry specimens were significantly faster than expected and do not agree well with published data. As fluids are not able to transmit shear energy, shear waves propagate through the soil skeleton. Leong et al. (2004) referenced a shear velocity of 235 m/sec for a slurry consolidated kaolin specimen at 800 kPa effective stress. Nakagawa et al. (1996) referenced shear velocities between 85 – 207 m/sec for slurry specimens of kaolin between 98 – 490 kPa effective stress. The high velocities recorded in this research are speculated to be complicated by some compressional wave energy and thus accurate assessment of the shear wave velocity was not accomplished.

Ultrasonic pulse velocity transmissions through compacted specimens were not successful due to significant attenuation. It is believed that specimen lengths would need to be reduced significantly to obtain cleaner data that lend itself to robust assessment of the wave arrivals. Tests previously performed at Missouri S&T on compacted silt specimens (Weidinger 2007) initially used specimens with an approximate length of 100 mm with similar results. The specimens lengths were ultimately reduced to 25 – 30 mm to yield results in which the wave arrivals could be determined. It should be noted that short specimen lengths lend themselves to increased influence from the near-field effect, as discussed in Section 2.4.2.

Overall the research confirmed that obtaining meaningful measurements of wave velocities for laboratory soil specimens is very difficult using ultrasonic platens. Saturated specimens tended to channel the wave energy through the pore fluid, and the ultrasonic pulse velocity transmission signals were not strong enough to accurately define wave velocities for specimens compacted to typical laboratory geometries with a height-to-width ratio of 2. Shorter specimen lengths could be used for future testing, but the recorded signal would most likely be influence by electromagnetic influences that would complicate the wave signature.

## 7.5.  DYNAMIC SOIL PROPERTIES

Dynamic soil properties for kaolin and EPS modified unit element soil specimens were determined using a variety of low-strain laboratory techniques. The maximum shear modulus,

$G_{max}$, was determined using both the resonant column apparatus and shear wave velocity measurements from bender element pulse transmission tests. The variation in shear modulus with cyclic strain (modulus reduction curves) was determined from resonant column tests. The maximum Young's modulus, $E_{max}$, was determined using compressional wave velocity measurements from bender element pulse transmissions, and Poisson's ratios were determined from the combined measurements of compression and shear wave velocity. Additional pulse tests were performed with ultrasonic pulse velocity transducers, but test data were inconclusive and $G_{max}$ and $E_{max}$ could not be determined with confidence. The variation in material damping was determined from free vibration decay measurements in the resonant column apparatus. Pulse velocity techniques are not able to accurately measure the material damping of specimens. Wave dispersion and boundary reflections mask the true attenuation occurring in a specimen and thus measuring material damping from recorded wave signatures was not possible.

      **7.5.1.   Maximum Shear Stiffness.** Both resonant column and bender element test data were reviewed to determine the influence of EPS content on $G_{max}$ and the modulus reduction curves. $G_{max}$ is primarily a function of S-wave velocity, and thus decreases with increasing void ratio in a similar manner as the S-wave velocity. $G_{max}$ is a secondary function of specimen density and thus the trends do not exactly follow the wave velocity trends.

      Canales (1980) studied the effects of latex membranes and filter paper strips on the measured shear modulus during resonant column testing and results indicated that for moduli greater than 5 MPa the effects were minimal. Conversely, for moduli less that 5 MPa the measured moduli were significantly influenced by the membrane and filter paper. Considering the stiffness of the specimens tested during this experimental program were generally greater than 10 MPa, the additional confinement from the latex membranes was assumed to not influence the measured shear stiffness.

      **7.5.1.1. Comparison of $G_{max}$ measured with different laboratory techniques.** $G_{max}$ values obtained from resonant column and bender element pulse velocity tests are compared in Table 7.3. The presented data is an average of the duplicate specimens tested using each technique. The reported shear modulus from resonant column testing considers the maximum value measured for the variable cyclic shear strains. Data from the slurry consolidated specimens tested using the resonant column and ultrasonic pulse velocity transmissions are also not presented due to the large variation between measurements and bender element testing on slurry consolidated specimens was not performed.

      It can be seen that the measured $G_{max}$ from the bender element pulse velocity tests consistently exceeded the measurements from the resonant column apparatus. This is attributed

to the difference in applied shear strains between the two tests, and the resolution of the transducers used in the laboratory. It was previously discussed in Section 6.1.2 that shear strain measurements for very low strain levels during resonant column testing were influenced by the resolution of the accelerometer, whereas a local displacement transducer would have provided better results.

The differences in results between the two laboratory tests are greater for pure kaolin specimens as compared to modified soils with 1.5% EPS content, as shown in Figure 7.1. The measured $G_{max}$ also appear to converge between the two tests at higher confining pressures, which could be attributed to better coupling of the test apparatus and the specimens. The percent relative compaction of the specimens does not appear to influence the relationship.

**Table 7.3. Comparison of $G_{max}$ (MPa) using different low-strain testing techniques**

| Mix Ratio (% Kaolin:% EPS, by mass) | $\sigma_{cell}$ (kPa) | ≈ 88% Relative Compaction | | ≈ 94% Relative Compaction | |
|---|---|---|---|---|---|
| | | RC | BE | RC | BE |
| 100 : 0 | 25 | 39.1 | 76.8 | 50.3 | 97.5 |
| | 50 | 45.5 | 78.3 | 55.8 | 97.4 |
| | 100 | 50.9 | 78.7 | 58.8 | 97.9 |
| | 200 | 54.9 | 80.8 | 63.9 | 105.4 |
| 99.5 : 0.5 | 25 | 36.2 | 58.7 | 43.8 | 73.5 |
| | 50 | 38.7 | 59.4 | 50.0 | 72.4 |
| | 100 | 41.5 | 61.5 | 51.6 | 74.3 |
| | 200 | 46.5 | 67.5 | 55.9 | 77.7 |
| 99 : 1 | 25 | 35.0 | 50.2 | 39.3 | 63.0 |
| | 50 | 39.5 | 51.1 | 45.1 | 62.8 |
| | 100 | 41.8 | 52.5 | 47.6 | 64.7 |
| | 200 | 45.9 | 58.4 | 51.6 | 68.4 |
| 98.5 : 1.5 | 25 | 27.5 | 40.7 | 33.1 | 51.2 |
| | 50 | 29.8 | 41.1 | 35.2 | 50.8 |
| | 100 | 32.3 | 42.9 | 37.8 | 52.3 |
| | 200 | 37.3 | 51.3 | 42.1 | 55.4 |

It is believed variation in $G_{max}$ could also be related to variations in induced strain levels between pulse velocity and resonant column techniques. Bender elements likely represent a lower strain measurement of $G_{max}$ as compared to the resonant column apparatus. Leong et al. (2005) presented a theoretical equation to estimate the free lateral deflection ($\delta$) of a Y-poled bender element wired in parallel (thus operating as an S-wave transmitter) as:

$$\delta = 3d_{31}V\left(\frac{l}{T}\right)^{2}\left(1+\frac{t}{T}\right)K \qquad\qquad (7.1)$$

Where '$d_{31}$' is the piezoelectric charge constant, 'V' is the applied voltage, 'l' is the cantilever length of the bender element, 'T' is the thickness of the bender element, 't' is the thickness of the metallic center shim, and 'K' is an empirical weighting factor that is always greater or equal to 1. Assuming K is equal to 1, the calculated deflection is 0.01 mm and the shear strain at the tip of the bender element would be approximately $10^{-1}$ %. It should be stressed that this would be the deflection of the bender element in a free-space and not confined within a test specimen. Actual strains would be much less. Dyvik and Madshus (1985) estimated the induced strains as approximately $10^{-3}$ % and Leong et al. (2005) estimated shear strains as approximately $10^{-4}$ %. It is likely that measurements obtained at the lowest strain possible in the resonant column apparatus obtained during this research, approximately $0.0002 - 0.0005\%$, would have slightly degraded the shear modulus from the maximum shear modulus.
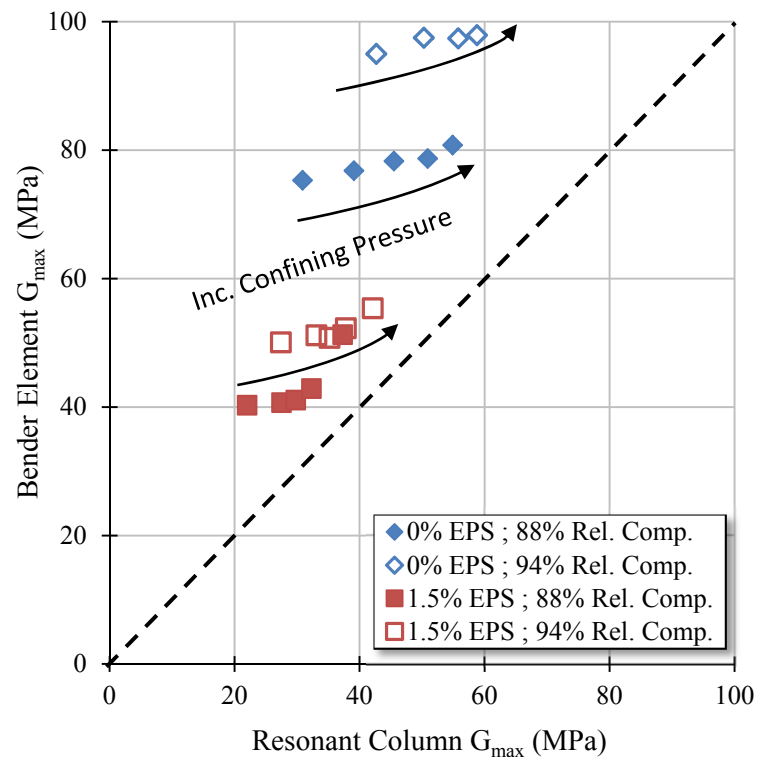


**Figure 7.1. Comparison of Measured $G_{max}$**

The difference between pulse velocity and resonant column measurements can also be attributed to strain rate effects. Kramer (1996) stated that rate effects can significantly influence the comparison of data derived from field investigations and that from laboratory investigations. In addition, the stiffness measured from field or laboratory investigations was thought to overestimate the actual stiffness of the soil in design applications due to the large mismatch between the loading rates. The resonant column apparatus applies an approximate 100 - 200 Hz loading rate whereas bender elements operate at approximately two orders of magnitude higher frequencies. Many researchers have studied the influence of frequency on the the measured shear modulus. Matesic and Vucetic (1994) showed that rate effects become increasingly important in cohesive soils as compared to cohesionless soil types, and they showed an approximate 1% - 11% increase in shear modulus per log cycle.

Measurements obtained from this research generally agree with published results. Thomann and Hryciw (1990) showed that bender element measurements of velocity for sands and silts, which are directly related to $G_{max}$, were slightly higher than resonant column measurements. Bennell and Taylor Smith (1991) showed that stiff cohesive specimens exhibited shear wave velocities were approximately 30% higher for bender element measurements as compared to resonant column tests, and the authors attributed a lot of the influence to poor coupling between the torsional motor and specimen in resonant column testing. The measured trends also agree with observations of Nakagawa et al. (1996) who showed ultrasonic pulse velocity measurements exceeded resonant column measurements.

Ultimately it is believed that the resonant column measurements provided a more accurate assessment of the shear modulus of EPS modified soils as compared to pulse transmission tests. The methodology produces a torsional loading that affects the entire specimen geometry, whereas pulse transmission tests have limited areas of influence. In addition particulate additives increase the scattering of transmitted signals and thus can influence the travel time determination. It is believed that this observation would also be true for other particulate inclusions such as tire chips and fibers. Conversely, the installed accelerometer on the resonant column device has limited precision as very low strains, which was evident during testing. The use of a proximeter for strains less than $10^{-3}$ % would improve measurements of deformation during low strain testing. Finally, the resonant column apparatus was limited to strain levels of approximately 0.01% or less.

**7.5.1.2. $G_{max}$ Compared to published data.** Low-strain measurements of shear stiffness for EPS modified soils are not available in the literature but data exists for pure kaolin specimens. Aggour et al. (1989) performed resonant column tests on compacted, saturated kaolin

specimens and measured $G_{max}$ between 28 – 30 MPa at 34.5 kPa effective stress. Athanasopoulos (1993) measured $G_{max}$ between 37 – 150 MPa for slurry consolidated specimens tested at effective stresses between 35 and 415 kPa. Duffy et al. (1994) measured $G_{max}$ of 55, 91, and 155 MPa for effective stress states of 100, 200, and 400 kPa, respectively using the resonant column apparatus. Leong et al. (2004) used ultrasonic platens and estimated Gmax to be approximately 94 MPa for a slurry consolidated kaolin specimen. Black et al. (2009) used bender elements tests and measured $G_{max}$ between 16 – 60 MPa for compacted specimens tested in unconsolidated, undrained conditions and at a cell pressure of 100 kPa. Overall, saturated specimens generally exhibited increased $G_{max}$ as compared to partially saturated specimens. The comparison of $G_{max}$ determined for kaolin specimens (Table 7.3) and the published data indicate that measurements obtained throughout the testing program using both the resonant column and bender elements are reasonable.

**7.5.1.3. Influence of EPS content on $G_{max}$.**   In general, $G_{max}$ measured using the resonant column apparatus decreased with increasing EPS content as shown in Table 7.3.  $G_{max}$ decreased by approximately 12 – 18 MPa for the addition of 1.5% EPS content by mass; a 30% – 34% reduction. The data for the 0.5% and 1% EPS content modified soil specimens was quite similar as shown in Figure 6.6, Figure 6.7, and Table 7.3. Bender element measurements indicate a systematic reduction in $G_{max}$ with increasing EPS content. For each 0.5% increase in EPS content the measured $G_{max}$ decreased by 6 – 16 MPa; a 10% - 20% reduction. The addition of 1.5% EPS content resulted in an approximate 40 – 44% reduction in $G_{max}$ as compared to pure kaolin specimens. These trends were not influenced by either confining pressure or percent relative compaction. Overall, increasing EPS content appears to influence measurements of $G_{max}$ more for bender element pulse velocity tests as compared to measurements from the resonant column apparatus.

The relationship between $G_{max}$ and equivalent void ratio is given in Figure 7.2 for compacted specimens tested in the resonant column apparatus and with bender elements pulse velocity transmissions. This relationship removes the influence of the different compactive energy and allows specimens compacted at different relative compactions to be directly compared. The data presented is from specimens tested at the lowest confining pressure during the multi-stage test program. A linear regression of the data is presented in Figure 7.2. As discussed in Section 5.1, the equivalent void ratio has an almost linear relationship to the EPS content and thus is an advantageous way to quantify the influence of increasing EPS content. The range in equivalent void ratios for the test specimens was approximately 0.900 to 1.900. The data indicates decreasing $G_{max}$ with increasing equivalent void ratio, but the rate of decrease is

different between the two test methods.  To determine if the rate of change was influenced by the confining pressure, a linear regression of the data was determined for each confining pressure used during the multi-stage testing program.  The linear regressions of a series of resonant column tests are shown in Figure 7.3.  Individual data points are shown only for the smallest and largest confining pressures to avoid an overly complicated plot.
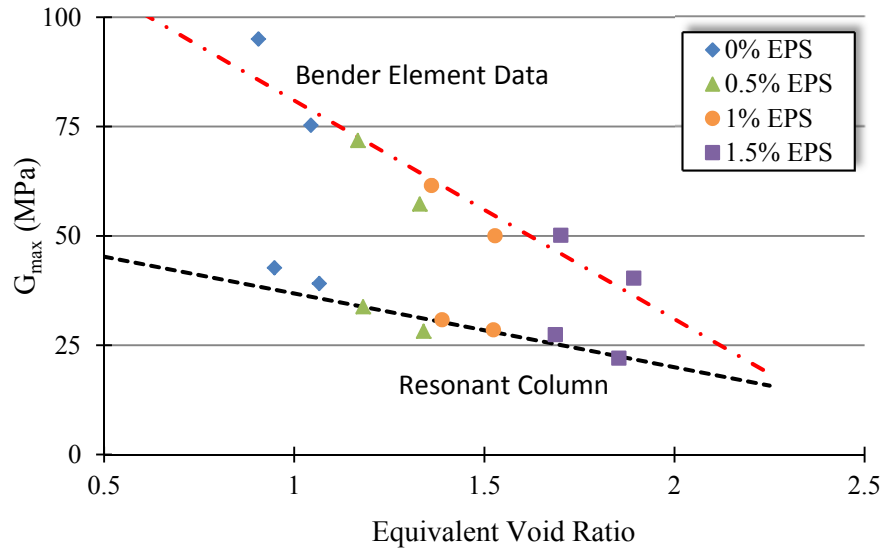


**Figure 7.2.  Variation in $G_{max}$ with Equivalent Void Ratio**
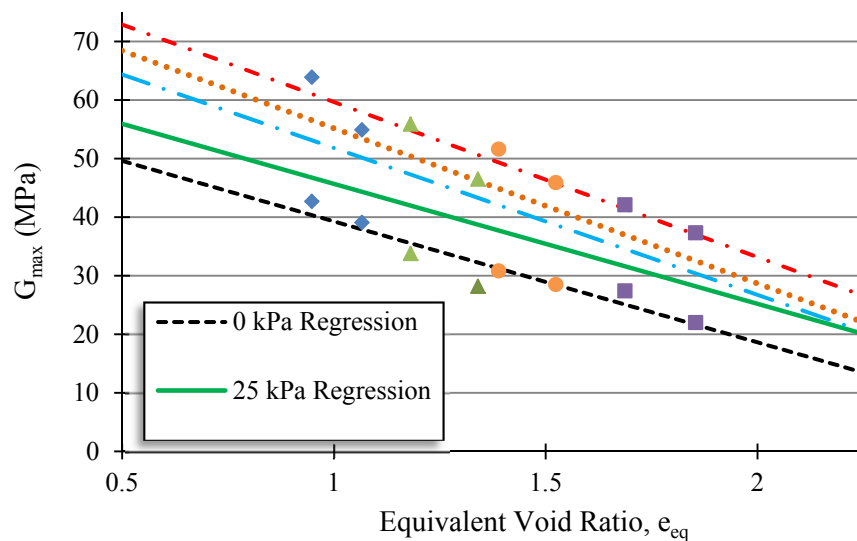


**Figure 7.3.  Linear Regression of $G_{max}$ vs. Equivalent Void Ratio (Resonant Column)**

The data indicates that $G_{max}$ decreases with increasing equivalent void ratio at a fairly constant rate and the vertical intercept (b) is a function of the confinement.  This decrease in the shear modulus can be generally expressed as:

$$Resonant\,Column \quad G_{max}\,(MPa) \approx -23e_{eq} + b \qquad (7.2)$$

As noted in Section 5.1 the equivalent void ratio is linearly related to EPS content for the range of EPS contents used within this research program, and thus the previous relationship could also be related to EPS content.  The slope varied from a minimum at the lowest confining pressure to a maximum at the largest confining pressure.  A similar process were used to analyze the data from bender element testing and resulted in the following relationship:

$$Bender\,Element \quad G_{max}\,(MPa) \approx -50.5e_{eq} + b \qquad (7.3)$$

Figure 7.2 indicates that the maximum shear modulus measured with the resonant column and bender elements would converge between an equivalent void ratio of 2.00 and 2.50.  Based on the data in Figure 5.2, an equivalent void ratio of 2.50 would correspond to compacted specimens with approximately 2.5 % to 3.0% EPS content by mass.  Additional tests at higher EPS contents are required to determine if the $G_{max}$ trends continue to vary linearly with the equivalent void ratio for increased EPS content.

**7.5.1.4. Influence of confining pressure on $G_{max}$.**  Since the use of EPS particulates in soil is such a new subject of research, the effects of confining pressure on the dynamic properties of soils modified with EPS was completely unknown.  Considering the density of EPS particulates, it was anticipated that they might collapse at higher confinement which subsequently could lead to significantly different response to dynamic loadings.  Increases in confining stress lead to compression of air void in partially saturated specimens which subsequently increases specimen density and stiffness.  In addition, increases in confining stress can lead to increased interlocking and bonding between adjacent soil particles as they rearrange into a denser configuration, thus increasing soil stiffness.

Multi-stage measurements of $G_{max}$ from resonant column and bender element tests as described in Chapter 6 were performed at confining pressures between 0 to 200 kPa.  In general, for a specific EPS content the maximum shear modulus increased for increasing confining

pressure as shown in Table 7.3, but the rate of increase was different for resonant column and bender element tests.

For each testing technique, $G_{max}$ was normalized by the measured $G_{max}$ at the lowest confining pressure and plotted against the confining pressure, as shown in Figure 7.4. The data presented in Figure 7.4 is from specimens compacted to approximately 88% relative compaction, but in general the results were not influenced by relative compaction.
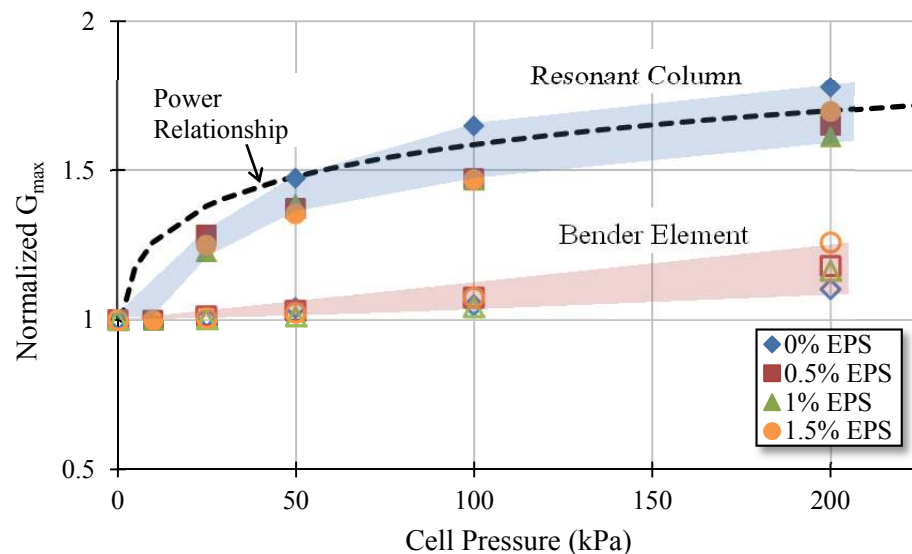


**Figure 7.4. Influence of Confining Pressure on $G_{max}$ for Compacted Specimens (Relative Compaction ≈ 88%)**

Results indicate that increases in confining pressure led to an increase in $G_{max}$, and that the trends were not influenced by increasing EPS content. Results were influenced by the type of testing technique. The confining pressure played a more important role in resonant column testing as compared to bender element tests. Bender element tests exhibited very small increases in $G_{max}$ with increasing confining pressure. It is suspected that this is a function of the area of influence of the propagating wave transmission primarily impacting the central portion of the compacted specimens and having less interaction with the specimen perimeter. Increases in confinement would preferentially compress air voids and potentially EPS particulates along the outer portions of the specimen with reduced impact in the specimen interior. Conversely, the area influenced during cyclic torsional loadings using the resonant column apparatus is the entire

cross-section of the specimen, and thus void compression in the exterior of the specimen would be registered by an overall stiffer specimen during testing. $G_{max}$ versus confining pressure relationship of the resonant column specimens is similar to that of the undrained shear strength of partially saturated specimens. At increasing confinement, air voids are compressed until complete saturation is obtained. Once completely saturated the shear modulus would not be expected to increase with additional confinement.

Various researchers have reported increased stiffness with increasing confining pressure (e.g. Seed & Idriss 1970; Sun et al. 1988; Santamarina 2001), but most of the relationships consider the long-term, drained effective stress state and thus the increases in $G_{max}$ would be a function of the specimen density/void ratio. Sun et al. (1988) stated that the influence of confining pressure on the shear modulus is much reduced for cohesive soils and gradually diminishes with increasing plasticity. Nakagawa et al. (1997) and Cascante and Santamarina (1996) related $G_{max}$ and confining pressure to a power relationship as:

$$G_{max} = a\sigma^{b}$$ 

(7.4)

The constant *a* is a magnitude scaling factor and the constant *b* is a function of secondary influences other than confining stress such as of fabric changes, particle arrangement and deformation during loading. The data from the resonant column test exhibited a strong power relationship, as plotted in Figure 7.4. The relationship best fits the resonant column curve using a value of 0.09 – 0.10 for the *b* constant depending on the specimen relative compaction. For partially saturated specimens the power relationship predicts changes in $G_{max}$ with increased confinement fairly well, but it is expected the *b* coefficient would be different for other soils types. The EPS content did not influence this relationship.

**7.5.2. Shear Modulus Degradation.** Shear modulus degradation curves were only developed from resonant column testing as this is the only dynamic test that allowed variation in the induced strain level. Two trends can be recognized from the shear modulus degradation curves measured (Figure 6.6 and Figure 6.7). First, there is a general reduction in the shear stiffness at all strain levels as the percent EPS particulates is increased. The percent reduction in stiffness is most significant in the lowest strain range (approximately $10^{-4}$ – $10^{-3}$ %), and at increasing strains the curves begin to converge. There was approximately a 30 – 40% reduction in shear modulus from the addition of 1.5% EPS particulates, with lesser percentages of EPS particulates exhibiting a smaller reduction in shear modulus. The data from the 99.5% kaolin : 0.5% EPS and 99% kaolin : 1% EPS particulate specimens often overlap, which indicates that the

addition of 0.5 - 1% EPS particulates did not produce a modified soil with drastically different stiffness for a given strain. A second trend indicates that the breakpoint where shear modulus rapidly decreases shifts to larger strain levels with increasing confining pressure. This phenomenon was expected as increasing isotropic stress generally results in a stiffer response for particulate mediums.

Normalized modulus reduction curves measured during resonant column testing were presented in Figure 6.8 and Figure 6.9. Surprisingly the data suggested that cohesive soils with increasing EPS content maintained its maximum shear modulus to larger strain levels as compared to pure kaolin specimens. It should be stressed that this does not mean that cohesive soils modified with EPS particulates will have a stiffer response than the parent soils, but instead the degradation of stiffness in soils modified with EPS particulates will occur at slightly higher strain levels than their parent soil types. Essentially increasing EPS content in the soils led to a larger range of strains in which the material exhibited an elastic response.

Modulus degradation curves for pure kaolin and 1.5% EPS content specimens are grouped according to the relative percent compaction of the specimens in Figure 7.5.
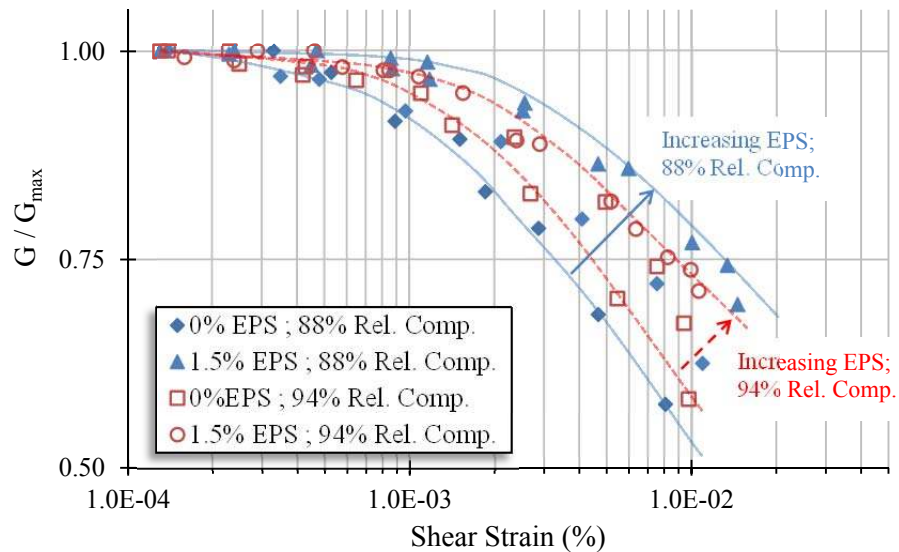


**Figure 7.5. Influence of Relative Compaction on Normalized Modulus**

The data suggests that increased compactive energy resulted in a smaller variation in material stiffness with increasing EPS content; ultimately the influence of increasing EPS content

was partially muted. This trend is most likely the result of a larger percentage of the EPS particulates being compressed and collapsed as the specimen is compacted into a denser arrangement, thus reducing the stiffening influence of the EPS. The data in Figure 7.5 is from specimens tested at a confining pressure of 10 kPa. Data from alternate confining pressures were also analyzed, and it was noted that the influence of relative compaction on the modulus reduction curves gradually diminishes with increasing cell confinement.

Finally, the strain limitations with the resonant column apparatus are apparent reviewing the data in Figure 6.8 and Figure 6.9. Based on the measured data, the resonant column apparatus at Missouri S&T is limited to shear strains of approximately 0.01% or less. To obtain measurements at larger strain levels the resonant column would need to be modified to a torsional shear apparatus and operated at a lower torsional frequency.

**7.5.2.1. Influence of confining pressure on normalized modulus reduction.** The normalized modulus curves were plotted based on the confining pressure applied to the specimens during resonant column testing and plotted in Figure 7.6. The data presented is based on tests performed on compacted specimens at an approximate relative compaction of 88%, but in general trends were not influenced by the percent relative compaction.

The transition for low-strain, linear behavior to intermediate, non-linear behavior is clearly a function of confining pressure for the compacted specimens. Results indicate that increases in confining pressure led to stiffer response at very low strains, but as the shear strain approaches intermediate ranges the reduction in shear stiffness is much more abrupt. For example, the strain level where this transition occurs is approximately 0.0002%, 0.0004%, 0.0008%, 0.001%, and 0.002% shear strain for pure kaolin specimens at isotropic confining pressures of 10, 25, 50, 100, and 200 kPa, respectively. Both pure kaolin and EPS modified specimens exhibited more gradual changes in shear modulus at lower pressures. Surprisingly, the influence of confining pressure on the normalized modulus reduction curves were less evident for increased EPS content. As discussed previously the EPS modified soils exhibited a larger range of low-strain, linear behavior as compared to pure kaolin specimens, and increases in confining pressure extended the low-strain elastic behavior to higher cyclic strain levels.
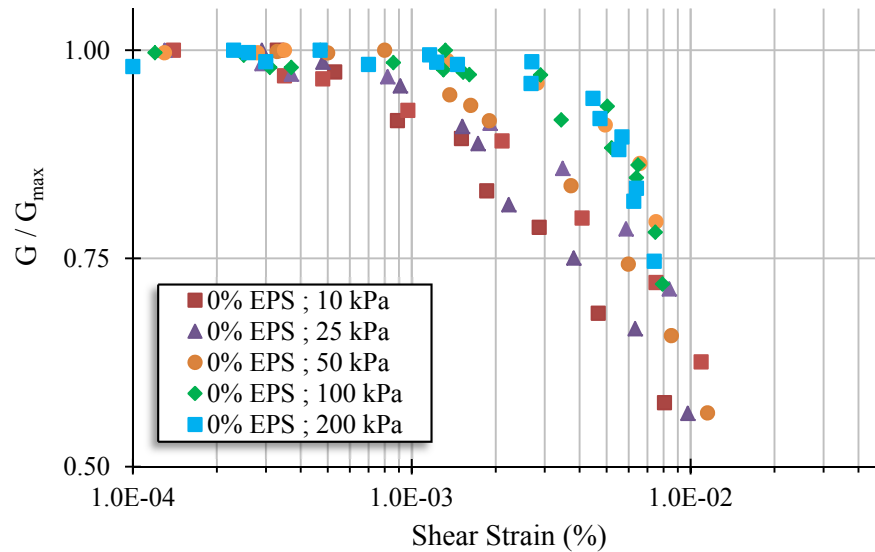
a)   0% EPS Content (by mass)
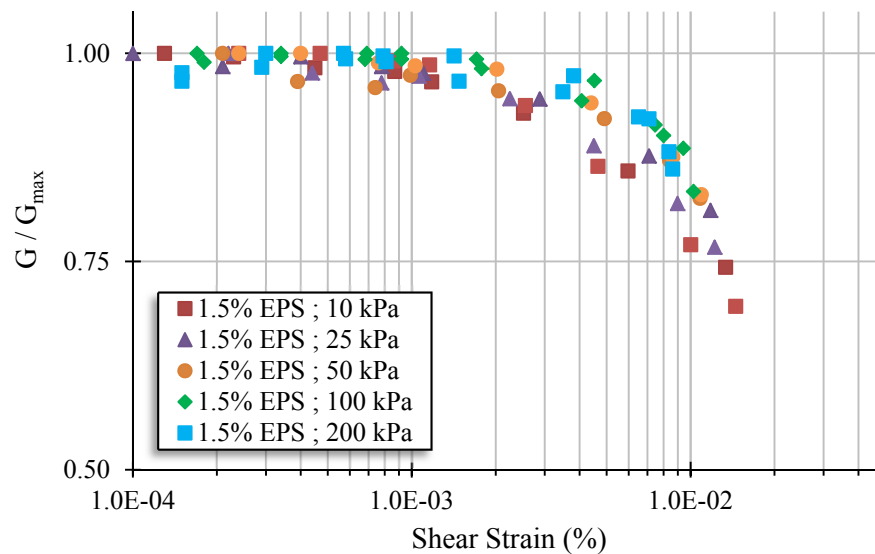


b)   1.5% EPS Content (by mass)

**Figure 7.6.  Influence of Confining Pressure on Normalized Modulus Reduction for Compacted Specimens (Relative Compaction ≈ 88%)**

**7.5.3.   Young's Modulus.**  Young's modulus was determined from P-wave pulse trans-missions using bender element transducers according to Equation 2.5.   Young's modulus is primarily a function of P-wave velocity and a secondary function of specimen density.  Since the

induced strain levels from bender element transducers are very small, the calculated Young's modulus represents a maximum value, $E_{max}$. Similar to the shear modulus, Young's modulus is constant at very low strain level and at larger strains displays non-linear behavior. Since Young's modulus was determined only with pulse velocity techniques where the strain levels cannot be adjusted, the variation with shear strain is unknown.

The variation of $E_{max}$ with increasing EPS content and confining stress were presented in Figure 6.24 and Figure 6.25. Increasing EPS content leads to a significant reduction in $E_{max}$. Each 0.5% increase in EPS content leads to an approximate 50 MPa decrease in $E_{max}$. The trends are not influenced by either the confining pressure or the relative compaction.

The relationship between $E_{max}$ and equivalent void ratio is given in Figure 7.7 for compacted specimens tested with bender elements. The data points presented are from specimens tested at atmospheric pressure, but linear regressions for larger confining pressures are also shown. For comparison $G_{max}$ values determined from bender element tests are also included, and it is clear that measurements of $E_{max}$ exhibit more scatter than $G_{max}$. A linear regression was fit to the tabulated data and indicates that $E_{max}$ decreases with increasing equivalent void ratio at a fairly constant rate and the vertical intercept (b) is a function of the confinement. The decrease in the Young's modulus can be generally expressed as,

$$E_{max}(MPa) \approx -285e_{eq} + b \qquad \textbf{(7.5)}$$
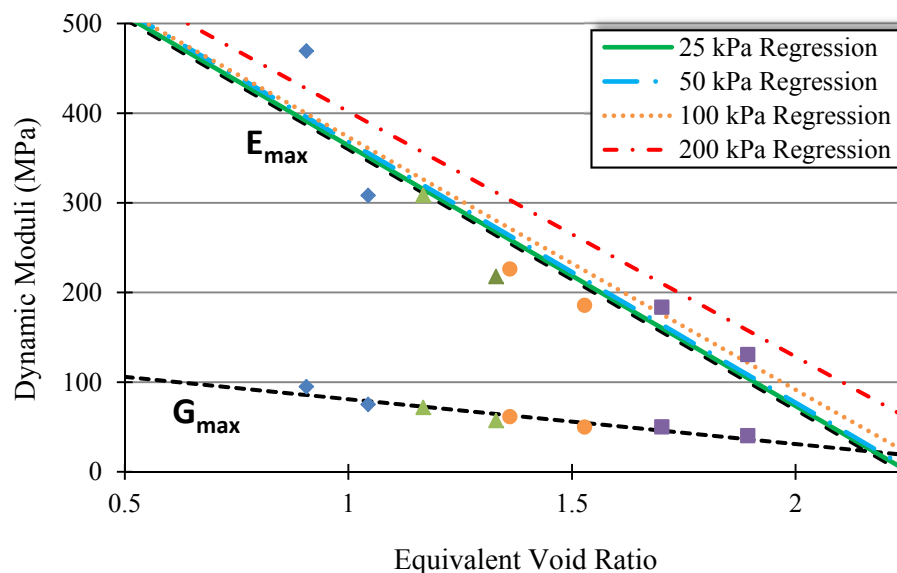


**Figure 7.7. Variation in $E_{max}$ with Equivalent Void Ratio for Compacted Specimens**

**7.5.4. Poisson's Ratio.** Poisson's ratio (υ) was calculated from measurements of P-wave and S-wave velocities during pulse transmissions tests using Equation 2.3. Poisson's ratio is presented in Figure 6.26 and Figure 6.27 as a function EPS content and confining pressure. Saturated, undrained specimens would be expected to have a Poisson's ratio of 0.5 based on elastic theory, but the test specimens were clearly not saturated. For a given confining pressure, Poisson's ratio decreased with increasing EPS content. The relationship between Poisson's ratio and equivalent void ratio was also investigated and is presented in Figure 7.8. The data presented is from specimens tested at atmospheric pressure. This relationship incorporates the influence of the percent compaction of the prepared specimens. Poisson's ratio was relatively unaffected by increasing confining pressure.
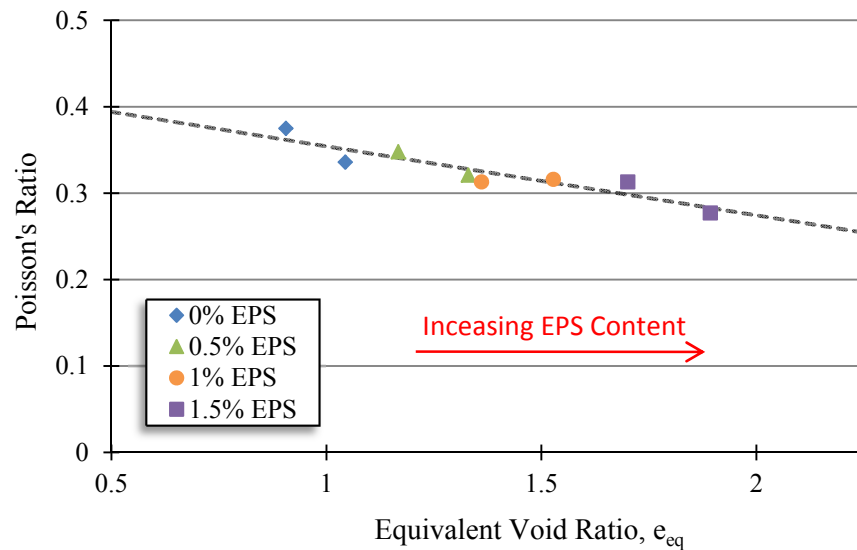


**Figure 7.8. Variation in Poisson's Ratio with Equivalent Void Ratio**

A linear regression was fit to the tabulated data and indicates that Poisson's ratio decreases with increasing equivalent void ratio at a fairly constant rate and can be generally expressed as,

$$\upsilon \approx -0.065 e_{eq} + b \qquad (7.6)$$

As discussed previously, equivalent void ratio is a proxy for the percent EPS. The calculated Poisson's ratio decreases with increasing equivalent void ratio, and is most likely an indication of increased EPS content that is assumed to be softer and more compliant than the surrounding soil matrix. A reduction in Poisson's Ratio with increasing EPS content would correlate to reduced lateral strain in the horizontal direction from the application of vertical loads, and thus would have positive implications for the use of EPS modified soils against structures. The EPS particulates function as compressible inclusions during loading and absorb some of the strain a typical soil would exhibit during loading through volumetric reduction.

**7.5.5. Damping Ratio.** Material damping as quantified by the damping ratio was determined from free vibrational decay measurements using the resonant column apparatus and results were given in Figure 6.11 through Figure 6.13. The damping ratio at low strain, $D_{min}$, was approximately 1.75 – 2.0% for most specimens with significantly more scatter for the slurry consolidated specimens. The measurements indicated that there was little to no influence of increasing EPS content on the damping ratio. Damping ratio was not influenced by the percent relative compaction of specimens. It was previously shown that pure kaolin specimens exhibited a smaller strain range for $G_{max}$ when compared to specimens with increasing EPS content. Since material damping and stiffness are inversely coupled, the pure kaolin specimens also exhibited an initial increase in damping ratio at smaller strains than modified specimens with EPS particulates. This was an unexpected since the addition of more void space in soils, assuming EPS particulates are essentially void space, was originally postulated to increase the material damping.

In general, measurements of free vibrational decay during torsional excitation provided the best results to measure material damping of specimens. Material damping estimates using the frequency response from the resonant column apparatus, the half-power bandwidth method, produced poor results. The installed accelerometer recorded scattered data at very low strain levels which complicated the selection of the appropriate values using the half-power bandwidth method. In addition, at larger strain levels the scatter was reduced but the shape of the frequency response curve was distorted and subsequently influenced estimates of damping. At this time half-power bandwidth measurements of material damping should not be utilized for the resonant column apparatus at Missouri S&T.

**7.5.5.1. Influence of confining pressure on damping ratio.** Damping ratio was shown to be a function of the confining pressure at strain levels greater than $10^{-3}$%. Damping ratio versus cyclic shear strain data from resonant column tests were plotted for increasing confining pressures in Figure 7.9. The data presented is based on tests performed on compacted specimens

at an approximate relative compaction of 88%, but as stated previously general trends were not influenced by the percent relative compaction.
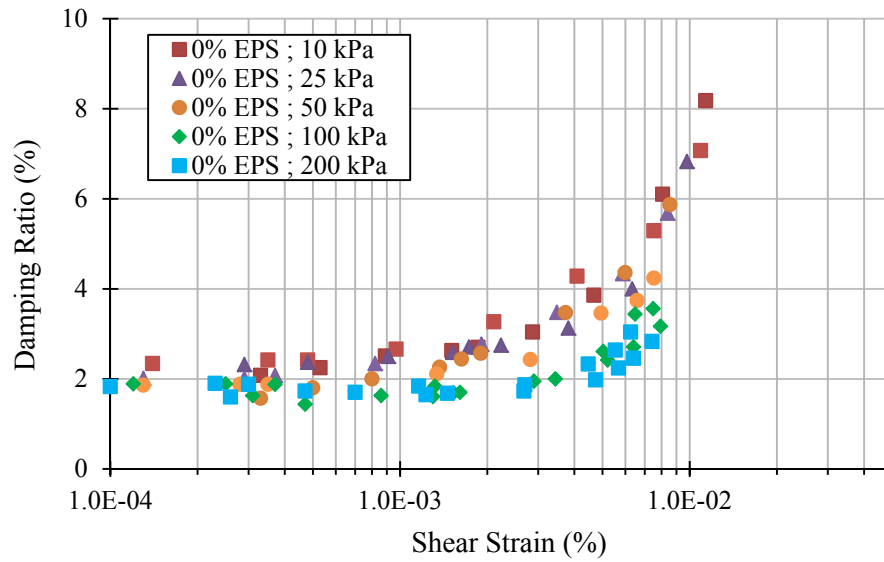


a)   0% EPS Content (by mass)
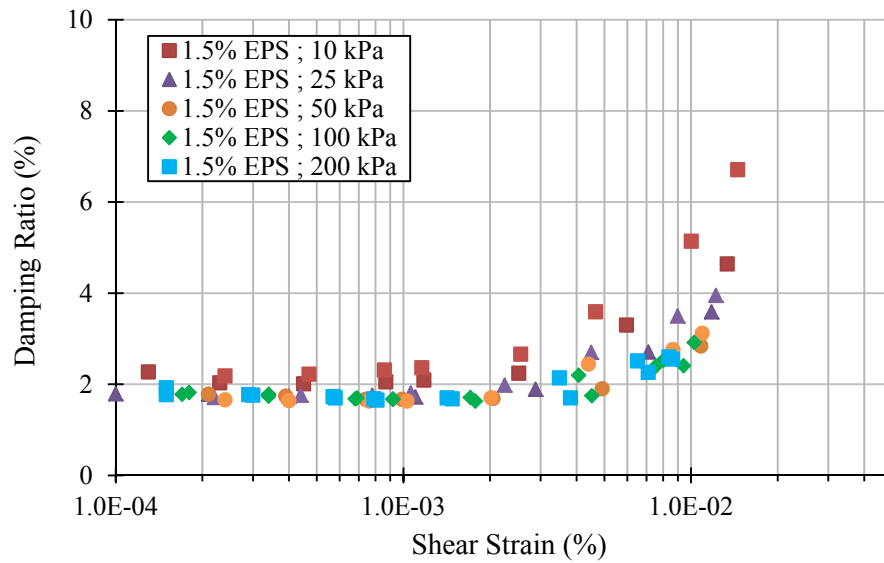


b)   1.5% EPS Content (by mass)

**Figure 7.9.  Influence of Confining Pressure on Damping Ratio**

Results indicated that increasing confining pressure did not influence the low-strain minimum damping ratio, $D_{min}$, but influenced the damping ratio in the intermediate strain ranges. These trends agree with the trends presented earlier in which the soil stiffness increased with increasing confining pressure. A stiffer soil would be expected to absorb less energy and thus a reduced damping ratio based on logarithmic decrement measurements would be reported. The data also agrees with published data in which decreased material damping was reported with increasing confining pressure (e.g. Hardin & Drnevich 1972a; Seed et al. 1984). Surprisingly, the influence of confining pressure on the damping ratio was less evident for increasing EPS content. This was not expected as conceptually the EPS particulates were expected to partially compress or collapse at high pressures leading to increased specimen density and thus a larger range of material damping for a given range of confining pressures.

## 7.6. COMPARISON OF DYNAMIC PROPERTIES WITH PUBLISHED RELATIONSHIPS

Published relationships that provide the variation of the maximum shear modulus ($G_{max}$), normalized shear modulus ($G/G_{max}$), and damping ratio versus cyclic shear strain are widely accepted and commonly used in practice. These relationships attempt to capture the stiffness and damping of soils in the elastic range, the non-linearity of these soil parameters with increasing shear strain, and also the secondary influencing factors such as stress state, void ratio, and plasticity. Some of the more commonly used relationships for cohesive soils were previously introduced in Chapter 2.

### 7.6.1. Maximum Shear Modulus Relationships. 
A classic empirical estimate of $G_{max}$ was developed for cohesive soils by Hardin and Black (1969) and introduced as Equation 2.18. The relationship was compared to estimates of $G_{max}$ from the resonant column apparatus and bender element pulse velocity tests. All specimens were normally consolidated, so the portion of the empirical relationship related to stress history was removed. The relationship is also based on effective stresses, which were unknown during the dynamic tests performed on compacted specimens in this research. It was assumed increases in cell pressure during testing predominantly compressed air voids within the soil matrix and secondarily compressed the EPS particulates without significantly affecting the pore water pressure. Based on this assumption, the cell pressure was assumed to be approximately equal to the mean effective stress on the test specimens. Duplicate specimens were tested during resonant column and bender element testing, and an average of the two specimens is reported. The modified void ratio expressions of Hardin (1978) and Jamiolkowski et al. (1991) were also used to compare with the measured data.

Results indicate that the simplified expressions for $G_{max}$ provided a poor fit to the measured data. Estimated $G_{max}$ deviated from measured data with increasing EPS content and decreasing cell confinement, as shown in Figure 7.10. The void ratio expressions of Hardin (1978) and Jamiolkowski et al. (1991) provided very similar estimated of $G_{max}$ and thus only the Hardin expression has been presented in Figure 7.10.
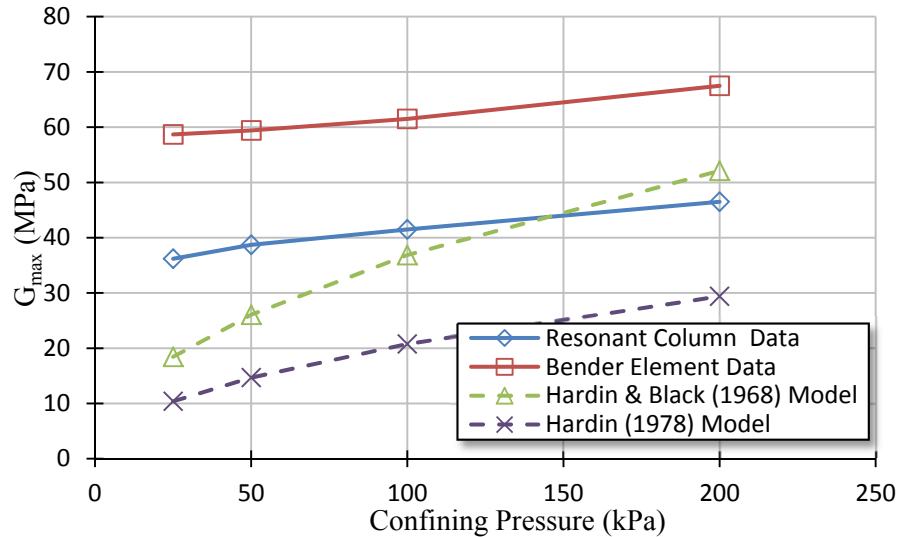


a)        0.5% EPS Content (by mass)
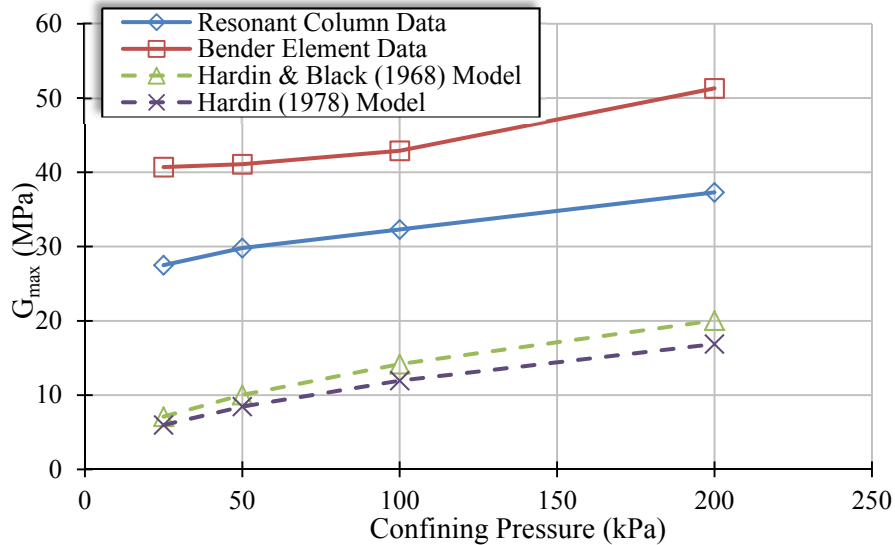


b)        1.5% EPS Content (by mass)

**Figure 7.10. Comparison of $G_{max}$ with Empirical Models**

The differences between the experimental measurements of this research and the published relationships are primarily attributed to the unknown effective stress state during testing and the influence of EPS content on the void ratio. The 'A" coefficient at the front of Equation 2.18 was modified in an attempt to provide a better fit, but results did not indicate significant improvements. The models were developed using data from saturated specimens, and thus their extension to partially saturated specimens is tenuous. The influence of EPS content on the specimen void ratio also influenced the model predictions. As discussed previously, increasing EPS content has a significant effect on the specimen void ratio and this is likely responsible for the poor fit with increasing EPS content.

**7.6.2. Normalized Shear Modulus Relationships.** The shear modulus reduction curves measured with the resonant column apparatus were compared to published models and design curves introduced in Section 2.3.4. Figure 7.11 compares the hyperbolic model (Hardin and Drnevich 1972) and the Ishibashi and Zhang (1993) model with the measured data. The 'a' and 'b' coefficients recommended by Hardin and Drnevich (1972b) for saturated cohesive soils were used with the hyperbolic model.
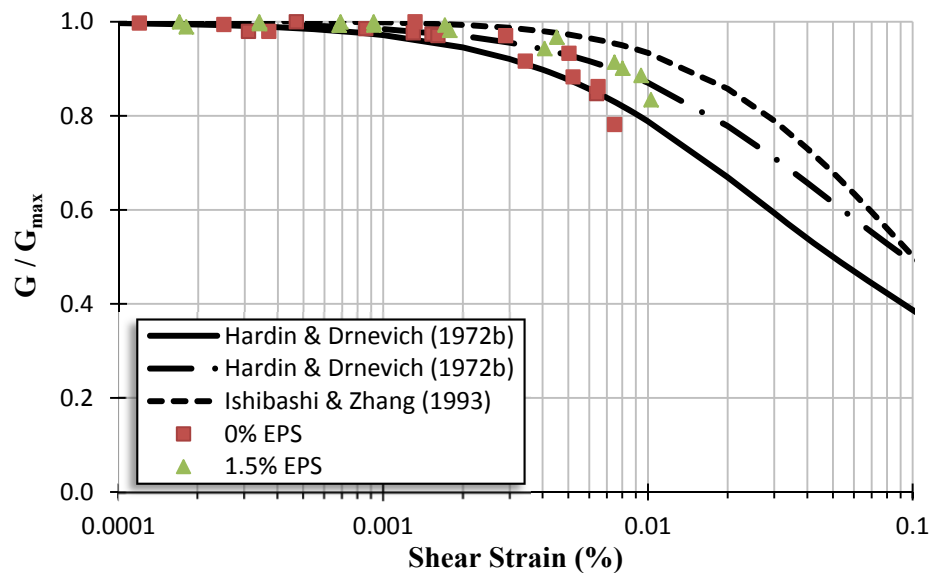


**Figure 7.11. Modulus Reduction Curve compared with Analytical Models for Compacted Specimens (Relative Compaction ≈ 88% ; $\sigma_{cell}$ = 100 kPa)**

A sensitivity analysis determined that the degradation curve shape was most influenced by the choice of reference strain. A reference strain of 0.08% provided a good fit to the pure kaolin specimen data and a reference strain of 0.15% provided the best fit for the soil specimens with 1.5% EPS particulates, as shown in Figure 7.11. Results indicated that the hyperbolic model can effectively characterize the modulus degradation curve of EPS modified cohesive soils if the reference strain is carefully chosen. If the reference strain cannot be calibrated with experimental data then an initial value between 0.1% and 0.15% is recommended for specimens with up to 1.5% EPS content by mass at moderate confining pressures.

Previously it was shown that increases in confining pressure led to an extension of linear elastic behavior to intermediate strain levels but a steeper degradation curve. The hyperbolic model provided an increasingly poor fit with increasing confinement; especially at intermediate strain levels. The analytical model of Ishibashi and Zhang (1993) provided a decent fit to the measured data at low strain levels, but poorly modeled the data for both the pure kaolin and EPS modified soils at moderate strain levels.

The measured data was also plotted on the design curves of Sun et al. (1988) and Vucetic and Dobry (1991) as shown in Figure 7.12 and Figure 7.13, respectively, for specimens tested at 100 kPa cell pressure. The design curves were developed for saturated cohesive soils and thus are divided into specific ranges based on plasticity index. The PI of the kaolin soil used in this study was 29. Both design curves slightly overestimate the stiffness of the pure kaolin specimen, and the data for the EPS soil mixtures correspond to curves with slightly higher PI than the pure kaolin samples.

Overall the empirical models and design curves have the potential to be used with EPS modified soils, but additional testing would further confirm their applicability. The measured data of this research program followed the general shape of the empirical based modulus degradation models. The effect of soil plasticity was not investigated for these compacted modified soil specimens. Additional testing at intermediate and large strain levels and a larger, more significant statistical database is recommended to improve comparison of measurements with the design curves.
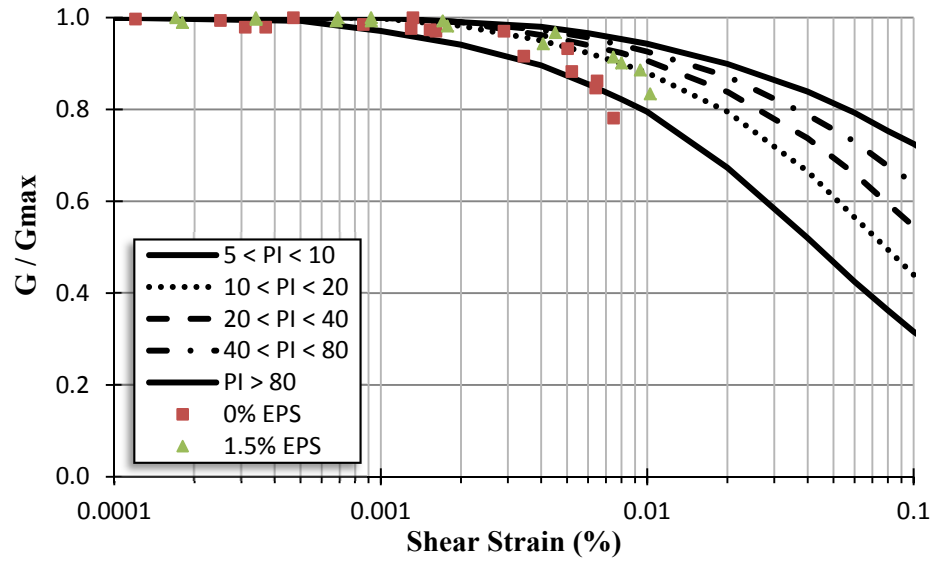
**Figure 7.12.  Modulus Reduction Curve compared with Sun et al. (1988) Curves for Compacted Specimens (Relative Compaction ≈ 88% ; $\sigma_{cell}$ = 100 kPa)**



**Figure 7.13.  Modulus Reduction Curve compared with Vucetic & Dobry (1991) Curves for Compacted Specimens (Relative Compaction ≈ 88% ; $\sigma_{cell}$ = 100 kPa)**

**7.6.3.  Damping Ratio Relationships.**  The increase in damping ratio with increasing cyclic strain measured with the resonant column apparatus were compared to the empirical based analytical models and design curves introduced in Section 2.3.4.  Figure 7.14 compares the hyperbolic model (Hardin and Drnevich 1972) and the Ishibashi and Zhang (1993) model with measured data at a cell pressure of 100 kPa.  The models were developed for saturated, cohesive soils.  The 'a' and 'b' coefficients recommended by Hardin and Drnevich (1972b) are a function of the resonant frequency and effective stress.  The resonant frequency decreased with increasing shear strain and thus an average value was considered for the hyperbolic model, and as discussed previously the confining stress was assumed to closely correlate to effective stress for compacted specimens.  A reference strain of 0.065% provided the best fit to the pure kaolin specimen and a reference strain of 0.12% provided the best fit for the soil specimens with 1.5% EPS particulates, which are the same values used when fitting the hyperbolic model to the modulus degradation curve.  The hyperbolic model provided a poor fit at strain levels less than $10^{-3}$%.  The Ishibashi and Zhang (1993) model slightly underestimated the damping ratio at all strain levels.
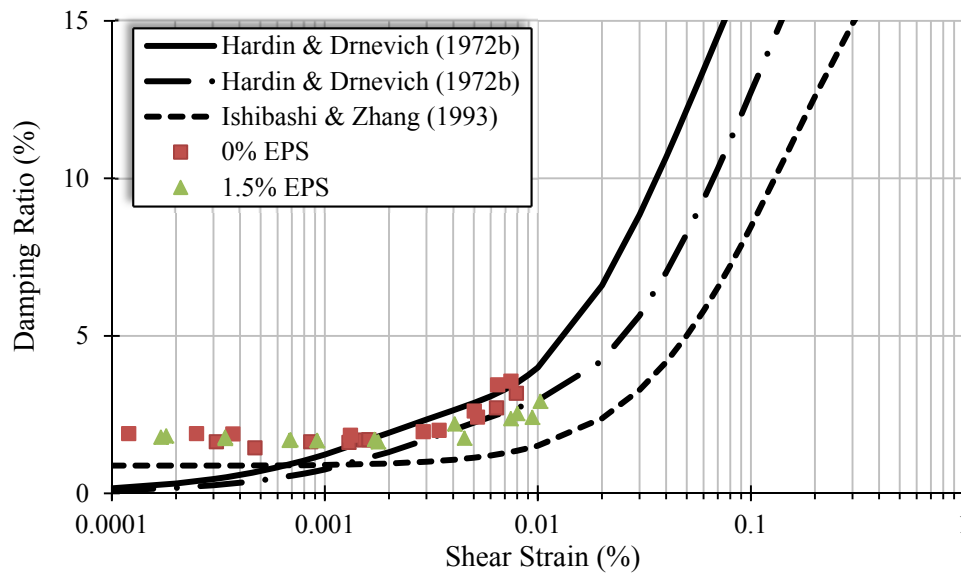


**Figure 7.14.  Damping Ratio compared with Analytical Models for Compacted Specimens**
**(Relative Compaction ≈ 88% ; $\sigma_{cell}$ = 100 kPa)**

The measured data was also plotted on the design curves of Seed and Idriss (1970) and Vucetic and Dobry (1991) as shown in Figure 7.15 and Figure 7.16, respectively.  Data is from

specimens tested with a 100 kPa cell pressure. Both sets of design curves do not attempt to define the low-strain damping ratio, $D_{min}$. The design curve of Seed and Idriss (1970) provide a reasonable fit to the measured data but the data tended to plot close to the lower limit. The design curves of Vucetic and Dobry (1991) were divided into specific ranges based on plasticity index. The relationship provided an accurate fit to the pure kaolin data, and the EPS modified soil specimens followed the curve of a high PI soil.

The variation between the measured results and the damping models are primarily attributed to the fact that the curves do not specifically consider the influence of confining stress on the soil, with the exception of the Ishibashi and Zhang model. It is well established that increases in confinement would result in a stiffer material with less damping capacity. The curves provide a general range of the damping ratio but in most cases cannot accurately model specific soil behavior.
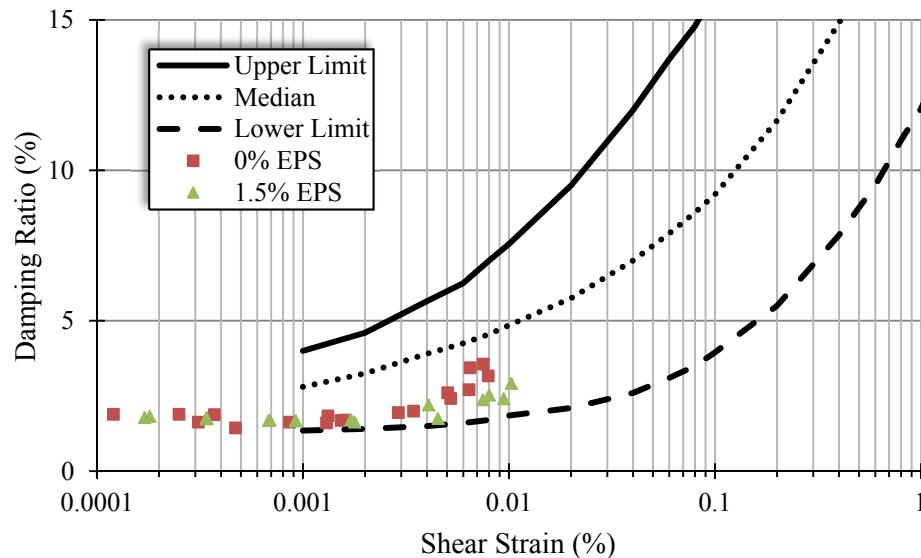


**Figure 7.15. Damping Ratio compared with Seed & Idriss (1970) Curves for Compacted Specimens (Relative Compaction ≈ 88% ; $\sigma_{cell}$ = 100 kPa)**
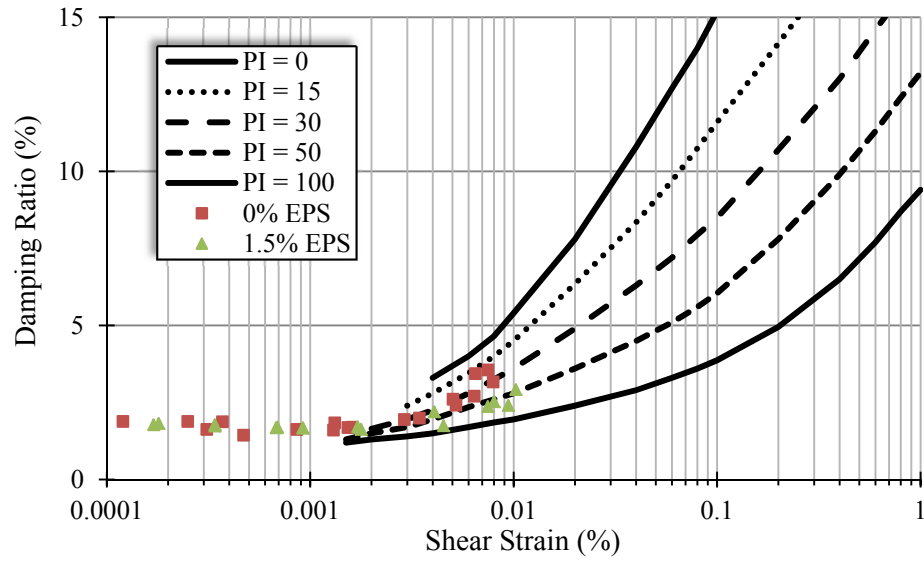
**Figure 7.16. Damping Ratio compared with Vucetic & Dobry (1991) Curves for Compacted Specimens (Relative Compaction ≈ 88% ; $\sigma_{cell}$ = 100 kPa)**



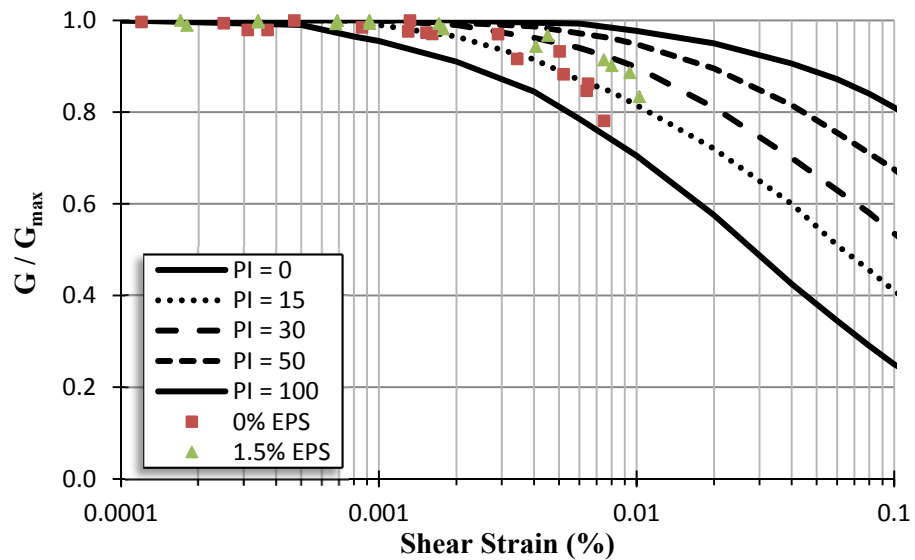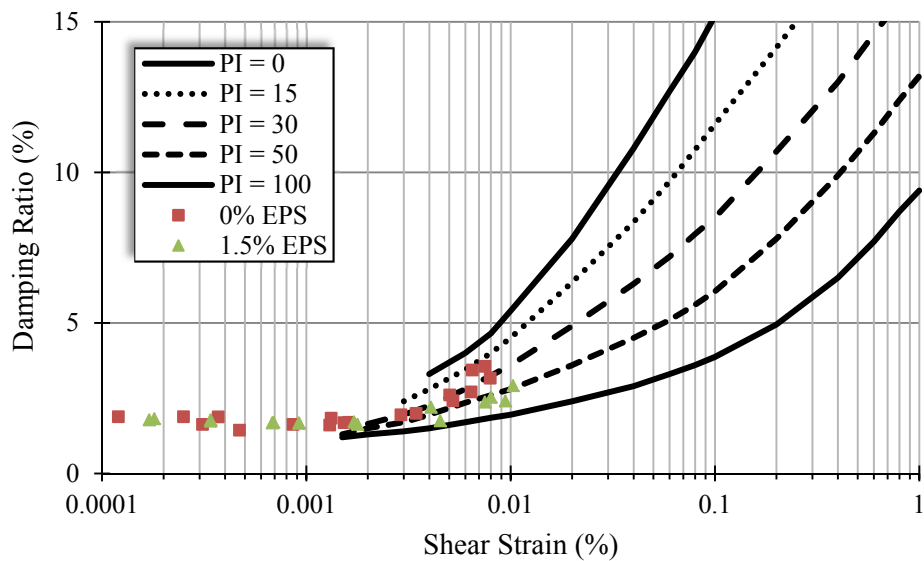**Figure 7.17. Damping Ratio compared with Vucetic & Dobry (1991) Curves for Compacted Specimens (Relative Compaction ≈ 88% ; $\sigma_{cell}$ = 100 kPa)**

## 8.    CONCLUSIONS & RECOMMENDATIONS

This following chapter presents the research conclusions developed from the data presented herein and recommendations for future research that were identified throughout the realization of the work.  It is stressed that the experimental program performed for this research was designed as an initial characterization of material properties for cohesive soils modified with EPS particulates.  For design purposes, additional testing should utilize the conclusions of this research to guide initial selection of EPS particulate content and further testing of in-situ soils that would be used during construction should be realized.

### 8.1.    CONCLUSIONS

In chapter 1 the primary questions to be addressed by this research (research objectives) were introduced and discussed.   Based on the results obtained during the experimental program, the following conclusions and responses were developed.

- *How does the addition of EPS particulates affect the strength of soils modified with EPS particulates?*

The undrained shear strength of saturated specimens, or EPS modified soils with a saturated soil matrix, was nearly constant with increasing EPS content, but partially saturated compacted specimens behaved differently.  Compacted specimens with EPS contents less than or equal to 1% by mass exhibited undrained shear strengths similar to the pure kaolin specimens, but EPS contents greater than 1% showed a distinct reduction in strength.  Drained shear strength results indicate that soils modified with EPS particulates up to 1.5% by mass do not exhibit decreased strength as the Mohr-Coulomb strength parameters were similar for the different mix ratios.   Overall the results indicated that if the dosage of EPS particulates are carefully considered, a reduced unit weight material could be produced with minimal loss in short-term undrained shear strength or long-term drained shear strength.

- *Does soil modified with EPS particulates show an improvement in dynamic soil properties?*

Results indicated that for a given strain level, the shear modulus decreased with increasing EPS content and the damping ratio was relatively unaffected by EPS content.  Based on these results, the addition of up to 1.5% EPS particulates by mass would not lead to improved

shear stiffness or material damping at any specific strain levels. At this time the inclusion of EPS particulates into fill soils for dynamic applications would not be expected to provide more damping of energy and it has been confirmed that they exhibit reduced shear stiffness for a given strain level. The one potentially advantageous aspect of EPS modified soils was that the inclusion tended to increase the range of strains in which they exhibited linear elastic behavior.

- *Based on the findings of the research program, what are the optimum mixing ratios for these soils and are these mixing ratios different for the modification of different engineering properties?*

Considering the results of this testing program the optimum mixing ratio for a lightweight fill composed primarily of a cohesive soil and maintained sufficient drained and undrained strength would be approximately 99% soil : 1% EPS particulates, by mass, which would constitute approximately 35% EPS per unit volume. The optimum mixing ratio for a modified soil that performed as a compressible inclusion for reduced earth pressures would be approximately 98.5% cohesive soil : 1.5% EPS particulates. Based on the swell-compression test results, the percent free swell systematically decreased with each 0.5% addition of EPS particulates. This indicates EPS particulate percentages greater than 1.5% would likely exhibit a further decrease in swell potential. It should be noted that increasing EPS content did not affect the swell pressure soils significantly. Based on the results of the dynamic tests it appears that EPS modified soils do not positively influence the damping capacity of the soil, and at this point EPS modified soils would not be expected to exhibit significant advantages for dynamic applications.

In addition to the research objectives, two additional working hypotheses were introduced in Chapter 1 and considered throughout the experimental program. Considering the measurements and data obtained the following responses and conclusions were developed:

- *The EPS particulate additives will not saturate under pressures and time periods of typical of geotechnical applications.*

Simple experimental tests that immersed EPS particulates in water for specific periods of time and subsequently required gravimetric mass determinations were inconclusive due to the very small individual mass of the particles. Based on the backsaturation and consolidation procedures used during preparation of specimens for CU triaxial testing the EPS particulates

remained impervious up to pressures of 310 kPa, which would correlate to a burial depth of approximately 15 meters in the field. The potential for increased permeability with increasing time or higher pressures is unknown, but it is expected there is some pressure in which water could be forced into the particulates.

- *The EPS particulate additives will not significantly degrade the soil stiffness and strength as they constitute such a small percentage of the overall soil mass.*

The strength of EPS modified soils were discussed previously based on experimental measurements from UU and CU triaxial tests. The EPS particulates constitute a small percentage of the specimen mass but a large percentage of the specimen volume. Saturated specimens, tested in both UU and CU triaxial compression, did not exhibit any specific decrease in stiffness with increasing EPS content. Partially saturated specimens tested in UU triaxial compression exhibited a decrease in stiffness when EPS contents exceeded 1% by mass. Dynamic tests indicated decreased dynamic stiffness with increasing EPS content; as defined by both the shear modulus and Young's modulus.

It is believed that the EPS particulates compress and potentially collapse at high confining stresses. Radial measurements of compacted, partially saturated specimens during undrained isotropic compression would result in better estimates of specimen density / void ratio at the time of testing, and provide more information on the performance to changing stress regimes.

## 8.2. RECOMMENDATIONS FOR EPS MODIFIED SOILS – FUTURE TESTING AND APPLICATIONS

The data, results, and interpretations contained herein expand the existing knowledge of soils modified with EPS particulates and provide a foundation for their potential use in industry. Based on the knowledge and experiences gleaned throughout this research program a more detailed discussion of potential applications and additional work needed to support the use of EPS modified soils for these applications is presented.

**8.2.1. Compressible Inclusion.** Geofoam's successful use as a compressible inclusion has been reported for a number of years (Horvath 1997; Ikizler et al. 2008;), and the potential use of EPS modified fill soils as compressible inclusions to counteract earth pressures was positively reinforced from the results of laboratory swell-compression tests performed during this research and the measured reduction in void ratio with increasing EPS content. Compressible inclusions

are commonly installed behind soil retention structures to reduce lateral loads, underneath slabs to reduce uplift pressures, or over subsurface pipes. A soil modified with EPS particulates could present an attractive option over geofoam blocks or select fill for applications with difficult access, variable geometries, or where importing inert soil is economically prohibitive. In these cases existing cohesive soils modified with EPS particulates could reduce the swell potential and potentially the earth pressure against soil retention structures, foundation elements, or basement diaphragm walls. The total heave of an expansive layer in the soil can be computed using the measured data from oedometer swell-compression tests and following methodologies presented by Fredlund and Rahardjo (1993). Chao et al. (2011) discuss a metric called the expansion potential that is related to both the percent free swell and the swell pressure. The measured swelling pressure could be used to model an upward force on foundation elements if water is introduced to swelling soils as discussed by both Nelson and Miller (1992) and Chen (1988). Increasing EPS content led to a systematic decrease in the percent free swell but only slightly affected the swell pressure.

Kaolin is known to be a relatively stable clay soil. Additional laboratory tests should be performed on a soil with increased swell potential (high PI and/or activity) to highlight the influence of increasing EPS content on the swell pressure and percent free swell.

Conceptually it is believed that soil modified with EPS particulates could be advantageously used as select fill against soil retention structures. The drastic reduction in unit weight with increasing EPS content would lead directly to reduced lateral loads, but it is believed that the compressibility of the particulates would also influence the lateral earth coefficients and further decrease lateral loads. Data from oedometer swell-compression tests cannot be tied directly to lateral earth pressure and thus the assumed positive influence of increased EPS content on the lateral earth coefficient is unknown. An alternate experiment is recommended in which and EPS modified soil is compacted into a cylinder and vertically loaded. Both horizontal and vertical strain measurement would be obtained along the outside perimeter of the cylinder and related to lateral stress via the hoop stress. The influence of the cylinder stiffness would need consideration and to be removed from the recorded data. This type of experiment has been performed for tire-derived aggregates and the publication of Humphrey and Manion (1992) offers further guidance.

Swelling soils also present design problems from seasonal shrinkage resulting from fluctuations in moisture content. Further testing on the use of EPS modified soils should consider their influence on the shrinkage potential.

**8.2.2. Lightweight Fill.** The use of EPS modified soils has the potential to be a viable alternative as a lightweight fill over compressible soils or on slopes to reduce the gravitational driving force. Often levees and embankments must be built over weak and compressible fills and the design must consider a significant amount of strain from the expected soil loads. In these cases a lightweight fill composed of EPS particulates and native soil could represent a design alternative. Similarly, EPS modified soils could be used as fill on slopes to improve the overall stability. The significant reduction in unit weight with increasing EPS content would reduce expected settlements or downslope driving force. If the results of the strength tests presented in this report are confirmed for other soil types, then little loss of strength would be expected and thus the design geometry (i.e. height and slope angle) would not require alteration. In addition the EPS additive represents a significant portion of the soil volume and could reduce the cost of imported select fill.

With approximately 1 – 1.5% EPS content by mass, the unit weight of the modified soil was less than water and thus the buoyancy of the fill could influence its applicability for levees and other embankments adjacent to water, but in reality the buoyancy is significantly less than traditional geofoam blocks often used in these type of applications. Further testing should determine if upward buoyancy of placed fill affects the design intent of the structure (i.e. strength, stability, and hydraulic conductivity).

**8.2.3. Dynamic Isolation.** It is still believed that EPS modified soils could produce a fill soil that has the potential to be used for vibrational isolation of structures. Geofoam installations have been shown to successfully isolate structures (Zarnani and Bathurst 2008; Murillo et al. 2009), and thus it is believed if similar results could be realized with the correct soil-to-EPS particulate mixing ratio. The EPS particulates could be added to the existing soil and used as compacted fill for isolation trenches or against structures to act as seismic buffers. They would present a safer alternative to open or slurry filled trenches often used in temporary applications such as pile driving activities or blasting operation. The laboratory tests performed as part of this research did not show improved material damping for cohesive soils with up to 1.5% EPS particulates, by mass.

It is recommended that additional experimental testing of EPS modified soils considering both EPS particulates of lower density that those used for this research and increased percentages of EPS particles. Generally the density of EPS particulates is directly related to the size of the particles. A lower density particulate will introduce more void space to the soil which might produce measurable improvements in material damping. It should be noted that a soil modified

with a lower density particulate than used in this research would most likely result in a larger influence on the strength and stiffness of the soil.

It is recommended that any additional experimental work performed in the laboratory and field consider cohesionless soil types, which could produce a marked difference from EPS modified cohesive soils. The influence of the EPS particulates in a granular material might lessen and soften the contacts between soil particles and thus produce a different effect on the damping capacity for cohesionless soil types.

Even though the experimental work performed on unit element specimens in the laboratory did not show superior shear stiffness or material damping with the addition of EPS particulates, it is uncertain if their addition to real soils would produce a notable influence and tested in-situ. A potential field test program should include installing a cutoff trench near a dynamic excitation source and measuring wave velocities with geophones placed along a survey line orthogonal to the cutoff trench. Railroad excitations are known to produce low frequency loadings in the soil and thus the test location could be installed at Schuman Park (after consulting the city of Rolla) or at the Missouri S&T experimental mine. Both of these locations are adjacent to frequent railroad traffic and an extensive data set could be acquired over a few days or weeks of monitoring.

**8.2.4. Environmental Stewardship.** The use of EPS particulates to modify existing soils is attractive for a variety of reasons, but one notable disadvantage of the EPS particulates utilized in this research was that they originated from a geofoam manufacturer and ultimately associated with a specific unit cost. Future research should consider the use of recycled EPS materials that could be obtained free of charge and provide an innovative way of utilizing waste materials from the manufacturing sector in engineering designs. Virgin EPS materials typically contain 10 – 15% "regrind" material that originates from trimming of larger geofoam pieces (Horvath 1993). Nonetheless manufacturers often contain an overabundance of the regrind material that must be hauled to a landfill for disposal (Pat Rosener, personal communication). Utilization of this waste stream could be beneficial for EPS manufacturers, project owners, and the designer in certain circumstances.

**APPENDIX**

STEREOSCOPY IMAGES, SCANNING ELECTRON MICROSCOPY IMAGES, PROCEDURES FOR CUTTING PIEZOELECTRIC ELEMENTS AND EXPOING CENTER ELECTRODE, COMPRESSION – SWELL TEST RESULTS, RESONANT COLUMN TEST RESULTS, RAW DATA FILES

## 1. INTRODUCTION

Included with this dissertation is a CD-ROM which contains the six sections of data. The stereoscopy images, scanning electron microscopy images and procedures for cutting piezoelectric elements are Microsoft Word 2010 document files. The compression – swell test results are a collection of PDF files. The resonant column test results are Microsoft Excel 2010 files. The raw test data files are a combination of Microsoft Excel and comma separated value (CSV) files obtained from the various data acquisition systems used throughout the research. The contents are as follow.

## 2. CONTENTS

Stereoscopy.DOCX

SEM.DOCX

Piezo_Machining.DOCX

COMPRESSION – SWELL TEST RESULTS:
Deformation_vs_Stress_100Kaolin.PDF
Deformation_vs_Stress_995Kaolin.PDF
Deformation_vs_Stress_99Kaolin.PDF
Deformation_vs_Stress_985Kaolin.PDF
Time_Deformation_Curve_100Kaolin.PDF
Time_Deformation_Curve_995Kaolin.PDF
Time_Deformation_Curve_99Kaolin.PDF
Time_Deformation_Curve_985Kaolin.PDF

<u>RESONANT COLUMN TEST RESULTS:</u>

RC_100Kaolin.XLSX

RC_995Kaolin.XLSX

RC_99Kaolin.XLSX

RC_985Kaolin.XLSX


<u>RAW DATA FILES:</u>

Unconsolidated Undrained Triaxial Compression Test Data Files (12 files)
Consolidated Undrained Triaxial Compression Test Data Files (4 files)
Resonant Column Test Data Files (854 files)
Bender Element Pulse Velocity Test Data Files (612 files)
Ultrasonic Pulse Velocity Test Data Files (88 files)

## BIBLIOGRAPHY

Aabøe, R., and Frydenlund, E. (2011). "40 years of experience with the use of EPS geofoam blocks in road construction." *Proceedings of the 4th International Conference on the use of geofoam blocks in construction applications*, Lillestrom, Norway, 6 – 8 June 2011.

Aggour, M.S., Taha, M.R., Tawfiq, K.S., and Amini, F. (1989). "Cohesive soil behavior under random excitation conditions." *Geotechnical Testing Journal*, Vol. 12 (2), 135 – 142.

Allam, M.M., and Sridharan, A. (1979). "The influence of aging on the shear strength behavior of two fine-grained soils." Canadian Geotechnical Journal, Vol. 16 (2), 391 – 397.

Amini, F. (1995). "Time effects on dynamic soil properties under random excitation conditions." *Soil Dynamics and Earthquake Engineering*, Vol. 14, 439 – 443.

Anderson, D.G., and Stokoe, K.H. (1978). "Shear modulus: A time-dependent soil property." *Dynamic Geotechnical Testing*, ASTM STP 654, American Society for Testing and Materials, 66 – 90.

APC International, Ltd. (2002). *Piezoelectric Ceramics: Principles and Applications*, Mackeyville, PA.

Arrellano, D., Zarrabi, M., Jafari, N.H., and Bailey, L.J. (2009). "Geosynthetic aggregate drainage systems: Preliminary large-scale laboratory test results for expanded recycled polystyrene." Geosynthetics 2009, Salt Lake City, UT, 25 – 27 February 2009.

Arroyo, M. (2001). "Pulse tests in soil samples." Ph.D. Thesis, University of Bristol, U.K.

Arroyo, M., Muir Wood, D., and Greening, P.D. (2003). "Source near-field effects and pulse tests in soil samples." *Geotechnique*, Vol. 53 (3), 337 – 345.

Arroyo, M., Muir Wood, D., Greening, P.D., Medina, L., and Rio, J. (2006). "Effects of sample size on bender-based axial $G_0$ measurements." *Geotechnique*, Vol. 56 (1), 39 – 52.

Arulnathan, R., Boulanger, R.W., and Riemer, M.F. (1998). "Analysis of bender element tests." *Geotechnical Testing Journal*, Vol. 21 (2), 120 – 131.

ASTM C 203 – 05. Standard test methods for breaking load and flexural properties of block-type thermal insulation. ASTM, West Conshohocken, Pennsylvania, USA.

ASTM C 272 – 01. Standard test methods for water absorption of core materials for structural sandwich constructions. ASTM, West Conshohocken, Pennsylvania, USA.

ASTM C 273 / C 273M – 07a.  Standard test method for shear properties of sandwich core materials.  ASTM, West Conshohocken, Pennsylvania, USA.

ASTM C 303 – 10.  Standard test method for dimensions and density of preformed block and board-type thermal insulation.  ASTM, West Conshohocken, Pennsylvania, USA.

ASTM C 578 – 11.  Standard specification for rigid, cellular polystyrene thermal insulation. ASTM, West Conshohocken, Pennsylvania, USA.

ASTM D422 – 63.  Standard test method for particle-size of soils.  ASTM, West Conshohocken, Pennsylvania, USA.

ASTM D 696 – 08.  Standard test method for coefficient of linear thermal expansion of plastics between -30°C and 30°C with a vitreous silica dilatometer.  ASTM, West Conshohocken, Pennsylvania, USA.

ASTM D 698 – 91.  Standard test methods for laboratory compaction characteristics of soil using standard effort (12,400 ft-lbf/ft$^3$ (600 kN-m/m$^3$)).  ASTM, West Conshohocken, Pennsylvania, USA.

ASTM D 1621 – 00.  Standard test method for compressive properties of rigid cellular plastics. ASTM, West Conshohocken, Pennsylvania, USA.

ASTM D 1622 – 08.  Standard test method for apparent density of rigid cellular plastics.  ASTM, West Conshohocken, Pennsylvania, USA.

ASTM D 1623 – 09.  Standard test method for tensile and tensile adhesion properties of rigid cellular plastics.  ASTM, West Conshohocken, Pennsylvania, USA.

ASTM D 2845 – 08.  Standard test method for laboratory determination of pulse velocities and ultrasonic elastic constants of rock.  ASTM, West Conshohocken, Pennsylvania, USA.

ASTM D 2850 – 03a.  Standard test method for unconsolidated-undrained triaxial compression test on cohesive soils.  ASTM, West Conshohocken, Pennsylvania, USA.

ASTM D 2863 – 10.  Standard test method for measuring the minimum oxygen concentration to support candle-like combustion of plastics (Oxygen Index).  ASTM, West Conshohocken, Pennsylvania, USA.

ASTM D 4015 – 07.  Standard test methods for modulus and damping of soils by the resonant-column method.  ASTM, West Conshohocken, Pennsylvania, USA.

ASTM D 4318 – 10.  Standard test methods for liquid limit, plastic limit, and plasticity index of soils.  ASTM, West Conshohocken, Pennsylvania, USA.

ASTM D 4546 – 08.  Standard test methods for one-dimensional swell or collapse of cohesive soils.  ASTM, West Conshohocken, Pennsylvania, USA.

ASTM D 4767 – 04.  Standard test method for consolidated undrained triaxial compression test for cohesive soils.  ASTM, West Conshohocken, Pennsylvania, USA.

ASTM D 6270 – 08.  Standard practice for the use of scrap tires in Civil Engineering applications.  ASTM, West Conshohocken, Pennsylvania, USA.

ASTM D 6817 – 07.  Standard specification for rigid cellular polystyrene geofoam.  ASTM, West Conshohocken, Pennsylvania, USA.

ASTM D 7180 – 05.  Standard guide for use of expanded polystyrene (EPS) geofoam in geotechnical projects.  ASTM, West Conshohocken, Pennsylvania, USA.

ASTM D 7557 – 09.  Standard practice for sampling of expanded polystyrene geofoam specimens.  ASTM, West Conshohocken, Pennsylvania, USA.

ASTM WK-23118 (2009) "New test method for determination of shear wave velocity by bender element." ASTM, West Conshohocken, PA.

Athanasopoulos, G.A. (1993).  "Effects of ageing and overconsolidatoin on the elastic stiffness of a remoulded clay." *Geotechnical and geological Engineering*, Vol. 11, 51 – 65.

Athanasopoulos, G.A., Pelekis, P.C., and Xenaki, V.C. (1999).  "Dynamic properties of EPS geofoam:  An experimental investigation." *Geosynthetics International*, Vol. 6 (3), 171 – 194.

Athanasopoulos, G.A., and Xenaki, V.C.  (2011).  "Experimental investigation of the mechanical behavior of EPS geofoam under static and dynamic / cyclic loading." *Proceedings of the 4th International Conference on the use of geofoam blocks in construction applications*, Lillestrom, Norway, 6 – 8 June 2011.

Atkinson, J.H, and Sallfors, G. (1991).  "Experimental determination of soil properties."  General Report to Session 1:  *Proceedings of the 10th ECSMFE*, Florence, Italy, 915-956.

Atkinson, J.H.  (2000).  "Non-linear soil stiffness in routine design." *Geotechnique*, Vol. 50 (5), 487 – 508.

BASF (2006).  Technical Information:  Styropor®. <http://www.basf-cc.co.in/en/products/Sustainable%20Construction/GEOFOAM/Documents/Geofoam.pdf > (June 25, 2012).

Bennell, J.D., and Smith, D.T. (1991). "A review of laboratory shear wave techniques and attenuation measurements with particular reference to the resonant column." *Shear Waves in Marine Sediments*, J.M. Hovem et al. (eds.), Kluwer Academic Publishers, Netherlands.

Bernal, A., Lovell, C.W., and Saldago, R. (1996). "Laboratory study on the use of tire shreds and rubber-sand in backfilled and reinforced soil applications." *Publication FHWA/IN/JHRP-96/12, Joint Highway Research Project*, Indiana Dept. of Transportation and Purdue University, West Lafayette, Indiana.

Biot, M.A. (1956). "Thoery of propagation of elastic waves in a fliuid-saturated porous solid. I. Low frequency range." *The Journal of the Acoustical Society of America*, Vol. 28 (2), 168 – 178.

Black, J.A., Stanier, S.A., and Clarke, S.D. (2009). "Shear wave velocity measurement of kaolin during undrained unconsolidated triaxial compression." *GeoHalifax 2009*, 20 – 24 September, Halifax, Canada.

Borden, R.H., Shao, L., and Gupta, A. (1996). "Dynamic properties of piedmont residual soils." *Journal of Geotechnical and Geoenvironmental Engineering*, Vol. 122 (10), 813 – 821.

Brocanelli, D., and Rinaldi, V. (1998). "Measurement of low-strain material damping and wave velocity with bender elements in the frequency domain." *Canadian Geotechnical Journal*, Vol. 35, 1032 – 1040.

Canales, A.R. (1980). "Measurement techniques and test related variables in resonant column testing." M.S. Thesis, University of Texas – Austin.

Cascante, G., and Santamarina, J.C. (1996). "Interparticle contact behavior and wave propagation." *Journal of Geotechnical Engineering*, Vol. 122 (10), 831 – 839.

Chan, C.M. (2012). "Variations of shear wave arrival time in unconfined soil specimens measured with bender elements." *Geotechnical and Geological Engineering*, Vol. 30, 461 – 468.

Chao, K.C., Nelson, J.D., Overton, D.D., and Nelson, E.J. (2011) "Commentaries on the consolidation-swell test." *UNSAT 2010: Proceedings of the Fifth International Conference on Unsaturated Soils*, Barcelona, Spain, 6 – 8 September, 2010, 641 – 646.

Chen, A.T.F., and Stokoe, K.H. (1979). "Interpretation of strain-dependent modulus and damping from torsional soil tests." *Report No. USGS-GD-79-002, NTIS No. PB-298479*, US Geologic Survey, Menlo Park, California.

Chen, F.H. (1988). *Foundations on Expansive Soils*. Elsevier Science, New York, NY, 2nd Ed.

Clayton, C.R.I., Theron, M., and Best, A.I. (2004). "The measurement of vertical shear-wave velocity using side-mounted bender elements in the triaxial apparatus." *Geotechnique*, Vol. 54 (7), 495 – 498.

Clayton, C.R.I. (2011). Stiffness at small strain: research and practice." *Geotechnique*, Vol. 61 (1),. 5-37.

Coleman, T.A. (1974). "Polystyrene foam is competitive, lightweight fill." *Civil Engineering*, Vol. 44 (2), 68 – 69.

Darendeli, M.B. (2001) "Development of a new family of normalized modulus reduction and material damping curves." Ph.D. Thesis, University of Texas – Austin.

de Alba, P., Baldwin, K., Janoo, V., Roe, G., and Celikkol, B. (1984). "Elastic-wave velocities and liquefaction potential." *Geotechnical Testing Journal*, Vol. 7 (2), 77 – 87.

de Alba, P., and Baldwin, K.C. (1991). "Use of bender elements in soil dynamics experiments." *Recent Advances in Instrumentation, Data Acquisition and Testing in Soil Dynamics*, ASCE, Geotechnical Special Publication (GSP) No. 29, 86 – 101.

Deng, A., and Xiao, Y. (2008). "Shear behavior of sand-expanded polystyrene beads lightweight fills." *Journal of the Central South University of Technology*, Vol. 15 (2), 174 – 179.

Deng, A., and Xiao, Y. (2010). "Measuring and modeling proportion-dependent stress-strain behavior in EPS-Sand Mixture." *International Journal of Geomechanics*, Vol. 10 (6), 214 – 222.

Dobry, R., and Vucetic, M. (1987). "Dynamic properties and seismic response of soft clay deposits." *Proceedings of International Symposium on Geotechnical engineering of Soft Soils*, Mexico City, Mexico, 13 – 14 August, Vol. 2, 51 – 87.

Drnevich, V.P., Hardin, B.O., and Shippy, D.J. (1978). "Modulus and damping of soils by the resonant-column method." *Dynamic Geotechnical Testing*, ASTM STP 654, American Society for Testing and Materials, 91 – 125.

Drnevich, V.P. (1985). "Recent developments in resonant column testing." *Proceedings Richart Commemorative Lectures,* R.D. Woods (eds.), ASCE, Detroit, Michigan, 79 – 107.

Duffy, S.M., Wheeler, S.J., and Bennell, J.D. (1991). "Shear modulus of kaolin containing methane bubbles." *Journal of Geotechnical Engineering*, Vol. 120 (5), 781 – 796.

Duskov, M. (1997). "Materials research on EPS20 and EPS15 under representative conditions in pavement structures." *Geotextiles and Geomembranes*, Vol. 15 (1-3), 147 – 181.

Dyvik, R., and Madshus, C. (1985). "Lab measurement of $G_{max}$ using bender elements." *Advances in the art of testing soils under cyclic conditions*, V. Khosla (eds.), ASCE, NY, 186 – 196.

EPS Molders Association (2008). "15-Year in-Situ research shows EPS outperforms XPS in R-value retention." Technical Bulletin, November.

Esch, D.C. (1994). "Long term evaluation of insulted roads & airfields in Alaska." *Publication FHWA/AK/RD_94/18*, Alaska Department of Transportation, Juneau, Alaska.

Feng, M., Gan, J. K-M, and Fredlund, D.G. (1998). "A laboratory study of swelling pressure using various test methods." *UNSAT 1998: Proceeding of the Second International Conference on Unsaturated Soils*, Beijing, China, 27 – 30 August, 350 – 355.

Feng, Z., and Sutter, K.G. (2000). "Dynamic properties of granulated rubber/sand mixtures." *Geotechnical Testing Journal*, Vol. 23 (3), 338 – 344.

Ferreira, C., Viana da Fonseca, A., and Santos, J.A. (2006). "Comparison of simultaneous bender elements and resonant column tests on Porto residual soil." *Soil Stress-Strain Behavior: Measurement, Modeling and Analysis Geotechnical Symposium,* Roma, Italy, 16 – 17 March.

Fredlund, D.G., and Rahardjo, H. (1993). "*Soil mechanics for unsaturated soils.*" John Wiley and Sons Inc., New York, NY.

Gohl, W.B., and Finn, W.D.L. (1991). "Use of piezoceramic bender elements in soil dynamics testing." *Proceedings of ASCE National Convention, Recent Advances in Instrumentation, Data Acquisition and Testing in Soil Dynamics*, S.K. Bhatia, and G.W. Blaney (eds.), Florida, GSP 29, 118 – 133.

Graesser, E.J., and Wong, C.R. (1992). "The relationship of traditional damping measures for materials with high damping capacity: A review." *M3D: Mechanics and Mechanisms of Material Damping*, ASTM STP 1169, V.K. Kinra and A. Wolfenden (eds.), American Society for Testing and Materials, Philadelphia, 316 – 343.

Greening, P.D., Nash, D.F.T., Benahmed, N, Ferreira, C., and da Fonseca, A.V. (2003). "Comparison of shear wave velocity measurements in different materials using time domain and frequency domain techniques." *Deformational Characteristics of Geomaterials*, Di Benedetto, H., Doanh, T., Geoffroy, H., & Sauzeat, C. (eds.), Swets and Zeitlinger, Lisse, 381 – 386.

Greening, P.D., and Nash, D.F.T. (2004). "Frequency domain determination of $G_0$ using bender elements." *Geotechnical Testing Journal*, Vol. 27 (3).

Gregory, A.R., and Podio, A.L. (1970). "Dual-mode ultrasonic apparatus for measuring compressional and shear wave velocities of rock samples." *IEEE Transactions on Sonics and Ultrasonics*, Vol. SU-17 (2), 77 – 85.

Gregory, G.H. (1996). "Laboratory testing of fiber-reinforced soils." *Proceedings of FHWA 29th annual southeastern transportation geotechnical engineering conference*, Cocoa Beach, Florida.

Gregory, G.H. (1997). "Slope reinforcement using randomly-distributed polypropylene fibers." *Proceedings of FHWA 22th annual southwestern geotechnical engineers conference*, Santa Fe, New Mexico.

Gregory, G.H. (1999). "Theoretical shear strength model of fiber-soil composite." *Proceedings of ASCE Texas section spring meeting*, Longview, Texas.

Gregory, G.H. (2011). "Sustainability and the fiber-reinforced soil repair of a highway embankment." *Geosynthetics*, Vol. 29 (4), 18 – 22.

Grubb, D.G., Gallagher, P.M., Wartman, J., Liu, Y., and Carnivale, M. (2006), "Laboratory evaluation of crushed glass – dredged material blends." *Journal of Geotechnical and Geoenvironmental Engineering*, Vol. 132 (5), 562 – 576.

Grubb, D.G., Liu, W., Cadden, A.W., and Humphrey, D.N. (2007a), "Bulkhead design using recycled materials as backfill." *Ports 2007: 30 years of sharing ideas: 1977 – 2007*, W. Watson (ed.), ASCE.

Grubb, D.G., Wartman, J.M., Malasavage, M.E., and Mibroda, J.G. (2007b), "Turning mud into suitable fill: Amending OH, ML-MH, and CH soils with curbside-collected crushed glass (CG)." *Geo-Denver 2007: New peak in geotechnics*, ASCE, GSP 163

Handy, R.L. (1981). "Linearizing triaxial test failure envelopes." *Geotechnical Testing Journal*, Vol. 4 (4), 188 – 191.

Hardin, B.O., and Richart, F.E. (1963). "Elastic wave velocities in granular soils." *Journal of the Soil Mechanics and Foundations Division*, Vol. 89 (SM1), 33 – 65.

Hardin, B.O. (1965). "The nature of damping in sands." *Journal of the Soil Mechanics and Foundations Division*, ASCE, Vol. 91 (SM1), 63 – 97.

Hardin, B.O., and Music, J. (1965). "Apparatus for vibration of soil specimens during triaxial testing." *Instruments and Apparatus for Soil and Rock Mechanics*, ASTM STP 392, American Society for Testing and Materials, 55 – 74.

Hardin, B.O., and Black, W.L.  (1968).  "Vibration modulus of normally consolidated clay." *Journal of the Soil Mechanics and Foundations Division*, ASCE, Vol. 94 (SM2), 353 – 369.

Hardin, B.O., and Black, W.L.  (1969).  Closure to "Vibration modulus of normally consolidated clay." *Journal of the Soil Mechanics and Foundations Division*, ASCE, Vol. 95 (SM6), 1531 – 1537.

Hardin, B.O., and Drnevich, V.P.  (1972a).  "Shear modulus and damping in soils:  Measurement and parameter effects." *Journal of the Soil Mechanics and Foundations Division*, Vol. 98 (SM6), 603 – 624.

Hardin, B.O., and Drnevich, V.P.  (1972b).  "Shear modulus and damping in soils:  Design equations and curves." *Journal of the Soil Mechanics and Foundations Division*, Vol. 98 (SM7), 667 – 692.

Hardin, B.O.  (1978).  "The nature of stress-strain behavior of soils." *Proceedings of Earthquake Engineering and Soil Dynamics*, ASCE, Pasadena, CA, Vol. 1, 3 – 89.

Holtz, R.D., and Kovacs, W.D.  (1981).  *An Introduction to Geotechnical Engineering*.  Prentice Hall, Englewood Cliffs, New Jersey.

Horvath, J.S. (1993).  "Expanded Polystyrene (EPS) Geofoam: An Introduction to Material Behavior." *Geotextiles and Geomembranes*, Vol. 13, 263 – 280.

Horvath, J.S.  (1997).  "The compressible inclusion function of EPS geofoam." *Geotextiles and Geomembranes*, Vol. 15, 77 – 120.

Horvath, J.S.  (2001).  "An introduction to cellular geosynthetics (Geofoams and Geocombs)." Manhattan College, NY.

Humphrey, D.N., and Manion, W.P.  (1992).  "Properties of tire chips for lightweight fill." Grouting, Soil Improvement and Geosynthetics, ASCE, GSP No. 30, Vol. 2, 1344 – 1355.

Humphrey, D.N., and Sandford, T.C.  (1993).  "Tire chips as lightweight subgrade fill and retaining wall backfill." *Symposium on Recovery and Effective Reuse of Discarded Materials and by-Products for Construction of Highway Facilities*, Denver, Colorado, 19 – 22 October.

Humphrey, D.N., and Tweedie, J.J. (2002), "Tire shreds as lightweight fill for retaining walls – Results of full scale field trials." *Proceedings of the Workshop on Lightweight Geomaterials*, Tokyo, Japan.

Ishibashi, I., and Zhang, X. (1993). "Unified dynamic shear moduli and damping ratios of sand and clay." *Soils and Foundations*, Vol. 33 (1), 182 – 191.

Ishihara, K. (1996). *Soil Behavior in Earthquake Geotechnics*. Oxford University Press, UK.

Ikizler, S.B., Aytekin, M., and Nas, E. (2008). "Laboratory study of expanded polystyrene (EPS) geofoam used with expansive soils." *Geotextiles and Geomembranes*, Vol. 26, 189-195.

Jamiolkowski, M., Leroueil, S., and LoPresti, D.C.F. (1991). "Theme lecture: Design parameters from theory to practice." *Proceedings of the International Conference on Geotechnical Engineering for Coastal Development – Theory and Practice on Soft Ground*, Geo-Coast '91, Japan.

Jardine, R.J. (1992). "Some observations on the kinematic nature of soil stiffness." *Soils and Foundations*, Vol. 32 (2), 111 – 124.

Johnson, D.H. (1981). "Attenuation: A state-of-the-art summary." *Seismic Wave Attenuation*, M.N. Toksoz and D.H. Johnson (eds.), Geophysical Reprint Series, Society of Exploration Geophysicists, Tulsa, OK.

Jovicic, V., Coop, M.R., and Simic, M. (1996). "Objective criteria for determining $G_{max}$ from bender element tests." *Geotechnique*, Vol. 46 (2), 357 – 362.

Khan, Z., Cascante, G., El Naggar, H, and Lai, C. (2008). "Evaluation of first mode of vibration, base fixity, and frequency effects in resonant-column testing." *Proceedings of the Fourth International Symposium on Deformational Characteristics of Geomaterials*, S.E. Burns, P.W. Mayne, and J.C. Santamarina (eds.), IOS Press/Millpress, London, UK.

Kim, Y.T., and Kang, H.S. (2011). "Engineering characteristics of rubber-added lightweight soil as a flowable backfill material." *Journal of Materials in Civil Engineering*, Vol. 23 (9), 1289 – 1294.

Kim, H.K., and Santamarina, J.C. (2008). "Sand-rubber imxtures (Large rubber chips)" *Canadian Geotechnical Journal*, Vol. 45 (10), 1457 – 1466.

Kondner, R.L. (1963). "Hyperbolic stress-strain response: Cohesive soils." *Journal of the Soil Mechanics and Foundations Division*, Vol. 89 (SM1), 115 – 143.

Kramer, S.L. (1996). *Geotechnical Earthquake Engineering*. Prentice Hall, New York.

Krautkramer, J., and Krautkramer, H. (1990). *Ultrasonic Testing of Materials*. 4th ed., Springer-Verlag, New York.

Kumar, S., and Tabor, E. (2003). "Strength characteristics of silty clay reinforced with randomly orientated nylon fibers." *Electronic Journal of Geotechnical Engineering* (EJGE), Vol. 8.

Ladd, R.S. (1978). "Preparing test specimens by undercompaction." *Geotechnical Testing Journal*, Vol. 1 (1), 16 – 23.

Lawrence, F.V. (1963). "Propagation of ultrasonic waves through sand." *Research Report R63-08*, Massachusetts Institute of Technology, Boston.

Lawrence, F.V. (1965). "Ultrasonic shear wave velocity in sand and clay." *Research Report R65-05*, Massachusetts Institute of Technology, Boston.

Lee, J.S., and Santamarina, J.C. (2005). "Bender elements: Performance and signal interpretation." *Journal of Geotechnical and Geoenvironmental Engineering*, Vol. 131 (9), 1063 – 1070.

Lee, C., Lee, J.S., Lee, W., Cho, T.H. (2007). "Experiment setup for shear wave and electrical resistance measurements in an oedometer." *Geotechnical Testing Journal*, Vol. 31 (2).

Leong, E.C., Yeo, S.H., and Rahardjo, H. (2004). "Measurement of wave velocities and attenuation using an ultrasonic test system." *Canadian Geotechnical Journal*, Vol. 41, 844-860.

Leong, E.C., Yeo, S.H., and Rahardjo, H. (2005). "Measuring shear wave velocity using bender elements." *Geotechnical Testing Journal,* Vol. 28 (5), 488-498.

Leong, E.C., Cahyadi, J., and Rahardjo, H. (2009). "Measuring shear and compressional wave velocities of soil using bender-extender elements." *Canadian Geotechnical Journal*, Vol. 46, 792 – 812.

Lings, M.L., and Greening, P.D. (2001). "A novel bender/extender element for soil testing." *Geotechnique*, Vol. 51 (8), 713 – 717.

Liu, H., Deng, A., and Chu, J. (2006). Effect of different mixing ratios of polystyrene pre-puff beads and cement on the mechanical behavior of lightweight fill. *Geotextiles and Geomembranes*, Vol. 24, 331 – 338.

Loehr, J. E., Axtell, P. J., and Bowders, J.J. (2000). "Reduction of soil swell potential with fiber reinforcement." GeoEng 2000, Melbourne, Australia, 19 – 24 November.

Mancuso, C., Simonelli, A.L., and Vinale, F. (1989). "Numerical analysis of in situ S-wave measurements." *Proceedings of the 12$^{th}$ International Conference on Soil Mechanics and Foundation Engineering*, Rio de Janeiro, Brazil, 13 – 18 August.

Matesic, L., and Vucetic, M. (1994). "Strain-rate effect on soil secant shear modulus at small cyclic strains." *Journal of Geotechnical and Geoenvironmental Engineering*, Vol. 129 (6), 536 – 549.

Mathwork Inc. (2011). MATLAB version 7.12.0.635: 2011a, Natick, MA.

Mitchell, J.K. (1993). *Fundamentals of Soil Behavior*. 2nd Ed., John Wiley & Sons, New York, NY.

Morgan, J.R. (1967). "Shear strength of a kaolin." *Proceedings of the Fifth Australia – New Zealand Conference of Soil Mechanics and Foundation Engineering*, Auckland, NZ, 72 – 78.

Moulson, A.J., and Herbert, J. M. (1990). *Electroceramics*. Chapman & Hall, London, UK.

Murillo, C., Thorel, L., and Caicedo, B. (2009). "Ground vibration isolation with geofoam barriers: Centrifuge modeling." *Geotextiles and Geomembranes*, Vol. 27, 423 – 434.

Nakagawa, K., Soga, K., and Mitchell, J.K. (1996). "Pulse transmission system for measuring wave propagation in soils." *Journal of Geotechnical Engineering*, Vol. 122 (4), 302 – 308.

Nakagawa, K., Soga, K., and Mitchell, J.K. (1997). "Observation of Biot compression wave of the second kind in granular soils." *Geotechnique*, Vol. 47 (1), 133 – 147.

Nataatmadja, A., and Illuri , H.K. (2009). "Sustainable backfill materials made of clay and recycled EPS." *Proceedings of the 3rd CIB International Conference on Smart and Sustainable Build Environments (SASBE 2009)*, Delft, Netherlands, 15 – 19 June.

Negussey, D. (2007). Design parameters for EPS geofoam. *Soils and Foundations*, Vol. 47 (1), 161 – 170.

Nelson, J.D., and Miller, D.J. (1992). *Expansive Soils: Problems and Practice in Foundation and Pavement Engineering*. John Wiley & Sons, Inc., New York.

Nirmalan, S. (2006). "*Strength and deformation characteristics of compacted scrap tire chips*", M.S. Thesis, University of Tokyo.

Oh, W.T., Garga, V.K., and Vanapalli, S.K. (2008). "Shear strength characteristics of statically compacted unsaturated kaolin." Canadian Geotechnical Journal, Vol. 45, 910 – 922.

Ossa, A., and Romo, M.P. (2009). "Micro- and macro-mechanical study of compressive behavior of expanded polystyrene geofoam." *Geosynthetics International*, Vol. 16 (5), 327 – 338.

Ossa, A., and Romo, M.P. (2011). Dynamic characterization of EPS geofoam. *Geotextiles and Geomembranes*, Vol. 29, 40 – 50.

Ozkul, Z.H., and Baykal, G. (2006). "Shear strength of clay with rubber fiber inclusions." *Geosynthetics International*, Vol. 13 (5), 173 – 180.

Ozkul, Z.H., and Baykal, G. (2007). "Shear behavior of compacted rubber fiber – clay composite in drained and undrained loading." *Journal of Geotechnical and Geoenvironmental Engineering*, Vol. 133 (7), 767 – 781.

Padilla, J.M. (2004). "GCTS Resonant Column Device." Geotechnical Consulting and Testing Systems, Tempe, AZ.

Pallara, O., Mattone, M., and Lo Presti, D.C.F. (2008). "Bender elements: Bad source – good receiver." *Deformational Characteristics of Geomaterials*, S.E. Burns, P.W. Mayne, and J.C. Santamarina (eds.), IOS Press/Millpress, London, UK, 697 – 702.

Parry, R.H.G., and Nadarajah, V. (1973). "Multistage triaxial testing of lightly overconsolidated clays." *Journal of Testing and Evaluations*, Vol. 1 (5), 374 – 381.

Pennington, D.S., Nash, D.F.T., and Lings, M.L. (2001). "Horizontally mounted bender elements for measuring anisotropic shear moduli in triaxial clay specimens." *Geotechnical Testing Journal*, Vol. 24 (2), 133 – 144.

Richart, F.E., Woods, R.D., and Hall, J.R. (1970). *Vibrations of Soils and Foundations*. Prentice-Hall, Inc., Englewood Cliffs, New Jersey.

Rio, J.F.M.E. (2006). "Advances in Laboratory Geophysics using Bender Elements." Ph.D. Thesis, University College London, UK.

Rossato, G., Ninis, N.L, and Jardine, R.J. (1992). "Properties of some kaolin-based model clay soils." Geotechnical Testing Journal, Vol. 15 (2), 166 – 179.

Sanchez-Salinero, I., Roesset, J.M., and Stokoe, K.H. (1986). "Analytical studies of body wave propagation and attenuation." *Report GR86-15*, University of Texas, Austin.

Santamarina, J.C. (2001). *Soils and Waves*. John Wiley & Sons, Ltd, West Sussex, England.

Santamarina, J.C. and Fratta, D. (2005). *Discrete Signals and Inverse Problems: An Introduction for Engineers and Scientists*. John Wiley & Sons, Ltd., West Sussex, England.

Santoni, R.L., Tingle, J.S., and Webster, S.L. (2001). "Engineering properties of sand-fiber mixtures for road construction." *Journal of Geotechnical and Geoenvironmental Engineering*, Vol. 127 (3), 258 – 268.

Satoh, T., Tsuchida, T., Mitsukuri, K., and Hong, Z. (2001). "Field placing test of lightweight treated soil under seawater in Kumamoto port." *Soils and Foundations*, Vol. 41 (5), 145 – 154.

Schneider, J.A., Hoyos, L., Mayne, P.W., Macari, E.J., and Rix, G.J. (1999). "Field and laboratory measurements of dynamic shear modulus of piedmont residual soils." *Behavioral Characteristics of Residual Soils*, GSP 92, ASCE, 12 – 25.

Seed, H.B., Mitchell, J.K., and Chan, C.K. (1960). "The strength of compacted cohesive soils." *Research Conference on Shear Strength of Cohesive Soils*, ASCE, Boulder, Colorado, June, 877 – 964.

Seed, H.B., and Idriss, I.M. (1970). "Soil moduli and damping factors for dynamic response analyses." *Report EERC 70-10, Earthquake Engineering Research Center*, University of California, Berkeley, California.

Seed, H.B., Wong, R.T., Idriss, I.M., and Tokimatsu, K. (1984). "Moduli and damping factors for dynamic analyses of cohesionless soils." *Report UBC/EERC 84/14*, Earthquake Engineering Research Center, University of California, Berkeley, California.

Senetakis, K., Anastasiadis, A., Pitilakis, K., and Souli, A. (2012). "Dynamic behavior of sand/rubber mixtures, Part II: Effect of rubber content on $G/G_0$-$\gamma$-$\Delta T$ curves and volumetric strain threshold." *Journal of ASTM International*, Vol. 9 (2).

Shi, Q. (1998). "Determination of the dynamic soil moduli by ultrasonic wave transmission method." Ph.D. Thesis, Arizona State University, Tempe, Arizona.

Shibuya, S., Koseki, J., and Kawaguchi, T. (2005). "Recent developments in deformation and strength testing of geomaterials." *Deformational Characteristics of Geomaterials*, H. Di Benedetto, T. Doanh, H. Geoffroy, and C. Sauzeat (eds.), A.A. Balkema, Netherlands.

Shirley, D.J., and Anderson, A.L. (1975). "In situ measurement of marine sediment acoustical properties during coring in deep water." *IEEE Transactions on Geoscience Electronics*, Vol. GE-13 (4), 163 – 169.

Shirley, D.J., and Hampton, L.D. (1978). "Shear-wave measurements in laboratory sediments." *Journal of the Acoustic Society of America*, Vol. 63 (2), 607 – 613.

Shirley, D.J. (1978). "An improved shear wave transducer." *Journal of the Acoustic Society of America*, Vol. 63 (5), 1643 – 1645.

Schultheiss, P.J. (1981). "Simultaneous measurement of P and S wave velocities during conventional laboratory soil testing procedures." *Marine Geotechnology*, Vol. 4 (4), 343 – 367.

Silvestri, V., Yong, R.N., and Mohamed A.M.O. (1988). "A true triaxial testing cell." *Advanced Triaxial Testing of Soil and Rock*, ASTM STP 977, R.T. Donaghe, R.C. Chaney, and M.L. Silver, (eds.), American Society for Testing and Materials, Philadelphia, 819 – 833.

Sivathayalan, S., Negussey, D., and Vaid, Y.P. (2001). "Simple shear and bender element testing of geofoam." *Proceedings of the 3$^{rd}$ International Conference on EPS Geofoam 2001*, Salt Lake City, Utah, December.

Stephenson, R.W. (1978). "Ultrasonic testing for determining dynamic soil moduli." *Dynamic Geotechnical Testing*, ASTM STP 654, American Society for Testing and Materials, 179 – 195.

Sun, J.I., Golesorkhi, R., and Seed, H.B. (1988). "Dynamic moduli and damping ratios for cohesive soils." *Report UBC/EERC 88/15*, Earthquake Engineering Research Center, University of California, Berkeley, California.

Thomann, T.G., and Hryciw, R.D. (1990). "Laboratory measurement of small strain shear modulus under $K_0$ conditions." *Geotechnical Testing Journal*, Vol. 13 (2), 97-105.

Tsuchida, T., Porbaha, A., and Yamane, N. (2001). Development of a geomaterial from dredged bay mud. *Journal of Materials in Civil Engineering*, Vol. 13 (2), 152 – 160.

Upright, W. (1989). "Colorado fights frost heave with insulation." *Public Works*, Vol. 120 (8), 81 – 82.

Viggiani, G., & Atkinson, J.H. (1995). "Interpretation of bender element tests." *Geotechnique*, Vol. 45 (1), 149 – 154.

Vucetic, M., and Dobry, R. (1991). "Effect of soil plasticity on cyclic response." *Journal of Geotechnical Engineering*, Vol. 117 (1), 89 – 107.

Vucetic, M. (1994). "Cyclic threshold shear strains in soils." *Journal of Geotechnical Engineering*, Vol. 120 (12), 2208 – 2228.

Wartman, J., Grubb, D.G., and Nasim, A.S.M. (2004a), "Select engineering characteristics of crushed glass." *Journal of Materials in Civil Engineering*, Vol. 16 (6), 526 – 539.

Wartman, J., Grubb, D.G., and Strenk, P. (2004b). "Engineering properties of crushed glass – soil blends." *Geotechnical Engineering for Transportation Projects*, M.K. Yegian and E. Kavazanjian (eds.), ASCE, Vol. 1, GSP 126, 732 – 739.

Wei, Z., Mingdong, L., Chunlei, Z. and Gan, Z. (2008). "Density and strength properties of sand-expanded polystyrene beads mixture." *GeoCongress 2008*, ASCE.

Weidinger, D.M. (2007). "Laboratory analysis of small strain moduli in compacted silts." M.S. Thesis, Missouri University of Science and Technology, Rolla, Missouri.

Woods, R. (1968). "Screening of surface waves." *Journal of Soil Mechanics and Foundations*, Vol. 94 (4), 951 – 979.

Woods, R.D. (1994). "Laboratory measurement of dynamic soil properties." *Dynamic Geotechnical Testing II*, ASTM STP 1213, R.J. Ebelhar, V.P. Drnevich, and B.L. Kutter (eds.), American Society for Testing and Materials, 165 – 190.

Yamashita, S., Kawaguchi, T., Nakata, Y., Mikami, T., Fujiwara, T., and Shibuya, S. (2009). "Interpretation of international parallel test on the measurement of $G_{max}$ using bender elements." *Soils and Foundations*, Vol. 49 (4), 631 – 650.

Yoonz, G., Jeon, S., and Kim, B. (2004). Mechanical characteristics of light-weighted soils using dredged materials. *Marine Georesources and Geotechnology*, Vol. 22, 215 – 229.

Zarnani, S., and Bathurst, R.J. (2008). "Numerical modeling of EPS seismic buffer shaking table tests." *Geotextiles and Geomembranes*, Vol. 26, 371 – 383.

Zen, K., Umehara, Y., and Hamada, K. (1978). "Laboratory tests and in-situ seismic survey on vibratory shear modulus of clayey soils with different plasticities." *Proceedings of Fifth Japan Earthquake Engineering Symposium*, Tokyo, Japan, 721 – 728.

Zen, K., Yamazaki, H., and Umehara, Y. (1986). "Time effect on the shear modulus of cohesive soils." *Proceedings of Seventh Japan Earthquake Engineering Symposium*, Japan, 619 – 624.

**VITA**

Nicholas Thomas Rocco was born in Missouri, United States of America in 1978. In December 2000 he graduated from the University of Missouri – Rolla with a B.S. degree in civil engineering. In March 2003 he received a M.S. degree in civil engineering with a geotechnical emphasis from the University of California – Davis. Mr. Rocco's M.S. research project included a kinematic back-analysis to determine the residual strength of a liquefied soil layer within an earthen dam located in central California. After receiving his M.S. degree he worked as a consulting engineer for Ausenco Vector (formally Vector Engineering Inc.) from 2004 to 2008 supporting geoenvironmental and geotechnical design tasks for the solid waste and surface mining industries. This consulting work included extended field assignments in Mexico, Colombia, Chile, Taiwan, and Vietnam. Mr. Rocco received his professional registration from the state of California in September 2006. In 2009 Mr. Rocco enrolled in a full-time, on-campus Ph.D. program at the Missouri University of Science and Technology, and a degree in civil engineering with a geotechnical emphasis was bestowed in December 2012.